

# **Directed differentiation of human pluripotent stem cells to telencephalic lateral ganglionic eminence progenitors using small molecules**

Shona Joy  
Supervisor: Professor Nicholas D. Allen

This thesis is submitted for the degree of Doctor of philosophy  
at Cardiff University

December 2016



**Dedicated to my Kunjothi**

## Summary

This thesis focused on directing the differentiation of pluripotent stem cells towards telencephalic lateral ganglionic eminence-like fate. The study aimed at developing chemically defined conditions for optimized production of cell types for application in Huntington's disease. The signalling pathways known to be involved in *in vivo* telencephalon development and regional specification were addressed. The temporal integration of pathways was achieved *in vitro* by utilizing small molecule pathway agonists or antagonists. In chapter 3, BMP antagonism by Dorsomorphin, LDN193189 and DMH1 was found to promote PAX6<sup>+</sup> neuroectoderm fate specification of hPSCs by day 8 of differentiation. In chapter 4, concomitant inhibition of BMP and WNT signalling by IWR1 and KY02111 was found to enhance FOXG1<sup>+</sup> telencephalic fate and regional specification towards LGE-like fate by day 16 of differentiation. In chapter 5 SHH pathway activation by Purmorphamine from day 8 to day 16 led to telencephalic fate specification towards MGE fate whereas Activin exposure in the same temporal window specifically enhanced LGE-like specification. In chapter 6, the day16 neural progenitors were terminally differentiated and analysed for DARPP32/CTIP2 expression indicative of LGE derived striatal MSN-like fate. BMP inhibitor+ WNT inhibitor patterned progenitors generated ~60% CTIP2<sup>+</sup> and ~16% DARPP32<sup>+</sup> neurons and addition of Activin nearly doubled the number of DARPP32<sup>+</sup> neurons. Activation of SHH signalling downregulated these markers. Thus, the study using hPSC as model system identified distinct cell responses to different signalling pathways involved in telencephalon specification.

## **Acknowledgements**

I would like to thank my supervisor Nick Allen for the providing me the opportunity to pursue this PhD under his guidance. I would also like to thank Anne Rosser and Paul Kemp for the support with this project. I would like to extend my gratitude to my advisor Ros Johns for the feedback and the encouragement.

I would like to acknowledge that Marco Straccia and Phil Sanders (University of Barcelona) carried out the high-throughput QRT-PCR analysis in this thesis.

My heartfelt thanks to Sian Rizzo for the constant encouragement, for being my mentor and for providing me with the feedback for thesis writing. Thank you to all the senior post docs; Susan Hunter for your friendly advice, Alysia Battersby and Amanda Redfern for sharing your expertise with QRT-PCR and cell culture and Andrew Hollins for your help with western blotting. I would also like to thank all my colleagues Alex Harrison, Belinda Thompson, Charlene Geater, David Rushton, Emma Cope, Joao Bigares, Rachel Steeg, Sali Bagabir, Shun Ming and Susannah William, for being such a supportive team.

I would like to extend my gratitude to my colleagues in St. Georges University of London and in UCL, London for helping me to meet the various demands of work whilst doing my thesis writing in parallel.

Special mention to Andreas Mezger, thank you Andy, for being a good friend and for always listening whenever I needed an ear.

The completion of this PhD has been quite a challenging experience. It would not have been possible without the enormous support of my family. Massive thanks to Mum and Dad, Simy, Sonia, George, Mannav and Michael for being there and keeping me motivated and determined to achieve this goal.

## Abbreviations

AME	Axial mesendoderm
ANR	Anterior Neural Ridge
A-P axis	Anterior-posterior axis
AVE	Anterior visceral endoderm
BDNF	Brain-derived neurotrophic factor
BMP	Bone Morphogenetic protein
BSA	Bovine serum albumin
CNS	Central Nervous system
D/V axis	Dorsal-ventral axis
DARPP32	Dopamine and cyclic adenosine 3',5'- monophosphate-regulated phosphoprotein
DMEM	Dulbecco's modified Eagle's medium
DMSO	Dimethylsulfoxide
E	Embryonic day
EB	Embryoid body
FGF	Fibroblast growth factor
GABA	$\gamma$ -aminobutyric acid
GADPH	Glyceraldehyde-3-phosphate dehydrogenase
GP	Globus pallidus
HD	Huntington's disease
Hesc	Human Embryonic stem cell
hiPSC	Human induced pluripotent stem cell
Hpsc	Human pluripotent stem cell
HTT	Huntingtin
ICM	Inner cell mass
KSR	Knock-out serum replacement
L	LDN193189 only treated culture
LGE	Lateral ganglionic eminence
LI	LDN193189+IWR1 treated culture
LIA	LDN193189+IWR1+Activin treated culture
LIP	LDN193189+IWR1+Purmorphamine treated culture
MEFi	Irradiated mouse embryonic fibroblast
MESC	Mouse Embryonic stem cell
MGE	Medial ganglionic eminence
MSN	medium spiny neurons
MZ	mantle zone
NII	Neuronal Intranuclear Inclusion
NMDA	N-methyl-D-aspartic acid
PDL	Poly-D-lysine
PFA	Paraformaldehyde
PS	primitive streak
PSB	Pallial Subpallial boundary
QA	Quinolinic acid

RA	Retinoic acid
SHH	Sonic Hedgehog
SN	substantia nigra
STN	subthalamus nucleus
SVZ	subventricular zone
VZ	Ventricular Zone
WGE	Whole ganglionic eminence
WNT	Wingless

# Table of Contents

<b>1</b>	<b>Introduction</b>	<b>1</b>
1.1	Huntington's disease	1
1.1.1	Clinical characteristics of HD	1
1.1.2	Selective Neurodegeneration in HD	1
1.1.3	The mutant Htt protein	2
1.1.4	HD research models	4
1.2	Striatum and Medium spiny neurons	9
1.2.1	Medium spiny neurons and Basal ganglia circuitry	10
1.2.2	DARPP-32	12
1.3	Neural development	13
1.3.1	Early patterning of the embryo	13
1.3.2	The principal events in telencephalon induction and LGE development	14
1.3.3	Signalling pathways involved in the telencephalon development and regional specification	19
1.3.4	Transcription factors involved in D-V regionalisation of the developing telencephalon	34
1.4	Stem cells	44
1.4.1	Embryonic stem cells	46
1.4.2	Induced pluripotent stem cells	46
1.4.3	Core transcriptional network of hPSC pluripotency and self-renewal	49
1.4.4	Signalling pathways in hPSC pluripotency and self-renewal	50
1.4.5	Application of hPSCs for HD	51
1.5	Small molecules mediated differentiation	66
1.5.1	BMP Inhibitors	66
1.5.2	WNT inhibitors	67
1.5.3	SHH agonists	67
1.6	Aims of the thesis	70
<b>2</b>	<b>Materials and Methods</b>	<b>72</b>
2.1	In-vitro Methods	72
	Derivation, Mitotic inactivation and Cryopreservation of	
2.1.1	mouse embryonic fibroblasts	73
2.1.2	Cell count using Haemocytometer	74
2.1.3	hES culture and maintenance on MEFi feeder layers	74
2.1.4	hPSC culture and maintenance on Matrigel in mTeSR1	76
2.1.5	Mycoplasma testing of hPSCs	77
2.1.6	Alkaline phosphatase staining of hPSCs	78
2.1.7	hPSC neural differentiation	78
2.2	Molecular Methods	81
2.2.1	Detection of gene expression at mRNA level	81
2.2.2	Detection of gene expression at protein level	89
2.3	. Statistical methods	94

2.4	Materials	94
<b>3</b>	<b>Investigation of small molecule mediated BMP antagonism on neural induction</b>	<b>99</b>
3.1	Aim	99
3.2	Background	99
3.3	Experimental design	100
3.4	Results	102
3.4.1	Small molecule mediated inhibition of induced BMP activity	102
3.4.2	QRT-PCR characterization of small molecule mediated inhibition of endogenous BMP activity during H9 neural induction	105
3.4.3	QRT-PCR characterization of neural induction	105
3.4.4	Immunocytochemistry characterization of neural induction	110
3.5	Discussion	124
3.5.1	Effect of BMP inhibitors on neuroectodermal and pluripotency markers	124
3.5.2	Effect of BMP inhibitors on neural crest and epidermal markers	128
<b>4</b>	<b>Investigation of small molecule mediated WNT antagonism on hPSC telencephalon specification</b>	<b>131</b>
4.1	Aim	131
4.2	Background	131
4.3	Experimental design	132
4.4	Results	134
4.4.1	Effect of IWR1 on inhibition of induced WNT activity	134
4.4.2	Effect of IWR1 on inhibition of endogenous WNT activity	134
4.4.3	Effect of IWR1 on telencephalon induction - time point analysis	136
4.4.4	QRT-PCR characterization of WNT inhibitors mediated telencephalon induction and specification	138
4.4.5	Immunocytochemistry characterization of WNT inhibitor mediated telencephalon induction and specification	140
4.4.6	High- through put QRT-PCR characterization of IWR1 or KY02111 mediated telencephalon differentiation	147
4.5	Discussion	153
4.5.1	Effect of WNT inhibitors on telencephalon induction	153
4.5.2	Effect of WNT inhibitors on telencephalon D/V specification	155
<b>5</b>	<b>Investigation of effect of HH and Activin signalling on hPSC ventral telencephalon specification</b>	<b>159</b>
5.1	Aim	159
5.2	Background	159
5.3	Experimental design	161
5.4	Results	162
5.4.1	Modulation of HH signalling by Purmorphamine and SAG	162

during hPSC differentiation.

5.4.2	QRT-PCR characterization of Purmorphamine or SAG mediated ventral telencephalon specification	164
5.4.3	Immunocytochemistry characterization of Purmorphamine or Activin mediated ventral telencephalon specification of H9 ESCs and 34D6 iPSCs	166
5.4.4	High-through put QRT-PCR characterization of Purmorphamine or Activin mediated ventral telencephalon specification of H9 ESC and 34D6 iPSCs	172
5.5	Discussion	189
5.5.1	Effect of SHH agonists or activin on dorsal and ventral markers	189
5.5.2	Effect of SHH agonists or Activin on neuroectodermal, anterior and neuronal markers	193
5.6	Limitations of the methods in the chapter	194
<b>6</b>	<b>Characterization of in vitro neuronal differentiation: Looking for striatal markers</b>	<b>195</b>
6.1	Aim	195
6.2	Background	195
6.3	Experimental design	195
6.4	Results	198
6.4.1	Analysis of striatal differentiation	198
6.4.2	Analysis of pre and post synaptic markers	207
6.5	Discussion	209
6.5.1	Effect of D16 treatments on generation of DARPP32+/CTIP2+ neurons	209
6.5.2	Effect of D16 treatments on generation of ISL1+ neurons	211
6.5.3	Effect of D16 treatments on generation of GABA, Calbindin, Synaptophysin and PSD95	212
<b>7</b>	<b>General Discussion</b>	<b>214</b>
7.1	Summary of the results	214
7.2	Small molecules-mediated directed differentiation of hPSCs	215
7.2.1	BMP antagonism promoted PAX6+ neuroectoderm fate specification	215
7.2.2	WNT antagonism promoted FOXG1+ telencephalic progenitor induction and ventral fate specification	218
7.2.3	SHH signalling and Activin signalling enhanced MGE-like and LGE-like fate specification respectively	219
7.2.4	Patterning effects persist when terminally differentiated into neurons	221
7.3	Scope of the project and future work	222
	Bibliography	223
	Appendix	

## List of Figures

Figure 1.1	Coronal section through a normal and HD brain	2
Figure 1.2	The basal ganglia	10
Figure 1.3	Photomontage of medium spiny neurons	10
Figure 1.4	Basal ganglia circuitry	11
Figure 1.5	Early embryo developmental stages	15
Figure 1.6	Neural Induction	16
Figure 1.7	Neurulation	17
Figure 1.8	Neural tube A-P and telencephalon D-V patterning	18
Figure 1.9	Schematic coronal section through E12.5 telencephalon	19
Figure 1.10	Canonical BMP signalling	20
Figure 1.11	Canonical WNT signalling	23
Figure 1.12	The SHH pathway	26
Figure 1.13	RA and paracrine RA signalling	31
Figure 1.14	Stem cell division	44
Figure 1.15	Multipotent adult and pluripotent embryonic or induced stem cells	45
Figure 1.16	Core signalling network that regulate pluripotency and self-renewal	51
Figure 1.17	Structure of small molecules	69
Figure 1.18	Thesis outline	71
Figure 3.1	Neural Induction culture regime	102
Figure 3.2	Attenuation of BMP4 induced phosphorylation of SMAD1/5/8 in undifferentiated H9 cells by small molecules	104
Figure 3.3	Modulation of endogenous BMP signalling by Noggin or small molecules during H9 differentiation	106
Figure 3.4	Effect of dual SMAD inhibition by SB431542 and either Noggin or small molecules on induction of neuroectoderm marker <i>PAX6</i>	108
Figure 3.5	Effect of dual SMAD inhibition by SB431542 and either Noggin or small molecules on induction of neuroectoderm marker <i>SLUG</i>	109
Figure 3.6	Fluorescent immunocytochemistry analysis of <i>PAX6</i> in D8 cultures	112
Figure 3.7	Fluorescent immunocytochemistry analysis of <i>SOX2</i> in D8 cultures	114
Figure 3.8	Fluorescent immunocytochemistry analysis of <i>NESTIN</i> in D8 cultures	116
Figure 3.9	Fluorescent immunocytochemistry analysis of <i>P75</i> in D8 cultures	119
Figure 3.10	Fluorescent immunocytochemistry analysis of <i>CK18</i> in D8 cultures	120
Figure 3.11	Fluorescent immunocytochemistry analysis of <i>KI67</i> in D8 cultures	122
Figure 3.12	Fluorescent immunocytochemistry analysis of <i>OCT4</i> in D8 cultures	123
Figure 4.1	Cell culture regime for hPSC telencephalon induction.	133

Figure 4.2	Modulation of WNT activity by WNT3a and IWR1 in day 12 neural progenitors	135
Figure 4.3	Modulation of endogenous WNT activity by IWR1.	136
Figure 4.4	Monitoring telencephalon induction on monolayer based protocol	137
Figure 4.5	Effect of time point addition of IWR1 on <i>FOXG1</i>	137
Figure 4.6	Effect of WNT inhibitors on telencephalon induction and specification	140
Figure 4.7	Fluorescent immunocytochemistry analysis of FOXG1 in D16 monolayer cultures	143
Figure 4.8	Fluorescent immunocytochemistry analysis of PAX6 in D16 monolayer cultures	144
Figure 4.9	Fluorescent immunocytochemistry analysis of GSX2 in D16 monolayer cultures	145
Figure 4.10	Fluorescent immunocytochemistry analysis of NKX2.1 in D16 monolayer cultures	146
Figure 4.11	Effect of WNT inhibitors on neuroectodermal markers-	147
Figure 4.12	Effect of WNT inhibitors on anterior markers	148
Figure 4.13	Effect of WNT inhibitors on pallial markers	149
Figure 4.14	Effect of WNT inhibitors on subpallial markers	150
Figure 4.15	Effect of WNT inhibitors on subpallial markers	151
Figure 4.16	Effect of WNT inhibitors on MGE markers	152
Figure 4.17	Effect of WNT inhibitors on neuronal markers	153
Figure 5.1	Cell culture regime for hPSC telencephalon induction and ventral specification	162
Figure 5.2	Modulation of HH activity by Purmorphamine and SAG in H9 day 16 neural progenitors	163
Figure 5.3	Effect of Purmorphamine and SAG on ventral telencephalon markers analysed by QRTPCR during H9 differentiation	166
Figure 5.4	Fluorescent immunocytochemistry analysis of PAX6 and NKX2.1 in H9 D16 monolayer cultures	168
Figure 5.5	Fluorescent immunocytochemistry analysis of PAX6 and NKX2.1 in 34D6 D16 monolayer cultures	169
Figure 5.6	Fluorescent immunocytochemistry analysis of GSX2 in H9 D16 monolayer cultures	170
Figure 5.7	Fluorescent immunocytochemistry analysis of GSX2 and CTIP2 in 34D6 D16 monolayer cultures	171
Figure 5.8	Effect of Purmorphamine or Activin treatment on neuroectodermal markers at D16	173
Figure 5.9	Effect of Purmorphamine or Activin treatment on anterior or floor plate markers at D16	175
Figure 5.10	Effect of Purmorphamine or Activin treatment on pallial markers at D16	177
Figure 5.11	Effect of Purmorphamine or Activin treatment on pallial markers at D16	180
Figure 5.12	Effect of Purmorphamine or Activin treatment on pallial markers at D16	182

Figure 5.13	Effect of Purmorphamine or Activin treatment on pallial markers at D16	184
Figure 5.14	Effect of Purmorphamine or Activin treatment on pallial markers at D16	186
Figure 5.15	Effect of Purmorphamine or Activin treatment on neuronal and glial markers at D16	188
Figure 6.1	Cell culture regime	198
Figure 6.2	Fluorescent immunocytochemistry analysis of CTIP2 and DARPP32 on 34D6iPSC derived neurons on D37	201
Figure 6.3	Confocal images of fluorescent immunostaining showing weaker CTIP2 expression in some DARPP32 positive neurons	202
Figure 6.4	Fluorescent immunocytochemistry analysis of MAP2 and ISL1 on 34D6iPSC derived neurons on D37	204
Figure 6.5	Fluorescent immunocytochemistry analysis of Calbindin on 34D6iPSC derived neurons on D37	205
Figure 6.6	Fluorescent immunocytochemistry analysis of GABA on 34D6iPSC derived neurons on D37	206
Figure 6.7	Fluorescent immunocytochemistry analysis of Synaptophysin and PSD65 on 34D6iPSC derived neurons on D37	207
Figure 6.8	Confocal images of fluorescent immunostaining showing co-registration of Synaptophysin and PSD65 on 34D6-iPSC derived neurons	208

## List of Tables

Table 1	hPSC directed differentiation protocols	63
Table 2	QRT-PCR primer sequences	86
Table 3	TaqMan probes ID	88
Table 4	Antibody Dilutions and Conditions for ICC	90
Table 5	Composition of gels and solutions used for Western blotting	94
Table 6	Materials	95
Table 7	Comparison of dual-SMAD inhibition protocols	127

# 1. Introduction

## 1.1 Huntington's disease

Huntington's disease (HD) is an inherited monogenic neurodegenerative disorder. It was first described by George Huntington in 1872, who identified both its familial transmission pattern and clinical features. Over 100 years later, the gene responsible for HD was mapped to chromosome 4 in humans (Gusella *et al.* 1983). Later in 1993, the disease causing mutation was found to be an abnormal expansion of a CAG trinucleotide repeat located in exon1 of IT15 gene (interesting transcript 15) now known as 'huntingtin' (*HTT*) gene (Huntington's disease collaborative research 1993). The mutation is inherited as autosomal dominant.

### 1.1.1 Clinical characteristics of HD

HD is characterized by progressive development of motor dysfunction (such as chorea, dysphasia, postural imbalance and akinesia), cognitive impairment (such as deficits in skilled learning, planning and short term memory) and psychiatric disorders (such as depression, personality changes, irritability and apathy) (Walker 2007). HD is late onset, manifesting in the third or fourth decade of life and gradually progressing over a number of years with increasing severity. Patients eventually die within 15-20 years from diagnosis.

Age of symptom onset inversely correlates with the number of CAG repeats. Adult onset is associated CAG expansions in the range of 36-56. CAG repeat length between 36 and 39 may be regarded as 'variable penetrance' and higher than 39, leads to a disease state (Rubinsztein *et al.* 1996; Langbehn *et al.* 2004). Juvenile onset occurs with expansion exceeding 70 (Andrew *et al.* 1993)

### 1.1.2 Selective Neurodegeneration in HD

The neuropsychiatric characteristics associated with HD results predominantly from selective neuronal degeneration in the caudate nucleus and putamen, collectively referred to as 'neostriatum', which is located in the ventral forebrain. Within the striatal neuronal population, medium spiny neurons (MSN) expressing neuropeptide enkephalin and containing inhibitory neurotransmitter  $\gamma$ -aminobutyric acid (GABA) that project to the globus pallidus are preferentially

affected in earliest stage of HD (Albin *et al.* 1992; Richfield *et al.* 1995). (Striatum and MSNs are discussed further in the following section 1.2). There is also loss of cortical neurons including those that project to striatum (Heinsen *et al.* 1994). In the late stages of HD, there is a significant brain atrophy measured as loss of cross-sectional tissue area in other core nuclei of brain including cortex, globus pallidus, substantia nigra, thalamus and hippocampus (de la Monte *et al.* 1988; Vonsattel *et al.* 1985; Rosas *et al.* 2003). In contrast to about 60% cross-sectional area loss in the caudate and putamen, the extent of late stage atrophy in other brain regions is 20-30%, which corresponds to the overall loss of brain mass in HD (Figure 1:1) (de la Monte *et al.* 1988).

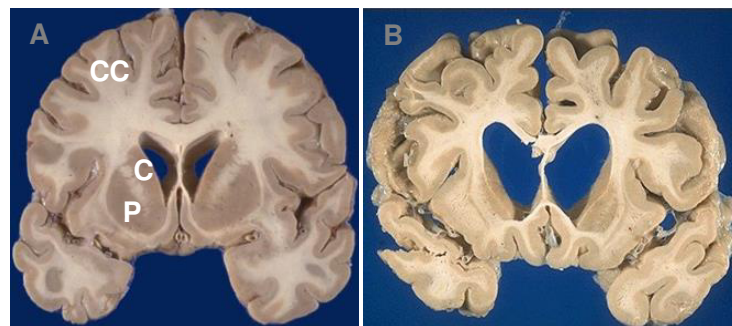


Figure 1:1 Coronal section through a normal and HD brain. A) Normal Brain showing caudate (C), putamen (P) and cerebral cortex(CC). B). HD brain showing atrophy in the C, P and CC. Adapted from Kelly *et al.* 2009

The commonly used grading system for standardization of HD pathology is based on the data from the gross and microscopical examination of 163 clinically diagnosed post-mortem brains of HD patients (Vonsattel *et al.* 1985). Striatum was consistently reported to have significantly reduced neuronal density in HD brains and exhibited marked variation in the severity of neuropathological involvement (Vonsattel *et al.* 1985). The mildest category grade 0 is indistinguishable from the normal brain but with 30-40% neuronal loss in caudate nucleus. The severe category grade 4 includes severe striatal atrophy and with 95% neuronal loss (Vonsattel *et al.* 1985). Neuronal loss and atrophy in non-striatal regions are evident in grade 3 and 4. At the time of death the majority of cases are grade 3 or 4 (Vonsattel and DiFiglia 1998).

### 1.1.3 The mutant Htt protein

The huntingtin protein (Htt protein) is a cytoplasmic protein found in the soma, proximal dendrites and synaptic terminals of neurons (DiFiglia *et al.* 1995;

Trottier *et al.* 1995). Htt associates with mitochondria, vesicles, microtubules and synaptic components and is involved in energy metabolism, cellular trafficking as well as neurotransmission (DiFiglia *et al.* 1995; Sapp *et al.* 1997; Velier *et al.* 1998). In HD the CAG repeat expansion in HTT gene encodes a polyglutamine stretch at the N-terminus end of protein, thus generating a mutant Htt (mHtt) protein (Huntington's disease collaborative research 1993). Immunostaining of HD brains with antibodies against the N terminus of Htt protein identified neuronal intranuclear inclusions (NII) containing mHtt protein aggregates in the striatum and cortex (DiFiglia *et al.* 1997; Becher *et al.* 1998). The significance of these aggregates in HD pathogenesis is not yet known. However, the aggregate formation is a hallmark of HD. Transgenic animal models for human HD gene carrying CAG repeats (animal models discussed further in section 1.1.4) developed NIIs as observed in biopsy materials from HD patients. Interestingly, it has been suggested that NII may form as a protective response. Transfection of striatal neurons with mHtt induced neurodegeneration which was protected by the addition of brain derived neurotrophic factor (BDNF) (Saudou *et al.* 1998). Blocking the nuclear localization of mHtt suppressed its ability to form NII and resulted in an increase in cell death. This suggested that mHtt may act to induce cell death and NII might be a protective mechanism against mHtt-induced cell death (Saudou *et al.* 1998). Neuronal death was observed to be dependent on mHtt dose and polyglutamine expansion (Arrasate *et al.* 2004). The presence of inclusion bodies in cytoplasm and nucleus was found to improve cell survival and decrease intracellular levels of diffuse mHtt. Neurons without NII showed increased degeneration (Arrasate *et al.* 2004).

How the mutation results in selective neuronal degeneration, is a central question in HD. Targeted disruption of the murine homolog of HD gene showed that wild type Htt protein is functionally indispensable. Homozygosity resulted in embryonic lethality (Duyao *et al.* 1995; Nasir *et al.* 1995) whereas, heterozygosity resulted in increased motor activity and cognitive deficits (Nasir *et al.* 1995). A comparative study between human homozygotes and heterozygotes for HTT mutation revealed a similar age of diseases onset and a subtle but significant clinical difference. Neuroimaging showed an extensive and severely progressive brain atrophy in the homozygotes (Squitieri *et al.* 2003). Post-natal forebrain specific inactivation of Htt in mice led to progressive apoptotic neuronal degeneration

(Dragatsis *et al.* 2000). To assess the role loss-of- function of wild type Htt in the presence of CAG expansion, Van Raamsdonk *et al.* (2005), compared 2 HD mice models -YAC128<sup>+/+</sup> expressing two endogenous wild type alleles (+/+) and mutant 128 CAG expansion and YAC128<sup>-/-</sup> expressing no wild type alleles (-/-) but expressing mutant 128 CAG expansion. The loss of wild type in YAC128<sup>-/-</sup>, led to severe motor dysfunction and shortened longevity. Both groups showed similar striatal neuropathology, however the modest worsening of striatal neuronal atrophy was evident in YAC128<sup>-/-</sup> (Van Raamsdonk *et al.* 2005). Thus, potential loss-of-function effects of wild type Htt conferred by toxic gain-of- function of mutant Htt protein may have a direct relevance to HD pathophysiology. This possible dual nature of pathogenic mechanism in HD can be explained by the functional differences between wild type and mutant Htt protein. Antibodies that discriminate between normal and mutant forms of Htt implied that the mutation caused a conformational change in the protein (Trottier *et al.* 1995). CAG expansion abolished the ability of wild type htt protein to bind to proteins, inhibited endocytosis and secretion of neurotransmitters and activated apoptosis (Gervais *et al.* 2002). Furthermore, CAG expansion was demonstrated to increase the proteolytic cleavage of Htt protein (Gervais *et al.* 2002; Goldberg *et al.* 1996). Mice expressing caspase 6 non-cleavable mHtt maintained normal neuronal function and did not develop striatal neurodegeneration, when compared with mice expressing cleavable mHtt (Graham *et al.* 2006). Altered N-methyl-D-aspartic acid (NMDA) receptor activity caused by CAG expansion was shown to result in striatal MSN degeneration (Huntington's disease collaborative research 1993; Vonsattel and DiFiglia 1998). The mHtt has been shown to disrupt multiple cellular functions by impairment of BDNF synthesis, vesicular trafficking and mitochondrial function which may contribute to neuronal degeneration (Sawa *et al.* 2003; Bano *et al.* 2011).

#### **1.1.4 HD research models**

##### *1.1.4.1 Human studies*

Human studies highlighted a metabolic defect and an involvement of mitochondrial dysfunction in HD pathology. Mitochondria are the site of tricarboxylic acid (TCA) and electron transport chain (ETC), where the bulk of ATP production within cells takes place. Mitochondria serve vital roles in cellular signalling, buffering intracellular Ca<sup>2+</sup> and regulating apoptosis (Wallace *et al.*

2010). The putative mechanisms contributing to neuronal death include metabolic deficit, oxidative stress, excitotoxicity. Evidence from positron emission topography (PET) showed a marked reduction in glucose utilization in the caudate, putamen and cerebral cortex in symptomatic HD patients (Kuhl *et al.* 1985; Kuwert *et al.* 1990). The rate of reduction in striatal glucose utilization precedes the bulk of tissue loss in HD and in asymptomatic at-risk subjects (Kuwert *et al.* 1993; Antonini *et al.* 1996). Nuclear magnetic resonance (NMR) imaging demonstrated elevated lactose concentration (a compensatory glycolytic response to mitochondrial dysfunction) in the striatum and occipital cortex of symptomatic HD patients, but not in at-risk or asymptomatic patients (Jenkins *et al.* 1993; Jenkins *et al.* 1998). The impaired metabolism was correlated with the degree of motor function in patients; the extent of caudate hypometabolism correlated with decline in clinical test scores for dementia, rigidity and bradykinesia. Similarly, putaminal hypometabolism predicted chorea, defects in eye movements and cortical hypometabolism was seen in patients suffering mood changes and physiological disturbances, before the onset of motor symptoms (Kuwert *et al.* 1990). mHtt has been shown to affect mitochondrial biogenesis and function (Bano *et al.* 2011). Biochemical studies of HD post-mortem tissues revealed impaired energy metabolism (Bano *et al.* 2011). Biochemical analysis of post-mortem samples of grade 3 and grade 4 (advanced) HD patients showed marked reduction in ETC complexes activity in the caudate and putamen (Brennan *et al.* 1985; Gu *et al.* 1996; Browne *et al.* 1997). Similar studies with grade 1 (early) patients samples showed no impairment in complexes in the striatum or cortex (Guidetti *et al.* 2001). Reduced activity of other mitochondrial enzymes such as aconitase (Tabrizi *et al.* 1999) and pyruvate dehydrogenase (Butterworth *et al.* 1985) was also reported in caudate and putamen from grade 3 and 4 patients. Another PET study in the striatum of early HD patient showed an increased oxygen consumption relative to glucose utilization and selective glycolysis defect but no defective mitochondrial oxidative metabolism (Powers *et al.* 2007). Furthermore, studies showed increased oxidative damage in HD, as evidenced by markers of oxidative stress such as DNA strand breaks and accumulation of oxidative damage products. In-situ end labelling to identify DNA fragmentation in apoptotic or necrotic nuclei showed increased levels of DNA breaks in postmortem HD striatal neurons, the extent of which was correlated with CAG repeat length (Browne *et al.* 1999). An increase in oxidation of DNA base deoxyguanosine to generate 8-hydroxy-

deoxyguanosine (OH8Dg) was observed in caudate nuclear DNA of grade 4 HD patient (Browne *et al.* 1997). In parallel, oxidative damage to lipids and proteins was also reported as seen by elevated levels of malonaldehyde, lipofuscin, heme oxygenase and 3-nitrotyrosine in HD striatum and cortex (Browne *et al.* 1999). Lysosomal and endosomal like organelles with Htt immunoreactivity have also been reported in HD brains (Sapp *et al.* 1997).

Post-mortem human brain from end stage HD patients, thus offer insight into disease pathology, however limit the study of longitudinal progression of disease. Currently, studies rely on animal and cellular models of HD to assess disease pathology and CAG expansion associated neuronal degeneration.

#### 1.1.4.2 Toxin induced animal models

The earliest animal models of HD were based on the selective vulnerability of striatal neurons to excitotoxins or mitochondrial toxins (reviewed in Ramaswamy *et al.* 2007). Quinolinic acid (QA) is a widely used excitotoxin to model the behavioural and neurochemical features of HD in transplantation studies. It induces cell death by binding to NMDA receptors on striatal neurons. Toxicity induced by QA involved increase in reactive oxygen species, DNA damage and peroxidative damage. Intra-striatal administration of QA resulted in striatal degeneration with predominant depletion of GABAergic MSNs. (Schwarcz and Köhler 1983; Beal *et al.* 1986). The mitochondrial toxin, 3-nitropropionic acid (3-NP) acts by inhibiting complex II of TCA and ETC in mitochondria and leads to elevated lactate concentrations and reduced ATP levels. Administration of 3NP resulted in free radical generation and produced progressive locomotor deterioration and striatal neuronal death in rodents (Borlongan *et al.* 1997). The acute nature of lesions in these models contrasts with the gradually progressive and age-dependent HD pathogenesis.

#### 1.1.4.3 Genetic animal models

The identification of the gene mutation led to the development of genetic animal models of HD (reviewed in Pouladi *et al.* 2013). The invertebrate models of HD have been generated using either full length HTT or truncated HTT N-terminal fragments in *Drosophila melanogaster* (Jackson *et al.* 1998; Romero *et al.* 2008) and *Caenorhabditis elegans* (Faber *et al.* 1999). These models exhibited mutant HTT

aggregates, as well as recapitulated the progressive degenerative phenotype and motor abnormalities.

Rodent HD models in which brain is more analogous to the primate brain than are invertebrates models, have been developed to characterize the many aspects of HD including behaviour deficit and neuropathology. These models fall into 3 categories- knockout, knock-in and transgenic models. In knockout murine models with targeted disruption of the *Htt* gene, homozygous knockouts were embryo-lethal whereas heterozygous knockouts survived and displayed increased motor activity and cognitive deficits as well as showing neuronal loss in subthalamic nuclei of basal ganglia (Nasir *et al.* 1995). Knock-in HD mice models are generated by replacing a part of endogenous *Htt* gene with either a full length or truncated human *HTT* with expanded CAG repeats. Carrying the mutation in its appropriate genomic and protein context, these models are considered a precise genetic HD model. *HdhQ92* and *HdhQ111* mice models with 92 and 111 CAG repeats respectively, displayed repeat instability; length of repeat was increased in subsequent generations predisposing them to juvenile onset of symptoms, similar to observations in human (Wheeler *et al.* 1999). Both *HdhQ92* and *HdhQ111* showed a few behavioural deficits and no overt striatal degeneration, but pathology was evident by the presence of NIIs. CAG140 knock-in mouse with full length human *HTT* containing 140 repeats, displayed progressive motor dysfunction. There was also progressive increase in size and number of NIIs in striatum, cortex, hippocampus and cerebellum (Menalled *et al.* 2003). CAG150 model with 150 CAG repeats, displayed late-onset behavioural deficits as well as a severe neuropathology with striatal NIIs, cellular dysfunction and degenerating axons (Lin *et al.* 2001). Knock-in models thus showed the profound effect of length of CAG repeats on HD phenotype and suggested that a substantive neuropathology more representative of human HD may be induced with knock-in models with higher CAG repeats.

Transgenic models express either full length or truncated human *HTT* randomly inserted into the genome. R6/2 models contains HD promoter exon 1 and with 144 CAG repeats (Mangiarini *et al.* 1996). Although 144 CAG repeats models that of juvenile HD, R6/2 mice mimicked the adult-onset HD with appearance of NIIs (Davies *et al.* 1997), overall reduction in brain volume, striatal atrophy, significant striatal neuronal loss as well as progressive neurological phenotype

including chorea, involuntary stereotypic movements and tremor (Mangiarini *et al.* 1996; Stack *et al.* 2005). The other transgene models, YAC 128 and BACHD were created using yeast artificial chromosome (YAC) (Slow *et al.* 2003) or bacterial artificial chromosome (BAC) (Gray *et al.* 2008) respectively. These models express entire human genomic mutant *HTT* transgene including all exons and introns as well as regulatory sequences ensuring temporal and tissue specific expression. YAC128 mice contain 128 CAG repeats and BACHD mice and rat contain 97 repeats. Both models exhibited progressive motor, cognitive and psychiatric disturbances as well as developed selective striatal and cortical atrophy with the expression of NIIs (Slow *et al.* 2003; Gray *et al.* 2008). In a comparative study of behavioural patterns of various HD models (knock-in model HdhQ111 and transgenic models -R6/2 mice with 240 CAG repeats, BACHD and YAC128) overall R6/2 and BACHD model exhibited robust and progressive phenotype (Menalled *et al.* 2009). However, rodent models do not often fully recapitulate the human neuronal phenotypes (Chan 2009). A transgenic non-human primate model of HD has been developed Transgenic rhesus macaque that express 84 CAG repeat show nuclear inclusions as well as display clinical HD features including dystonia and chorea (S. Yang *et al.* 2008). Overall, animal models of HD have allowed extensive study on some aspects of HD. Each animal model has different strengths and should be chosen to match specific research questions. The main limitations of the animal models include fundamental differences from humans, cost and availability. In terms of developing therapeutic approaches, the results from animal studies do not necessarily cross over into human clinical trials with the same level of success

#### 1.1.4.4 Cell culture models of HD (Non stem cells models)

Various *in vitro* models using non-neuronal and neuronal cell lines have been generated by transfection with full length Htt with normal or expanded CAG repeats. Primary neuronal cells lines from animal models of HD have been also been established as *in vitro* HD models. These models have allowed the study of the intracellular mechanism including Htt protein distribution within cells and role of Htt aggregates in pathogenesis.

Non-neuronal lines 293T (human embryonic kidney cell line) and monkey kidney cells expressing full length or truncated Htt with 15 CAG showed cytoplasmic distribution of huntingtin and expression of higher repeats of 44 or 128

CAG resulted in perinuclear aggregates (Martindale *et al.* 1998). In mouse Neuro2a (N2a) neuroblastoma cells, transient transfection with full length Htt showed diffuse cytoplasmic localization of protein, whereas transfection with truncated N-terminal Htt fragment, resulted in aggregates in both cytoplasm and nucleus as well as enhanced cell toxicity to apoptosis inducing agents (Cooper *et al.* 1998). Similarly, expression of polyglutamine expanded huntingtin induced apoptosis in HN33 (immortalized rat hippocampal neuronal cell line), whereas expression of normal Htt showed no toxic effect (Liu 1998). With PC-12 (rat pheochromocytoma) model, stable expression of mutant Htt lead to formation of inclusion bodies in both cytoplasm and nucleus in a time and polyglutamine length-dependent manner (Lunkes and Mandel 1998). A truncated N-terminal Htt fragment was involved in inclusion bodies in cytoplasm at early time points and in the nucleus at later time points (Lunkes and Mandel 1998). Primary neuronal cultures have been established from knock-in model HdhQ111 (Trettel *et al.* 2000) and transgenic models-YAC and BACHD. Striatal cells generated from HdhQ111 expressed the mutant protein and displayed a disrupted striatal homeostasis (Trettel *et al.* 2000). YAC128 MSNs co-cultured with cortical cells partially recapitulated cortico-striatal circuitry and highlighted the aberrant pathways in HD (Milnerwood *et al.* 2012). BACHD striatal neurons provided a platform to develop neuroprotective drugs to ameliorate HD memory deficit (Doria *et al.* 2013)

## 1.2 Striatum and Medium spiny neurons

Striatum is a part of basal ganglia, which extends from ventral forebrain through the midbrain (Figure 1:2). It is a major component of basal ganglia circuitry along with globus pallidus (GP), substantia nigra (SN) and subthalamic nucleus (STN) and is critically involved in control of motor movements and cognitive functions. Striatum receives input from SN, cerebral cortex and thalamus and sends outputs to SN and GP.

Striatum comprises of caudate nucleus and putamen. It is heterogeneous both anatomically and neurochemically and displays multiple levels of compartmental organization. It comprises a variety of neurons that can be characterized based on size, spine density, axon target destination, utility of neurotransmitters/neuropeptide (Prensa *et al.* 1999).

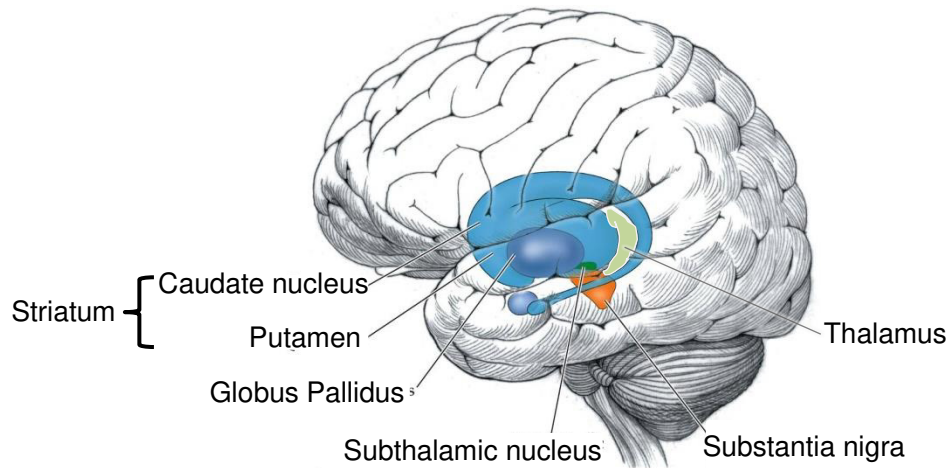


Figure 1:2 The basal ganglia. Striatum consists of the caudate nucleus and the putamen. Striatum receives input from substantia nigra, cerebral cortex and thalamus and send outputs to subthalamic nucleus and globus pallidus. Adapted from Biological Psychology 6e, figure 11.18

### 1.2.1 Medium spiny neurons and Basal ganglia circuitry

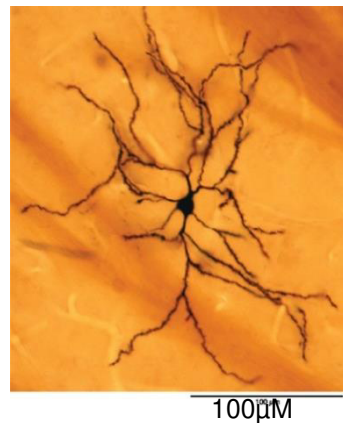


Figure 1:3 Photomontage of medium spiny neurons. MSNs with branched spiny dendrites. Taken from Kita and Kita 2011.

Medium spiny neurons (MSNs) constitute about 95% of striatal neurons in rodents (Chang *et al.* 1982) and over 80% in humans (Victorin 1992), whilst aspiny interneurons make up 2-3% in rodents (Rymar *et al.* 2004) and upto 23% in primates (Graveland *et al.* 1985). MSNs have a medium sized cell body with a diameter of 20-25 $\mu$ m and branched dendrites with densely studded spines (Figure 1:3). MSNs are the predominant projection neurons of striatum and are sub-classified by the neuropeptide and receptor expression and patch or matrix localization (Gerfen 1992).

MSNs use inhibitory transmitter, gamma amino butyric acid (GABA) as the principle neurotransmitter. GABAergic MSNs give rise to two major pathways. (Figure 1:4). The direct pathway involves striatonigral MSNs that project to GP

internal (GPi) and midbrain –SN and ventral tegmental area. The indirect pathway involves striatopallidal MSNs that project to GP external (GPe) and indirectly influence GPi and SN via subthalamic nucleus (STN) (Gerfen 1992; Leisman *et al.* 2012). Striatonigral MSNs express neuropeptides substance P and dynorphin and D1 dopamine receptor (Drd1a) whereas striatopallidal neurons express neuropeptide enkephalin, D2 dopamine receptor (Drd2) and A2a adenosine receptor (A2aR) (Gerfen 1992). MSNs receive excitatory glutamatergic input from cortex and thalamus as well as modulatory dopaminergic inputs from midbrain SN pars compacta (SNc) (Leisman *et al.* 2012). Dopamine modulates the relative responsiveness of striatonigral and striatopallidal MSNs to cortical input which determines the pattern of activity of output (Gerfen 1992). Dopaminergic projections from SN to D1 dopamine receptors of striatonigral MSNs facilitates cortical glutamatergic signalling in activation of direct pathway to GPi and SN which project to thalamus. Dopaminergic projections to D2 receptors of striatopallidal MSNs attenuate excitatory cortical input in activation of indirect pathway to GPe that via STN feeds into direct pathway (Leisman *et al.* 2012). Striatonigral MSNs promotes movements by disinhibition of thalamocortical projections, whereas striatopallidal MSNs inhibits movements by inhibition of thalamocortical projections (Leisman *et al.* 2012).

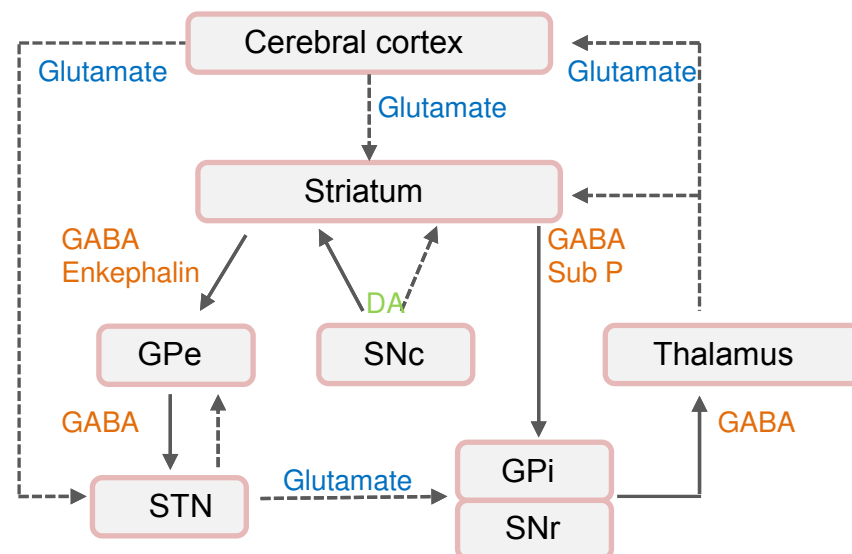


Figure 1:4 Basal ganglia circuitry. Striatum receives inputs from cerebral cortex and thalamus (excitatory pathways). It also receives dopaminergic (DA) projections from substantia nigra pars compacta (SNc). Striatum sends output to globus pallidus external and internal (GPe and GPi) as well as substantia nigra pars reticula (SNr) (inhibitory pathways). Subthalamic nucleus (STN) sends excitatory projections to GPe, GPi and SNr. Gpi or SNr inhibits thalamus. The thalamus projects to cortex. In the direct pathway, striatum inhibits GPi which in turn inhibits its normal inhibitory action

on thalamus and leads to greater excitation from thalamus to cortex. The indirect pathway excites GPi thereby increasing its inhibition on thalamus. (Leisman *et al.* 2012).

Based on neurochemical properties, striatum is divided into patch (or striosome) and the matrix compartments. MSNs segregated into patch or matrix compartments have distinct project targets; patch neurons provide inputs to dopamine neurons in SNc and matrix neurons provide inputs to GABAergic neurons in SNr (Gerfen 1989; Gerfen 1992). Both patch and matrix receives input from cortical regions to affect motor, cognitive and emotional behaviours; patch receives cortical input from deep layers V and VI whereas matrix receives cortical input from superficial layer V and supragranular layers (Gerfen 1989; Gerfen 1992). In the adult striatum, patch neurons express high levels of opiate receptors, and matrix neurons express acetylcholinesterase, calcium-binding protein calbindin and somatostatin (Gerfen 1989; Gerfen 1992).

Interestingly, at the earlier stages in HD, MSNs in the indirect pathway are affected largely than MSNs in the direct pathway (Deng *et al.* 2004; Han *et al.* 2010). The functional abnormalities in the indirect pathway were associated with chorea-like movement. At late stage in HD, abnormalities in the direct pathway were associated with rigidity and bradykinesia (Han *et al.* 2010). Differential vulnerability was also observed in cerebral cortex, with loss of layer V and VI neurons to a greater extent than layer III neurons (Han *et al.* 2010).

### 1.2.2 DARPP-32

Dopamine and cyclic adenosine 3',5'- monophosphate-regulated phosphoprotein, with a molecular weight of 32kDa (DARPP-32) is a striatal enriched protein expressed by more than 90% of GABAergic MSNs in rodent brain (Anderson and Reiner 1991; Ouimet *et al.* 1998). DARPP-32 plays the key role in the integration of neuromodulator dopamine and neurotransmitter glutamate signals in striatum (Fernandez *et al.* 2006). Both dopaminergic and glutamatergic stimulation regulate DARPP-32 phosphorylation, but in opposite directions. Stimulation of dopamine 1 receptor enhances cyclic adenosine 3',5'- monophosphate (cAMP) dependent-protein kinase (PKA) which in turn phosphorylates DARPP-32 (Walaas *et al.* 1983). The phosphorylated form D34 inhibits protein phosphatase-1 (PP1) (Hemmings *et al.* 1984). PP1 dephosphorylates glutamate receptors or GABA receptors or voltage-gated ion-channels or calcium/calmodulin kinases and

transcription factors, reviewed in (Svenningsson *et al.* 2004). Stimulation of glutamate receptor such as NMDA elevates intracellular calcium and activates calcineurin which in turn dephosphorylates DARPP-32, thereby reducing inhibitory activity on PP1 (Halpain *et al.* 1990). Cell division kinase 5 (CDK5) mediated phosphorylated form DARPP D75 inhibits PKA and thereby reduces effect of dopamine signalling on PKA target such as glutamate receptor AMPA (Bibb *et al.* 1999). Activation of protein phosphatase-2A (PP2A) by calcium upon glutamate receptor activation enhances PKA and dephosphorylates D75 (Fernandez *et al.* 2006). To summarise, DARPP32 plays a critical role in basal ganglia circuitry in response to dopaminergic and glutamatergic inputs.

### 1.3 Neural development

The neural development discussed here focuses on the developing telencephalon and the signalling and molecular mechanism leading to cell fate specification of lateral ganglionic eminence (LGE), the origin of putative striatum. The scarcity of human material is a major limiting factor for the detailed study of human embryogenesis and development. Nevertheless, extrapolation from mammalian, avian and amphibian models have provided a working model of early events in the development of human telencephalon. In this section, I discuss briefly the early patterning of the embryo (section 1.3.1), the principle events in telencephalon induction and LGE specification (section 1.3.2), the role of relevant signalling pathways (section 1.3.3) and finally, the transcription factors in the developing telencephalon (section 1.3.4).

#### 1.3.1 Early patterning of the embryo

In vertebrates, the development of the nervous system is linked to the early patterning of the embryo and is triggered by multiple signalling pathways from 'signalling centres'. During early embryogenesis (Figure 1:5), following fertilization, the diploid zygote undergoes multiple cell divisions, compaction and progress to a structure called the blastocyst. The early blastocyst consists of an inner cell mass (ICM) or embryoblast and outer cell mass called trophoblast. At day 6 post fertilization, the blastocyst begins to implant into uterine wall via trophoblast. The embryo at this stage consists of extraembryonic ectoderm and the ICM segregated into hypoblast (primitive endoderm) and epiblast, together called the bilaminar disc.

Prior to and during gastrulation, the epiblast is patterned by multiple signalling pathways that initially establish the axis of the embryo and then specify the three germ layers- ectoderm, mesoderm and endoderm that form the embryo. The hypoblast divides into embryonic endoderm and extraembryonic endoderm. In early mouse embryonic development, just prior to gastrulation, a small population of embryonic endoderm cells translocate to the prospective anterior end of embryo to give rise to anterior visceral endoderm (AVE). The anterior-posterior axis (A-P axis) of the embryo emerges gradually as the AVE represses posteriorizing signals in the overlying epiblast. In the posterior region of the embryo, the subset of epiblast cells initiate formation of primitive streak (PS) (a linear midline condensation of cells). The appearance of PS marks beginning of gastrulation. The epiblasts cells egressing through the anterior PS forms definitive endoderm and mesoderm, together referred to as mesendoderm. The endoderm emerges onto the embryo outer surface. The epiblast after the formation of mesoderm and endoderm is called ectoderm. The mesenodermal cells emerging through the anterior most end of primitive streak give rise to major signalling centres- the primitive node which generates axial mesendoderm (AME), which will populate the embryo midline to form the prechordal plate and the notochord (Figure 1:6 and Figure 1:7) (Beddington and Robertson 1999; Lu *et al.* 2001). These structures are the source of key growth factors that play a critical role in the induction of neuroectoderm, neurulation and subsequently patterning of the neural tube that eventually establishes the embryo nervous system. At neuroectoderm and neural tube stages, local signalling centres, such as anterior neural ridge (ANR) at the anterior border of the neural plate and roof plate and floor plate at dorsal and ventral midline of neural tube, act as ‘organizing centre’ to pattern and specify molecularly distinct domains of neural tube.

### **1.3.2 The principal events in telencephalon induction and LGE development**

The entire central nervous system originates from the embryonic ectoderm through three subsequent events- neural induction, neurulation and neural patterning. During neural induction, under the influence of AVE signals, the embryonic ectoderm thickens and is specified to form the neural plate (neuroectoderm) and becomes distinct from the surface ectoderm (Figure 1:6). The ectoderm at this stage thus contains two distinct progenitor domains: the neural plate

that forms the central nervous system and the non-neural ectoderm that forms the future epidermis. The neural plate gradually elongates the entire length of the vertebrate axis. During neurulation (Figure 1:7), the lateral folding of neural plate results in elevation of each side, along a midline neural groove. Gradually, the neural folds meet, fuse at dorsal midline to form neural tube and separate from the overlying ectoderm. During this process, the cells at the junction between neural plate and non-neural ectoderm form the neural crest cells and begin to migrate to different regions in the embryo to form peripheral neurons, glia, melanocytes, bone and connective tissue. (Beddington and Robertson 1999; Gammill and Bronner-Fraser 2003).

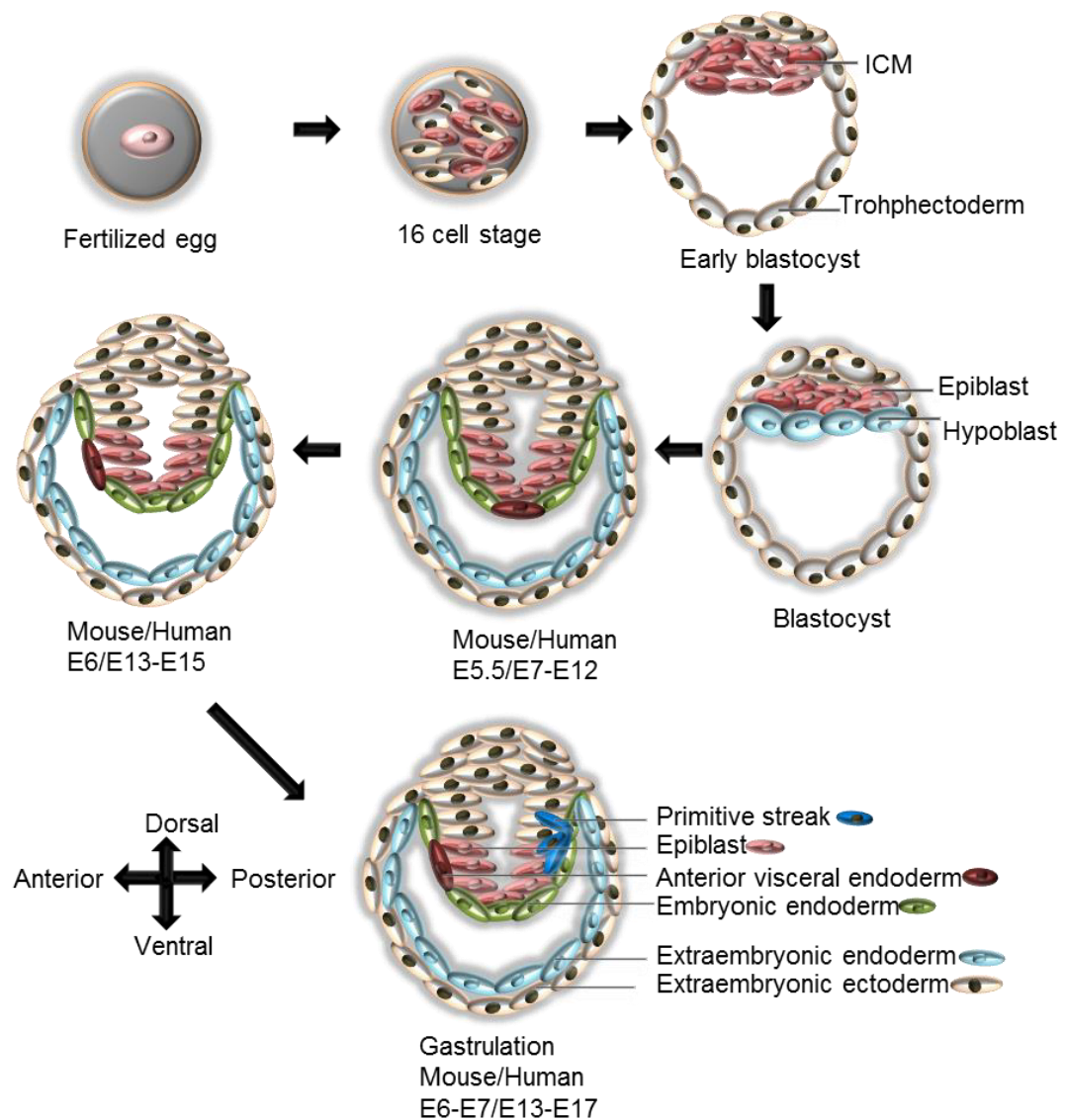


Figure 1:5 Early embryo developmental stages. Fertilized egg gives rise to blastocyst formed of ICM and trophoblast. At post-implantation blastocyst stage, ICM segregated into epiblast and hypoblast.

During subsequent development, the hypoblast divides into embryonic endoderm and extraembryonic endoderm. Distal visceral endoderm cells from the embryonic endoderm migrate anteriorly and form anterior visceral endoderm (AVE). Primitive streak is formed at the opposite pole from AVE. Adapted from Zirra *et al.* 2016.

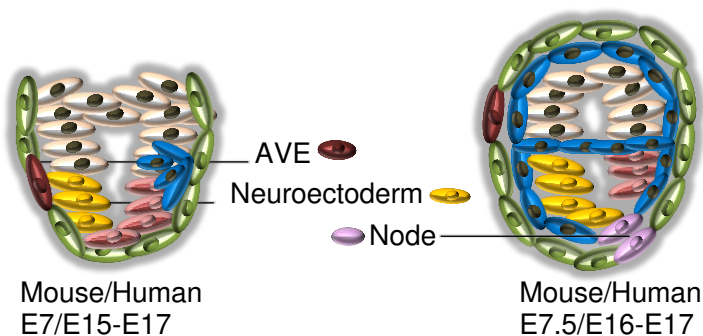


Figure 1:6 Neural Induction. Under the influence of AVE signals, the neuroectoderm is induced. The mesodermal cells migrate in all directions and envelope the embryo between the ectoderm and endoderm. At the anterior most end of primitive streak, the node develops. Adapted from Zirra *et al.* 2016.

As the neural tube develops, it bends, resulting in flexures that give rise to vesicles along the A-P axis: telencephalon and diencephalon (together make up the forebrain), mesencephalon (midbrain), rhombencephalon (hind brain) and the spinal cord (Figure 1:8A) (Wilson and Houart 2004). The embryonic telencephalon develops from the anterior most part of neural tube. The dorsal telencephalon (pallium) forms the neocortex and ventral telencephalon (subpallium) forms the striatum, also is the origin of neurons that populate olfactory bulb, GP and cortex (Figure 1.8.B). (Evans *et al.* 2012). In the subpallium, the progenitors proliferation and the rapid migration of the post mitotic neurons result in three intraventricular bulges- lateral, medial ganglionic eminence (LGE/MGE), collectively called as whole ganglionic eminence (WGE) and the septum. At E10.5, MGE was seen as a neuroepithelial protrusion into lateral ventricle. Between E11.5 and E12.5, LGE emerged between the cortex and MGE. By E12.5, the telencephalon was composed of three molecularly distinct layers (Sussel *et al.* 1999). The neuronal progenitors are born in the two proliferative zones - ventricular zone (VZ), which lies on the perimeter of lateral ventricles and subventricular zone (SVZ), which spans the basal regions of VZ. The postmitotic cells migrate out of the proliferative zones towards the mantle zone (MZ) where they complete differentiation to generate mature neurons and interneurons (Sussel *et al.* 1999; Evans *et al.* 2012). The dorsal LGE progenitors give rise to olfactory bulb neurons and ventral LGE progenitors give rise to MSNs that populate the caudate and the putamen of the striatum (Wichterle *et al.* 2001). MSNs make up nearly 90% of LGE neurons. Interneurons born in the LGE

migrate to populate cortex, olfactory bulb and striatum. MGE forms amygdaloid body and GP and MGE born interneurons migrate to cortex, GP and striatum (Evans *et al.* 2012)

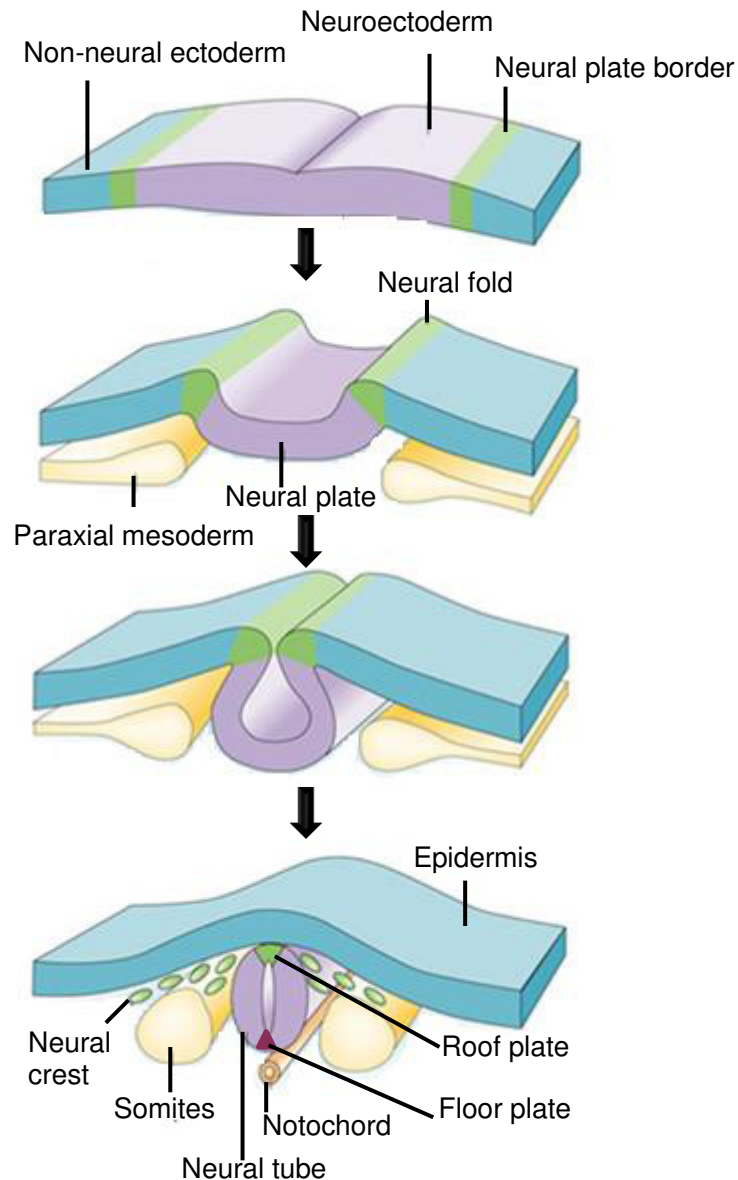


Figure 1:7 Neurulation. The neural plate border is induced by signalling between the neuroectoderm and the non-neural ectoderm and from the underlying paraxial mesoderm. During neurulation, the neural plate borders elevate and form neural fold. This causes the neural plate to roll into a neural tube. Neural crest cells are derived from the dorsomedial borders of the neural fold. The non-neural ectoderm forms the epidermis. The mesodermal cells emerging through the anterior most end of primitive streak form the prechordal plate (lies under forebrain) and the notochord (lies under the rest of CNS), to further act as signalling centres of developing CNS. The roof plate (at dorsal midline) and the floor plate (at ventral midline) influence the dorso-ventral patterning of the newly formed neural tube. Adapted from Gammill and Bronner-Fraser 2003

During early gastrulation, the signals produced in the node and its anterior derivatives, mesendodermal (AME) and prechordal plate influence the telencephalon development (Figure 1:7 and Figure 1:8). For the rest of the CNS, the notochord takes the role of prechordal plate. By mid to late gastrulation, at neural plate and neural tube stage, signals from the anterior margin of neural plate, called anterior neural ridge (ANR, at the junction between anterior neural and non-neural ectoderm) and the roof plate and the floor plate influence telencephalon specification (Wilson and Houart 2004). The morphogens such as FGF, WNT, RA, BMP and SHH emanating from these signalling centres spread away forming a concentration gradient (Figure 1:8 C). The positional identity and regional specification along anterior-posterior (A-P) and dorso-ventral (D/V) axis of neural tube depends on the concentration of these morphogen signals. The synergism of the signals spatiotemporally induces the expression transcription factors (Figure 1:9, discussed in detail in 1.3.4) that in turn induce patterning and eventually establishes the CNS.

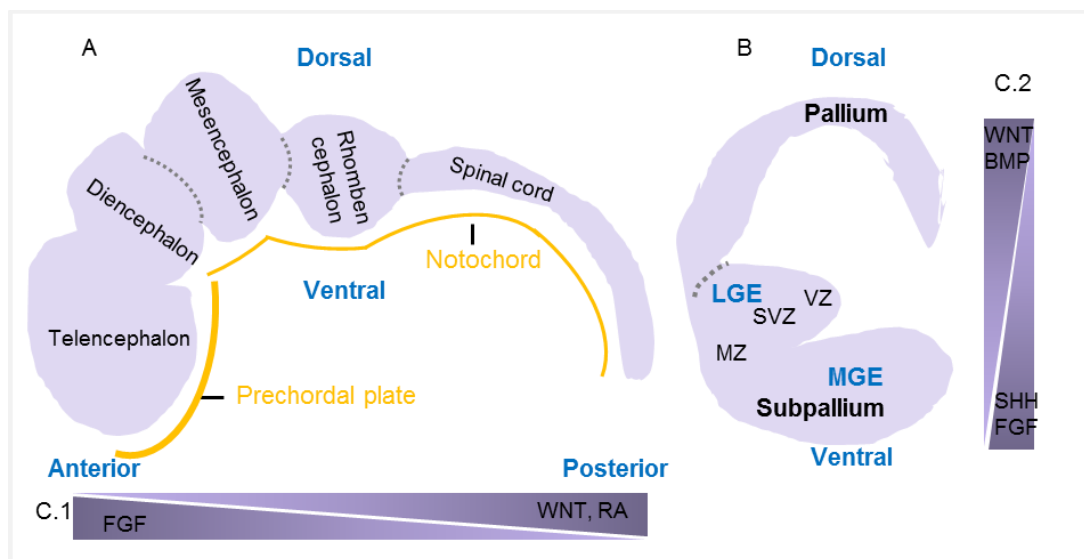


Figure 1:8 Neural tube A-P and telencephalon D-V patterning- (A, C.1) The neural tube is patterned to form the telencephalon and diencephalon (together forebrain), mesencephalon (midbrain), rhombencephalon (hindbrain) and spinal cord by the anterior-posterior gradient of FGF and posterior-anterior gradient of WNT and RA. (B, C.2) Dorso-ventral gradient of BMP and WNT and ventro-dorsal gradient of SHH and FGF establish the dorsal and ventral identity. The dorsal telencephalon (pallium) forms the neocortex and the ventral telencephalon (subpallium) (LGE and MGE) forms the striatum and globus pallidus. The dotted line indicates the pallial-subpallial boundary (PSB). The ventricular zone (VZ) and the subventricular zone (SVZ) contain proliferative neuronal progenitors. The progenitors migrate tangentially and radially to populate the specific regions of the brain. Adapted from Kiecker and Lumsden 2005; Evans *et al.* 2012.

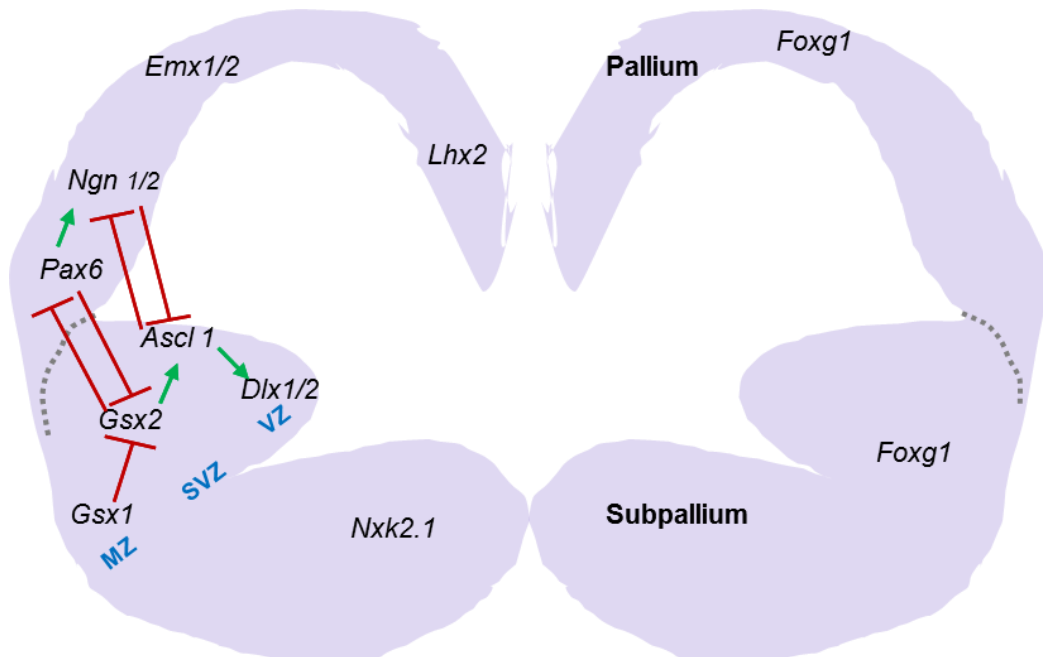


Figure 1:9 Schematic coronal section through E12.5 telencephalon showing dorsal and ventral domains: The expression of pallial markers (*Pax6*, *Emx1*, *Emx2*, *Ngn1*, *Ngn2*) and subpallial markers (*Dlx1*, *Dlx2*, *Gsx2*, *Gsx1*, *Ascl1*, *Nkx2.1*) is shown. Some of the important gene interactions are also shown. The interaction between *Pax6* and *Gsx2* maintains the pallial-subpallial boundary. Figure adapted from Evans *et al.* 2012.

### 1.3.3 Signalling pathways involved in the telencephalon development and regional specification

#### 1.3.3.1 BMP antagonism

The Bone Morphogenetic proteins (BMPs) belong to transforming growth factor $\beta$  (TGF- $\beta$ ) family of secreted proteins. They were initially discovered in extract of bone by their ability to induce ectopic bone formation when implanted into muscle pouches in rabbit, hence the name BMP (Urist 1965). In the canonical BMP pathway (Figure 1:10), BMPs bind to single pass transmembrane serine/threonine kinase receptors- type I BMP receptors (BMPRI) (activin receptor-like kinase ALK3 (BMPRIa), ALK6 (BMPRIb)) and BMPRII (activin type IIa and activin type IIb). Upon binding, the constitutively active BMPRII, transphosphorylates BMPRI intracellular domain, which then recruits and phosphorylates R-SMAD- SMAD 1/5/8 (P-SMAD1/5/8). P-SMAD1/5/8 forms a heterotrimeric complex with CO-SMAD- SMAD4. It is then translocated to the nucleus and cooperates with other transcription factors to regulate target genes (Whitman 1998).

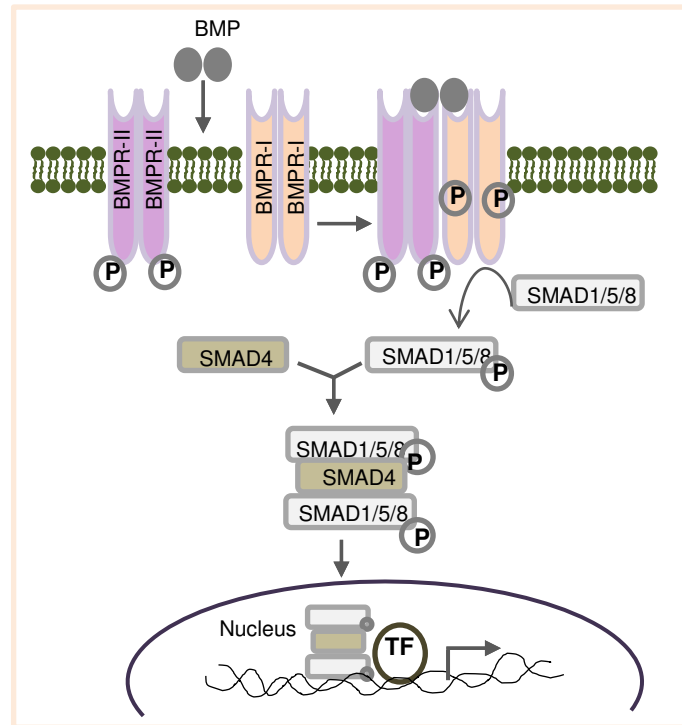


Figure 1:10 Canonical BMP signalling - Upon BMP binding, BMPRII transphosphorylates BMPRI that in turn phosphorylates SMAD1/5/8. P-SMAD1/5/8 heterotrimeric complex with SMAD4 translocate to the nucleus and modulate target gene expression by cooperating with other transcription factors. Adapted from Anderson and Darshan 2008.

During neural induction, BMPs and their inhibitors specify the epidermal and neural fate of ectoderm. The fundamental insight into the present understanding of mammalian neural induction came from the work of Spemann and Mangold (1924). They found that grafting tissues from dorsal blastopore lip of early salamander gastrula to the ventral side of another embryo, induced a second set of axial structures including host derived second nervous system, on the ventral side. The ventral ectodermal cells would normally give rise to epidermis, suggesting that signals from dorsal blastopore induced neural fate (Spemann and Mangold 1924). The dorsal blastopore lip was termed ‘Spemann’s organizer’. Analogous grafting experiments in other vertebrates reinforced the ‘organizer’ as ‘neural inducer’, called ‘henson’s node’ in chick (Waddington 1933) and the ‘node’ in mouse (Beddington 1994). Years later following the discovery of the organizer, the animal cap experiments in *Xenopus* proposed the first model of neural induction. The animal cap (ectoderm cells of blastula) when cultured intact, formed epidermal tissue and when dissociated into single cells, neural fate was induced (Grunz and Tacke 1989). It was proposed that the factors lost upon cell dissociation negatively control neural

induction in animal cap. Supporting this notion, over expression of synthetic RNA encoding the dominant negative mutant form of a TGF- $\beta$  receptor (Activin receptor) in animal cap, led to conversion of epidermal fate to neural fate (Hemmati-Brivanlou and Melton 1994). Subsequently, it was demonstrated that treatment of dissociated animal cap cells with members of TGF- $\beta$  family- Activin or BMP4 inhibited neural fate. Activin did so by inducing mesoderm, whereas BMP4 did so by inducing epidermis (Wilson and Hemmati-Brivanlou 1995). Later, the inhibitors of TGF- $\beta$  family such as Noggin, Chordin and Follistatin secreted by the ‘organizer’ were found to be the endogenous neural inducers. Simultaneous depletion of these factors from organizer by specific morpholinos prevented acquisition of neural fate (Khokha *et al.* 2005). These findings demonstrated that antagonism of BMP signalling is essential for neural induction.

BMP antagonists have been implicated in forebrain development. During early development in mouse (E7.5-8.5), Noggin (Nog) and Chordin (Chrd) were found to expressed in the node and AME derivatives including prechordal plate as well as in ANR (Bachiller *et al.* 2000; Anderson *et al.* 2002). *Chrd*<sup>-/-</sup>;*Nog*<sup>-/-</sup> and *Chrd*<sup>-/-</sup>;*Nog*<sup>+/-</sup> mice double mutants lacked anterior neural structures but preserved posterior structures (Bachiller *et al.* 2000; Anderson *et al.* 2002). *Chrd*<sup>-/-</sup>;*Nog*<sup>+/-</sup> mutants showed decreased *Fgf8* expression in the ANR (Anderson *et al.* 2002). Ectopic application of BMPs in mice and chick forebrain explants reduced *Fgf8* and inhibited the expression of telencephalon markers *Foxg1* and *Six3* (Furuta *et al.* 1997; Anderson *et al.* 2002; Ohkubo *et al.* 2002; Yang and Klingensmith 2006). In contrast, application of BMP2 had no effect, when forebrain explant was co-cultured with the underlying AME (Yang and Klingensmith 2006). Thus, these studies indicated that BMP antagonists promote forebrain establishment.

Further BMPs function in telencephalon D/V patterning. At E8.5- E13.5 mice, *Bmps* were expressed in dorsomedial telencephalon (roof plate) where it overlapped with that of *Msx1* and was complementary to *Foxg1* (Furuta *et al.* 1997). BMP4 soaked beads induced *Msx1* in lateral telencephalic neuroectoderm explants (where BMPs are not expressed) and inhibited ventral markers *Nkx2.1* and *Dlx2* (Furuta *et al.* 1997). Similarly, ectopic BMP expression in developing chick embryo was found to inhibit *Dlx2* and *Nkx2.1* (Golden *et al.* 1999; Ohkubo *et al.* 2002). *Chrd*<sup>-/-</sup>;*Nog*<sup>+/-</sup> mutants showed increased *Msx1* expression indicative of ectopic BMP

signalling. These mutants displayed reduced expression of ventral marker *Nkx2.1* and a loss of *Shh* expression in the prechordal plate (Anderson *et al.* 2002). Additionally, ablation of telencephalic roof plate caused reduction in cortex volume and reduced cortical marker *Lhx2* (Monuki *et al.* 2001). Taken together, BMPs promote dorsal fate and restrict ventral telencephalon specification.

### 1.3.3.2 WNT antagonism

Wingless (Wnt) ligands are secreted glycoproteins. In the canonical Wnt pathway (Figure 1:11), Wnts bind to membrane bound Frizzled (Frz)/low-density lipoprotein receptor-related protein (LRP) complex that recruits intracellular Dishevelled (Dsh). This destabilizes destruction complex which included glycogen synthase kinase 3 $\beta$  (GSK-3 $\beta$ )- adenomatosis polyposis coli (APC)- axin complex and thereby prevents degradation of  $\beta$ -catenin. Upon translocation to nucleus,  $\beta$ -catenin binds and activates transcription factors such as TCF/LEF which regulate the expression of Wnt target genes. In the absence of WNT, FRZ and LRP5/6 are not bound.  $\beta$ -catenin joins the destruction complex and subsequently degraded and there is no gene expression (Komiya and Habas 2008).

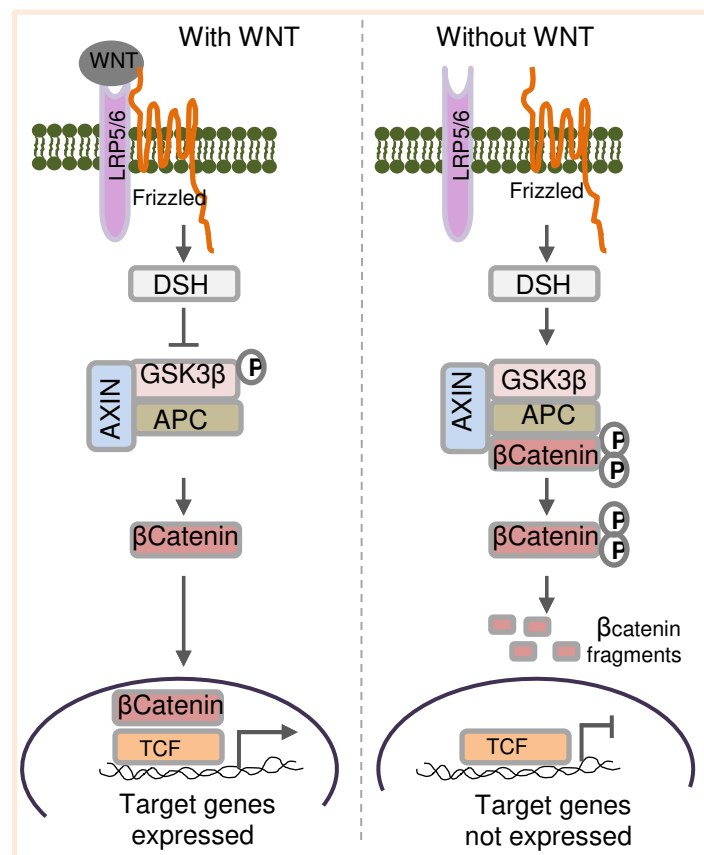


Figure 1:11 Canonical WNT signalling- Upon WNT stimulation, signalling through Frizzled receptor/LRP5/6 co-receptor complex allows activation of Dishevelled (DSH) and repression of GSK $\beta$ -APC-AXIN destruction complex. This prevents  $\beta$ -catenin degradation, enabling it to translocate to the nucleus and activates TCF to modulate target gene expression. In the absence of WNT,  $\beta$ -catenin is phosphorylated by the GSK3 $\beta$ -APC-AXIN complex and is targeted for degradation and target genes are not expressed. Adapted from Staal and Clevers 2005.

In early mouse embryo, Wnt proteins are expressed in the primitive streak at the posterior side, while their antagonists such as Cerberus (Cer-1, inhibitor of both Wnt and BMP) (Belo *et al.* 1997) and Dkk1 (Kemp *et al.* 2005) are expressed in the AVE and AME. In mouse, grafts of organizer alone induced ectopic axis lacking anterior tissues whereas a combination of organizer and AVE induced complete secondary axis. Yet, AVE alone was not able to ectopically induce anterior neural markers (Tam and Steiner 1999). However, surgical removal of AVE resulted in loss of anterior neural tissue and did not affect more posterior regions of developing CNS (Thomas and Beddington 1996). On the other hand, loss of WNT activity in *Wnt3*<sup>-/-</sup> mice mutants resulted in loss of primitive streak, node or its derivative. Despite preserving a normal AVE, these mutants lacked normal A-P patterning (Liu *et al.* 1999). Thus, AVE signals alone are not sufficient and that signals from primitive streak or its derivatives (i.e., posteriorizing signals) are required to drive A-P patterning. AVE signals acts by repressing posteriorizing signals in adjacent anterior ectoderm as evidenced in embryonic explants assays in which co-culture of ectoderm with AVE, resulted in repression of posterior markers and no anterior neural induction (Kimura *et al.* 2000). In line with this, other studies further identified the role of Wnt inhibitors in the suppression of the posterior fate and induction of anterior structures. In *Xenopus*, dominant negative Bmp receptor (tBR) alone or in combination with noggin or chordin yielded incomplete secondary axis, whereas tBR or noggin in combination with Wnt antagonists- XCer, dkk1 and frzb- induced a complete secondary axis including heads with anterior neural structures (Glinka *et al.* 1997; Glinka *et al.* 1998). On the other hand, targeted deletion of Dkk1 in mice or co-inhibition of Dkk1 as well as Noggin and chordin in both mice and *Xenopus* lead to anterior truncations (Mukhopadhyay *et al.* 2001; Barco Barrantes *et al.* 2003). Thus, while inhibition of BMP signalling is the major molecular determinant of neural induction, concomitant inhibition of posteriorizing signal such as WNT is required for induction of anterior neural structures.

In addition to promoting posterior neural fates, WNT pathway is involved in regional patterning within prosencephalon which forms the

telencephalon and diencephalon. Genetic inactivation of TCF3 (a member of Tcf/Lef family, a transcriptional repressor of Wnt targets) and Axin1 (negative intracellular WNT signalling scaffolding protein) in zebrafish *headless* (*hdl*) and masterblind (*mb1<sup>-/-</sup>*) mutants respectively, resulted in loss of telencephalon (Kim *et al.* 2000; Heisenberg *et al.* 2001). *mb1<sup>-/-</sup>* mutants displayed anteriorly expanded diencephalon with ectopic expression of Wnt8b (Houart *et al.* 2002). Abrogation of Wnt8b activity or overexpression of wild-type Axin1 restored telencephalon in *mb1<sup>-/-</sup>* mutants (Houart *et al.* 2002; Heisenberg *et al.* 2001), indicating that local Wnt antagonism within anterior neural plate is required for telencephalon development. Supporting this notion, transplantation of Wnt1 or Wnt8 expressing cells into anterior neural border of zebrafish wildtype embryos, resulted in the inhibition of telencephalic markers *bfl*, *emx1* and *fgf8* and complementary expansion of midbrain marker *pax2.1* (Houart *et al.* 2002). Whereas Tlc (secreted Frizzled-related protein sFRP that bind to and antagonize Wnt by inhibiting ligand/receptor interaction), promoted telencephalic gene expression in a concentration dependent manner and abrogation of its function compromised telencephalon development (Houart *et al.* 2002). Further, in *mb1<sup>-/-</sup>* mutants, Tlc expressing cells suppressed ectopic *wnt8b* expression and restored telencephalon (Houart *et al.* 2002). Thus, WNT antagonism promote telencephalic fate.

Wnt signalling also contributes to telencephalon D/V patterning. BAT-gal reporter mice (in which the expression of  $\beta$ -galactosidase under the control of TCF/LEF binding site reflected Wnt signalling) showed active Wnt signalling in the pallium but not in the subpallium between E11.5 and E16.5 (Backman *et al.* 2005). Inactivating Wnt target  $\beta$ -catenin using a conditional Cre/loxP system before neurogenesis (E8.5-11) resulted in downregulation of dorsal markers *Ngn2*, *Emx1* and *Emx2* and in ectopic expansion of ventral markers *Dlx2*, *Gsx2* and *Ascl1* in the pallium. Interestingly, the expression of *Pax6* and *Nkx2.1* in these mutants was similar to that of wildtype. Activating  $\beta$ -catenin in the subpallium led to repression of ventral markers including *Nkx2.1* and expansion of dorsal markers including *Pax6* (Backman *et al.* 2005). Similarly, in chick embryo ventral explants, Wnt3a exposure dose dependently resulted in reduction of *Nkx2.1<sup>+</sup>* cells and increase in *Pax6<sup>+</sup>*, *Ngn2<sup>+</sup>* and *Emx1<sup>+</sup>* cells, whereas exposure to Wnt antagonist Frz receptor8 protein blocked generation of *Pax6<sup>+</sup>*, *Ngn2<sup>+</sup>* and *Emx1<sup>+</sup>* cells (Gunhaga *et al.* 2003). Thus, WNT

signalling maintains the pallial identity by suppressing the ventral markers and by controlling dorsal marker expression. However, inactivating  $\beta$ -catenin after the onset on neurogenesis did not alter D/V specification of telencephalon progenitors, suggesting that the role of WNT signalling in telencephalon D/V patterning is relatively early (Backman *et al.* 2005).

Later, WNT signalling regulates progenitor expansion and neurogenesis in the ventral telencephalon. MGE proliferative zone showed expression of Tcf4 at E12.5 mice embryo. Inhibition of Tcf4 by expression of dominant repressor form of Tcf/Lef1 or treatment with Dkk1 reduced cell proliferation in MGE slice cultures (Gulacsi and Anderson 2008). Eliminating  $\beta$ -catenin from Nkx2.1 expressing cells greatly diminished the size of MGE by E14.5 resulting from reduced cell proliferation. Normal expression pattern of PAX6 and GSX2 and ectopic expansion of mantle zone Calbindin<sup>+</sup> and LHX6<sup>+</sup> neurons into proliferative zone in these mutants suggested that removal of  $\beta$ -catenin mediated Wnt signalling in MGE caused cells to exit cell cycle prematurely (Gulacsi and Anderson 2008). Moreover, mutants displayed reduced number of MGE derived cholinergic and cortical interneurons. A role of non-canonical Wnt signalling has been implicated in neuronal fate decision in the ventral telencephalon. Loss of non-canonical Wnt receptor Ryk resulted in increased production of oligodendrocytes at the expense of GABAergic neurons. Wnt3a stimulation mediated by RyK promoted GABAergic neuronal fate over oligodendrocyte fate (Zhong *et al.* 2011). Thus, following forebrain A-P and D/V domains establishment, WNT signalling regulates the progenitor expansion and cell fate decision and drives the differentiation.

### 1.3.3.3 SHH signalling

SHH, a member of Hedgehog (Hh) family of proteins, is a secreted morphogen. In SHH pathway (Figure 1:12), upon SHH binding to PATCHED (PTC), SMOOTHENED (SMO) is released. This activates GLI (glioma-associated oncogenes) family of transcription factors, which induce the expression of SHH target genes. In the absence of SHH, PTC binds and inhibits SMO and cannot activate GLI complex genes and target genes are not expressed.

SHH acts in a temporal and concentration dependent manner to specify distinct progenitor subtypes within ventral telencephalon (Stamatakis *et al.* 2005; Yu

*et al.* 2009). During telencephalon development, Shh was initially expressed by the prechordal plate (Shimamura *et al.* 1995). By E9, it was expressed mainly in the ventral telencephalon (Shimamura *et al.* 1995) and by E12.5, it was shifted into the mantle area (Nery *et al.* 2001).

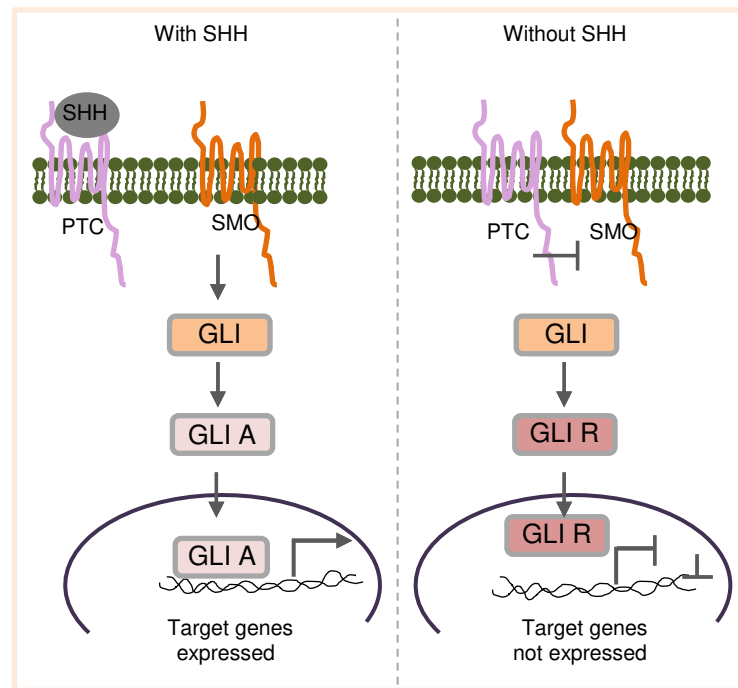


Figure 1:12 The SHH pathway- Upon SHH binding to PATCHED (PTC), SMOOTHEND (SMO) is released. This allows activation of GLIA which binds to the DNA to activate gene expression. In the absence of SHH, PTC represses SMO by binding to it and cannot activate GLI complex. The GLI repressor (GLIR) represses target gene expression. Adapted from Szkandera *et al.* 2013.

*Shh* null mutant mice displayed a complete lack of ventral telencephalon structures resulting in a single vesicle with *Emx1* expression throughout (Chiang *et al.* 1996). Similarly, ablation of Hh signalling at E8.5, using *Smo<sup>cl-/-</sup>;Foxg1<sup>cre</sup>* (Cre recombinase under regulatory control of *Foxg1* removes *Smo* flanked by loxP sites, resulting loss of expression *Gli1*) resulted in loss of ventral telencephalon patterning with absence of *Nkx2.1* and *Gsx2* and concomitant expansion of *Pax6* expression throughout dorsal and ventral telencephalon at E10 (Fuccillo *et al.* 2004). By E12.5, the mutants completely lacked all ventral ganglionic eminences, showed absence of MGE derived cortical interneurons (as judged by absence of *Lhx6* and *GAD67*) and oligodendrocyte precursors (as judged by absence of *Olig2* and *Pdgfra*) as well as displayed ventrally expanded expression of dorsal markers *Ngn2* and *Emx2* (Fuccillo *et al.* 2004). Interestingly, abrogation of Hh signalling, (specifically loss of expression *Ptch1* and *Gli1*) between E10 and E12 using *Smo<sup>n/c</sup>;Nestin<sup>cre</sup>* resulted in grossly normal telencephalic patterning with normal expression domains of *Pax6*,

*Ngn2*, *Gsx2*, *Dlx2*, *Nkx2.1* and *Lhx6* (Machold *et al.* 2003). However, in some mutants *Nkx2.1* expression was diminished, MGE was reduced by 50% in size and was often fused with LGE. There was also a deficit in the production of oligodendrocytes precursors and severe reduction in progenitor population in the cortex, olfactory bulb and hippocampus (Machold *et al.* 2003). Collectively, loss-of-function studies indicated that HH signalling is required for ventral specification and that a temporal change in the signalling specifies the different cell populations originating within ventral telencephalon

Further supporting evidences for temporal and spatial responsiveness to Shh, come from *in vitro* exposure and ectopic expression studies. Rat E9.5 presumptive telencephalic explants cultured in the presence of recombinant Shh protein (6nM) induced widespread *Nkx2.1* expression. By contrast, E11.5 explants cultured in the presence of same or high Shh (960nM) showed no expression of *Nkx2.1*, but at 6nM, showed induction of *Dlx*, *Isl1/2* and *Ikaros* as well as repression of *Emx1* and *Tbr1* suggesting a LGE/striatal identity rather than MGE or pallial (Kohtz *et al.* 1998). Interestingly, beyond E12.5, Shh was not able to ventralize, but induced 50% higher Nestin<sup>+</sup> cells suggesting a mitogenic effect on progenitors (Kohtz *et al.* 1998). Retroviral mediated activation of Shh signalling in E8.5 to E10.5 mouse telencephalon resulted in differential induction of ventral markers; *Nkx2.1* induction was restricted to LGE, whereas *Gsx2* and *Dlx2* induction was observed throughout neocortex, with concomitant repression of *Pax6* and dorsal proneural genes *Ngn2*, *Math2* and *NeuroD* (Rallu *et al.* 2002). Furthermore, *Gli1* (usually expressed at border between LGE and MGE) and *Ptc* (usually expressed in MGE) induction all along D/V and A/P axis suggested that all regions within telencephalon were equally competent to respond to Shh signalling (Rallu *et al.* 2002).

Shh signalling is mediated by Gli transcription factors- Gli1, Gli2 and Gli3. Both Gli1 and Gli2 act as transcriptional activators, whereas Gli3 functions as transcriptional repressor. Studies on *Gli* mutants have revealed their role in D/V patterning and specification of cell types generated from the ventral telencephalon. *Gli3*<sup>-/-</sup> mutants displayed defective dorsal telencephalon with ectopic expansion of *Gsx2* (co-expressed with *Pax6*), *Dlx2*, *Ascl1* and *Isl1* into cortex which was severely reduced in size (Tole *et al.* 2000; Rallu *et al.* 2002) and lacked expression of *Emx2*, *Emx1*, *Bmp2,4,6,7* and *Wnt3a* (Theil *et al.* 1999; Tole *et al.* 2000). A normal ventral

patterning was evident in *Gli3*<sup>-/-</sup> mutants, by the expression of *Shh*, *Gli1* and *Nkx2.1* confined to ventral telencephalon (Tole *et al.* 2000), thus suggesting that *Gli3* is required for suppression of ventral markers in dorsal telencephalon. Interestingly, removal of *Gli3* from *Shh*<sup>-/-</sup> mutant (which showed markedly diminished ventral most expression of *Dlx2* and *Gsx2* and absence of *Nkx2.1*) largely rescued D/V patterning; the expression of *Dlx2*, *Gsx2*, *Ascl1* and *Nkx2.1* was restored to their normal domains and the mutually exclusive expression pattern of *Pax6* and *Gsx2* confirmed existence of corticostriatal boundary (Rallu *et al.* 2002). On the other hand, *Gli1*<sup>-/-</sup>;*Gli2*<sup>-/-</sup> and *Gli1/2*<sup>-/-</sup> double mutants, showed establishment of telencephalon D/V patterning as evidenced by normal expression pattern of *Pax6*, *Gsx2*, *Dlx2*, *Lhx6* and *GAD67*. *Gli1*<sup>-/-</sup> mutants also maintained normal expression of *Nkx2.1* and *Nkx6.2*, whereas *Gli2*<sup>-/-</sup> and *Gli1/2*<sup>-/-</sup> expressed *Nkx2.1* in MGE with a decreasing gradient towards LGE and was lost in the region where its expression normally would overlap with *Gli1*. These mutant lacked *Nkx6.2* expression and by E14.5, showed a reduction in *Lhx6* expression but had normal *Ebf1* striatal expression (Yu *et al.* 2009). Thus, perturbation of *Gli1/2* mediated SHH signalling affected specification of ventral most progenitors and differentiation of telencephalic neurons. *Gli2/3*<sup>-/-</sup> mutants lacking the expression of all three *Gli* genes lost the positional identity of ventral telencephalic cells; there was ectopic dorsal expansion *Dlx2*, *Gsx2*, *Isl1*, *Lhx6* and *GAD67*, MGE-restricted *Nkx2.1* expression as well as a severe reduction in *Lhx6*<sup>+</sup>, *GAD67*<sup>+</sup> and *Ebf1*<sup>+</sup> and *PGGFRα*<sup>+</sup> neurons (Yu *et al.* 2009). Taken together, these studies demonstrate that GLI3 and SHH antagonize each other's function. GLI3 suppresses ventral markers. SHH signalling in the ventral telencephalon primarily functions to repress GLI3 as well as activate downstream targets through GLI activators.

#### 1.3.3.4 FGF signalling

FGF signalling through RAS/MAPK is explained in Figure 1.17. FGFs most notably *Fgf8* and *Fgf3* and FGF receptors *Fgfr1*, *Fgfr2* and *Fgfr3* were expressed in ANR and later in ventral telencephalon. They play an important role in the induction and patterning of telencephalon. *Fgf8* in the ANR regulates *Foxg1* expression; removal of ANR resulted in loss of *Foxg1* and FGF8 soaked beads induced *Foxg1* expression in mouse anterior neural plate explants lacking ANR (Shimamura and Rubenstein 1997). Within prosencephalon explants, ectopic FGF8

by means of FGF8 beads induced sulcus (which separates telencephalon into anterior (rostral) and posterior (caudal) vesicles) and inhibited *Otx2* (caudal forebrain marker) (Crossley *et al.* 2001), thus revealing that FGF signalling promote telencephalic fate within prosencephalon. *Fgf8*<sup>-/-</sup> mutant mice (in which some *Fgf8* expression persisted) displayed abnormally small telencephalon, which resulted from reduced *Foxg1* expression, reduced cell proliferation and increased apoptosis. There was also rostral expansion of *Otx2* and *Wnt8b*, suggesting caudalization in the anterior prosencephalon in the absence of *Fgf8* (Storm *et al.* 2006). Targeted deletion of increasing number of FGF receptors in the anterior neural plate affected the extent of telencephalon truncations; *Fgfr1* mutants showed slight reduction in telencephalon size, *Fgf1:Fgfr2* double mutants displayed more severe truncations and *Fgfr1:Fgfr2:Fgfr3* triple mutants completely lost telencephalon with no *Foxg1* expression (Paek *et al.* 2009). Consistent with the loss of telencephalon, there was increased cell death in *Fgfr* triple mutants suggesting that FGF signalling acts to promote survival of *Foxg1*+ cells (Paek *et al.* 2009).

Further, loss-of-function studies revealed a role of FGF signalling in ventral telencephalon specification. In zebrafish, inhibition of FGF signalling by injecting dominant negative form of Ras (RasN17) or by FGF receptor antagonist SU5402 did not alter normal expression of *foxg1* and *otx2* (Shinya *et al.* 2001), suggesting normal establishment of telencephalic and diencephalic territories in the absence of Ras/MAPK signalling. However, these mutants showed aberrant telencephalon patterning with loss of ventral markers *dlx2*, *isl1* and *nkx2.1b* and extended expression of dorsal markers *emx1* and *tbr1* throughout pallium and subpallium (Shinya *et al.* 2001; Walshe and Mason 2003). Reduced FGF signalling in zebrafish *ace*<sup>-/-</sup> (*fgf8* homologue) and *fgf3/8*-depleted (using morpholinos) mutants also led to similar ventral defects (Shanmugalingam *et al.* 2000; Walshe and Mason 2003). Consistent with these studies, mice *Fgf8*<sup>-/-</sup> and *Fgf1:Fgfr2* double mutants showed reduced ventral structures with repression of ventral markers and ectopic expansion of dorsal markers in subpallium (Storm *et al.* 2006; Gutin *et al.* 2006; Paek *et al.* 2009).

*Shh* expression is intertwined with *Fgf8* expression in ventral telencephalon (Ohkubo *et al.* 2002). The ventralization reported in GLI3 mutants (explained in 1.3.3.3) correlates with FGF signalling. In *Shh*<sup>-/-</sup> mutants, the ventral

structures were lost and lacked FGF expression whereas, in both *Gli3*<sup>-/-</sup> and *Shh*<sup>-/-</sup>; *Gli3*<sup>-/-</sup> mutants, the ventral telencephalon development was preserved or restored and there was expansion of FGF expression (Theil *et al.* 1999; Rallu *et al.* 2002; Kuschel *et al.* 2003). Therefore, SHH through its ability to attenuate GLI3 repressor, indirectly promote FGF function. In *Fgfl:Fgfr2* double mutants, *Shh* and *Gli* expression remained despite the lack of most or all of ventral telencephalon precursors as observed with loss of SHH signalling. Removal of *Gli3* in *Fgfl:Fgfr2* mutants, did not rescue ventral structures as observed in *Shh*<sup>-/-</sup>; *Gli3*<sup>-/-</sup> mutants (Gutin *et al.* 2006). Thus, FGF receptors are required for SHH-ventralizing effect and FGF signalling acts downstream of *Shh* and *Gli3* to specify ventral telencephalon. Additionally, FGF8 soaked beads induced ectopic expression of ventral markers in mouse dorsal telencephalon explants and inhibition of SHH signalling did not prevent this effect (Kuschel *et al.* 2003), thus suggesting that FGF8 can specify ventral telencephalon independent of SHH signalling.

Within ventral telencephalon, FGFs act to promote MGE fate and suppress LGE fate. In chick ventral telencephalic explants, FGF2 or FGF8 increased the number of Brdu<sup>+</sup> cells, induced normal numbers of NKX2.1<sup>+</sup> cells and blocked generation of ISL1<sup>+</sup> neurons (Gunhaga *et al.* 2000), whereas FGFR4 an inhibitor of FGF signalling blocked generation of NKX2.1<sup>+</sup> progenitors and largely induced PAX6<sup>+</sup> MEIS2<sup>+</sup> LGE-like phenotype (Marklund *et al.* 2004). Furthermore, in dorsal telencephalic explants FGF8 blocked induction of retinoic acid-induced MESI2<sup>+</sup> ISL1<sup>+</sup> neurons (Marklund *et al.* 2004). These studies suggested that a) FGF signalling prevents LGE fate induced by retinoic acid and thereby promotes MGE fate in the ventral telencephalon and b) in addition to patterning, FGF signalling prevents generation of post-mitotic neurons and increases proliferation of telencephalic progenitors.

#### 1.3.3.5 RA signalling

Retinoic acid (RA) is a morphogen, implicated in LGE and striatal neuronal differentiation. RA is generated through sequential oxidation of retinol (vitamin A) (Figure 1:13). Retinol enters the cell through interaction with receptor STRA. Inside the cell, retinol can bind to cellular retinol binding protein (CRBP) or for storage, converted to retinylesters via lecithin retinol acyltransferase (LRAT). CRBP-bound retinol is oxidised by two classes of enzymes; alcohol

dehydrogenases/retinol dehydrogenases (ADH/RDH) oxidise retinol to retinaldehyde, and retinaldehyde dehydrogenases (RALDHs) oxidise retinaldehyde to RA. CYP26 can further oxidise RA for degradation. Cellular RA binding protein (CRABP) transports RA into the nucleus. RA then binds to retinoic acid receptors (RARs) and retinoid X receptors (RXRs) and subtypes ( $\alpha$ ,  $\beta$  and  $\gamma$ ) which upon heterodimerization, binds to RA responsive elements (RARE) and regulates their expression. RA can diffuse to adjacent cells to activate target gene expression (Kin *et al.* 2012).

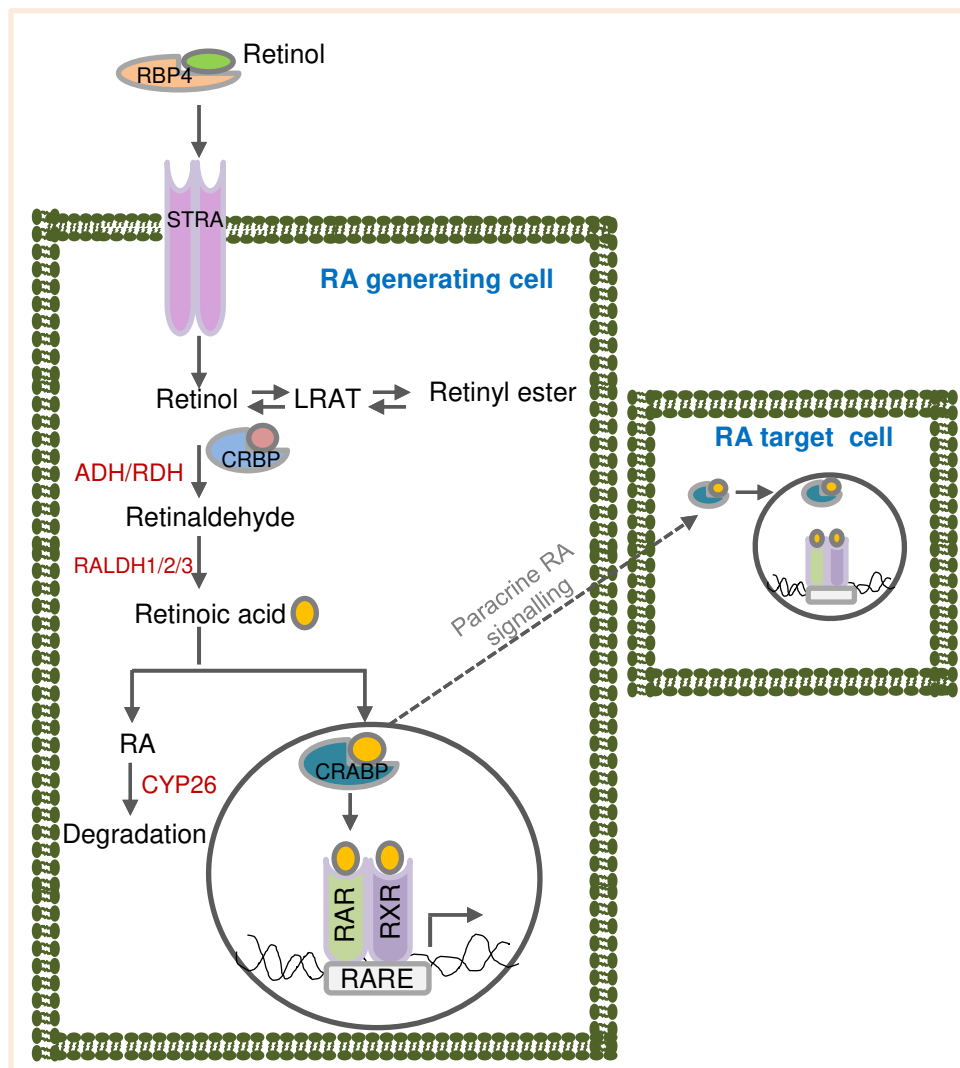


**Figure 1:13 RA and paracrine RA signalling-** In serum, retinol is bound to retinol-binding protein 4 (RBP4), synthesized in the liver. Retinol enters cells through STRA. In the cell, retinol is either converted into retinyl esters via LRAT or binds to the CRBP. The CRBP-bound retinol is oxidized to retinaldehyde by ADH/RDH and retinaldehyde is oxidized to RA by RALDH1/2/3. CYP26 can oxidize RA for degradation. CRABP facilitates transportation of RA into the nucleus where RA binds its receptors-RAR and RXR. The ternary complex binds to RARE and activates the RA target genes. RA can diffuse to adjacent cells to activate target gene expression. Adapted from Maden 2002; Kin *et al.* 2012

Radial glial cells in LGE were found to produce high levels of retinoids and LGE represents a localized source of retinoid signalling (Toresson *et al.* 1999). As compared to MGE or cortex, LGE and developing striatum showed enriched expression of markers of RA synthesis, including CRBP1 in VZ (E12.5- E16.5), *Raldh3* in SVZ (E14.5), *RAR $\alpha$*  in SVZ (E12.5-E16.5), *RAR $\beta$*  (E16.5) and *RXR $\gamma$*  in striatal primordium (Toresson *et al.* 1999; Marklund *et al.* 2004; Li *et al.* 2000; Liao and Liu 2005; Liao *et al.* 2005; Molotkova *et al.* 2007).

Studies utilizing either agonists or antagonists for RARs or genetic ablation of RADLHs or RARs have highlighted the role of RA in telencephalon development and LGE specification. In chick embryos, early inhibition of RA signalling by citral or by RAR/RXR antagonists soaked beads at stage 10 resulted in lack of telencephalon, whereas late inhibition at stage 18 had no effect. At the molecular level, RAR/RXR antagonists treatment resulted in loss of *FGF* and *SHH* expression as well as downregulation of *FOXP1*, *NKX2.1*, *NKX6.2* and *DLX2* (Schneider *et al.* 2001). Administration of RA restored the expression of *FGF* and *SHH* and either RA or FGF2/SHH treatment rescued telencephalon defects, indicating that RA mediated expression of *FGF* and *SHH* at early stage is required for early telencephalon morphogenesis (Schneider *et al.* 2001). Treatment of prospective LGE explants from stage 14 chick embryos with RAR antagonist blocked generation of MEIS2<sup>+</sup> LGE progenitors, whereas inhibitors of FGF, SHH and BMP signalling had no effect (Marklund *et al.* 2004). Conversely, exogenous RA treatment induced MEIS2<sup>+</sup> ISL1<sup>+</sup> LGE phenotype in both dorsal and ventral explants and blocked generation of NKX2.1<sup>+</sup> phenotype in ventral explants (Marklund *et al.* 2004). Similarly, in intact embryos, RAR antagonist-soaked beads grafted adjacent to the prospective telencephalon suppressed normal LGE specification and RA soaked beads induced LGE character in prospective dorsal telencephalon (Marklund *et al.* 2004). Thus, RA signalling was required to specify LGE fate in chick embryo studies. However, in contrast to chick embryos, *Raldh2*<sup>-/-</sup>; *Raldh3*<sup>-/-</sup> mice lacking all RA activity showed normal expression of *Fgf* and *Shh* at E8.75 and *Meis2* at E10 (Molotkova *et al.* 2007). An alternative approach utilizing Cre-dependent expression of dominant negative receptor (DN-RAR $\alpha$ ) to ablate RA signalling in telencephalon from E9, led to defective cell proliferation in dorsal telencephalon and increased cell death in both dorsal and ventral telencephalon

(Rajaii *et al.* 2008). However, the expression of *Fgf8*, *Shh* and *Foxg1* remained unaltered and the mutants showed normal D/V patterning, thus contradicting the reports in chick embryos. Paradoxically, in the absence of RA signalling, Nkx2.1+ MGE progenitors co-expressed *Isl1* thus suggesting that RA signals may function by suppressing some intrinsic LGE differentiation within MGE progenitors (Rajaii *et al.* 2008).

RA signalling in the LGE regulates the development of striatal neurons and interneurons. Stimulation of RA signalling either by treatment with agonists for RAR/ RXR or by supplementation of RA specifically induced DARPP32+ neurons in E13.5 LGE cultures, whereas there was no DARPP32 induction in MGE or cortical cultures (Toresson *et al.* 1999). RA supplementation of *Gsx2*<sup>-/-</sup> mutants (which exhibited marked reduction in LGE *Raldh3* expression), during the period of striatal neurogenesis, increased DARPP-32 expression (Waclaw *et al.* 2004). Involvement of RAR $\beta$  mediated signalling was further demonstrated in a gain-of-function study; ectopic expression of RAR $\beta$  in cortical explants (that lacked RA receptors), upregulated DARPP-32 (Liao and Liu 2005). Further evidences for RA activity came from knock out studies. Null mutation of RAR $\beta$  in *RAR $\beta$* <sup>-/-</sup> mice led to aberrant striosomal compartmentalisation in rostral striatum (made up of late-born striosomal cells) but the caudal striatum (made up of early born striosomal cells) was spared. The defective neurogenesis of late-born neurons resulted from reduction in both cyclin E2 (cell cycle protein regulating G1 to S transition) and *Ascl1* (proneural gene) (Liao *et al.* 2008). *RAR $\beta$* <sup>-/-</sup> rostral striatum showed loss of striosomal enriched tyrosine phosphatase (STEP),  $\mu$ opioid receptor (MOR1), dynorphin, DARPP32 and tyrosine hydroxylase (TH) (Liao *et al.* 2005; Liao *et al.* 2008). This could be correlated to the *in vivo* endogenous RA signalling; LGE RA signalling was found to be low during neurogenesis of early-born S cells whereas a substantial level was present during neurogenesis of late-born S cells (Liao *et al.* 2008). Loss of RALDH3 activity in *Raldh3*<sup>-/-</sup> embryos resulted in reduction of GAD+/TUJ1+ interneurons migrating to cortex and olfactory bulb as well as Foxp1+ striatal projection neurons, at E14.5 *in vitro* cultures (Chatzi *et al.* 2011). At E18.5, *Raldh3* loss led to specific loss of *Drd2* expression in the nucleus accumbens and significant reduction in RAR $\beta$  expression in striatum (Molotkova *et al.* 2007).

### 1.3.4 Transcription factors involved in D-V regionalisation of the developing telencephalon

#### 1.3.4.1 Developmental transcription factor profile in Human samples

Recently, a pioneering study by Onorati *et al.* (2014) that involved a systematic immunohistochemistry analysis of human embryos 2 to 20 post-conception weeks showed regional domains of TF expression and their refinement during human striatal development. The expression of TFs at early neuroectoderm as it acquired dorsal or ventral telencephalic fates was identified in 2-8 week embryos. At 2 weeks + 5 days (2w+5d) embryo, when the neural plate invagination gives rise to neural folds, expression of OTX2, PAX6 and NKX2.1 was detected in neural folds. Starting at 3w+3d, PAX6 and SOX2 expression were identified in closing neural tube. The first molecular sign of telencephalic fate was evident at 3w+ 4d embryo by the expression of OTX2 and FOXG1 in prosencephalon and expression of NKX2.1 confined to ventral prosencephalon. At 7w+2d, OTX2 and FOXG1 were found in entire telencephalon particularly in VZ and the beginning of dorsal ventral organization was evident by complementary expression of TFs; PAX6 expression was restricted to pallium while GSX2 expression was detected in subpallium, thus defining the pallial-subpallial boundary (PSB) and NKX2.1 expression marked MGE. The progenitor domains and mature neurons compartment within LGE were evident at the beginning of foetal stage at 8w and striatal neurons were defined at 8-11 week embryos. At 8w, proliferating LGE VZ progenitors expressed FOXG1, OTX2, GSX2 and ASCL1 while LGE SVZ progenitors expressed ASCL1, EBF1 and ISL1. The mutually exclusive subpallial expression of GSX2 and ASCL1 and pallial expression of PAX6 and TBR2 clearly demarcated the PSB. At 8-11 w, in the ventral post mitotic MZ where internal capsules began to appear, striatal neurons were defined by the co-expression of ISL1, EBF1, FOXP1, FOXP2, CTIP2, DARPP-32, GABA and NKX2.1. At 11w, massive SVZ overlaid the developing striatum separated into the caudate and putamen by the internal capsule. During mid-foetal development at 20 w embryo where neurogenesis continued, a dynamic change in expression pattern of some TFs was seen. ISL1 initially expressed in all striatal precursors was restricted to a few cells in caudate-putamen and some ISL1<sup>+</sup> cells did not co-express FOXP1 or FOXP2 or CTIP2, but expressed DARPP32. NKX2.1 was restricted to only 4% of striatal cells and did not co-express CTIP2. FOXP2

expression was reduced to ~ 25% of striatal cells. CTIP2<sup>+</sup> striatal cells co-expressed CALB, FOXP1, FOXP2 and DARPP32 and displayed a GABAergic identity. Interestingly at this stage, neocortex also showed expression of FOXP1, FOXP2, CALB, NKX2.1 and DARPP-32. However, unlike striatal MSNs CTIP2/DARPP-32 co-localization was rarely seen and DARPP-32<sup>+</sup> neocortical neurons were not GABAergic.

Very recently, Straccia *et al.* (2015), compared mRNA expression profile of 7-9 weeks human WGE and fetal cortex as well as adult caudate, putamen and motor cortex and identified markers characteristic of each developmental stage. The high expression of *SIX3*, *DLX1*, *DLX5*, *DLX6*, *LHX6* and *EBF1* distinguished WGE from cortex. Compared to WGE, the adult striatum down regulated the expression of *DLX1*, *DLX2*, *DLX5*, *LHX6* and *EBF1* and upregulated the expression of *DARPP-32*, *ADORA2A*, *CALB1*, *DRD1*, *DRD2*, *PENK* and *TAC1* (Straccia *et al.* 2015).

The expression domains of core transcription factors involved in telencephalon D/V development is shown in Figure 1:9 and their role is discussed below.

#### 1.3.4.2 *FOXP1*

*FOXP1* (Brain factor 1 BF-1) belong to HNF3/forkhead family of transcription factors (Tao and Lai 1992). In mammals, it was first identified in rat foetal brain. No expression was found in liver, intestine, lung, kidney, spleen and testis (Tao and Lai 1992). Detection by in situ hybridisation, revealed an expression from embryonic day E10 (at which no telencephalon-diencephalon boundary is distinguished) in anterior neuroepithelium. As development progressed, the expression pattern was restricted to the telencephalon and was absent from the diencephalon (Tao and Lai 1992). *Foxg1* plays a role in establishing the early regional subdivision of developing forebrain and in further telencephalon development.

Xuan *et al.* 1995 generated *Foxg1* null mutant mice, by replacing most of coding sequence of *Foxg1* with a lac Z and neomycin cassette. The expression of  $\beta$ -galactosidase enzyme was thus under the control of *Foxg1* promoter and expression of  $\beta$ -gal detected by X-gal histochemistry, identified *Foxg1* expression. *Foxg1* was

detected in neural tube from E8.5 and E9.5 at which *Foxg1*<sup>-/-</sup> mutants appeared grossly similar to that of wild types. However, from E10.5, mutants displayed a progressive reduction in size of telencephalic vesicles and at E12.5, ganglionic eminences were not present and showed only thin neuroepithelium (Xuan *et al.* 1995; Martynoga *et al.* 2005). E12.5 mutants expressed only dorsal telencephalic markers *Emx2* and *Pax6* and no ventral telencephalic markers *Dlx2* and *Dlx1* (Xuan *et al.* 1995). Consistent with this study, absence of ventral markers *Nkx2.1*, *Ascl1*, *Dlx2* and *Gsx2* and expansion of dorsal markers *Pax3* and *Pax6* were reported in *Foxg1*<sup>-/-</sup> mutant telencephalon (Martynoga *et al.* 2005). Analysis of cell proliferation by Bromodeoxyuridine (BrdU) labelling (that incorporate into cells in S phase) revealed that only dorsal telencephalic cells and not ventral telencephalic cells were actively proliferating in mutants (Xuan *et al.* 1995). Characterization of cell proliferation by BrdU and iododeoxyuridine (IdU) double labelling (that determines the total length of cell cycle and the length of S phase), demonstrated prematurely lengthened cell cycle in *Foxg1*<sup>-/-</sup> mutant telencephalon (Martynoga *et al.* 2005). Concurrently from E10.5 in *Foxg1*<sup>-/-</sup> mutants, an excess of neurons was produced, thus depleting progenitor populations and limiting growth of telencephalon. In addition, *Foxg1*<sup>-/-</sup> mutants showed significant reduction in the expression of *Fgf8* at E10.5 and increased BMP expression at E11.5 (Martynoga *et al.* 2005). In *Xenopus*, over expression of *XBF-1*, suppressed neural differentiation and resulted in proliferation (Bourguignon *et al.* 1998). Collectively these studies demonstrate that *Foxg1* regulates telencephalon progenitor proliferation and neurogenesis and in its absence, ventral telencephalon fate is not specified

Subsequently, *foxg1* was shown to inhibit dorsal telencephalic identity by repression of Wnt/ $\beta$ catenin signalling pathway, specifically *wnt8b* in zebra fish (Danesin *et al.* 2009). By using by morpholino knocking down *foxg1*, this study reinforced the earlier findings and demonstrated that absence of ventral fate in *foxg1* morphants was caused by their transformation into dorsal fates and partial displacement into hypothalamic territory. Furthermore, broad overexpression of *foxg1* in Hh-depleted embryos induced ventral fate in ventral telencephalon and *shh* overexpression in *foxg1* morphants inhibited dorsal marker *tbr1*. Thus indicating that FOXG1 and SHH act independently in repression of dorsal fate and induction of ventral fate (Danesin *et al.* 2009). FOXG1 was observed to act cell autonomously in

*Foxg1*<sup>-/-</sup>/*Foxg1*<sup>+/+</sup> chimeric embryos. *Foxg1*<sup>-/-</sup> cells located in dorsal telencephalon expressed dorsal markers *Pax6*, *Tbr1* and *Ng2*. *Foxg1*<sup>-/-</sup> cells in the LGE failed to express ventral markers *Gsx2* and *Mash1*, instead expressed dorsal markers, whereas surrounding wild type cells in the LGE expressed ventral markers. This indicated that *Foxg1*<sup>-/-</sup> cells did not alter specification of wild type cells and that *Foxg1* is required in ventral telencephalon in a cell autonomous manner to ensure cell competence to adopt ventral identity (Manuel *et al.* 2010). The proportion of *Foxg1*<sup>-/-</sup> cells in S phase of cell cycle was significantly smaller compared to wild type indicating a reduction in their proliferation (Manuel *et al.* 2011). The expression of *Pax6* (which is also a cell cycle regulator) was lower than normal in these cells. Over expression of *Pax6* in *Foxg1*<sup>-/-</sup>/*Pax77* chimeric embryos, resulted in partial rescue of proliferation defects, thus indicating that *Foxg1* regulates progenitor proliferation cell autonomously by mechanisms that include regulation of *Pax6* (Manuel *et al.* 2011).

#### 1.3.4.3 PAX6

PAX6 is a paired box (Pax) transcription factor, first detected in the neuroectodermal cells of mouse developing forebrain at E8.5-E9.5 (Stoykova and Gruss 1994). Analysis of human foetal samples revealed PAX6 co-expression with SOX2 at E18 (Carnegie stage 8-9) in neuroectodermal cells, when the neural plate began to form (X. Zhang *et al.* 2010). The expression was retained in multi-layered neural plate at E21 (Carnegie stage 8-9). By E26 (Carnegie stage 11-12), when forebrain and midbrain had clearly demarcated, PAX6 expression was restricted to forebrain (X. Zhang *et al.* 2010). In mouse at E12.5, when both LGE and MGE were morphologically distinct, PAX6 was expressed in the dorsal telencephalon throughout cortical VZ and in the lateral most part of LGE (Stoykova *et al.* 1997; Toresson *et al.* 2000). PAX6 expression was largely complementary to that of GSX2 in the ventral telencephalon and this expression pattern was maintained throughout the embryogenesis marking a boundary between cortical VZ and the LGE (Toresson *et al.* 2000).

PAX6 modulates D/V patterning of the developing telencephalon. The mice small eye mutant, *Pax6*<sup>Sey/Sey</sup> which lacked functional Pax6 protein displayed severe forebrain patterning defects with abnormal cortical-striatal boundary (pallial-subpallial boundary) (PSB) (Stoykova *et al.* 1997). The expression of dorsal markers

such as *Ngn2* and *Emx1* were diminished and ventral markers *Gsx2*, *Dlx2* and *Ascl1* showed ectopic expression across the boundary into dorsal regions (Toresson *et al.* 2000; Stoykova *et al.* 1997; Stoykova *et al.* 2000; Kroll and O'Leary 2005). The expression of MGE markers *Shh*, *Nkx2.1* and *Lhx6* was expanded into LGE territory and shifted LGE-MGE boundary (Stoykova *et al.* 2000). By mid-neurogenesis, there was ectopic production of GABAergic interneurons (LGE/MGE derived) and the cortical plate appeared thinner due to the diminished production of glutamatergic neurons (generated in dorsal telencephalon, normally) (Kroll and O'Leary 2005). Taken together, PAX6 plays a critical role in establishing PSB and it specifies pallial identity by repressing subpallial fates in dorsal telencephalon.

#### 1.3.4.4 GSX2

*Gsx2* (formerly known as *Gsh2*) belongs to homeobox transcription factor family, (Hsieh-Li *et al.* 1995) first detected within developing mouse forebrain between E9 and E14. During telencephalon development, its abundant expression was restricted to the ganglionic eminences (Hsieh-Li *et al.* 1995; Szucsik *et al.* 1997).

Targeted deletion of *Gsx2* in *Gsx2*<sup>-/-</sup> mutants resulted in reduction in size of LGE at E12.5-E14.6 (Szucsik *et al.* 1997). There was a loss of PSB (which is established as early as E10.5 in mouse through differential expression of markers) in *Gsx2*<sup>-/-</sup> mutants (Yun *et al.* 2001). Altered gene expression pattern was evident in E12.5 mutants as seen by reduced expression of *Dlx1*, *Dlx2* and *Ascl1* (Szucsik *et al.* 1997; Corbin *et al.* 2000; Toresson *et al.* 2000), accompanied by ectopic expansion of *Pax6*, *Ngn2* and *Tbr2* into LGE (Corbin *et al.* 2000; Toresson *et al.* 2000; Yun *et al.* 2001). Conversely, *Pax6*<sup>-/-</sup> mutants displayed expansion of *Gsh2* and *Ascl1* into *Pax6* domains (Toresson *et al.* 2000; Yun *et al.* 2001) and removal of *Pax6* from *Gsx2* mutants (*Gsx2*<sup>-/-</sup>;*Pax6*<sup>-/-</sup> double homozygous mutants), rescued telencephalic patterning (Toresson *et al.* 2000; Waclaw *et al.* 2004). Interestingly, expression of MGE marker *Nkx2.1* was not affected in the *Gsx2*<sup>-/-</sup> mutants (Szucsik *et al.* 1997). Taken together, these studies demonstrate that *Gsx2* is required for expression of *Dlx1*, *Dlx2* and *Ascl1* while repressing dorsal fate via cross-repression with *Pax6*.

E12.5 *Gsx2*<sup>-/-</sup> mutants also showed a decrease in expression of *Ebf1* (essential for cell transition from SVZ to striatal mantle zone), *Gad67* (catalyses

formation of GABA) and *Raldh3* and decreased retinoid production (Corbin *et al.* 2000; Waclaw *et al.* 2004). Although, *Gsx2<sup>-/-</sup>;Pax6<sup>-/-</sup>* showed improved striatal patterning and larger striatum compared to *Gsx2<sup>-/-</sup>* mutants, the expression of *Raldh3* was not rescued (Toresson *et al.* 2000). Furthermore, both *Gsx2<sup>-/-</sup>* and *Gsx2<sup>-/-</sup>;Pax6<sup>-/-</sup>* mutants had reduced number of DARPP-32 neurons (Corbin *et al.* 2000; Waclaw *et al.* 2004). Supplementation of RA during striatal neurogenesis increased DARPP-32 *Gsx2<sup>-/-</sup>* mutant (Waclaw *et al.* 2004), thus identifying the requirement of *Gsx2* for retinoid production. Collectively, these studies establish the role of *Gsx2* for normal striatal development to maintain the correct molecular identity of LGE precursors.

Interestingly, as development progressed, by E15.5-E18.5 (mid-neurogenesis), *Gsx2<sup>-/-</sup>* mutants showed a recovery in expression of *Dlx1*, *Dlx2*, *Ascl1*, *Ebf1* and *Gad67* within VZ of the developing striatum. However, striatum remained reduced in size (Corbin *et al.* 2000). Concomitantly, *Gsx1* expression was notably expanded in the *Gsx2<sup>-/-</sup>* LGE. No obvious striatal defects were detected in *Gsx1<sup>-/-</sup>* mutant, whereas *Gsx1<sup>-/-</sup>;Gsx2<sup>-/-</sup>* double homozygous mutant displayed more severe disruption than *Gsx2<sup>-/-</sup>* mutant, indicating that *Gsx1* compensates at least in part for the loss of *Gsx2* in *Gsx2<sup>-/-</sup>* mutant (Toresson and Campbell 2001). In wild type, at E12.5 and onwards, *Gsx2* was shown to be expressed in a high dorsal (in dLGE) to low ventral (in vLGE and MGE) gradient (Yun *et al.* 2001; Pei *et al.* 2011) whereas *Gsx1* expression was localised in vLGE and MGE near VZ/SVZ boundary (Pei *et al.* 2011). This *Gsx2* gradient was perturbed with an increased number of *Gsx2<sup>+</sup>* cells in vLGE of *Gsx1<sup>-/-</sup>* mutants between E16.5 and E18.5. Furthermore, overexpression of *Gsx1* resulted in dramatic down-regulation of *Gsx2* expression in the ventral telencephalon and overexpression of *Gsx2* significantly reduced *Gsx1* expression (Pei *et al.* 2011). Thus, *Gsx2* and *Gsx1* reversely control the expression of each other. Misexpression of *Gsx1* lead to lengthening of cell cycle, as a result enhanced neurogenesis, whereas, misexpression of *Gsx2* caused an increase in cell cycle retention index, as a result maintained progenitors in an undifferentiated state (Pei *et al.* 2011).

#### 1.3.4.5 DLX2

*Dlx* genes belong to homeodomain transcription factors and comprise six known mammalian members, organized as three clusters- *Dlx1/2*, *Dlx3/4* and *Dlx5/6* (Panganiban and Rubenstein 2002). *Dlx2*, *Dlx1*, *Dlx5* and *Dlx6* showed overlapping

but distinct temporal sequence of expression in the LGE (Eisenstat *et al.* 1999). In situ hybridization and immunoreactivity studies at E12.5 showed expression of *Dlx2* in subset of VZ, co-expression of *Dlx1*, *Dlx2* and *Dlx5* in SVZ and expression of *Dlx5* and *Dlx6* in post mitotic migrating neurons in SVZ and mantle zone (Liu *et al.* 1997; Eisenstat *et al.* 1999). This expression pattern indicates that *Dlx* genes function at different stages in striatal differentiation.

Histological analysis of brains of mice single mutants for *Dlx1* (*Dlx1*<sup>-/-</sup>) and *Dlx2* (*Dlx2*<sup>-/-</sup>) showed a subtle phenotype, whereas *Dlx1/2*<sup>-/-</sup> double mutant had an enlarged SVZ- like region with low number of proliferating cells (Anderson *et al.* 1997). In the double mutants, early born neurons migrated into striatum like region that was enriched with striosomal (patch) markers- DARPP32, acetylcholinesterase (AChE) and tyrosine hydroxylase (TH). However, Brdu birth-dating (single injection of Brdu at different developmental stages from E11.5 and analysing location of Brdu positive cells) and organotypic slice cultures (analysing cell migration of Dil labelled cells) revealed that the later born neurons (beginning at E12.5), failed to migrate into mantle zone. They accumulated within defective LGE where they partially differentiated into MAP2 positive and DARPP32 negative neurons (Anderson *et al.* 1997). Furthermore, molecular abnormalities were evident at E12.5 by the absence of *Dlx5*, *Dlx6* and *Oct6* (Anderson *et al.* 1997). At E15.5, there was a reduction in expression of retinoid receptors- *Rarb* and *RXRγ* and reduction in number of MSNs expressing striatonigral markers - *D1R* and *Substance P* and striatopallidal markers- *D2R* and *Enkephalin* (Long *et al.* 2009). There was also a severe reduction in expression of *Er81*, *Sp8*, *Meis1*, *Meis2* and *Foxp1* in SVZ and moderate reduction in expression of *Ctip1*, *Ebf1*, *Foxp2*, *Islet1* in MZ. This was compounded with an ectopic expression of pallial markers- *Ebf3* and *Id2* and MGE markers- *Gbx1* and *Gbx2* in dLGE SVZ ( Long *et al.* 2009). Further, *Dlx1/2*<sup>-/-</sup> had low expression of *GAD67* and *vesicular GABA transporter* (vGAT) and displayed massive reduction in cortical GABAergic interneurons that are derived from VZ and SVZ (Anderson *et al.* 1997; Long *et al.* 2009). Thus, *Dlx2* and *Dlx1* are required for generation and migration of later born neurons (striatal matrix) and for proper LGE development and striatal differentiation in addition to promoting GABAergic neurons fate. Interestingly, *Dlx1/2*<sup>-/-</sup> mutant SVZ showed increased expression of *Gsx2*, *Gsx1*, *COUP-TF1*, *Ascl1* and genes in Notch signalling pathway- *Notch1*, *Notch3*, *Delta*-

like *1(Dll1)* and *Hes5* (Yun *et al.* 2002), suggesting a role of *Dlx1/2* in repressing the expression of these genes for differentiation of SVZ progenitors.

#### 1.3.4.6 *ASCL1*

*ASCL1* (Achaete-scute homolog 1, originally named as mammalian achaete scute homolog-1, MASH1) is a basic helix-loop-helix (bHLH) gene essential for ventral telencephalon development (Casarosa *et al.* 1999; Fode *et al.* 2000; Castro *et al.* 2011). *Ascl1* was broadly expressed in VZ and SVZ at E12.5 ventral telencephalon (Parras *et al.* 2004; Castro *et al.* 2011). It was co-expressed with *Dlx2* (Yun *et al.* 2002) and was complementary to *Ngn1/2* (Fode *et al.* 2000).

*Ascl1* controls neuronal progenitor specification and later steps of neuronal differentiation as well as regulates genes in cell cycle progression (Casarosa *et al.* 1999; Yun *et al.* 2002; Castro *et al.* 2011). *Ascl1* null mutant showed decreased number of Brdu<sup>+</sup> cells in VZ and SVZ and displayed pronounced reduction in MGE at E12.5. Interestingly, LGE progenitors appeared unaffected (Casarosa *et al.* 1999). However, there was loss of Notch ligand *Dll1*, *Dll3* and Notch target *Hes5*, indicative of decreased notch signalling in both LGE and MGE VZ and SVZ. Additionally, there was ectopic expression of SVZ markers such as *Dlx1*, *Dlx5*, *Dlx6* and *Gad67* in VZ, suggesting that in the absence of *Ascl1*, VZ cells prematurely acquired SVZ phenotype (Casarosa *et al.* 1999; Yun *et al.* 2002). At E17.5-E18.5, LGE early born GABAergic interneurons were absent in MZ (Casarosa *et al.* 1999; Yun *et al.* 2002). *Dll1*<sup>-/-</sup> mutants shared a similar phenotype to that of *Ascl1*<sup>-/-</sup> mutants, thus suggesting that *Ascl1* influences Notch pathway to control progenitor specification and drive early neurogenesis.

Forced expression of *Ascl1* in *Ngn* mutants resulted in misspecification of early born cortical neurons with ectopic expression of *Dlx1*, *Dlx2*, *Dlx5* and *Gad67* (Fode *et al.* 2000). *Ascl1* has been shown to bind to an E-box sequence in I12b enhancer located in *Dlx1/2* intergenic region and regulate their expression (Poitras *et al.* 2007). An increased expression of *Ascl1* and Notch pathway genes was observed in *Dlx1/2*<sup>-/-</sup> mutant (as explained above) and there was a loss of DARPP-32 and DRD2 expression (Yun *et al.* 2002). Removal of *Ascl1* from *Dlx1/2*<sup>-/-</sup> background further exacerbated striatal phenotype (Long *et al.* 2009). Thus, combined function of *Ascl1* and *Dlx1/2* regulate LGE development and striatal

differentiation. *Ascl1* and activation of Notch signalling are required for early neurogenesis. *Dlx1/2* act, in part, by downregulating notch signalling to drive late neurogenesis (Yun *et al.* 2002).

#### 1.3.4.7 NKX2.1

*NKX2.1* (also known as Thyroid Transcription factor TTF1) is a homeobox transcription factor. The initial expression of *Nkx* genes was found in the medial neural plate overlying SHH-secreting axial mesoderm (Shimamura *et al.* 1995; Shimamura and Rubenstein 1997). Consistently, the expression of *Nkx2.1*, *Nkx2.2* and *Nkx6.1* was induced by SHH (Ericson *et al.* 1995; Shimamura and Rubenstein 1997; Kohtz *et al.* 1998; Sussel *et al.* 1999). *Nkx2.1* expression is restricted to the forebrain. Within telencephalon, *Nkx2.1* was expressed in the MGE VZ and SVZ as well as in post mitotic cells (Sussel *et al.* 1999). Elimination of *Shh* resulted in reduced *Nkx2.1* expression (Gulacsi and Anderson 2006) with dorsalization of ventral telencephalon (Chiang *et al.* 1996), whereas, over-activation of *Shh* lead to dorsal expansion of *Nkx2.1* (Goodrich *et al.* 1997). As mentioned above, SHH acts by repressing *Gli3* repressor function. Elimination of *Gli3* did not alter *Nkx2.1* expression that remained confined to the enlarged MGE in *Gli3*<sup>-/-</sup> mutants, whereas, Cyclopamine (SHH signalling antagonist) treatment of *Gli3*<sup>-/-</sup> slice cultures resulted in downregulation of *Nkx2.1* expression, suggesting that SHH-induced *Nkx2.1* expression is mediated by *Gli3*-independent mechanism (Gulacsi and Anderson 2006).

NKX2.1 is involved in regulating MGE progenitor specification. *Nkx2.1* null mutants displayed severely reduced MGE (Sussel *et al.* 1999). At molecular levels, there was ventral expansion of *Pax6* and MGE acquired LGE markers, thus was specified to form caudate and putamen at the expense of MGE derivatives- globus pallidus, cholinergic striatal interneurons and cortical interneurons (Sussel *et al.* 1999). Similarly, early loss of *Nkx2.1* at E9.5-10.5, in conditional knockout mutants favoured the production of MSNs at the expense of cortical interneurons (Butt *et al.* 2008). Interestingly E12.5 mutants, displayed neither ectopic generation of MSNs nor loss of cortical interneurons, instead showed an increased ectopic production of caudal ganglionic eminence (CGE) derived interneurons that migrate into cortex (Butt *et al.* 2008). Thus, suggesting that *Nkx2.1* acts in a temporal manner and might induce MGE identity by repressing LGE and CGE fate. In support of this

notion, *Nkx2.1* was shown to regulate MGE markers *Lhx6*, *Lhx7* and *Shh* and repress LGE markers, and CGE markers (Elias *et al.* 2008) and ectopic expression of *Lhx6* in *Nkx2.1* null mutants rescued interneurons generation (Du *et al.* 2008).

*Nkx2.1* directs the migration and differentiation of post mitotic neurons. *Nkx2.1* expression was found to be downregulated in GABAergic interneurons migrating to the cortex and it was maintained in cholinergic interneurons migrating to the striatum (Nóbrega-pereira *et al.* 2008). *Nkx2.1* overexpression led to reduction in neurons reaching the neocortex. Interestingly, loss of *Nkx2.1* in conditional knockouts (under the control of *Lhx6* promoter which turns on in post mitotic cells) did not increase the number of cortical interneurons (Nóbrega-pereira *et al.* 2008). However, post mitotic loss of *Nkx2.1* inhibited neuronal migration to the striatum (Nóbrega-pereira *et al.* 2008)

## 1.4 Stem cells

Stem cells are undifferentiated cells capable of self-renewal and differentiation into various specialized cell types in the body (Figure 1:14) (Gardner and Beddington 1988). Stem cells are generally termed according to differentiation potential (pluripotent or multipotent) and place of development (embryonic or adult) (Figure 1:15). A multipotent adult stem cell can self-renew and can form multiple differentiated cell types within a distinct tissue/organ. They reside in a variety of tissues in the adult body and contribute to replenishing and regeneration of diseased and damaged tissue (Dor and Melton 2004). For example, haematopoietic stem cells in bone marrow differentiate into all lineage of blood cells. A pluripotent stem cell (PSC) can self-renew and can form all the different cell types in the developing embryo excluding extra-embryonic tissue such as placenta (Smith 2006). *In vivo*, pluripotency is possessed transiently by the inner cells mass of the blastocyst stage of the developing embryo (explained previously in 1.3.2) and can be maintained *in vitro* by deriving embryonic stem cells (ESC) (Figure 1:15.B). Pluripotency could also be ‘induced’ by *in vitro* reprogramming of somatic cells and can be maintained as induced pluripotent stem cells (iPSCs) (Takahashi and Yamanaka 2006). Human pluripotent stem cells (hPSC)-including both hESC and hiPSC the particular focus of this project are discussed here

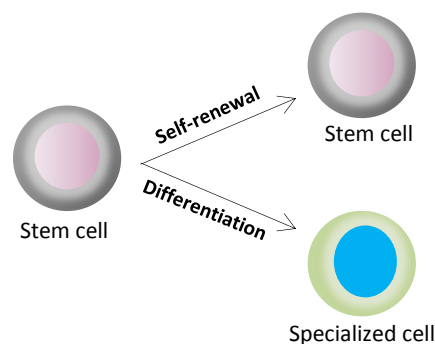


Figure 1:14 When a stem cell divides, it produces either identical daughter cells (self-renewal) or specialized cell types (differentiation), in response to signalling cues

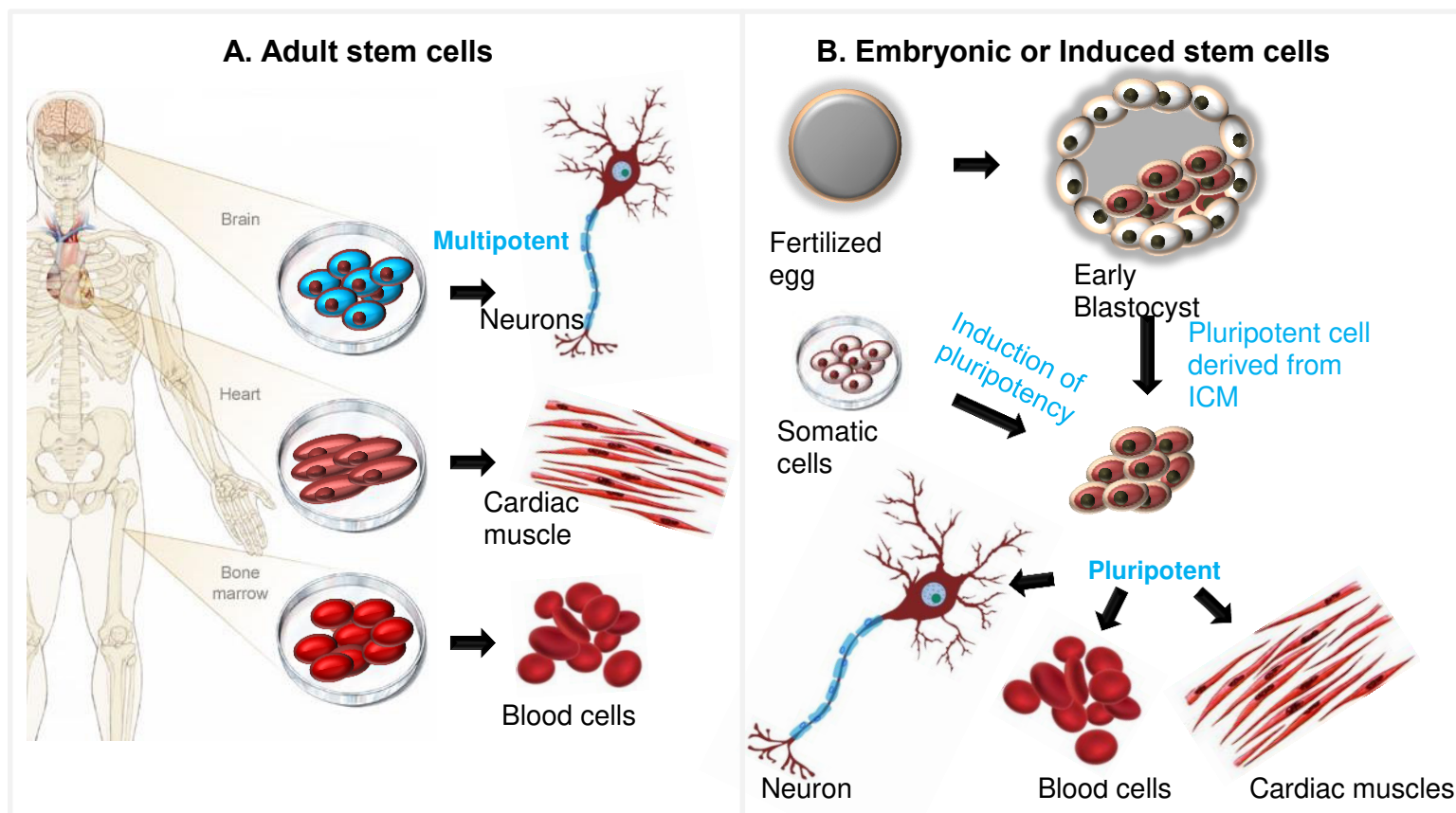


Figure 1:15 **Multipotent adult and pluripotent embryonic or induced stem cells:** **A).** Multipotent adult stem cells reside in various organs such as brain, heart and bone and give rise to tissue specific cells. **B).** Pluripotent stem cells are derived from blastocyst ICM or induced *in vitro* from somatic cells by forced expression of transcription factors and can form cells of all 3 germ layers. Adapted from Stemcellhealthcare.com 2014; Medicinenet.com 2010

### 1.4.1 Embryonic stem cells

Evans and Kaufman (1981), established the first pluripotent mouse ESC line by plating down delayed-implantation blastocyst (the embryonic development delay was induced at 2.5 days post fertilization, causing embryos not to implant into uterine wall). The ICM from the expanded blastocyst was isolated and cells were grown on a layer of mitotically inactivated STO fibroblasts. The resulting cells displayed characteristics of pluripotent cells and retained a normal karyotype. 17 years later, Thomson *et al.* (1998) derived hESCs from the blastocyst stage of human embryos that were produced for clinical purpose by *in vitro* fertilization. The stem cells colonies formed, fulfilled all the criteria for hESC; retained pluripotency and self-renewal as well as normal karyotype when grown on mouse embryonic fibroblasts (MEF). When grafted to severe combined immunodeficient (SCID) mice, they generated large germ cell tumors containing a diversity of differentiated cells (Thomson *et al.* 1998). Later advances in culturing methods and techniques for ICM isolation led to derivation of hundreds of hESC lines from donated embryos (Vazin and Freed 2010).

### 1.4.2 Induced pluripotent stem cells

Induced pluripotent stem cells (iPSC) are generated from somatic cells using defined transcription factors and are capable of self-renewal and differentiation, like ESCs. iPSCs not only overcome the ethical issues regarding the use of human embryos but also allow generation of patient-specific cells. The groundbreaking discovery of iPSCs technology was made by Takahashi and Yamanaka (2006). iPSCs were generated from mouse embryonic or adult fibroblasts by genome-integrating retrovirus-mediated constitutive expression of four ESC transcription factors– *Oct3/4* (Octamer binding transcription factor-3/4), *Sox2* (Sex determining region Y-box2), *cMyc* and *Klf4* (Kruppel like factor-4), termed ‘Yamanaka factors’. Subsequently, human iPSCs were generated using ‘Yamanaka factors’ from foetal, neonatal and adult human dermal fibroblasts (Takahashi *et al.* 2007; Park *et al.* 2008). These iPSCs were similar to ESCs in morphology, proliferation, surface markers, gene expression and epigenetic state, in addition, demonstrated differentiation potency both *in vitro* and *in vivo* (Takahashi and Yamanaka 2006; Takahashi *et al.* 2007; Park *et al.* 2008).

The original iPSC reprogramming strategy using Yamanaka factors remains robust and largely unaltered to date. However, identification of ESC-enriched

genes and screening for transcription factor combinations to reprogram somatic cells led to various adaptations to improve efficiency or safety. Lentiviral expression of reprogramming cocktail –*OCT4*, *SOX2*, *NANOG* and *LIN28*- eliminated both *CMYC* and *KLF4* oncogenes and successfully generated iPSCs from human fibroblasts, although with decreased efficiency compared to Yamanaka factors (Yu *et al.* 2007). An enhancement of efficiency (~10 fold increase in number of iPSC colonies) was achieved by combining all 6 transcription factors- *OCT4*, *SOX2*, *NANOG*, *CMYC*, *KLF4* and *LIN28* cloned into lentivirus (J. Liao *et al.* 2008). A much improved efficiency of 23-70 fold was reported from human foetal and adult fibroblasts, by addition of SV40 large T antigen to reprogramming cocktail from Takahashi *et al.* (2007) and Yu *et al.* (2007), which acts by inhibiting p53(Mali *et al.* 2008). Silencing *p53* expression by addition of *p53*siRNA to Yamanka factors increased iPSC generation up to 100 fold even when *CMYC* was eliminated, by blocking cellular apoptosis (Zhao *et al.* 2008). Exploration of cell signalling pathways and mechanisms underlying reprogramming led to use of small molecules to replace exogenous reprogramming factors and to enhance the process. Valproic acid (inhibitor of histone deacetylase) replaced *CMYC* and *KLF4* and enhanced reprogramming (Huangfu *et al.* 2008). CHIR99021 (glycogen synthase 3 inhibitor, activates WNT signalling) and Parnate (inhibitor of lysine-specific demethylase-1) combined or PS48 (activator of PI3K/AKT signalling) alone, enhanced reprogramming of human keratinocytes (which endogenously express *CMYC* and *KLF4*) using *OCT4* and *KLF4* and thus replaced exogenous *SOX2* and *CMYC* (W. Li *et al.* 2009; Zhu *et al.* 2010). Further, CHIR99021 and Parnate enhanced reprogramming of *OCT4* only transduced human keratinocytes, umbilical vein endothelial cells and amniotic fluid-derived cells (Zhu *et al.* 2010). A combination of SB431542 (inhibitor of TGF $\beta$  signalling) and PD0325901 (inhibitor of MAPK/ERK signalling) increased efficiency to >100 fold (Lin *et al.* 2009) and both together with sodium butyrate (inhibitor of histone deacetylase) greatly accelerated the reprogramming of human fibroblasts, using retroviral expression of Yamanaka factors (Zhang *et al.* 2011). There have been major advancement in the method of delivering reprogramming factors also. Retroviral or Lentiviral vectors showed random integration into iPSC genome and led to tumour formation in chimeric animals (Yu *et al.* 2007; Takahashi *et al.* 2007; Okita *et al.* 2007) which hinders the utilization of resulting cells. iPSCs free of transgenes and vector integration have been derived using OriP/EBNA1 (Epstein-Barr nuclear antigen-1) based episomal vectors (J. Yu *et al.*

2009; Okita *et al.* 2013), Sendai virus (Fusaki *et al.* 2009), cell penetrating peptide (D. Kim *et al.* 2009), modified synthetic mRNA (Warren *et al.* 2010) and piggyBac transposon (Wang *et al.* 2011). The various delivery methods with different combination of reprogramming factors differed in their efficiency. To date, divergent human cell types have been reprogrammed to iPSCs including keratinocytes (Aasen *et al.* 2008), amniotic cells (C. Li *et al.* 2009), neural stem cells (J. B. Kim *et al.* 2009), hepatocytes (Liu *et al.* 2010), adipose cells (Qu *et al.* 2012) and cord blood and peripheral blood cells (Okita *et al.* 2013) for myriad applications.

Despite the advances in reprogramming technology, the mechanistic understanding of reprogramming remains incomplete. At the molecular level, the generally accepted model of iPSC reprogramming consists of 3 sequential phases - initiation, maturation and stabilization (Samavarchi-Tehrani *et al.* 2010; David and Polo 2014; Hawkins *et al.* 2014). Initiation occurs in virtually all transfected cells and is characterized by somatic genes expression being switched off, reactivation of telomerase activity, increase in cell proliferation, cell metabolic switch from mitochondrial oxidative phosphorylation to glycolysis and mesenchymal to epithelial transition (MET). During the maturation phase, the epigenetic changes in pre-iPSC colonies allow the activation of endogenous expression of pluripotency genes. By stabilization phase, stable iPSC colonies gain transgene independency and maintain self-renewal and pluripotency. Mechanistically, *SOX2* was shown to suppress mesenchymal genes and *KLF4* induced epithelial gene expression such as *E-CADHERIN* (a cell adhesion molecule), thus promoted MET which is critical and is a hallmark of reprogramming (Liu *et al.* 2013). As explained above various inhibitors of TGF $\beta$  and MAPK signalling have been used to enhance reprogramming. It is likely due to the prevention of TGF $\beta$ -induced epithelial to mesenchymal transition *in vivo* (EMT, the opposite of MET, involved in embryogenesis and differentiation) (Thiery and Sleeman 2006). The metabolic switch from oxidative phosphorylation to glycolysis is likely to be an adaptation to the *in vivo* hypoxic environment of early embryo where ESCs are originated. In support of this notion, reprogramming under hypoxic condition has been shown to improve efficiency (Yoshida *et al.* 2009). Upregulation of glycolytic genes by PS48 (explained above) therefore explains its effect on promoting reprogramming (Zhu *et al.* 2010). *CMYC*, when combined with *OCT4*, *SOX2* and *KLF4* greatly enhanced the generation of partially reprogrammed iPSCs, which had not turned on endogenous pluripotency genes, however, *CMYC* also

increased tumorigenicity (Nakagawa *et al.* 2008; Maekawa *et al.* 2011). In mice, substituting cMyc with *Glis1* (GLIS family zinc finger 1) promoted pro-reprogramming pathways including MET, *Lin28*, *Nanog* and *Wnt* and enhanced stable iPSC generation (Maekawa *et al.* 2011). *LIN28* expression and *p53/p21* inhibition stimulated cell proliferation by regulating cell cycle genes (Hanna *et al.* 2009). *LIN28* expression and TGF $\beta$  inhibition also promoted NANOG expression which appeared to play the pivotal role in transition from pre-iPSC maturation phase to reprogrammed-iPSCs stabilization phase of (Hanna *et al.* 2009; Samavarchi-Tehrani *et al.* 2010). Similarly, activation of WNT signalling enhanced *NANOG* expression and replaced exogenous *SOX2* (W. Li *et al.* 2009). The expression of endogenous pluripotency genes in stable-iPSC colonies is facilitated by demethylation of gene promoters, therefore various DNA and histone methyltransferases inhibitors have been employed (explained above) to accelerate iPSC reprogramming.

### 1.4.3 Core transcriptional network of hPSC pluripotency and self-renewal

Understanding the factors that regulate the unique hPSC characteristics is fundamental for harnessing the potential of these cells for various applications. Several lines of evidence in mESC and hESC show that precise levels of core transcription factors –*OCT4*, *SOX2* and *NANOG* robustly maintains ESC identity, yet permit cells to respond to developmental cues. During early mouse development, *Oct4*, *Nanog* and *Sox2* was required to maintain pluripotent cells of ICM and epiblast (Nichols *et al.* 1998; Mitsui *et al.* 2003; Avilion *et al.* 2003). In mESC, a conditional expression and repression of *Oct3/4* showed that a two fold increase in expression lead to differentiation into primitive endoderm and mesoderm, whereas its repression, induced loss of pluripotency and dedifferentiation to trophoblast. Thus, a precise level of *Oct4* maintained pluripotency (Niwa *et al.* 2000). *Nanog* knockdown in mESCs drove differentiation into extra-embryonic endoderm (Mitsui *et al.* 2003). *Nanog* also blocked neuroectoderm (Ying *et al.* 2003) and mesoderm (Suzuki *et al.* 2006) differentiation. Unlike *Oct4*, *Nanog* overexpression promoted self-renewal and maintenance of pluripotent state (Mitsui *et al.* 2003). *Sox2* knockdown in mESCs induced multilineage differentiation. However, unlike *Oct4* and *Nanog*, *Sox2* expression is not restricted to ESCs and is also present in multipotent cells of extraembryonic ectoderm and neuroectoderm (Avilion *et al.* 2003). A slight over expression of *Sox2* in ESC decreased expression of its own gene as well as *Oct4* and

*Nanog* (Boer *et al.* 2007). Thus, a precise *Sox2* expression levels is critical for ESC state.

In hESCs, consistent with the findings in mESC, OCT4 knockdown resulted in loss of expression of stem cell markers and results in trophoblast differentiation (Matin *et al.* 2004; Hay *et al.* 2004). NANOG knock down resulted in differentiation to extraembryonic lineages (Hyslop *et al.* 2005). And *SOX2* knock down resulted in reduced expression levels of *OCT4* and *NANOG* as well as trophoblast differentiation (Fong *et al.* 2008). It has been showed that the core transcription factors (TF) trio of OCT4, SOX2 and NANOG governs pluripotency and self-renewal in hESC (Boyer *et al.* 2005). Genome-wide ChIP-on chip analysis (to identify the DNA binding sites of these transcription factors) showed that these 3 TFs act as core regulators; they bound to a large number of genes and that they co-occupied the promoters of target genes. These target genes were found to be either active genes or inactive genes. The notable targets among the active genes included *OCT4*, *SOX2*, *NANOG* and components of TGF- $\beta$  and WNT signalling pathways that play a role in hES pluripotency. The inactive genes included many of those implicated in developmental process, such as transcription factors for differentiation into extra-embryonic tissues or germ layers (Boyer *et al.* 2005). A regulatory circuitry with interconnected autoregulatory loop between these core transcription factors was postulated in the same publication. *OCT4* and *SOX2* act together as heterodimer on the transcription of their own gene as well on that of *NANOG*, whereas *NANOG* acts on its own gene and *OCT4* and *SOX2* (Boyer *et al.* 2005). To summarise, the OCT4, NANOG, SOX2 trio prevents differentiation along other lineages and maintains hPSC pluripotency and self-renewal.

#### **1.4.4 Signalling pathways in hPSC pluripotency and self-renewal**

The predominant signalling pathways involved in hPSC pluripotency and self-renewal are TGF- $\beta$ /Activin/nodal and basic fibroblast growth factor (FGF) signalling (Figure 1:16). TGF- $\beta$ /Activin/nodal bind to Alk4/5/7Activin receptors and activate SMAD2/3. It has been demonstrated that SMAD2/3 binds and directly controls *NANOG* to maintain the pluripotent state (Xiao *et al.* 2006; Xu *et al.* 2008; Vallier *et al.* 2009). SMAD2/3 signalling is involved in self-renewal as well as differentiation. This dual role was shown to be governed by PI3K signalling (Singh *et al.* 2012). PI3K signalling, when active, limited the absolute levels of phosphorylated

SMAD2/3 within a range to maintain self-renewal by activating target including *NANOG*. Under low PI3K signalling activity, phosphorylated SMAD2/3 was increased and in conjunction with WNT effectors promoted target genes involved in differentiation (Singh *et al.* 2012). Fibroblast growth factor-2 (FGF2) regulates PI3K and MAPK/ERK signalling in hPSCs (Dalton 2013). At low concentration, FGF2 activated MAPK/ERK signalling. Under these conditions, ERK threshold for differentiation was not exceeded and self-renewal state was maintained. At elevated concentration, Fgf2 activated both ERK and PI3K/AKT, but AKT suppressed MEK/ERK activity and maintained ERK activity within a range for self-renewal. (Dalton 2013).

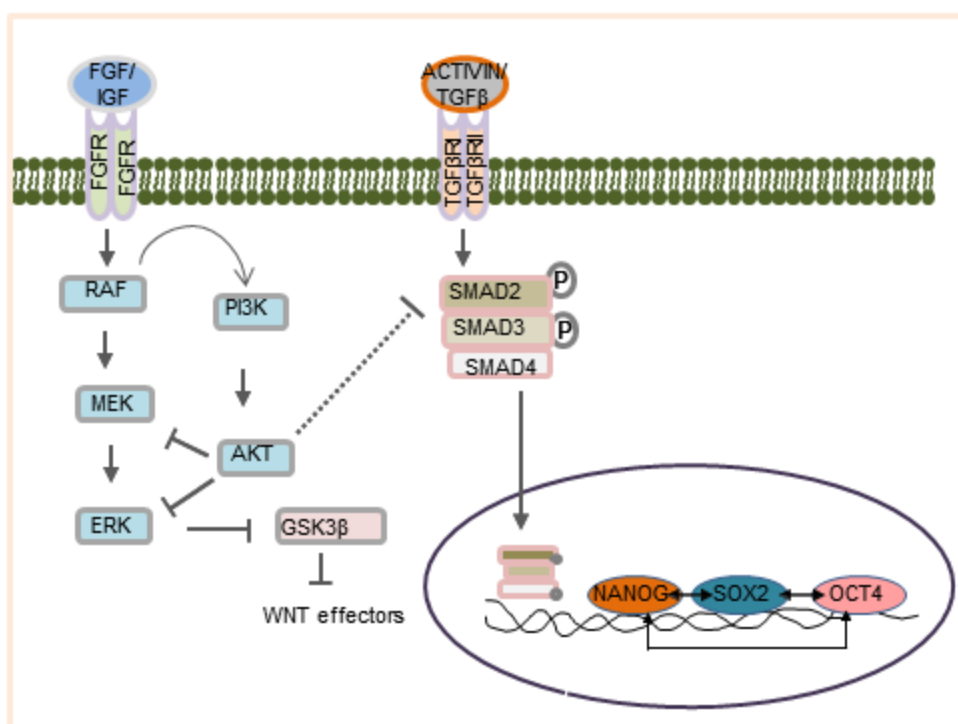


Figure 1:16 Core signalling networks that regulate pluripotency and self-renewal of human pluripotent stem cells: FGF2 at low concentration promotes self-renewal by activation of MAPK/ERK, by maintaining ERK threshold. Elevated FGF2 concentration drives ERK as well as PI3K/AKT which feeds back to suppress MEK/ERK activity. AKT also modulates SMAD2/3 threshold and maintains GSK3 $\beta$  activity, compatible with NANOG expression to maintain the self-renewing state. Adapted from Dalton 2013

#### 1.4.5 Application of hPSCs for HD

A major focus of HD research is directed towards understanding and modelling the mechanisms that contribute to degeneration of GABAergic MSNs. Derivation of hESC lines and discovery of hiPSC technology have created the

opportunities to model early human development and disease states *in vitro*. Deciphering early developmental mechanisms to drive *in vitro* differentiation of hPSCs harbouring mutant *HTT* allele, into striatal neuronal cell types provides a human cell based powerful platform to monitor disease related changes during neurogenesis. It may simultaneously enable the identification of target for drug screening as well as offer renewable source of specialized cells for cell based therapies. Here, I discuss the recent literature demonstrating the derivation of *in vitro* models of HD established by ESC and iPSC technologies and current hPSC differentiation strategies to generate MSN like neurons.

#### 1.4.5.1 hPSC models of HD

The common aspiration is that hPSC models of HD will overcome the limitations of using post-mortem tissues and animal models. HD-hESCs have been derived by several groups from preimplantation genetic diagnosis (PGD) *in vitro* fertilization (IVF) embryos, that carry *HTT* allele (Mateizel *et al.* 2006; Niclis *et al.* 2009; Tropel *et al.* 2010; Seriola *et al.* 2011; Bradley *et al.* 2011; Niclis *et al.* 2013). These various HD-ESCs lines expressed pluripotent markers at both mRNA levels and proteins levels and showed the ability to differentiate into cell types of three germ layers both *in vivo* and *in vitro* (Tropel *et al.* 2010; Seriola *et al.* 2011; Bradley *et al.* 2011). All the lines had normal karyotype and could be maintained in culture long term. Importantly, the HD-ESC lines showed the presence of 40-51 CAG repeats and expression of mutant gene at protein and mRNA levels that remained stable in the undifferentiated stage (Niclis *et al.* 2009; Seriola *et al.* 2011; Bradley *et al.* 2011). Compared to wild type-hESCs, *in vitro* neural differentiation of HD-hESCs showed similar levels of SOX2 and PAX6 at early progenitor stage and  $\beta$ -III-tubulin and MAP2 at later neuronal stage ((Niclis *et al.* 2009; Bradley *et al.* 2011; Feyeux *et al.* 2012). Although a short expansion, compared with large CAG expansion seen in neurons of HD patients, there was a low level CAG instability with 5-6 CAG repeat expansion in mutant allele of HD-ECS derived neurons (Niclis *et al.* 2009). Furthermore, some transcriptional changes linked to *HTT* mutation was captured during *in vitro* neural differentiation that included upregulation of *coiled-coil-helix-coiled-coil-helix domain containing 2* (*CHCHD2*, involved in mitochondrial function) and *tripartite motif family protein4* (*TRIM4*, involved in protein kinase A pathways) in HD-hESCs derived neurons (Feyeux *et al.* 2012). There was also elevated glutamate-evoked response in CGA51 HD-hESC derived neurons (Niclis *et al.* 2013).

hiPSCs avoid any ethical concerns related to hESC research and permit utilization of patient derived cells that mirror HD mutation in the donor. The first human HD-iPSC line was derived from juvenile onset HD patient fibroblasts with 72 CAG repeat in the *HTT* gene, using retroviral vector delivery of yamanaka factors (Park *et al.* 2008). These HD-iPSCs exhibited pluripotency markers at both mRNA and protein levels. Characterization by quantitative proteomic analysis revealed the pathological conditions, in particular, an increased susceptibility to oxidative stress, induction of apoptotic pathways and dysregulation of cytoskeleton associated proteins- in HD-iPSCs compared to normal hiPSC or hESCs (Chae *et al.* 2012). Subsequent neural differentiation of HD-iPSC produced SOX1<sup>+</sup> PAX6<sup>+</sup> NESTIN<sup>+</sup> neural progenitors which upon terminal differentiation generated ~10% DARP32<sup>+</sup> striatal neurons (N. Zhang *et al.* 2010). Both neural progenitors and neurons maintained same CAG expansion as in patients. Some features of HD phenotype were exhibited during *in vitro* differentiation, such as enhanced caspase 3/7 activity in neural progenitors upon growth factor withdrawal (N. Zhang *et al.* 2010), HTT aggregate formation upon addition of proteasome inhibitor MG132 (Jeon *et al.* 2012) and increased cell death and stunted neurite outgrowth in MAP2<sup>+</sup> neurons (Chae *et al.* 2012). *In vivo* at 9 months transplantation to mouse brain, HD-iPSC-derived neuronal cells showed HTT aggregates (Jeon *et al.* 2012). Camnasio *et al.* (2012) generated HD-iPSC lines from two patients- one heterozygous mutant *HTT* (44 repeats) and a homozygous mutant *HTT* (39–44 repeats) using lentiviral vectors. Analysis of pluripotency markers and *in vitro* and *in vivo* differentiation into derivatives of three germ layers confirmed pluripotency of these lines. CAG repeat length was maintained during reprogramming, long-term culture and neuronal differentiation. Neural differentiation efficiency of these HD-iPSCs was similar to that was seen in wild type iPSCs and yielded NESTIN<sup>+</sup> PAX6<sup>+</sup> neural progenitors which upon terminal differentiation generated  $\beta$ -III tubulin<sup>+</sup> or MAP2<sup>+</sup> neurons. Unlike previously reported by Zhang *et al.* (2010) in HD-iPSC with 72 CAG repeat, there was no difference in caspase activation. However, there was increased lysosomal activity in HD-iPSCs and HD-iPSC-derived neurons compared with wild type iPSCs (Camnasio *et al.* 2012). Juopperi *et al.* (2012) generated HD-iPSC lines from a father (50 CAG repeats) and daughter (109 CAG repeats) using a retroviral method. Both lines demonstrated pluripotency, as described previously for other HD-iPSC lines. Interestingly, differentiation to neural lineage produced phenotypically normal functional neurons, whereas differentiation into

astrocytic lineage showed the presence of clear cytoplasmic vacuoles (a phenomenon previously reported in blood lymphocytes from HD patients) which were more pronounced in HD-iPSC with 109 repeats (Juopperi *et al.* 2012). Remarkably, the vacuoles appeared without addition of stressors and increased over time. The HD iPSC Consortium (2012) reported generation of various HD-iPSC lines with 60, 109 and 180 CAG repeats using lentiviral vectors. Most of the lines exhibited CAG stability with passage or upon differentiation. Neural differentiation of HD-iPSC yielded SOX1<sup>+</sup> SOX2<sup>+</sup> NESTIN<sup>+</sup> PAX6<sup>+</sup> progenitors that expressed mutant HTT proteins and showed dysregulation of actin cytoskeleton, decreased cell-cell adhesion properties and reduction in energy metabolism. Further differentiation and maturation of progenitors yielded MAP2<sup>+</sup> GABA<sup>+</sup> neurons with functional expression of voltage activated K<sup>+</sup>, Na<sup>+</sup> and Ca<sup>2+</sup> currents and generated induced and spontaneous action potential, however in the HD180 line, no spontaneously firing neurons were detected. These neurons had increased caspase 3/7 activity and showed increased cell death (The HD iPSC Consortium 2012). Furthermore, microarray profiling of neural progenitors and neurons revealed CAG repeat-associated gene expression that distinguished patient lines from control and early onset vs late onset (The HD iPSC Consortium 2012). Genetic correction of *HTT* gene has been attempted in HD-72 iPSCs generated by Park *et al.* (2008) to replace CAG expansion with 21 repeat via homologous recombination. The corrected HD-iPSCs generated DARPP32<sup>+</sup> neurons *in vitro* and *in vivo*. The correction normalized pathological HD signalling such as cadherin, BDNF and caspase activation as well as reversed HD phenotypes such as altered mitochondrial bioenergetics and susceptibility to cell death (An *et al.* 2012).

Together, the studies described here demonstrate that hPSC models recapitulate HD pathogenesis and provide insight into underlying cellular and molecular events. They are advantageous over post-mortem tissues and animal models in that neuronal differentiation and disease pathology could be reproduced and be monitored. hiPSCs provide proof-of-concept for future high-throughput therapeutic screens.

#### 1.4.5.2 Directed differentiation of hPSC into medium spiny neurons

Over the last few years, the establishment of hPSCs lines has led to the generation of protocols for directing their differentiation into cell types of interest. For generation of striatal cell types that are of direct relevance to HD, the present protocols

in literature are targeted at specifying hPSCs into DARPP32 expressing MSN like neurons (summarised in Table 1). A small number of publications have also reported on functionality of these hPSC derived progenitors for striatal reconstruction from grafting into HD animal models.

The directed differentiation protocols have exploited the knowledge on the *in vivo* embryo developmental pathways to drive hPSC differentiation sequentially through neuroectoderm, telencephalon and LGE intermediates to a striatal like neuronal population. The protocols exploit either a non-adherent embryoid body (EB) culture or an adherent monolayer culture using substrates. Recapitulation of neural development is achieved *in vitro* by temporal integration of developmental signals by means of exogenous growth factors or small molecules. For the purpose of this thesis, LGE-like specification of hPSCs is reviewed here as 3 successive developmental stages neural induction, progenitor specification and neuronal differentiation.

#### 1.4.5.2.1. Neural Induction

The various approaches to drive hPSC differentiation along neural lineage include co-culture on stromal cells (murine stromal cells MS5 or PA6), culture in neuralizing medium and dual smad inhibition. Co-culture method relies on the neural inducing properties of stromal cells. hES co-culture on MS5 (in DMEM/F12 containing 15% knock out serum replacement (KSR) and amino acids) with subsequent culture in N2 medium (containing DMEM/F12 supplemented with insulin, transferrin, putrescine, selenium chloride and progesterone) yielded neural rosettes expressing PAX6, NESTIN, NCAM and SOX1 at 3 weeks of differentiation (Perrier *et al.* 2004; Aubry *et al.* 2008). Co-culture of HD-iPSCs on PA6 followed by growing neural rosettes in suspension in N2 medium yielded high levels of SOX2 and NESTIN (Jeon *et al.* 2012). Although seemingly efficient, the stroma feeder neural induction has the drawback of relying on nonhuman cell derived unidentified factors. Many studies have focused on developing more defined culture conditions. Culture of hES EB (chopped hESC colony fragments maintained in suspension as spheres) in neuralizing medium containing human serum albumin, insulin, transferrin, lipids and amino acids resulted in loss of pluripotent markers POUF1 and NANOG and acquisition of PAX6, NCAM and SOX1 by 16 days (Joannides *et al.* 2007). hESC EBs grown in ESC medium (containing 15% knock out serum replacement and FGF-b) for 4 days, then in N2 medium (containing DMEM/F12, aminoacid, heparin and N2

supplement) for 2 days and plated down onto laminin formed SOX1<sup>+</sup> SOX2<sup>+</sup> PAX6<sup>+</sup> neural rosettes over 10-15 days (Pankratz *et al.* 2007; Ma *et al.* 2012). A modification of this EB protocol by replacing ESC medium gradually over 8 days with 20% foetal bovine serum containing medium and then plating EB onto poly-orinithine/laminin in medium supplemented with 25ng/ml bFGF induced 95% SOX1<sup>+</sup> PAX6<sup>+</sup> NESTIN<sup>+</sup> neural progenitors from HD-iPSCs (N. Zhang *et al.* 2010). Understanding of developmental cues has not only allowed to refine the neural induction protocols but also to investigate these early events under *in vitro* condition. Inhibition of BMP signalling by Noggin treatment of hESCs (cultured in the presence of serum), blocked BMP-mediated differentiation into extra-embryonic endoderm and induced the expression of PAX6 and NESTIN (Pera *et al.* 2004). This effect of Noggin was reproduced for neural specification of hES EBs under chemically defined serum free condition (Itsykson *et al.* 2005). Supplementing Noggin during neural induction on MS5 also promoted neural specification (Lee *et al.* 2007; Chambers *et al.* 2009). Nodal inhibition accomplished by over expression of full length Lefty2 or truncated form of Cerberus in hESC and culture as EB in CDM (50% IMDM and 50% F12NUT-MIX supplemented with insulin, transferrin and bovine serum albumin) enhanced neural specification as seen by increased expression of NESTIN and SOX1 (Smith *et al.* 2008). Similar effects were reproduced during hESC EBs differentiation for 14-16 days in CDM supplemented with small molecule inhibitor of Activin/Nodal signalling-SB431542 (Smith *et al.* 2008). Synergistic action of Noggin and SB431542 for a highly efficient neural conversion of hESCs was demonstrated by Chambers *et al.* (2009). Under monolayer adherent culture conditions, supplementing KSR medium with Noggin and SB431542 for 11 days increased efficiency to > 80% compared with < 10% PAX6<sup>+</sup> cells when Noggin or SB431542 were used alone (Chambers *et al.* 2009). Temporal analysis of gene expression revealed that SB431542 treatment alone induced rapid loss of NANOG, suppressed mesodermal marker *BRACHYURY* and increased expression of trophoblast marker CDX2. Addition of Noggin suppressed CDX2 and endodermal marker SOX17. Thus, SB431542 and Noggin synergistically would promote neural specification by destabilizing pluripotency network and suppressing differentiation towards trophoblast/mesodermal/endodermal fate. Temporal fate analysis of Noggin/ SB431542 treatment revealed a transient FGF5<sup>+</sup> OTX2<sup>+</sup> epiblast like stage at day 5 followed by induction of SOX1 and PAX6 by day 7 (Chambers *et al.* 2009). Furthermore, in comparison to MS5/Noggin protocol,

Noggin/ SB431542 yielded high efficiency neural conversion (Chambers *et al.* 2009). Noggin/ SB431542 dual smad inhibition protocol thus obviates the need for feeder cells and induces high neural conversion of hESCs under more defined conditions. It is advantageous over other protocols in terms of scalability for generating clinical grade neural progenitors.

#### 1.4.5.2.2. Progenitor specification towards LGE like fate

hPSC differentiation could be directed to a specific progenitor type by exposing to signals that establish early AP axis and D/V regionalization and specification. During my research study, I analysed the role of WNT and SHH signalling at this context. Here I review the key findings published in the same period by other research groups.

As described in session 1.3.3, during early development, antagonism of WNT activity is required to establish the telencephalon. Neural progenitors derived using stromal co-culture, serum free EB method or dual smad inhibition protocol exhibit  $FOXG1^+$  telencephalic progenitors by default (Elkabetz *et al.* 2008; Pankratz *et al.* 2007; Chambers *et al.* 2009; DelliCarri *et al.* 2013). Use of WNT inhibitor DKK1 (100ng/ml) to efficiently induce  $FOXG1^+$  telencephalic precursors was first described with mouse ESC (Watanabe *et al.* 2005; Ten Berge *et al.* 2008). Similarly, plating of neurogenic hES EBs (generated using serum free EB method), in the presence of DKK1 (500ng/ml), as well as Lefty A and BMP inhibitor- BMPRIA-Fc induced telencephalic fate; at day 35, the cultures contained  $FOXG1^+$  (~34%),  $PAX6^+$  (~98%) and  $NKX2.1^+$  (<1%) progenitors (Watanabe *et al.* 2007). Dual-SMAD inhibition combined with DKK1 (100ng/ml) treatment highly enhanced expression of *FOXG1* and *SIX3* and downregulated expression of caudal markers *OTX1* and *LMX1A* (Nicoleau *et al.* 2013). In contrast, treatment with WNT3a promoted *OTX1* and most caudal *HOXB3* markers (Nicoleau *et al.* 2013). In the absence of any morphogen,  $FOXG^+$  hPSC progenitors adopted  $PAX6^+$  dorsal telencephalon fate (Chambers *et al.* 2009; Li *et al.* 2009; Nicoleau *et al.* 2013). This default dorsal telencephalon fate is attributed to endogenous WNT ligands which promote a repressive form of *GLI3* which in turn antagonizes SHH signalling (Li *et al.* 2009). Treatment with 100ng/ml or 500ng/ml DKK1 did not alter proportion of  $PAX6$  or  $NKX2.1$  among  $FOXG1^+$  cells (X. Li *et al.* 2009). Thus inhibition of WNT signalling efficiently induced  $FOXG1^+$ , however it did not mediate ventral telencephalon specification.

SHH, as described in 1.3.3, is a known morphogen for ventral telencephalon patterning. SHH, either a defined dose or with combinatorial WNT inhibition, has been used to promote ventral telencephalon specification during mESC and hPSC differentiation. SHH treatment increased Nkx2.1<sup>+</sup> or Isl1/2<sup>+</sup> among Foxg1<sup>+</sup> cells during mESC EB (Watanabe *et al.* 2005) and hESC EB differentiation (Watanabe *et al.* 2007). A dose dependent SHH effect has been demonstrated; the highest dose lead to MGE fate while a moderate dose specified LGE during mESC (Danjo *et al.* 2011) and hESC neural conversion (Ma *et al.* 2012). The highest SHH doses (500-1000ng/ml) reduced PAX6 while increased NKX2.1 and MEIS2 and did not affect FOXG1 and OTX2 (Li *et al.* 2009; Ma *et al.* 2012). Moderate SHH dose (200ng/ml) minimally elevated NKX2.1, optimally reduced PAX6, highly induced MASH1, MEIS2 and GSX2, suggesting LGE fate (Ma *et al.* 2012). In conjunction with DKK1, SHH significantly enhanced *GSX2*, *DLX2*, *ASCL1* and *NKX2.1* (Watanabe *et al.* 2007; Aubry *et al.* 2008; Li *et al.* 2009; Delli Carri *et al.* 2013; Nicoleau *et al.* 2013) and downregulated *PAX6*, *EMX1* and *TBR2* (Li *et al.* 2009; Nicoleau *et al.* 2013). Interestingly, SHH mediated ventralization (at optimal 50ng/ml that enhanced LGE markers) was shown to be enhanced by small molecule WNT antagonist XAV939 (explained in 1.5.2) in a dose dependent manner; there was proportional upregulation of *GSX2*, *DLX2*, *ASCL1* and *MEIS2* from 0.25 to 1 $\mu$ M XAV-939. There was no further increase of these genes at 4 $\mu$ M XAV-939, in contrast, there was progressive increase in *NKX2.1* and *LHX6* indicating MGE fate (Nicoleau *et al.* 2013). However, in the absence of SHH, this ventralizing property of XAV-939 was reduced, even the highest dose was not sufficient to promote MGE identity (Nicoleau *et al.* 2013). Thus coordination between WNT and SHH pathways may mediate LGE specification of hPSCS (Li *et al.* 2009; Nicoleau *et al.* 2013).

Studies indicate that SHH mediated ventral telencephalon specification is both temporal and dose dependent. Early SHH treatment during mESC neural conversion was not able to generate telencephalic progenitors (Danjo *et al.* 2011). Similarly during hESC differentiation (dual smad inhibition combined with WNT inhibition and SHH activation), an early SHH exposure suppressed FOXG1 induction, whereas late exposure did not have significant effect on telencephalon markers (Fasano *et al.* 2010; Ma *et al.* 2012; Maroof *et al.* 2013). In XAV-939 treated day 20 cultures, addition of SHH or cyclopamine at day 4 or 10 did not alter telencephalic fate, but induced ventralization in dose dependent manner (Nicoleau *et al.* 2013). In

*vitro* timing of SHH is also shown to affect MGE derived cortical interneuron identity during hPSC derived NKX2.1:GFP<sup>+</sup> cells differentiation; late SHH exposure (10-18 days), robustly induced cortical interneuron progenitor markers OLIG2 and NKX6.2 and LHX6 (Maroof *et al.* 2013). And in all SHH treated cultures (2-18, 6-18 and 10-18 days ), there was also an induction of floor plate marker FOXA2 (Maroof *et al.* 2013).

Recently, a novel method using Activin A (referred to as Activin hereafter) was shown to induce LGE characteristics in hPSC derived anterior neural progenitors (Arber *et al.* 2015). Activin treatment induced upregulation of *GSX2*, *DLX2*, *ASCL1*, *NOLZ1*, *EBF1* and *CTIP2* and downregulation of *PAX6* mRNA. At protein level, abundant expression of GSX2<sup>+</sup> (55±10%), DLX2<sup>+</sup> (25±12%), CTIP2<sup>+</sup> (50±12%), FOXP2<sup>+</sup> (16±6.7%) and NOLZ1<sup>+</sup> (16.7±1.7%) were detected (Arber *et al.* 2015). The same study reported that Activin and SHH act differentially in regulating LGE fate. Compared to Activin treatment, SHH treatment alone or in combination with Activin, upregulated mRNA expression of *NKX2.1* and *LHX8*, but did not increase LGE specific *CTIP2*, *NOLZ1*, *GSX2* and *DLX2* mRNA expression (Arber *et al.* 2015). Blocking endogenous SHH signalling by cyclopamine (at a dose that inhibited NKX2.1 induction) did not affect Activin mediated upregulation of GSX2, CTIP2 or FOXP2 (Arber *et al.* 2015). This finding suggested that Activin induces LGE/striatal characteristics independently of SHH signalling. A steady increase in the number of CTIP2<sup>+</sup> with increasing time of Activin treatment may suggest its requirement for stable maintenance of CTIP2 phenotype and induction of MSN like fate (Arber *et al.* 2015). Interestingly, Nicoleau *et al.* (2013) showed that in conjunction with DKK1, high dose of SHH (200ng/ml) decreased CTIP2<sup>+</sup> and increased NKX2.1<sup>+</sup> cells (Nicoleau *et al.* 2013). These finding suggests that SHH mediated LGE specification may occur via an indirect signalling of MGE fate induction, whereas Activin may directly mediate LGE specification.

#### 1.4.5.2.3 Neuronal differentiation towards MSN phenotype

The relevance and quality of exogenous signal-mediated LGE progenitor specification of hPSCs, is largely dependent on the strength of this commitment during terminal neuronal differentiation and maturation. Neuronal differentiation of ventral progenitors patterned by SHH treatment, generated GABA<sup>+</sup> DARPP32<sup>+</sup> neurons in SHH dose-dependent manner; progenitors generated at 200ng/ml produced the best yield compared to 500ng/ml (Ma *et al.* 2012). At day 47 of differentiation in the presence for VPA for 6 days followed by BDNF, GDNF, Insulin-like growth factor (IGF1) and cAMP, the majority of neurons were  $\beta$ III-tubulin<sup>+</sup>, among which 1.2 $\pm$ 0.8% were choline acetyltransferase<sup>+</sup> (ChAT) and 90.2 $\pm$ 4.2% were GABA<sup>+</sup> MEIS2<sup>+</sup> GAD65/67<sup>+</sup> neurons with numerous spines on their dendrites. 89.7 $\pm$ 9.3% GABA<sup>+</sup> neurons co-expressed DARPP32 (Ma *et al.* 2012). *In vivo* at four months post transplantation, day40 LGE-like progenitors transplanted into QA lesioned SCID mice generated GABA<sup>+</sup> MEIS2<sup>+</sup> CTIP2<sup>+</sup> DARPP32<sup>+</sup>(58.6 $\pm$ 3%) neurons with numerous synaptophysin<sup>+</sup> dendritic buttons along MAP2<sup>+</sup> dendrites (Ma *et al.* 2012). Presence of human specific synaptophysin<sup>+</sup> DARPP32<sup>+</sup> neurons in substantia nigra indicated striatal projection neuron characteristics. Furthermore, GABA<sup>+</sup> cell bodies showed robust co-labelling of TH and vGlu suggestive of dopaminergic and glutamatergic input respectively. Collectively, these results indicated that graft derived GABA neurons connected with endogenous circuit (Ma *et al.* 2012).

Neuronal differentiation of PA6-stromal induced rosettes EBs by plating down EBs in the presence of BDNF produced LGE progenitors as well as striatal neurons ((Jeon *et al.* 2012). LGE progenitors were OTX2<sup>+</sup> (76.0 $\pm$ 1.3%) FOXG1<sup>+</sup> (38.4 $\pm$ 3.4%), GSX2<sup>+</sup> (28.8 $\pm$ 2.8%) and DLX2<sup>+</sup> (34.1 $\pm$ 4.5%). Co-localized expression of DARPP32<sup>+</sup> (27.0 $\pm$ 1.7%) with GSX2 and DLX2 and the presence of GABA<sup>+</sup> (75.1 $\pm$ 2.2%) confirmed striatal MSN like phenotype. The cultures also contained neuronal proteins such as CALB<sup>+</sup> (19.1 $\pm$ 2.1%), MAP2<sup>+</sup> (89.1 $\pm$ 5.5%), Synaptophysin<sup>+</sup> (20 $\pm$ 3.8%) and NeuN<sup>+</sup> (88%) (Jeon *et al.* 2012). *In vivo*, at 12 weeks post-transplantation, the graft derived cells contained some NESTIN<sup>+</sup> progenitors as well as striatal neurons that were GABA<sup>+</sup> DARPP32<sup>+</sup> GAD65/67<sup>+</sup> (Jeon *et al.* 2012). Terminal differentiation of MS5 stroma-induced rosettes with subsequent DKK (100ng/ml) +SHH (200ng/ml) patterning, was carried out by mechanically isolating neural rosettes and re-plating in medium containing dibutyryl-cAMP (dbcAMP) and valproic acid

(VPA) (Aubry *et al.* 2008). At day 63, the cultures contained numerous PAX6<sup>+</sup>/NESTIN<sup>+</sup> (60-70%) progenitors as well as MAP2<sup>+</sup> (22±2%) mature neurons. Among MAP2<sup>+</sup> neurons, 53±6% co-expressed DARPP32, 36±2% co-expressed GABA, 10±2% co-expressed Calbindin (CALB) and 55±7% co-expressed Calretinin. At mRNA level, expression of *DARPP32*, *GAD67* and *CALB* were upregulated (Aubry *et al.* 2008). *In vivo* differentiation upon transplantation of day 45 cultures into QA lesioned rat striatum, generated human nuclear antigen<sup>+</sup> (HNA) MAP2<sup>+</sup> NeuN<sup>+</sup> neurons among which 21±7% were DARPP32<sup>+</sup> (Aubry *et al.* 2008). Ventral progenitors derived from EB based neural induction followed by DKK1, SHH (250ng/ml) and BDNF patterning, generated ~10% DARPP32 upon terminal differentiation in the presence of BDNF, VPA, cAMP and Y27632. The neurons were also immunoreactive for β-tubulin, GABA and CALB (N. Zhang *et al.* 2010).

Li *et al.* (2009) reported that default dorsal telencephalic progenitors (induced in the absence of any morphogens) at 6 weeks of terminal differentiation, generated 9% ISL1<sup>+</sup> post mitotic neurons, whereas DKK1+SHH patterned progenitors generated 40% ISL1<sup>+</sup> cells. Further differentiation of DKK1+SHH progenitors till week10, resulted in neuronal maturation into striatal GABAergic identity as evidenced by expression of βIII tubulin, MAP2, CTIP2 (14%) and some staining for GAD65/67, GABA and DARPP32 (Li *et al.* 2009). In contrast, default dorsal progenitors differentiated into CTIP2<sup>+</sup> (57%) vGLUT1<sup>+</sup> glutamatergic neurons (Li *et al.* 2009). *In vitro* differentiation of LGE like progenitors generated by dual smad inhibition with combinatorial SHH (200ng/ml)/ DKK (100ng/ml), yielded neurons of GABAergic MSN phenotype (DelliCarri *et al.* 2013). At day 45 of differentiation in the presence of B27 and BDNF, neuronal network contained βIII-tubulin<sup>+</sup> (80%), MAP2<sup>+</sup> and TAU<sup>+</sup> cells along with proteins of GABAergic specification- GAD65/67 and GABA- as well as proteins of striatal specification- CALB1, CTIP2, FOXP1, FOXP2 and DARPP32 (DelliCarri *et al.* 2013). Temporal mRNA expression analysis revealed gradual increase of *ARPP21*, *DARPP32* and *DRD1* from day 45 to day 80 and high expression of ISL1 at day 45 and downregulation thereafter. At day80, the cultures contained βIII-tubulin<sup>+</sup> (17%), NESTIN<sup>+</sup> (7%), MAP2<sup>+</sup> (50%) and GFAP<sup>+</sup> (25%). MAP2<sup>+</sup> neurons co-expressed DARPP32<sup>+</sup> (20%), GABA<sup>+</sup> (78%), CTIP2<sup>+</sup> (60.3%) and CALB1<sup>+</sup> (53%). βIII-tubulin<sup>+</sup> co-expressed DRD2 and CTIP2. Striatal interneurons were also detected as CALB1<sup>+</sup>/ CTIP2<sup>-</sup> (15.7%), Calretinin<sup>+</sup> (7%) and SST<sup>+</sup> (0.2%) (DelliCarri *et al.* 2013). Furthermore, *in vivo* maturation of progenitors towards MSN fate was

demonstrated; at 9 weeks post transplantation in QA lesioned HD rat brain extensive FOXP1, FOXP2 and DARPP32 staining was detected (DelliCarri *et al.* 2013). *In vitro* differentiation of LGE like progenitors generated using SHH (50ng/ml) and increasing dose of XAV-939 (0.25, 1 and 4 $\mu$ M), yielded striatal characteristics in XAV-939 dose dependent manner (Nicoleau *et al.* 2013). The best yield of MSNs was observed at 1 $\mu$ M XAV-939. After 45 days of differentiation in medium containing BDNF, cAMP and valproic acid (VPA), culture persisted expression of FOXP1 and expressed post mitotic markers MAP2 (~70%), alpha synuclein (SNCA) or synaptophysin (SYP). Robust maturation into MSN like neurons were evident; ~30% of MAP2<sup>+</sup> neurons co-expressed DARPP32, CTIP2, FOXP1 and DRD2 and ~25% of MAP2<sup>+</sup> neurons co-expressed Calbindin. The cultures were also immunoreactive for HuCD (~70%) of which ~5% co-expressed Calretinin (Nicoleau *et al.* 2013). *In vivo*, at 5 months post transplantation into QA lesioned rat, graft derived cells HNA<sup>+</sup> FOXP1<sup>+</sup> DARPP32<sup>+</sup> neurons co-expressed CTIP2 and FOXP1 (Nicoleau *et al.* 2013).

Differentiation of Activin A patterned progenitors, in media supplemented with BDNF and GDNF showed an increase in striatal markers (Arber *et al.* 2015). At day 36 of differentiation, there was an upregulation of *PPP1R1B* (*DARPP32*), *ARPP21* (cAMP regulated phosphoprotein), *CALBINDIN*, *PENK* (proenkeohalin), *TAC1* (tachykinin), *DRD2* and *GAD1* and downregulation of *TH* (tyrosine hydroxylase associated with dopamine neurons) (Arber *et al.* 2015). At protein level, there was 20 to 50% DARPP32<sup>+</sup> neurons, depending on cell line tested. All DARPP32<sup>+</sup> co-expressed MAP2, NeuN, PSD65 and CTIP2. A proportion of CTIP2<sup>+</sup> co-expressed Calbindin and all CTIP2<sup>+</sup> cells co-expressed GAD65/67 (*GAD2/1*) revealing GABAergic striatal projection neurons phenotype. A small number of TBR1<sup>+</sup>, SST<sup>+</sup> (somatostatin) were also detected (Arber *et al.* 2015). Furthermore, at 16 weeks post transplantation in rat HD model, graft derived cells exhibited GABA (86+4.6%) and DARPP32 (~50%) co-expressing HuNu. 43+11% and 35+8% of HuNu+ cells co-expressed FOXP2 and Calbindin respectively. There were also cells immunoreactive for substance P and DRD2 suggesting the presence of both direct and indirect pathway MSNs (Arber *et al.* 2015).

Table 1 hPSC directed differentiation protocols

References	Cell lines	Patterning using growth factors		In vitro differentiation			In vivo differentiation markers
		Neural Induction	LGE like Progenitor specification	Media supplements	Progenitor markers	Striatal neuron markers	
Arber <i>et al.</i> 2015	hESC (H1,H7 ,H9) hIPSC (2F8,4FH)	Noggin + SB431542 or Dorsomorphin/ LDN+ SB431542 in N2B27 media (DMEM-F12/Neurobasal (2:1)+ N2+B27 (-Retinoic acid))	Activin A in N2B27 media	BDNF + GDNF in N2B27 media	At protein level : NESTIN, FOXG1, OTX2, GSX2 <sup>+</sup> (55±10%), DLX2 <sup>+</sup> (25±12%), CTIP2 <sup>+</sup> (50±12%), FOXP1 <sup>+</sup> (16±6.7%), NOLZ1 <sup>+</sup> (16.7±1.7%) At mRNA level: <i>GSX2, DLX2, ASCL1, NOLZ1, EBF1, CTIP2</i>	At protein level : MAP2, NeuN, DARPP32 <sup>+</sup> (20-50%), CTIP2, SST <sup>+</sup> (<1%), CALBINDIN, GAD65/67, CR <sup>+</sup> (6±1.2%), TBR1 (10%) At mRNA level: <i>PPP1R1B, ARPP21, CALB, PENK, TAC1 DRD2, GAD1</i>	At protein level : GABA (86±4.6%), DRD2, SUBSTANCE P, PSD65, TBR1. And as a percentage of HuNu <sup>+</sup> cells (49±5%); DARPP32 <sup>+</sup> (49±5%), FOXP2 <sup>+</sup> (43±11%), CALB <sup>+</sup> (35±8%)
Nicoleau <i>et al.</i> 2013	hESC (H9, RC9) hIPSC (190c17)	Noggin + SB431542 or LDN+ SB431542 in N2B27 media	DKK1+ SHHC25II or XAV939+ SHHC25II in N2B27 media	BDNF + dbcAMP+ VPA in N2B27 media	At protein level : FOXG1 (78-90%), OTX2 (81±1%), GSX2 (~40-60%), NKX2.1 (~30%) CTIP2 (<10%) . At mRNA level: <i>FOXG1, SIX3, GSX2, DLX2, ASCL1, NKX2.1, MEIS2, LHX6</i>	At protein level : FOXG1 and as a percentage of MAP2 <sup>+</sup> (~70%); DARPP32 <sup>+</sup> (~30%), CALB <sup>+</sup> (~25%) And as % of HuCD <sup>+</sup> (~70%); Calretinin <sup>+</sup> (5%) At mRNA level: <i>MAP2, CTIP2, ARPP21, DARPP32, GAD1, CALB, DRD1,</i>	At protein level : FOXG1, CTIP2, DARPP32, D2DR, SubsP, FOXP1

						SubstP	
Aubry <i>et al.</i> 2008	hESC (SA-01, H9)	MS5 stromal co-culture	DKK1+ SHH in N2 medium	BDNF + dbcAMP+ VPA in N2 medium	At mRNA level: GSX2, DLX2	At protein level : PAX6 <sup>+</sup> (60%), NESTIN <sup>+</sup> (70%) and as % of MAP2 <sup>+</sup> (22±7%); DARPP32 <sup>+</sup> (53±6%), GABA <sup>+</sup> (36±2%), CALB <sup>+</sup> (10±2%), Calretinin <sup>+</sup> (55±7%) At mRNA level: <i>DARPP32</i> , <i>GAD67</i> and <i>CALB</i>	At protein level : HNA, MAP2, NeuN, DARPP32
Ma <i>et al.</i> 2012	hESC (H9, H1)	Serum free EB method	SHH or pumorphamine in N2 medium	VPA + BDNF + GDNF+ cAMP+ IGF1 in N2B27 medium	At protein level : MASH1, MEIS2 GSX2	At protein level : GABA <sup>+</sup> /MEIS2+/GAD65/67+ (90.2±4.2%) of which 89.7±9.3% DARPP32+	At protein level : GABA <sup>+</sup> MEIS2 <sup>+</sup> CTIP2 <sup>+</sup> DARPP32 <sup>+</sup> (58.6±3%), synaptophysin <sup>+</sup> MAP2 <sup>+</sup>
Delli Carri <i>et al.</i> 2013	hESC (H9, HS401) hIPSC (DF3F)	Noggin + SB431542 or Dorsomorphin + SB431542 in N2 media	DKK1+ SHHC25II in N2 medium	B27+ BDNF in N2 medium	At protein level : FOXG1 (58%), OTX2 (88%) PAX6 (64%) GSX2 (63.7±8%)	At protein level : βIII-tubulin <sup>+</sup> (17%), NESTIN <sup>+</sup> (7%), GFAP <sup>+</sup> (25%) and as a percentage of MAP2 <sup>+</sup> (50%); DARPP32 <sup>+</sup> (20%), GABA <sup>+</sup> (78%), CTIP2 <sup>+</sup> (60.3%) and CALB1 <sup>+</sup> (53%) CALB <sup>+</sup> /CTIP2 <sup>-</sup> (15.7%), Calretinin <sup>+</sup> (7%) and SST <sup>+</sup> (0.2%)	At protein level : FOXP1, FOXP2 and DARPP32

						At mRNA level: <i>ARPP21, DARPP32, ISL1, DRD1</i>	
Watanabe <i>et al.</i> 2007	hESC (KhES-1,2 and 3)	Serum free EB method	DKK1+SHH+Lefly A+ BMPRIAFc		At protein level : As a % of FOXG1 <sup>+</sup> (34%); PAX6 <sup>+</sup> (~20%), NKX2.1 <sup>+</sup> (~42%), $\beta$ -tubulin	Not tested	Not tested
Zhang <i>et al.</i> 2010	HD iPSC	EB method in 20% FBS media	DKK1+ SHH in N2 medium	BDNF + dbcAMP+ VPA in N2 medium	Not tested	At protein level : DARPP32 <sup>+</sup> (~10%), $\beta$ -tubulin, GABA and CALB	Not tested
Li <i>et al.</i> 2009	hESC (H9, H1)	Serum free EB method	DKK1+ SHH in N2 medium	VPA + BDNF + GDNF+ cAMP+ IGF1 in N2B27 medium	At protein level : FOXG1, NKX2.1, PAX6	At protein level : ISL1 (41%), $\beta$ III tubulin, MAP2, CTIP2(14%) GAD65/67, GABA DARPP32	Not tested
Jeon <i>et al.</i> 2012	HDiPSC 72 CAG	PA6 stromal co-culture followed by EB culture		BDNF in N2 medium		At protein level : OTX2+ (76.0+1.3%) FOXG1+ (38.4+3.4%), GSX2+ (28.8+2.8%), DLX2+ (34.1+4.5%), MAP2+ (89.1+5.5%) DARPP32+ (27.0+1.7%) CALB+ (19.1+2.1%) SYNAP+ (20+3.8%) GABA+ (75.1+2.2%)  NeuN+ (88%)	At protein level : NESTIN+ GABA+ DARPP32+ GAD65/67+

## 1.5 Small molecules mediated differentiation

Small molecules offer a powerful tool to target signalling pathways in a controlled manner to study the molecular mechanisms of differentiation. Small molecules can replace the expensive recombinant proteins and therefore are suitable for the development of chemically defined and cost effective culture conditions for generating clinical- grade hPSC derivatives. This thesis aims to use small molecules to direct hPSC differentiation. Here, I briefly introduce the small molecules used in this thesis and present the recent progress (other similar studies published during the period of my research) on the use of small molecules in neural induction and telencephalon/LGE specification

### 1.5.1 BMP Inhibitors

Dorsomorphin (6- [4- (2-Piperidin-1-ylethoxy) phenyl] -3-pyridin-4-ylpyrazolo [1,5-a] pyrimidine, also referred to as compound C) was the first identified small molecule inhibitor of BMP signalling (Figure 1:17A.1). Dorsomorphin was identified by screening a diverse chemical library that perturbed zebrafish embryo D-V axis formation. Dorsomorphin selectively inhibits BMP type I receptors ALK2, ALK3 and ALK6 and blocks BMP mediated SMAD 1/5/8 phosphorylation ( $IC_{50}=0.47 \mu M$ ) (Yu *et al.* 2008). Structure-activity relationship (SAR) studies of Dorsomorphin led to the discovery of more potent analogue LDN193189 (4(6-(4-(piperazin-1-yl) phenyl) pyrazolo[1,5-a] pyrimidin-3-yl) quinoline hydrochloride (Figure 1:17A.2), which like Dorsomorphin, inhibits BMP type I receptors ALK2 and ALK3 but at lower concentrations ( $IC_{50}=5nM$  and  $30nM$  respectively) (Cuny *et al.* 2008; Boergermann *et al.* 2010). At higher concentrations, both Dorsomorphin and LDN193189 were also shown to have “off target” effects against vascular endothelial growth factor (VEGF), Platelet-Derived Growth Factor Receptor- $\beta$  (PDGFR $\beta$ ) and BMP induced non-smad signalling such as p38 MAPK, Akt and ERK1/2 (Hao *et al.* 2010; Boergermann *et al.* 2010; Vogt *et al.* 2011). Another structural derivative of DM called, DMH1 (4-[6-[4-(1-Methylethoxy) phenyl] pyrazolo[1,5-a] pyrimidin-3-yl]-quinoline) (Figure 1:17A.3) specifically inhibits ALK2 receptor ( $IC_{50}=108nM$ ) and exhibits no detectable inhibition of AMPK, VEGFR-2 or PDGFR $\beta$  receptors (Hao *et al.* 2010).

During hPSC neural differentiation, Dorsomorphin, LDN193189 or DMH1 in combination with SB431542 generated PAX6<sup>+</sup> neuroectodermal cells to a level

comparable to Noggin treatment (Morizane *et al.* 2011; Surmacz *et al.* 2012; Neely *et al.* 2012; Nicoleau *et al.* 2013; Delli Carri *et al.* 2013; Arber *et al.* 2015) (Table 1).

### 1.5.2 WNT inhibitors

XAV939 (3,5,7,8-Tetrahydro-2-[4-(trifluoromethyl)phenyl]-4*H* thiopyrano [4,3-*d*] pyrimidin-4-one) (Figure 1:17 B.1) identified through a chemical genetic screen was found to antagonize WNT/  $\beta$ -catenin mediated transcription by directly binding to Tankyrase (TNKS) (IC<sub>50</sub>=4-11nm) (Huang *et al.* 2009). Another inhibitor, IWR-1-endo (4- (1,3,3a,4,7,7a-Hexahydro-1,3-dioxo-4,7-methano-2*H*-isoindol-2-yl)-N-8-quinolinyl-Benzamide), (inhibitors of Wnt response-1, referred to as IWR-1), (Figure 1:17 B.2) was identified through cell based screening from a synthetic chemical library and was shown to block Wnt-stimulated transcriptional response in reporter assays (IC<sub>50</sub>=180nm). IWR1 induced an increase in Axin2 protein level at least in part through TNKS1 and S2 inhibition and promoted  $\beta$ -catenin destruction by promoting the stability of Axin-scaffolded destruction complexes (Chen *et al.* 2009; Huang *et al.* 2009). KY02111 (*N*-(6-Chloro-2-benzothiazolyl)-3, 4-dimethoxy-benzenepropanamide) (Figure 1:17 B.3) another potent inhibitor was discovered in hPSC-based screening. KY02111 treatment dose dependently inhibited TCF reporter activity and induced downregulation of WNT target genes possibly by acting downstream of APC and GSK3 $\beta$  in  $\beta$ -catenin destruction complex, a manner distinct from XAV939 and IWR-1 (Minami *et al.* 2012).

During hPSC differentiation, XAV939 (0.25 to 4  $\mu$ M) was able to replace DKK1 and induced *FOXL1* and *SIX3* expression (Nicoleau *et al.* 2013; Maroof *et al.* 2013). In addition, XAV939 treatment dose dependently enhanced SHH mediated ventralization with upregulation of ventral markers (Nicoleau *et al.* 2013) (explained previously in 1.4.). Use of IWR-1 and KY02111 specifically for telencephalon induction has not been reported yet.

### 1.5.3 SHH agonists

Small molecule modulation of receptor Smoothened activation by Purmorphamine or SAG has been demonstrated to activate Hh signalling and replace SHH protein. Purmorphamine (9-Cyclohexyl-*N*-[4-(4-morpholinyl)phenyl]-2-(1-naphthalenyloxy)-9*H*-purin-6-amine) (Figure 1:17 C.1) was originally identified through high-throughput cell based screening as an osteoblast inducing agent (Wu *et al.* 2002). Purmorphamine directly binds and activates SMO (EC<sub>50</sub>=1 $\mu$ M) and

modulates its effects through upregulation of Hh pathway downstream members Gli and Patched (Sinha and Chen 2006). SAG (N-Methyl-N'-(3-pyridinylbenzyl)-N'-(3-chlorobenzo[b] thiophene-2-carbonyl)-1,4-diaminocyclohexane) (Figure 1:17 C.2) is a synthetic chlorobenzothiophene-containing compound which acts binding to SMO (EC50= 0.03 $\mu$ M), but inhibits Hh signalling at >1 $\mu$ M (Chen *et al.* 2002).

During human striatal line STROC05 neuronal differentiation, Purmorphamine at 1.0 $\mu$ M increased DARPP32<sup>+</sup> MSNs (El-akabawy *et al.* 2011). In hPSC models of telencephalon development, PM at 0.65 $\mu$ M concentration induced MEIS2<sup>+</sup>, ASCL1<sup>+</sup> LGE-like progenitors, which differentiated into DARPP32<sup>+</sup> MSNs (Ma *et al.* 2012). At higher concentrations, Purmorphamine alone at 2 $\mu$ M or at 1.0 $\mu$ M in combination with dual smad inhibition (SB431542+LDN193189) and Wnt inhibition (XAV 939), induced MGE progenitors with upregulation of *NKX2.1*, *NKX6.2*, *GSX2*, *DLX2*, *OLIG2*, and *LHX6* which differentiated into GABAergic cholinergic neurons and cortical interneurons (Nat *et al.* 2012; Maroof *et al.* 2013). Similarly, SAG at 0.01- 0.1 $\mu$ M dose dependently induced MGE progenitors at the expense of LGE fate and generated GABAergic interneurons (Kim *et al.* 2014)

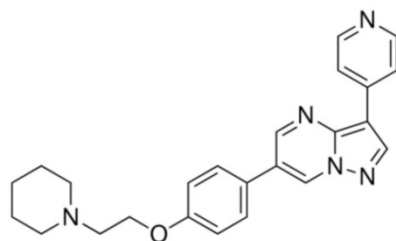
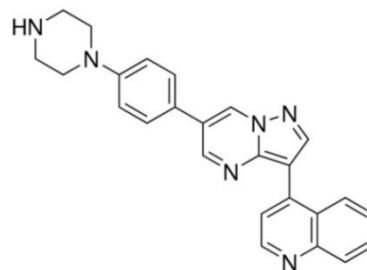
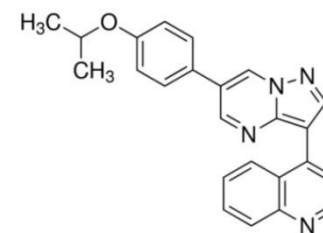
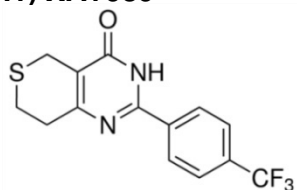
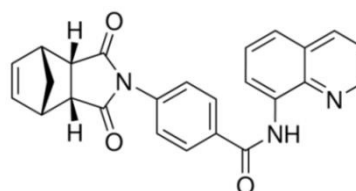
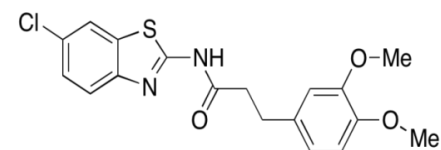
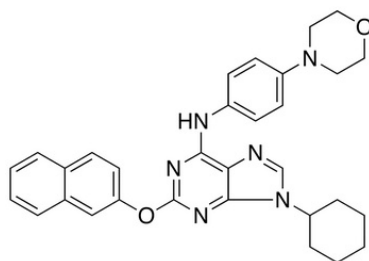
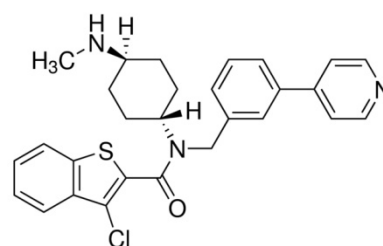
**A.1) Dorsomorphin****A.2) LDN193189****A.3) DMH1****B.1) XAV939****B.2) IWR-1****B.3) KY02111****C.1) Purmorphamine****C.2) SAG**

Figure 1:17 Structure of small molecules.  
A) Inhibitors of BMP signalling- A.1) Dorsomorphin, A.2) LDN193189, A.3) DMH1.

B) Inhibitors of WNT signalling- B.1) XAV939, B.2) IWR-1, B.3) KY02111.

C) Agonists of Hh signalling- C.1) Purmorphamine, C.2) SAG

## 1.6 Aims of the thesis

The generation of neuronal progenitors from hPSCs by directed differentiation offers significant opportunities for *in vitro* disease modelling and regenerative medicine. This thesis will focus on understanding the mechanisms underlying the generation of LGE-like progenitors from hPSC that are of direct relevance to HD. To achieve this, the insight from neural developmental biology will be applied and the timing and the context of developmental signals will be studied using small molecules. The stages of neuronal differentiation will be characterized for molecular markers at mRNA and protein levels.

The sequential stages of neuronal differentiation and thesis chapters focus are outlined in Figure 1:18. Chapter 3 addresses neural induction and investigates the effect of BMP inhibition by DM, LDN or DMH. Chapter 4 addresses forebrain specification and investigates the role of WNT inhibition by IWR or KY. Chapter 5 address ventral forebrain specification and investigates the role of SHH activation by PM or SAG. Following this, in chapter 6 the neuronal progenitors are differentiated *in vitro* and neurons are characterized for a striatal phenotype.

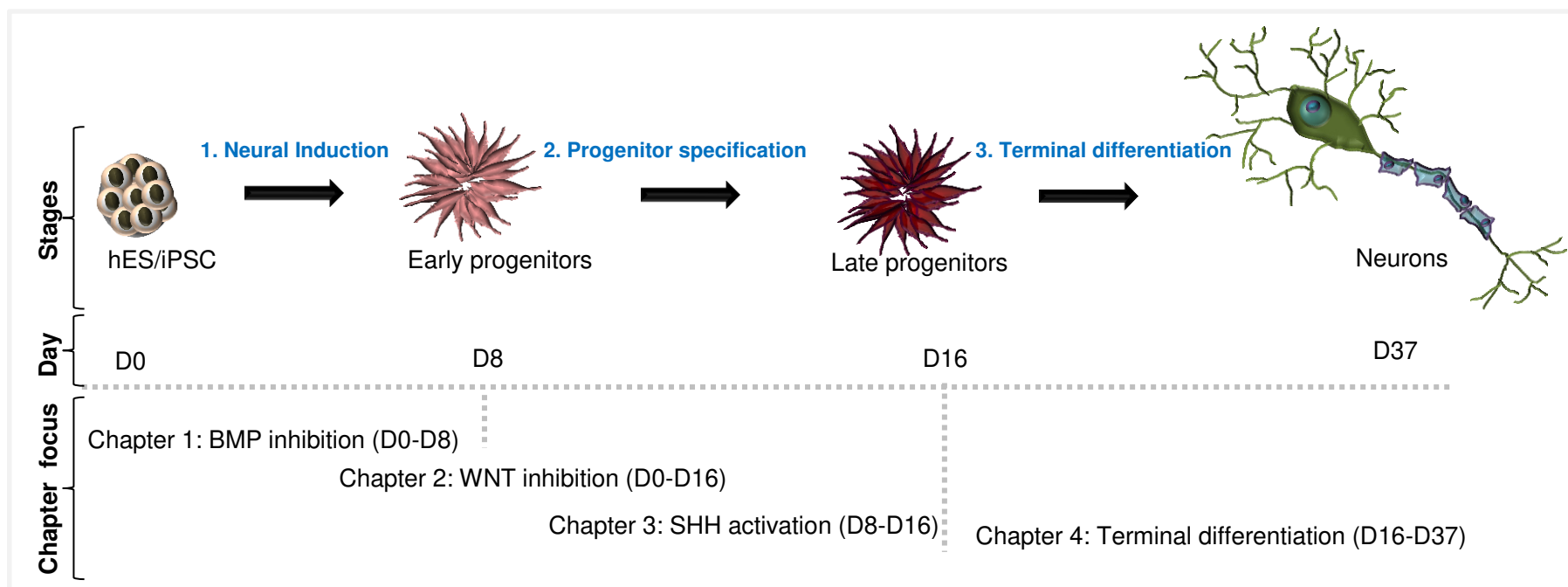


Figure 1:18 Thesis outline: hPSC are directed to differentiate into MSN like phenotype through sequential steps- Neural Induction, progenitor specification and terminal neuronal differentiation. The thesis chapter focuses on temporal integration of signalling pathways- BMP inhibition in chapter 3, WNT inhibition in chapter 4, SHH activation in chapter 5. Following which in chapter 6, the differentiated neurons are analysed for a striatal like phenotype

## 2. Materials and Methods

This chapter details the materials and *in-vitro* methodologies for the maintenance and directed neural differentiation of the human embryonic (hES) and induced pluripotent stem cells (hiPSc) as well as the molecular methods for the analysis of gene expression at mRNA and protein levels

### 2.1 *In-vitro* Methods

Initially during my project, the hESc were grown and maintained in hES medium containing serum replacement on a layer of mitotically inactivated mouse embryonic fibroblast (MEF). Later during the project, this feeder-based undefined culture containing xenogeneic elements was replaced with commercially available mTeSR1 medium and matrigel substrate for a standardized and better-defined culture condition.

Neural differentiation of hESC was achieved initially in the project, by embryoid body (EB) culture in which hESC aggregates were grown in suspension. EBs were then attached to poly-L-Lysin and Laminin coated plates to expand the neural progenitors. The EB culture system provides the advantage of mimicking *in vivo* embryonic developmental process to some extent. However, the heterogeneous size of EBs, difficulty in culture maintenance due to EBs sticking together and low yield of neural progenitors were problematic for studies to analyse the effect of different small molecules modulators of signalling pathways. So later in the project, EB culture conditions were adapted to an adherent monolayer small molecule based protocol, where hPSCs were grown on matrigel coated plate for early differentiation of neural progenitors and then onto poly-D-lysine and matrigel coated plates for their terminal differentiation.

Unless stated otherwise, all cell culture reagents and all tissue culture plates were purchased from Life technologies, Paisley, UK and Fisher Scientific, Loughborough, UK, respectively. All cells were grown at 37<sup>0</sup>C in 95% air, 5% CO<sub>2</sub> incubator (Binder, Germany). More information on materials and equipment including suppliers and catalogue numbers are listed in section 2.4

## **2.1.1 Derivation, Mitotic inactivation and Cryopreservation of mouse embryonic fibroblasts**

### *2.1.1.1 Derivation of primary culture*

Mouse embryos (Bl6 or 129sv genetic background) were harvested at 12.5 days post-coitum from timed matings. After removing head and all internal organs, embryos were transferred to a dry sterile 90mm Sterilin culture dish, washed twice with 10ml phosphate buffered saline (PBS) pH 7.4 and minced using a sterile scalpel blade. The minced tissues were collected in a 50ml falcon and incubated with collagenase type IV (at a concentration of 2mg/ml in pre-warmed medium and filtered using 0.2µm syringe filter (Fisher Scientific)) for 20 minutes at 37<sup>0</sup>C. Using a 10ml serological pipette (Sigma-Aldrich, Dorset, UK), the cells were pipetted vigorously up and down to acquire a cell suspension and centrifuged at 3000 rpm for 5min. The cell pellet was re-suspended in mouse embryonic fibroblast medium (MEF medium) consisted of Dulbecco's Modified Eagle Medium (DMEM) supplemented with 10% foetal bovine serum (FBS) and 1% Antibiotic/Antimycotic solution and plated at a ratio of 2embryos/144mm Nunc plate. This was labelled as passage 0 (MEF-P0). Cultures were fed daily

### *2.1.1.2 Propagation of MEF culture*

P0 cultures were passaged upon reaching 80% confluency. For passaging, the media was aspirated off, cells were washed once with 10ml PBS per plate and incubated with 0.05% Trypsin-EDTA (5ml/plate) for 5 min at 37<sup>0</sup>C in 5%CO<sub>2</sub> incubator. Trypsin-EDTA was inactivated by adding double the amount of MEF medium and the cells were harvested to a 50ml falcon and centrifuged at 3000rpm for 5 min. The cell pellet was re-suspended in fresh MEF medium and plated at 1:5 ratio (i.e., cells from 1 plate were plated into 5 plates). The cells were labelled as MEF-P1. Cultures were fed daily. MEF-P1 cultures were passaged and maintained until P3. Cultures were terminated at P3

### *2.1.1.3 Mitotic inactivation of MEF with $\gamma$ -irradiation*

MEF cultures were irradiated upon reaching 80% confluency. MEF cultures at P1 to P3 were used to generate irradiated MEF (MEFi) stocks. For irradiation, cells were harvested from culture dishes using 0.05% Trypsin-EDTA as

described above and cell pellet was re-suspended in 20ml MEF media in a 50ml falcon. The cells were irradiated for 30 min at 216 rad/min for total of 6480 rad.

#### 2.1.1.4 Freezing inactivated MEF

For freezing, the cell suspension after irradiation was centrifuged at 3000rpm for 5 min. The cell pellet was re-suspended in freezing medium consisted of MEF medium with 10% dimethyl sulfoxide (DMSO) (Sigma-Aldrich). Cell count was performed using haemocytometer as described below. Cells were frozen at  $1-2 \times 10^6$  cells/1ml cryovial (VWR, Leicestershire, UK) in 1ml freezing media. These cells were labelled as MEFi. The vials were placed in -80 freezer overnight in cryochamber Mr.Frosty (Fisher scientific) containing isopropanol for a cooling rate of 1°C per minute. The next day, vials were transported to liquid nitrogen dewar.

### 2.1.2 Cell count using Haemocytometer

To determine viable cell count, dye exclusion method was performed, for which single cell suspension was mixed with 0.4% Trypan Blue solution (Sigma-Aldrich) at a ratio of 1:1. The haemocytometer and glass slide (Fisher scientific) were cleaned with distilled water and ethanol. 10µl of the cell-trypan blue suspension was pipetted into the space between hemocytometer and glass slide and was viewed under microscope. Viable cells being impermeable would appear colorless whereas permeable dead cells would appear blue. The viable cells in the centre square of the haemocytometer were counted. The total number of viable cells/ml was calculated using the formula:

Total number of cells= Cell count  $\times 10^4$   $\times$  dilution factor, where  $10^4$  is the volume of small square in the haemocytometer calculated by multiplying the width by the height (1mm each) by the depth (0.1mm each).

### 2.1.3 hES culture and maintenance on MEFi feeder layers

#### 2.1.3.1 Preparation of MEFi feeder layers

For generating feeder layers, 6cm,Nunc culture plates were coated with 0.1% gelatin (2ml/plate) (Merck Millipore,UK) for 1 hour in incubator. The MEFi frozen vial after spraying thoroughly with 70% ethanol was transported to Class II safety cabinet and was thawed by dropwise addition of 1ml pre-warmed MEF media. The semi-thawed cell suspension was transferred to a 15ml falcon containing 4ml

media and was centrifuged at 1000rpm for 3 min. The cell pellet was re-suspended in fresh MEF medium and cells were plated at a cell density  $250 \times 10^3$  cells/6cm gelatin-coated plate. MEFi plates was used upto 5 days for maintaining hES cells.

#### 2.1.3.2 Maintenance of hES colonies

Human ES cells (H9, WiCell Research Institute) were maintained on MEFi feeder layers in hESC complete medium which consisted of knock-out DMEM (KO-DMEM) supplemented with 15% Knock-out serum replacement (KSR), 1% MEM non-essential amino acids, 1% 200mM L-glutamine, 1% Penicillin-streptomycin, 0.1mM  $\beta$ -mercaptoethanol and Fgf2 (Peprotech, London, UK) at final concentration of 10ng/ml. hESs were passaged every 3-4 days. For passaging, the culture medium was aspirated off, cells were washed with PBS and incubated with Collagenase type IV (at a concentration of 1mg/ml in KO-DMEM and filtered before use) and 10 $\mu$ M/ml rock inhibitor for 25 min at 37<sup>0</sup>C in 5%CO<sub>2</sub> incubator until the colony edges began to lift. The culture plate was gently tapped and colonies were lifted off by addition of hES medium using a P1000 gilson. The colonies were harvested to 15ml falcon and centrifuged for 3 min at 1000 rpm. The cell pellet was re-suspended in 200ul hES medium and was broken down into smaller clumps using P200 gilson. hES complete medium with Fgf2 for plating was then added. Y-27632 dihydrochloride, the Rho kinase inhibitor (Rock inhibitor) (Abcam, Cambridge,UK) at a concentration of 10 $\mu$ M/ml was added in the media on the day of passaging. To prepare feeder plates, medium from MEFi feeder plates was aspirated off before washing with PBS. H9 cell clumps were then plated onto these feeder layers at 1:4 ratio (i.e., cells from 1 plate were plated to 4 plates) and maintained in hES complete medium. The media was replaced daily.

#### 2.1.3.3 Freezing and Thawing hES colonies

For freezing, H9 colonies were harvested using Collagenase as described above. The cell pellet was re-suspended gently without breaking the colonies much, in freezing media consisted of 10% DMSO in FBS plus 10 $\mu$ M/ml rock inhibitor. The cryovials were placed in Mr.Frosty overnight before placing in liquid N<sub>2</sub> dewar. hES from at 1 x6cm plate was frozen into 1 cryovial.

hESc was thawed by drop wise addition of hES medium and care was taken to maintain the colonies intact. Following centrifugation at 1000 rpm for 3 min,

cell pellet was re-suspended in hES complete medium with 10ng/ml FGF-b. Cells from 1 cryovial was plated onto 3x6cm MEFi feeder layers. 10 $\mu$ M/ml Rock inhibitor was supplemented in the media on the day of thawing. Cultures were fed daily and were passaged at 3-4 days after thawing as described above.

#### **2.1.4 hPSC culture and maintenance on Matrigel in mTeSR<sup>TM</sup>1**

##### *2.1.4.1 Coating plates with Matrigel*

BD Matrigel<sup>TM</sup> (VWR) was thawed overnight at 4<sup>0</sup>C and aliquots volumes between 275-350 $\mu$ l as per dilution factor in the data sheet provided for each batch was frozen at -20<sup>0</sup>C. On the day before plating hPSCs, aliquot was thawed overnight at 4<sup>0</sup>C .On the day of plating, one aliquot was added to 25ml cold KO-DMEM in a 50ml falcon and used immediately to coat plates (1ml/well for 6 well plate, nunc and 2ml per 6cm plate, nunc). Coated plates were incubated at 37<sup>0</sup>C in 5%CO<sub>2</sub> incubator for at least 1 hour and matrigel was removed just prior to plating down the cells

##### *2.1.4.2 Preparation of mTeSR media*

mTeSR1 media (Stem cell Technologies, Manchester, UK) was prepared as per manufacturer's instructions. Briefly, to prepare mTeSR1 complete media, 5x supplement provided in the kit thawed overnight at 4<sup>0</sup>C and 1% Penicillin-streptomycin were added to the basal media. The complete media was aliquoted into 50ml falcons and froze at -20<sup>0</sup>C. On the day before cell plating, aliquot was thawed overnight at 4<sup>0</sup>C.

##### *2.1.4.3 Maintenance of hPSC colonies*

hPSCs (H9, passage 40-60 ,WiCell Research Institute) and hiPSC (34D6, passage 20-35, kind gift of Prof. Siddharthan Chandran, Edinburgh,UK and generated as previously described Bilican *et al.*, 2012) were maintained on matrigel coated 6cm nunc plates in mTeSR<sup>TM</sup>1 complete media. hPSCs were passaged every 4-5 days using dispase (1ml/6cm plate of 1mg/ml solution) (Stem cell Technologies) with 10 $\mu$ M/ml rock inhibitor for 20 min at 37<sup>0</sup>C in 5%CO<sub>2</sub> incubator. After 20min, dispase was aspirated off. Cells were washed once with KO-DMEM to dilute away any residual dispase. hPSC colonies were detached from culture dish by addition of KO-DMEM using a P1000 gilson, transferred to a 15ml falcon and centrifuged at 1000 rpm for 3

min. The cell pellet was re-suspended in 200ul mTeSR medium to break down the colonies into smaller clumps. The required amount of mTeSR complete medium with 10µM/ml rock inhibitor was added. Rock inhibitor was supplemented in the media only on the day of passaging. The cells were plated onto matrigel coated dishes at 1:5 ratio. Cultures were fed daily.

#### 2.1.4.4 Freezing and Thawing hPSCs

hPSC colonies were harvested using dispase as described above. The cell pellet was re-suspended taking care to maintain the colonies intact in Cryostor™ CS10 supplemented with 10µM/ml rock inhibitor. Colonies from 1x6cm plate was frozen into 1 cryovial.

Frozen hPSCs were thawed by dropwise addition of 1ml pre-warmed mTeSR1 media, transferred rapidly as semi-thawed cell suspension to 15ml falcon containing 4ml media and centrifuged at 1000rpm for 3 min. The cell pellet was re-suspended in fresh mTeSR™1 medium and plated onto matrigel coated dishes. hPSCc from 1 cryovial was plated onto 2x6cm plates. Cultures were fed daily and passaged 4 days after thawing

#### 2.1.5 Mycoplasma testing of hPSCs

Mycoplasma being a common contaminant of eukaryotic cell cultures, cell cultures were routinely analysed by MycoProbe™ Mycoplasma Detection Assay (R&D systems, Abingdon, UK). This colorimetric assay detects the presence 16S ribosomal RNA (rRNA) of the eight most common species of mycoplasma contaminants through an enzyme linked substrate reaction assay.

For the assay, all the microplates and reagents provided in the kit (cell lysis diluent, capture and detection probes, wash buffer, substrate solution, amplifier solution and positive control) were prepared to working concentration as per kit instructions.

Cell culture supernatant samples were prepared by dilution in the lysis buffer provided in the kit. All samples were done in duplicates. The lysed samples were stored on ice or at -20°C for use at a later time. For the assay, samples alongside with positive and negative control samples were hybridized with biotin-labelled capture oligonucleotide probes and digoxigenin-labeled detection probes targeted to 16S rRNA. This hybridisation solution was transferred to streptavidin microplate to

capture rRNA/probe. Following washes to remove unbound material, an anti-digoxigenin alkaline phosphatase conjugate was added. The substrate solution followed by amplifier solution was added. The colour would develop in proportion to the amount of mycoplasma. The colour development was stopped by addition of stop solution and the intensity of colour was measured using a microplate reader set to 690nm (Fluro Optima, BMG lab tech). The average optical density (OD) of negative control was subtracted from all average OD values of all samples. The calculated value below 0.05, in the range 0.05-0.10, above 0.1 was taken as negative, suspect and positive respectively as per kit instructions

### **2.1.6 Alkaline phosphatase staining of hPSCs**

For quick routine characterization of undifferentiated hPSCs, Alkaline phosphatase (AP), a membrane marker of undifferentiated hPSC was detected using NBT/BCIP substrate (Sigma-Aldrich). Cells were grown in 6 well plate. The media was aspirated off and cells were washed with PBS containing  $\text{Ca}^{2+}$  and  $\text{Mg}^{2+}$  (PBS  $\text{Ca}^{2+}\text{Mg}^{2+}$ ). The cells were fixed with freshly made 4% ice-cold paraformaldehyde (4% PFA) (Sigma-Aldrich) for 20 min at 4°C. Following three times washes with PBS  $\text{Ca}^{2+}\text{Mg}^{2+}$ , the cells were incubated with NBT/BCIP substrate (1ml/well, 6 well plate) for 30 min in dark. The cells were washed with PBS  $\text{Ca}^{2+}\text{Mg}^{2+}$  and viewed under bright field microscope. The undifferentiated hPSC colonies expressing AP would appear as purple red colonies whereas differentiated colonies would appear colourless.

### **2.1.7 hPSC neural differentiation**

#### *2.1.7.1 Embryoid body differentiation*

H9 ESC colonies grown on MEFi were harvested using collagenase as described above. The colonies were re-suspended in chemically defined medium, (ADF+ medium) consisted of advanced DMEM/F12, supplemented with 1% Penicillin-streptomycin, 1% 2mM L-glutamine, 1% lipid concentrate, 12.5mg/ml transferrin (final concentration of 150 $\mu\text{g}/\text{ml}$ ), 10mg/ml Insulin (final concentration 14 $\mu\text{g}/\text{ml}$ ) and 0.1mM  $\beta$ -mercaptoethanol. Colonies were chopped to 150 $\mu\text{M}$  fragments using tissue chopper and plated on untreated bacteriological grade sterlin culture dish as floating aggregates. This was referred to as day 0 of differentiation (D0). The colonies from 2 x 6cm nunc dishes were plated onto 1 x10cm sterlin dish. Half media change was performed every other day by swirling the plate to bring the embryoid

bodies (EB) to the middle of the plate and carefully taking off half media and adding fresh media.

To analyse the effect of SMAD pathway modulation, the medium was supplemented with small molecule modulators of the pathway from D0 of differentiation. SB431542 was re-suspended in ethanol and used at 10 $\mu$ M until D4. Recombinant protein Noggin was re-suspended in PBS+0.1% BSA and used at 300ng/ml until D8. To replace Noggin with small molecules Dorsomorphin, LDN193189 or DMH1, were re-suspended in DMSO and used at 0.25,0.5 and 1 $\mu$ M.

On D8, EBs were plated down to expand as monolayer adherent neural progenitor cultures. 13mm glass coverslips (VWR) was first coated with poly-L-Lysin (PLL) (Sigma) at a concentration of 10 $\mu$ g/ml in PBS Ca<sup>2+</sup>Mg<sup>2+</sup> for at least 1 hour. Following washes with PBS, they were allowed to air dry overnight in the safety cabinet. On the day of cell plating, the PLL-coated coverslips were coated with 80 $\mu$ l of Laminin at a concentration of 10 $\mu$ g/ml in distilled water for at least 1 hour. Laminin was removed prior to plating down cells without letting coverslips to dry off.

D8 embryo bodies were collected in 15 falcon and centrifuged at 500 rpm for 2 min. For plating, EBs were dissociated into single cells by incubating EBs with Stempro accutase containing 10 $\mu$ M rock inhibitor for 20 min at 37<sup>0</sup>C, followed by triturating the cells gently using P1000 gilson. The cell suspension was spun at 1000 rpm for 3 minutes and the cell pellet was re-suspended in ADF+ medium. Cell count was performed using haemocytometer and cells were plated as 80 $\mu$ l droplet at a density 50x10<sup>3</sup> cells per PLL/Laminin coated coverslip placed in the bottom of 24 well plate. The cells were allowed to adhere for an hour at 37<sup>0</sup>C and then 500 $\mu$ l of medium was added to each well. For some of the experiments, ADF+ medium was supplemented with small molecules between D8 and D16 to analyse their effects on neural progenitor cultures.

#### 2.1.7.2 Monolayer differentiation

For monolayer differentiation, hPSCs were plated in mTeSR1 on matrigel coated 6cm nunc plate. On day 2 post-plating when the plate reached 60-70% confluency, the mTeSR1 media was replaced with SLI medium (4ml/6cm nunc plate) which consisted of advanced DMEM/F12 supplemented with 2% NeuroBrew21 without retinoic acid (Miltenyi, Surrey, UK), 1% 200mM L-glutamine, 1% Penicillin-streptomycin, 10 $\mu$ M SB431542 and 1 $\mu$ M LDN 193189 (both from CHDI, Los

Angeles, USA). This was labelled as D0 of differentiation. The media was changed daily. On D4 of differentiation when cells were fully confluent, they were passaged at a ratio of 1:2. Cells were pre-treated with 10  $\mu$ M rock inhibitor for an hour and incubated with stempro accutase (2ml/6cm plate) containing 10 $\mu$ M rock inhibitor for 5 minutes at 37<sup>0</sup>C. By addition of some culture media, the cells were harvested to 15 ml falcon and spun at 1000rpm for 3 minutes. The cell pellet was re-suspended in SLI media with 10 $\mu$ M rock inhibitor and plated at 1:2 ratio onto matrigel coated 6cm nunc plates. The medium was replaced daily. On D8 of differentiation, cultures were passaged again as above. The cells pellet were re-suspended in LI medium which consisted of advanced DMEM/F12 supplemented with 2% NeuroBrew21 without retinoic acid, 1% 200mM L-glutamine, 1% Penicillin-streptomycin, and 0.25  $\mu$ M LDN 193189.

For studies on neural patterning, cells were plated onto matrigel coated coverslips placed in the bottom of 24 well plate. SLI and LI medium was supplemented small molecules to analyse their effect. All small molecules were re-suspended in DMSO. IWR1 was added either at D0 or D8 until D16 at 0 to 10  $\mu$ M concentration. KY02111 was added at D0 until D16 at 0 to 10  $\mu$ M concentration. Purmorphamine was added at D8 until D16 at 0.5 to 1 $\mu$ M concentration. SAG was added at D8 until D16 at 0.001 to 0.1 $\mu$ M concentration. Activin A was added at 20ng/ml at D8

#### *2.1.7.2.1 Terminal differentiation of neural progenitors*

13mm glass coverslips (VWR) were treated with nitric acid (Sigma-aldrich) overnight in 50ml falcon on rocker (Stuart mini see saw rocker, Bibby Scientific Ltd., Staffordshire, UK) at room temperature. Following 5 washes in distilled water and final wash in absolute ethanol, the coverslips were spread in a glass petridish and baked overnight at 150<sup>0</sup>C in oven (Swallow, LTE Scientific Ltd., Lancashire, UK). Baked coverslips were placed in the bottom of 24 well plates using ethanol and flame-sterilized tweezers. Coverslips were first coated with 80 $\mu$ l of 100 $\mu$ g/ml poly-D-lysine (PDL) (Sigma-aldrich), in borate buffer pH 8.4 for about an hour at room temperature and then washed 3 times with sterile water and air dried. Then the coverslips were coated with 50 $\mu$ l matrigel for an hour at 37<sup>0</sup>C. Immediately prior to plating down the cells, the matrigel was removed

For terminal neural differentiation, D16 neural progenitors were harvested using accutase as described above. The single cell suspension was re-suspended in SCM1 medium which consisted of advanced DMEM/F12 supplemented with 2% NeuroBrew21 with retinoic acid (Miltenyi), 1% 200mM L-glutamine, 1% Penicillin-streptomycin, 2 $\mu$ M CDK4/6 inhibitor PD0332991 (CHDI), 10 $\mu$ M  $\gamma$ -secretase inhibitor DAPT (CHDI), 10ng/ml brain-derived neurotrophic factor (BDNF) (Miltenyi), 10 $\mu$ M adenylate cyclase activator Forskolin (CHDI), 3 $\mu$ M glycogen synthase kinase-3 (GSK3) inhibitor CHIR 99021 (CHDI), 300 $\mu$ M  $\gamma$ -amino butyric acid (GABA)(Tocris, Oxfordshire, UK), 1.8mM CaCl<sub>2</sub> (Sigma-aldrich) and 200 $\mu$ M Absorbic acid (Sigma-aldrich)). Cell count was performed using haemocytometer and cells were plated at density of 50x10<sup>3</sup> cells/PDL-matrigel-coated coverslip in 80 $\mu$ l droplet in SCM1. Cells were allowed to adhere for an hour at 37<sup>0</sup>C and then 500 $\mu$ l SCM1 was added to each well. A 50% media change was performed on 2nd and 5th day after plating i.e., on D18 and D21 of differentiation. At 1 week i.e., on D23, SCM1 was 100% replaced with SCM2 which consisted of 1:1 advanced DMEM/F12: neurobasal A medium supplemented with NeuroBrew21 with retinoic acid, 1% 200mM L-glutamine, 1% Penicillin-streptomycin,, 2 $\mu$ M PD0332991, 10ng/ml BDNF, 3 $\mu$ M CHIR 99021, 1.8mM CaCl<sub>2</sub> and 200 $\mu$ M absorbic acid. Cells were maintained in SCM2 for 3 weeks i.e., until D37 with 50% media change at every 3rd day

## 2.2 Molecular Methods

### 2.2.1 Detection of gene expression at mRNA level

#### 2.2.1.1 RNA extraction and quality check

RNA was extracted using RNAeasy mini kit, QIAshredder spin columns and RNase-free Dnase set (all from Qiagen, Hilden, Germany). First, the cell culture medium was aspirated off and cells were washed with PBS once. The workbench, all surfaces and pipettes for RNA extraction were cleaned with RNase zap. The RNA extraction reagents were prepared as per the kit instructions. The cells were lysed and simultaneously homogenized directly in the cell culture plate using RLT buffer; a highly denaturing guanidine-thiocyanate-containing buffer that immediately inactivates RNases. As per kit instruction, 350 $\mu$ l RLT buffer was used for <5x10<sup>6</sup> cells and lysate harvested to eppendorf and vortexed. The lysate at this stage could be stored in -80<sup>0</sup>C for months. Frozen lysate was thawed at 37<sup>0</sup>C in water bath for approximately 2 minute until completely thawed. The samples were homogenized further using

QIAshredder spin columns. Homogenization shears high molecular weight genomic DNA and cellular components that may otherwise cause clogging of columns and inefficient binding of RNA to RNeasy spin column. Thawed lysate was loaded onto QIAshredder column placed in a 2ml collection tube and spun at 13000 rpm for 2 minute. 1 volume of 70% ethanol was then added to the homogenized lysate and mixed well by pipetting. Ethanol promotes appropriate binding conditions. The whole sample was then transferred to RNeasy spin column placed in a 2ml collection tube and spun as above. The total RNA binds to the silica-based membrane of the column. RNeasy technology removes most of the DNA. However, further DNA removal was achieved using RNase-free DNase I as per kit instruction. The DNase was removed in subsequent wash steps as per kit instructions using the provided buffers. Finally, RNA was eluted into 30µl RNase free water.

The amount and quality of RNA was determined using Nanodrop ND1000 spectrophotometer (Labtech international, Uckfield, UK). The ratio of absorbance at 260nm and 280nm, A<sub>260</sub>/A<sub>280</sub> for pure RNA is ~ 2. Contamination from any residual buffers or reagents alters this ratio

#### 2.2.1.2 C-DNA synthesis

RNA extracted was used on the same day of extraction for C-DNA synthesis. RNA concentration from 250ng to 1000ng was transcribed. The same RNA concentration was used in every sample in an experiment. The required amount of RNA was pipetted out into PCR tubes. For the first strand synthesis, the following reagents were added into each PCR tube

Random primers (1/12 dilution of 3µg/ml)	1µl
10mM dNTPs	1µl
Water to make upto 12µl	Xµl
(all from <i>Life Technologies</i> )	

The mix was then incubated at 65<sup>0</sup>C for 5 minutes. Following a brief chill on ice and a quick spin, the following reagents were added

5x first strand buffer	4µl
0.1M DTT	2µl
RNase Out Rnase Inhibitor	1µl
(all from <i>life technologies</i> )	

The mix was then incubated at 25<sup>0</sup>C for 2 minutes. Finally, 1µl of Superscript II reverse transcriptase (Life technologies) was added and incubated at 25<sup>0</sup>C for 10 minutes, then 42<sup>0</sup>C for 50 minutes and then 70<sup>0</sup>C for 15 minutes. For every C-DNA synthesis reaction, a minus RT reaction, i.e., a sample without any superscript II reverse transcriptase was also set. The C-DNA could be stored in -20<sup>0</sup>C for months. The C-DNA samples were used for qPCR reactions

### 2.2.1.3 Quantitative Real-time polymerase chain reaction( QRT-PCR)

Real time detection of PCR products were achieved using fluorescent based DyNAmo HS SYBR Green qPCR kit (Fisher scientific) which contains Hot-Start DNA Polymerase, SYBR Green I, PCR buffer, MgCl<sub>2</sub>, dNTPs and dUTP. SYBR Green I fluoresces when bound to double-stranded DNA (dsDNA). When free in the reaction mix, SYBR Green I exhibits little fluorescence and as dsDNA is generated during PCR cycles, it gives upto a 1000 fold increase in fluorescence. The dye emits at 520nm and overall fluorescent signal which is proportional to the amount of dsDNA generated as the target is amplified, can be detected

For QPCR reaction, the C-DNA and minus RT samples were diluted in water. If 1µg RNA was used for reverse transcriptase reaction, C-DNA was diluted at 1:20 and 1µl was used per well,96 well plate (optical plate, Life technologies) for QPCR reaction. Each biological C-DNA sample was prepared in 3 replicate wells and each reaction mix contained,

C-DNA1:20	1µl
Sybergreen mastermix	10µl
Forward and reverse primers, 10pmol	1µl
Water ( <i>Life technologies</i> )	8µl

Along with minus RT sample, a non-template control (NTC) i.e., all above reagents minus C-DNA template was also included for every primer pair used. This would detect any PCR contamination as wells distinguish the unintended amplification products for example, primer dimers from intended products. Each sample was analyzed for gene of interest (GOI) as well reference genes, to offset for technical variations. The reaction was set up was singleplex i.e., GOI and reference genes were analyzed in different wells. In an experiment with many treatments and biological replicates, all treatments from a single biological replicate were run on a single plate.

Ideally, all primer pairs for GOI and reference genes would be analysed on a single 96 well plate. When multiple GOIs were analysed using the same samples, different genes were analyzed on different plates to be more economical.

The plates containing samples were sealed using clear adhesive polyester film (Biorad) to avoid sample evaporation during PCR. The sealed plates could be stored in  $-20^{\circ}\text{C}$  freezer. Amplification conditions used were  $95^{\circ}\text{C}$  for 15 minute followed by 40 cycles of  $95^{\circ}\text{C}$  for 30 seconds,  $60^{\circ}\text{C}$  for 30 seconds and  $72^{\circ}\text{C}$  for 30 seconds. Melt curves were generated between  $53^{\circ}\text{C}$  and  $95^{\circ}\text{C}$  from readings every  $0.5^{\circ}\text{C}$ .

Biorad CFX connect real time thermocycler was used to amplify the target and monitor the fluorescence that reflected the amount of target sequence amplified in each cycle. The PCR amplification plot shows an exponential phase in which the amount of target is almost doubled every cycle. As the reaction proceeds, a non-exponential plateau phase follows the exponential phase when one or more PCR reaction components becomes limiting. Biorad CFX connect real time software uses the exponential phase of PCR for quantification. The more abundant the target sample, the earlier the quantification cycle value (Cq) is given. Biorad software provides the options to determine Cq value either at a baseline threshold value set for all samples above background fluorescent level or based on the kinetic parameters of amplification curve of each replicate of samples. To account for any asymmetric amplification efficiency variations among PCR runs, the latter option was used. The Cq value is the intersection point between the abscissa axis and tangent of the inflection point of amplification curve obtained by the non-linear regression of raw data.

The differences in Cq values between samples can be correlated for quantification. Target amplification was quantified by relative quantification method, referred to as comparative Cq method or  $2^{-\Delta\Delta\text{Cq}}$  method (Schmittgen et al., 2012). This method assumes that the PCR efficiency of GOI is similar to the reference gene and is close to 100% (please see below under the session ‘primer designing’ for PCR efficiency calculation) and relative gene expression is presented as  $2^{-\Delta\text{Cq}}$ , where  $\Delta\text{Cq} = \text{Cq}(\text{GOI}) - \text{Cq}(\text{Reference})$ . This normalization to reference gene accounts for variation in extraction yield, C-DNA synthesis yield and efficiency of PCR amplification. Fold change,  $2^{-\Delta\Delta\text{Cq}}$  is presented as the ratio between relative expression of treatment sample and that of untreated control sample. For data analysis, means of 3 technical replicates of a sample within an experiment were calculated and then means of sample

in all biological replicates were calculated. Standard error of mean (SEM) was calculated after  $2^{-\Delta\Delta Cq}$  transformation. Final data was represented as mean  $\pm$  SEM. Statistical analysis was performed on  $\Delta Cq$  values of biological replicates for assessing the significance of differences between treatments.

Cq value  $>33$  was analysed with caution as it may imply a low efficiency or a low target. If all the samples in an experiment or positive control had Cq  $> 33$ , the data was not reported to avoid false-positive results. If one or more of the treatment had Cq  $< 25$ , then Cq=33 was taken as cut off value.

#### *2.2.1.4 QPCR primer designing*

The information on sequence and mRNA transcript variants was retrieved using NCBI tools and the primers were designed using NCBI Primer-BLAST (<http://www.ncbi.nlm.nih.gov/tools/primer-blast/>). The primer pairs were designed to; span exon-exon boundary to avoid potential genomic DNA contamination, be 18-24 nucleotides in length for practical annealing temperatures, contain 50%GC content, melt at temperature in the range of 57-62<sup>0</sup>C and generate an amplicon  $< 250$  base pairs in size as longer products do not amplify as efficiently. The primer pairs were analysed using Oligo analyser tool (<https://www.idtdna.com/calc/analyzer>) for secondary structure.

All primers were verified for specificity and efficiency. Melt curve analysis was performed to verify the specificity by identifying the products amplified. DNA melts at a characteristic temperature and the melting temperature ( $T_m$ ) is defined as the temperature at which half of the helical structure of DNA is lost. During melt curve analysis, each sample is slowly heated from user defined temperature below  $T_m$  of desired product to a temperature above melting point. Melting of amplicons releases SYBER Green I bound to it. This results in a significant change in fluorescence and provides a  $T_m$  (the midpoint of fluorescence transition), characteristic of every amplified product and thus permits to distinguish between desired product from primer dimer or non-specific product. Primer dimer due to their small size melts at lower temperature than the desired product and any non-specific amplification product melts above or below that of desired product. Biorad real time thermocycler plots the fluorescence as a function of temperature and calculates melting peak by taking the differential derivative ( $dF/dT$ ) of this melt curve plot. Primer pairs that produced a

single amplicon peak in positive sample and no peak in NTC were used for qPCR analysis.

A serial dilution of known template concentration (RNA prepared in house from human foetal brain whole ganglionic eminence or Total RNA - Human Fetal Normal Tissue: Brain: Frontal Lobe (Amsbio, Abingdon, UK)) was used to verify the amplification efficiency. The independent variable i.e., log of concentration of each dilution was plotted on X axis and the dependent variable C<sub>q</sub> for that concentration was plotted on Y axis. Correlation coefficient (R<sup>2</sup>), and the slope were used to provide information about PCR reaction. R<sup>2</sup> close to 0.999 indicated linearity of the standard curve. Amplification efficiency was determined from the slope of log-linear phase of amplification curve by the following equation.

$$\text{PCR efficiency} = 10^{-1/\text{slope}} - 1$$

A slope of -3.32 gives an efficiency close to 100%. Primer sets with efficiency between 90 and 110% which corresponds to a slope between -3.58 and -3.10 was accepted for qPCR. (See Table 2. for qPCR primers and Appendix 2.1 for melt curve analysis and efficiency testing)

Table 2 QRT-PCR primer sequences

<i>Gene</i>	<i>Primer sequence (5' -3')</i>	
	<i>Forward</i>	<i>Reverse</i>
<i>DLX2</i>	GCCTCAACAACGTCCCTTAC	TCACTATCCGAATTCAGGCTC
<i>DLX5</i>	CGCTAGCTCCTACCACCAGT	GGGCTCGGTCACTTCTTTC
<i>FOX G1</i>	AGGAGGGCGAGAAGAAGA	ACTCGTAGATGCCGTTGAGC
<i>GLI 1</i>	CTACATCAACTCCGGCCAAT	CGGCGTTCAAGAGAGACTG
<i>GSX2</i>	ATGTCGCGCTCCTTCTATGT	ATGCCAAGCGGGATGAAGAAA
<i>ID1</i>	GGTGCCTGTCTGTCTGAG	CTGATCTCGCCGTTGAGG
<i>ID3</i>	CTGGACGACATGAACCACT	GTAGTCGATGACGCGCTGTA
<i>LEF1</i>	ACCAGATTCTTGGCAGAAG	CAGACCAGCCTGGATAAAGC
<i>NKX2.1</i>	AGGACACCATGAGGAACAG	CCCATGAAGCGGGAGATG
<i>OCT4</i>	CTCACCCCTGGGGTTCTATT	CTCCAGGTTGCCTCTCACTC
<i>PATCHED1</i>	GGAGCTTCGGCACTACGA	ATTCGGGATGGACCACAGT
<i>PAX6</i>	AGGCCAGCAACACACCTAG	AGCCAGATGTGAAGGAGGAA
<i>SLUG</i>	AAGCATTTCAACGCCTCCAA	AGGATCTCTGGTTGTGGTATG
<i>B-ACTIN</i>	CCCAGCACAATGAAGATCA	ACATCTGCTGGAAGGTGGAC
<i>GAPDH</i>	TGCACCACCAACTGCTTAGC	GGCATGGACTGTGGTCATGAG

### 2.2.1.5 High-throughput QRT-PCR

Quantitative high-throughput open array platform (Life technologies) uses TaqMan gene expression assays (see Table 3 for the probes) preloaded onto open array plates and enables multiple PCR assays to run simultaneously. The C-DNA samples of

A260/280 close to 1.8, were sent to Dr. Joseph M Canals, University of Barcelona-IDIBAPS where the assays were conducted and analysed as per manufacture's instructions.

The software assesses the gene expression by relative quantification as described above in 2.2.1.3. Software integrated algorithms calculate the geometric mean of 3-4 reference genes as 'normalization factor'. Fold change gene expression was determined as ratio between normalized expression of treatment and that of control. Means of 3 biological replicates with technical PCR replicates were assessed and data was represented as mean fold change  $\pm$  SEM. Statistical analysis was performed on  $\Delta$ Cq values of biological replicates for assessing the significance of differences between treatments

Table 3 TaqMan probes ID

Gene name	Probe Ids
ISL1	Hs00158126_ml
LMX1B	Hs00158750_ml
MSI1	Hs00159291_ml
PVALB	Hs00161045_ml
NKX2-1	Hs00163037_ml
TH	Hs00165941_ml
DCX	Hs00167057_ml
ALDH1A3	Hs00167476_ml
ADORA2A	Hs00169123_ml
GATA4	Hs00171403_ml
EOMES	Hs00172872_ml
IKZF1	Hs00172991_ml
NPY	Hs00173470_ml
KIT	Hs00174029_ml
PENK	Hs00175049_ml
CALB1	Hs00191821_ml
DLX5	Hs00193291_ml
SIX3	Hs00193667_ml
IKZF2	Hs00212361_ml
FOXP1	Hs00212860_ml
SLC17A7	Hs00220404_ml
SLC17A6	Hs00220439_ml
OTX2	Hs00222238_ml
DLX6	Hs00231999_ml
LHX1	Hs00232144_ml
TBR1	Hs00232429_ml
LHX6	Hs00232660_ml
FOXA2	Hs00232764_ml
MMP9	Hs00234579_ml
PDX1	Hs00236830_ml
PAX3	Hs00240950_ml
DRD2	Hs00241436_ml
TAC1	Hs00243225_ml
EMX2	Hs00244574_ml
BCL11B	Hs00256257_ml
HOXB4	Hs00256884_ml
HOXB9	Hs00256886_ml
MAP2	Hs00258900_ml
PPP1R1B	Hs00259967_ml
ZNF503	Hs00262121_ml
CNP	Hs00263981_ml
CHRM4	Hs00265219_sl
ASCL1	Hs00269932_ml
DLX2	Hs00269993_ml
TLX1	Hs00271457_ml
OLIG2	Hs00300164_sl
SST	Hs00356144_ml
KFL4	Hs00358836_ml
FOXP2	Hs00362817_ml
GSX2	Hs00370195_ml
ARPP21	Hs00372261_ml
DRD1	Hs00377719_sl
EBF1	Hs00395513_ml
EMX1	Hs00417957_ml

CALB2	Hs00418693_ml
NR4A2	Hs00428691_ml
POU3F1	Hs00538614_sl
MEIS2	Hs00542638_ml
GLI3	Hs00609233_ml
GAD2	Hs00609534_ml
T	Hs00610080_ml
AIF1	Hs00610419_sl
DLX1	Hs00698288_ml
NEUROG2	Hs00702774_sl
NES	Hs00707120_sl
OLIG1	Hs00744293_sl
NKX6-2	Hs00752986_sl
CHAT	Hs00758143_ml
GSX1	Hs00793699_sl
TUBB3	Hs00801390_sl
NR2F1	Hs00818842_ml
NR2F2	Hs00819630_ml
PBX2	Hs00855025_sl
S100B	Hs00902901_ml
MNX1	Hs00907365_ml
GFAP	Hs00909233_ml
GPR6	Hs00920605_sl
RARA	Hs00940446_ml
NCAM1	Hs00941830_ml
SNAI2	Hs00950344_ml
OTX1	Hs00951099_ml
ETV1	Hs00951941_ml
ZBTB16	Hs00957433_ml
DACH1	Hs00974297_ml
RARB	Hs00977140_ml
CDH2	Hs00983056_ml
B2M	Hs00984230_ml
CDH1	Hs01023894_ml
NEUROG1	Hs01029249_sl
FTSJD1	Hs01052115_sl
SOX2	Hs01053049_sl
OPRM1	Hs01053957_ml
PAX2	Hs01057416_ml
SOX1	Hs01057642_sl
CDX2	Hs01078080_ml
PAX6	Hs01088112_ml
GLI1	Hs01110766_ml
DBX2	Hs01117258_ml
RBFOX3	Hs01370653_ml
TJP1	Hs01551861_ml
RARG	Hs01559234_ml
POU5F1	Hs01654807_sl
FOXP1	Hs01850784_sl
UBC	Hs01871556_sl
SP8	Hs01941366_sl
KRT18	Hs01941416_sl
NANOG	Hs02387400_sl
HPRT1	Hs02800695_ml
GPR88	Hs03027832_sl
HSP90AB1	Hs03043878_sl
RPL13A	Hs04194366_sl
18S	Hs99999901_sl

## **2.2.2 Detection of gene expression at protein level**

### *2.2.2.1 Immunocytochemistry*

To detect and generate a quantitative data on the amount of protein of interest within cells, immunocytochemistry (ICC) was performed. During this project, an indirect immunofluorescence was performed in which protein antigen was detected by use of specific primary antibody that binds to it. The affinity between antigen and antibody was visualised under a fluorescence microscope by using fluorophore-conjugated secondary antibody that binds to primary antibody.

For ICC, the culture media was removed and cells attached to coverslips in culture dishes were washed with 1 x PBS (Life technologies). Cells were fixed with fresh 4% paraformaldehyde (PFA) (Sigma-Aldrich) in PBS for 10-15 minute at room temperature and were subsequently washed 3 times in PBS. The fixing step immobilizes the antigen of interest while retaining cellular and subcellular architecture. PFA through free amino group form intermolecular bridges and thus cross links antigen. Following fixation, to allow access of antibody to antigen, cells were permeabilized using either 0.1%-0.3% triton-X (Sigma-Aldrich) in PBS for 20 min or ice cold absolute ethanol for 2 min, depending on the antibodies used. No permeabilization was required for surface antigens. The cells were washed 3 times in PBS. For some antigens, extensive cross-linking during fixation may mask the epitope that antibody binds to and antigen retrieval was performed by using either 1M Glycine (Sigma-Aldrich) for 20 minutes at room temperature or heating at 60<sup>0</sup>C for 10 min. To prevent any non-specific antibody binding, a blocking buffer containing 3% bovine serum albumin (BSA) (Sigma-Aldrich), 3% normal goat serum (Dako) and 0.1% Triton-X in PBS (filtered before use) was applied to cells for an hour at room temperature. Triton-X was excluded in blocking buffer for surface antigens. Following blocking, the cells were incubated for an hour at room temperature with the primary antibody at appropriate dilution in blocking buffer. For double immuno-labelling, both primary antibodies were added simultaneously. The primary antibodies used were either monoclonal (pure immunoglobulins with known specificity) or polyclonal (containing a mixture of immunoglobulins against a specific antigen with subtle changed in epitope specificity). A droplet method of antibody incubation was performed for all cells, except terminally differentiated neurons in which antibody incubation was performed directly in culture plates where cells were grown. In droplet

method, 60µl of antibody dilution was placed on parafilm on the top of a bed of moist filter paper in a 10cm petridish. The coverslip with cells was gently inverted onto this droplet ensuring a tight contact between cells and antibody. For all staining, 2 controls- a biological negative sample and a no primary antibody sample were performed. After an hour, the coverslips were placed in bottom of a 24 well plate and were washed gently 3 times in PBS. Care was taken to minimize cells peeling off from coverslips. The cells were then incubated for 45 minutes at room temperature in dark with appropriate secondary antibody droplet (all at 1:400 dilution in blocking buffer) as described above. The secondary antibody used was specific to the primary antibody class i.e., IgGs or IgM and was against the species in which primary antibody was raised. Please see table 4 below for the list of antibodies used and details of permeabilization and blocking buffer. Following secondary antibody incubation, coverslips were placed back in the bottom of 24 well plates and washed 3 times in PBS. Coverslips were mounted with vector shield containing DAPI nuclear stain onto a glass microscope slide. The edge of coverslips was sealed with clear nail varnish. The mounted sealed coverslips could be stored at 4<sup>0</sup>C in dark until imaging.

Table 4 Antibody Dilutions and Conditions for ICC

Antibody	Species and specificity	Dilution	Permeabilization	Antigen retrieval	Blocking
Calbindin	Rabbit polyclonal IgG ( <i>Swant</i> )	1:500	0.3% Triton in PBS, 20 min, RT		2%NGS+ 3% BSA in PBS
CK18	Guinea pig polyclonal IgG ( <i>Progen Biotechnik</i> )	1:500			2%NGS+ 3% BSA+ 0.1% Triton X in PBS
CTIP2	Rat monoclonal IgG ( <i>Abcam</i> )	1:500	0.1% Triton X in PBS, 20 min, RT		2% NGS+ 3% BSA + 0.1% Triton x in PBS
DARPP32	Rabbit monoclonal IgG ( <i>Abcam</i> )	1:200	0.1% Triton X in PBS, 20 min, RT	1M Glycine, 20 min RT	2% NGS+ 3% BSA + 0.1% Triton x in PBS
FOXG1	Rabbit polyclonal IgG ( <i>Tebu-Bio</i> )	1:1000	0.1% Triton X in PBS, 20 min RT	1mM EDTA, 10 min at 60 degree water-bath	2%NGS+ 3% BSA+ 0.1% Triton X in PBS
GABA	Rabbit polyclonal	1:100			2%NGS+ 3% BSA

	IgG ( <i>Sigma</i> )				
GSX2	Rabbit polyclonal IgG ( <i>Millipore</i> )	1:500	0.1% Triton X in PBS, 20 min, RT		2% NGS+ 3% BSA+ 0.1% Triton x in PBS
ISL1	Rabbit monoclonal IgG ( <i>Abcam</i> )	1:500	Ice cold absolute ethanol, 2min		2%NGS+ 3% BSA in PBS
KI67	mouse monoclonal IgG ( <i>Vector Labs</i> )	1:100	0.1% Triton X in PBS, 10 min RT		2% NGS+ 3% BSA+ 0.1% Triton X in PBS
MAP2	Mouse monoclonal IgG ( <i>Sigma</i> )	1:600	Ice cold absolute ethanol, 2min		2% NGS+ 3% BSA
NESTIN	Mouse monoclonal IgG ( <i>Millipore</i> )	1:500			2%NGS+ 3% BSA+ 0.1% Triton X in PBS
NKX2.1	Rabbit monoclonal IgG ( <i>Abcam</i> )	1:150	0.1% Triton X in PBS, 20 min , RT		2%NGS+ 3% BSA+ 0.1% Triton X in PBS
OCT4	Mouse monoclonal IgG ( <i>Santa Cruz</i> )	1:100	Ice cold absolute ethanol, 2min		2%NGS+ 3% BSA+ 0.2% Triton X in PBS
PAX6	Mouse IgG ( <i>DSHB</i> )	1:10	0.1% Triton X in PBS, 20 min RT		2%NGS+ 3% BSA+ 0.1% Triton X in PBS
PSD95	Rabbit IgG ( <i>Abcam</i> )	1:100			2% NGS+ 3% BSA+ 0.05 % Tween 20 in PBS
SOX2	Rabbit polyclonal IgG ( <i>Millipore</i> )	1:500	Ice cold ethanol, 2 min RT		2%NGS+ 3% BSA+ 0.2% Triton X in PBS
Synapto-physin	Mouse monoclonal IgG ( <i>Abcam</i> )	1:200			2% NGS+ 3% BSA+ 0.05% tween 20 in PBS

### 2.2.2.2 Imaging and quantification of cells

Cells were visualised under UV fluorescence using Olympus BX61 microscope. Cells were imaged for nuclear stain as well as counterstaining with antibodies using different filters. Images were processed using Analysis software and Adobe photoshop. All images across treatments within an experiment were processed in the same manner.

For quantification of cells, 5-10 random fields per coverslip covering the edges and centre were imaged at 20X magnification. The images (straight from the microscope and not processed in photoshop) were quantified using either manually or

Cell profiler (Carpenter et al., 2006, <http://www.cellprofiler.org/citations.shtml>). For analysis by Cell profile software, the objects were identified by set size of nuclei with fixed intensity threshold; for each channel the size range was set to distinguish objects from any noise in the image and the intensity threshold was set to decide whether each pixel was foreground (region of interest) or background. 2 biological replicates per tested condition were quantified and the total cell count was averaged. The number of cells immuno-positive for antigen of interest was calculated as a percentage of total nuclei.

### 2.2.2.3 Western blotting

Western blotting was performed to detect the expression of phosphorylated SMAD1/5/8. The culture medium was aspirated and cells were washed with ice-cold PBS. The culture dishes were placed in ice and cells were lysed in 300µl ice-cold radio-immunoprecipitation assay buffer (RIPA) containing phosphatase inhibitor and protease inhibitor (all from Sigma-Aldrich). The cells were scraped, lysate was transferred to eppendorf tubes and incubated at 4<sup>0</sup>C for 30 minutes with intermittent agitation. The samples were then centrifuged at 12000 rpm for 20 minutes at 4<sup>0</sup>C. The supernatant was aliquoted and frozen at -80<sup>0</sup>C.

Samples were thawed on ice and the amount of proteins was quantified using Pierce BCA protein assay kit (Thermoscientific, Waltham, MA, USA). This colorimetric detection of protein is based on reduction of Cuprous, Cu<sup>2+</sup> to Cu<sup>1+</sup> by protein in an alkaline medium and detection of colored reaction product using a reagent containing bicichoninic acid (BCA) that chelates to Cu<sup>1+</sup>. Protein concentrations were determined with reference to a standard protein BSA provided in the kit. For this, a serial dilution of BSA ranging from 25µg/ml to 2000µg/ml was made. 25µl of each standard and sample in triplicate were pipetted into a microplate well (Fisher Scientific). 200µl of BCA working reagent prepared as per manufacture's instruction, was added to each well and the plate was mixed thoroughly on a plate shaker for 30 seconds. The plate was incubated at 37<sup>0</sup>C for 30 minutes. The plate was then cooled to room temperature and the absorbance was read at 562nm on a spectrophotometer (Fluro Optima, BMG lab tech). The protein concentration in samples was determined from the standard curve generated by plotting BSA standards concentration vs. their absorbance.

Western blotting was performed using polyacrylamide gel with a 10% resolving gel and 5% stacking gel (Table 5). Resolving gel was prepared and left to set with distilled water layered on the surface. The water was then replaced with stacking gel and left to set with the appropriate comb. Samples (volume aliquoted for 30µg protein) were prepared by adding sample loading buffer to samples at a ratio of 1:1 in 0.2ml PCR tubes and denatured at 95<sup>0</sup>C for 5 minutes in Techne TC512 thermocycler (Bibby Scientific Ltd). The gel set was placed in running tank containing 1X running buffer (Table 5) and the comb was removed. The samples were then loaded alongside a full range rainbow ladder Novex® Sharp Pre-Stained Protein Standard (Life technologies). The proteins in the samples were separated by running the samples at 100V through stacking gel and 120 V through resolving gel until the dye front of loading reached the base of the resolving gel.

For electro-blotting of the protein onto membrane, Hybond ECL 0.2µ pore size nitrocellulose membrane (GE healthcare) was soaked briefly in distilled water and in transfer buffer (TBS) (Table 5) for 10 minutes. The gel was placed on the top of the membrane and was layered between filter papers and sponges previously soaked in TBS (as sponge: filter: gel: membrane: filter: sponge). This gel-membrane cassette was then placed in Mini-PROTEAN apparatus set-up (Biorad) containing TBS buffer. The protein transfer was carried out at 100V for an hour. The membrane was carefully removed, rinsed in water once and with wash buffer (Table 5). The protein transfer was checked by staining with Ponceau S solution. The stain was removed subsequently in wash buffer.

The protein of interest, phosphorylated SMAD1/5/8 was detected by immuno-detection. The membrane was blocked with 5% w/v milk (Marvel,UK) in TBST (Table 5) for 1 hour. Membrane was first incubated with rabbit polyclonal P-SMAD1,5,8 antibody (Cell signalling, Danvers,MA) at 4<sup>0</sup>C overnight and washed 3x 5 minutes in TBST at room temperature. The membrane was then incubated with goat anti-rabbit horseradish peroxidase conjugated secondary antibody (GE life science) at 1:10000 dilution for an hour at room temperature and washed 3x 5 minutes in TBST. Signal generation was undertaken using SuperSignal WestDura substrate (Thermoscientific) as per manufacture's instruction. The signals were detected using chemiluminiscent film (Roche, Hertfordshire, UK) placed over the membrane in Hypercassette (Amersham Bioscience, Buckinghamshire, UK) and exposing for an

hour. The film was developed using an automatic developer Xograph Compact X4. The intensity of protein bands in the film was quantified by ImageJ software.

Table 5 Composition of gels and solutions used for Western blotting

		Composition*
Gels	10% Resolving gel	10% (w/v) Acrylamide ( <i>Biorad</i> ), 0.37M Tris pH 8.8, 0.1% SDS, 0.1 % Ammonium persulphate, and 0.06% tetramethylethylenediamine (TEMED)
	5% Stacking gel	5% Acrylamide, 0.125M Tris pH 6.8 ( <i>Roche</i> ), 0.1% SDS, 0.05 % Ammonium persulphate, and 0.5% TEMED
Buffers	Sample loading buffer	2 % SDS, 10% Glycerol, 60mM Tris pH 6.8, 0.005% Bromophenol blue and 500 mM DTT
	10x Running buffer	0.25 M Tris base, 1.92 M Glycine, 0.1 % SDS, and pH 8.3. Diluted to 1x before use.
	Transfer buffer	0.25 M Tris base, 1.92 M Glycine, and 20 % Methanol.
	Wash buffer	0.1 % Tween 20 in 1x PBS ( <i>Life technologies</i> )
Stain	Ponceau S	0.1% (w/v) in 5 % acetic acid

\*All materials from *Sigma-Aldrich* unless stated otherwise.

## 2.3 Statistical methods

Statistical analyses of data were performed in Graphpad prism v6.0 (*GraphPad Software Inc., La Jolla, CA, USA*). Parametric data were analysed using two-sample t-tests or one-way analysis of variance (ANOVA) with Dunn's comparison post doc when appropriate to compare differences between pairs. Non-parametric data were analysed using Kruskal-Wallis with Dunn's comparison. Where experiments were performed once or twice, i.e. N = 1 or 2, the results presented are semi-quantitative and could not be tested for statistical significance.

## 2.4 Materials

Initially in the project, all the small molecules were purchased from different supplier which are listed in the table 6 and later some of the small molecules were provided by *CHDI, Los Angeles, CA, USA*.

Table 6 Materials

<b>Materials/reagents</b>	<b>Catalogue No</b>	<b>Supplier</b>
Accutase, stempro	A1110501	Life Technologies
Acetic acid, glacial	A/0360/PB17	Fisher Scientific
Acrylamide (30%)	161-0158	Biorad
Advanced DMEM/F12	12634028	Life technologies
Alexa Fluor 488 goat $\alpha$ mouse IgG (H&L)	A11001	Life technologies
Alexa Fluor 488 goat $\alpha$ rabbit IgG (H&L)	A11008	Life technologies
Alexa Fluor 488 goat $\alpha$ rat IgG (H&L)	A11006	Life technologies
Alexa Fluor 594 goat $\alpha$ mouse IgG (H&L)	A11005	Life technologies
Alexa Fluor 594 goat $\alpha$ rabbit IgG (H&L)	A11012	Life technologies
Ammonium persulfate	A/6160/53	Fisons
Antibiotic/Antimycotic Solution	15240-062	Life technologies
Ascorbic acid	A4544	Sigma-Aldrich
BCA protein assay kit	13276818	Fisher scientific
BCIP/NBT liq substrate system (Alk Phosph Detection Kit)	B1911	Sigma
BD Matrigel Growth Factor Reduced	354230	VWR
BDNF – Human Research Grade	130-096-286	Milteny
Blotting paper	Z74759-100	Sigma-Aldrich
Boric Acid	B6768	Sigma
Bovine Serum Albumin	A9418	Sigma
Box, Microslide	MNK 337050M	Fisher scientific
Calbindin antibody	CB38a	Swant
Calcium chloride (anhydrous)	499609-1G	Sigma
CHIR 99021	4423	Tocris
CHIR 99021	CHDI-00401952-000	CHDI
CK18 antibody	GP-CK18	Progen Biotechnik
Collagenase Type IV	17104019	Life Technologies
Complete mini EDTA-free protease inhibitor cocktail tablets	11873580001	Roche
coverslip round 13mm	631-0149	VWR
Cryostor CS10	7930	Stem cell Technologies
CTIP2 antibody	ab18456	Abcam
Cyclopamine-KAAD	239804	Calbiochem Merck Millipore
DAPT	2634	Tocris
DAPT	CHDI-00396736-000	CHDI
DARPP32 antibody	ab40801	Abcam
DEPC treated DNase free H <sub>2</sub> O	46-2224	Life Technologies
Dimethylsulfoxide ampules	D2650	Sigma-Aldrich
Dispase	7923	Stem cell

		Technologies
Distilled Water, Sterile	15230188	Life Technologies
DMEM Glutamax	61965-059	Life Technologies
DMH1	4126	Tocris
dNTPs- Set of dATP, dCTP, dGTP, dTTP	U1240	Promega
Donkey $\alpha$ rabbit IgG HRP	NA934V	GE
Dorsomorphin	P5499-5MG	Sigma-Aldrich
EmbryoMax® ES Cell Qualified 0.1% Gelatin Solution	ES-006-B	Millipore
Ethanol 99.8+%, Absolute	10437341	Fisher Scientific
Foetal Bovine Serum	10270106	Life Technologies
Forskolin	1099	Tocris
Forskolin	CHDI-00000087- 0000	CHDI
FOXG1 antibody	NCFAB	Tebu-Bio
GABA	0344	Tocris
GABA antibody	A2052	Sigma-Aldrich
Glycerol 990%	G5516	Sigma-Aldrich
Glycine	G8898	Sigma
GSX2 antibody	ABN162	Millipore
Haemacytometer cover glass 21mm x 26mm	MNK-504-030M	Fisher Scientific
Haemacytometer improved neubauer	MNK-420-010N	Fisher Scientific
Human Activin A	120-14	Peprtech
Human FGF Basic	100-18B	Peprtech
Insulin from Bovine Pancreas	I6634	Sigma
Islet1 antibody	Ab109517	Abcam
Isopropanol	10326503	Fisher Scientific
IWR1	CHDI-00476979- 0000	CHDI
IWR1,endo	3532	Tocris
KI67 antibody	VP-K452 clone MM1	Vector Labs
Knockout DMEM 1 X	10829018	Life Technologies
Knockout Serum Replacement	10828-028	Life Technologies
KY 02111	4371	Tocris
Laminin, mouse	06-0002	Stemgent
LDN 193189	04-0019	Stemgent
LDN 193189	CHDI-00396388- 0000	CHDI
L-Glutamine 200mM	25030-024	Life Technologies
Lipid concentrate, Chem. Defined	119-05-031	Life Technologies
Lumi-film chemiluminescent detection film	11666916001	Roche
MACS NeuroBrew-21	130-093-566	Milteny
MACS NeuroBrew-21 w/o Vitamin A	130-097-263	Milteny
MAP2 (Mouse) antibody	M1406	Sigma-Aldrich
Matrigel BD	734-1440	VWR

MEM non essential amino acids	11140-035	Life Technologies
Methanol	32213	Sigma-Aldrich
MicroAmp™ Fast 96-Well Reaction Plate, 0.1 ml (qPCR plates)	4314320	Life Technologies
Microscope, Bright field inverted	Diavert	Leitz
Microscope, Phase contrast	EVOS AMG	Fisher Scientific
Microseal B adhesive seals (qPCR plate seal)	MSB-1001	Biorad
mTeSR™1	5850	Stem cell Technologies
Nanodrop ND1000		Labtech international
NESTIN antibody	MAB5326	Millipore
Neurobasal- A	10888-022	Life Technologies
Neurobasal-A medium 1X Liquid	10888-022	Life Technologies
Nitric acid	438073-500ML	Sigma
NKX2.1 antibody	ab76013	Abcam
Normal goat serum	X0907	DAKO
Novex® Protein ladder	LC5800	Life Technologies
OCT4 antibody	sc5279	Santa Cruz
Paraformaldehyde	P6148	Sigma
PAX6 antibody		DSHB
PBS (1x) pH 7.24	10010056	Life Technologies
PBS DULB, with Ca & Mg	140-40-091	Life Technologies
PD 0332991 isethionate	4786	Tocris
PD 0332991 isethionate	CHDI-00482855-0001	CHDI
Penicillin/Streptomycin (5000U/5000µg)	15070063	Life Technologies
Poly-L-lysine hydrobromide	P6407	Sigma
PSD-95 antibody	ab18258	Abcam
Purmorphamine	540220	Calbiochem
Purmorphamine	CHDI-00396749-0000	CHDI
Qiashredder	79654	Quiagen
QPCR , Biorad	CFX™ connect Real time	Biorad
Rack, 100 well, assorted colours	11700344	Fisher Scientific
Random Primers	48190-011	Life Technologies
Recombinant Human Noggin	120-10C	Peptotech
RIPA lysis buffer	R0278	Sigma-Aldrich
Rnase Inhibitor, Rnase Out Recombinant	10777-019	Life Technologies
RNase Zap	R-2020	Sigma
RNase-Free DNase Set	79254	Quiagen
Rneasy mini kit	74104	Quiagen
Rock Inhibitor (Y-27632)		Abcam
SAG	566660	Calbiochem Merck Millipore
SB431542 - Alk4,5 and 7 inhibitor	ab120163	Abcam
SB431542 - Alk4,5 and 7 inhibitor	CHDI-00447536-	CHDI

	0000	
SDS (powder)	L3771	Sigma-Aldrich
Slides (microscope), polysine, 75x25x1mm	10149870	Fisher scientific
Sodium tetraborate	221732	Sigma
SOX2 antibody	AB5603	Millipore
SSEA4 antibody	clone MC-813-70	DSHB
SuperscriptII RnaseH- Reverse Transcriptase	18064022	Life Technologies
SuperSignal West Dura chemiluminescent substrate	34075	Thermo Scientific
SYBR Green DyNAmo qPCR Kit	FZF-410L	Fisher scientific
Synaptophysin antibody	ab8049	Abcam
TEMED	T9281	Sigma-Aldrich
Thermal cycler,PCR	TC512-PCR	Techne
Total RNA - Human Fetal Normal Tissue: Brain: Frontal Lobe	R1244051-50	Ambio
Transferrin	T8158-100MG	Sigma
Tris base (121.4 MW)	10 708 976 001	Roche
Triton® X-100	T8787	Sigma-Aldrich
Trypan blue	T8154	Sigma-Aldrich
Trypsin - EDTA 1X	25300-054	Life Technologies
Tween-20	P1379	Sigma-Aldrich
Vectashield	H-1400	Vector laboratories
Water, Ultra pure DEPC treated	750024	Life Technologies
Y27632 dihydrochloride, rock inhibitor	688000	Abcam
Y27632 dihydrochloride, rock inhibitor	CHDI-00197406- 0001	CHDI

## 3. Investigation of small molecule mediated BMP antagonism on neural induction

### 3.1 Aim

To analyse the effect of BMP antagonism on neural induction of hPSCs, utilizing the small molecule BMP inhibitors Dorsomorphin, LDN193189 and DMH-1

### 3.2 Background

During neural induction *in vivo*, the embryonic ectoderm is specified to form neuroectoderm and non-neuroectoderm. Neuroectoderm forms the neural tube that will give rise to the CNS and separates from the non-neuroectoderm that will form the epidermis. During this process, the neural crest originates at the junction between these two cell domains and migrates away to form the peripheral nervous system, skeletal cranial and connective tissue and pigment cells (Beddington and Robertson 1999; Gammill and Bronner-Fraser 2003). Since the ground breaking discovery by Spemann and Mangold, the role of BMP, TGF- $\beta$ /Activin inhibition in neural induction has been well established. Over expression of dominant negative TGF- $\beta$  receptor or BMP inhibitors- Noggin, follistatin and chordin strongly induced neural fate (Hemmati-Brivanlou and Melton 1994; Sasai and De Robertis 1997), whereas treatment with TGF- $\beta$  family members- Activin and BMPs or morpholinos-mediated depletion of BMP inhibitors prevented the acquisition of neural fate (Wilson and Hemmati-Brivanlou 1995; Khokha *et al.* 2005). In the presence of BMP4, epidermal fate was induced in the ectoderm (Wilson and Hemmati-Brivanlou 1995).

*In vitro*, supplementing Noggin (which acts by binding to BMP ligands and prevents their binding to receptors) to hESC neural differentiation cultures under serum or serum free condition or on MS5 cells enhanced neuroectoderm markers PAX6 and NESTIN (Pera *et al.* 2004; Itsykson *et al.* 2005; Lee *et al.* 2007; Elkabetz *et al.* 2008). Similarly, NESTIN and another neural marker SOX1 expression was enhanced by inhibition of TGF- $\beta$ /Activin/Nodal signalling by overexpression of Lefty2 or Cerberus or by small molecule SB431542 (which acts by specifically inhibiting ALK receptors ALK4, ALK5 and ALK7, blocks SMAD2/3 phosphorylation and has no effect on BMP signalling) (Smith *et al.* 2008). Synergistic action of Noggin

and SB431542 under chemically defined conditions efficiently yielded >80% PAX6<sup>+</sup> neuroectodermal cells which was higher than Noggin or SB431542 only treatment. Also SB431542+Noggin treatment efficiently suppressed differentiation to other lineages (Chambers *et al.* 2009).

In this chapter, I investigated the effect of Dorsomorphin and its structural derivatives- LDN193189 and DMH-1 on hPSC neural induction to replace the function of recombinant Noggin. Dorsomorphin, LDN193189 and DMH-1 block BMP mediated SMAD 1/5/8 phosphorylation. Dorsomorphin and LDN193189 act by inhibiting BMP type I receptors ALK2, ALK3 and ALK6 and DMH-1 by selectively inhibiting ALK2 receptor (Yu, Hong, *et al.* 2008; Cuny *et al.* 2008; Boergermann *et al.* 2010; Hao *et al.* 2010). (Other similar studies published during the period of my study, utilizing the same small molecules are discussed later in this chapter).

### 3.3 Experimental design

For hPSC neural induction, the dual inhibition of SMAD signalling (i.e., simultaneous inhibition of SMAD2/3 phosphorylation by SB431542 and inhibition of SMAD1/5/8 phosphorylation by BMP inhibitors) was applied to an embryoid body (EB) culture. H9ESC colonies were lifted from MEF feeder layers, chopped to 150µM fragments and transferred to neural induction medium containing 10µM SB431542 till day 4 and either noggin (300ng/ml) or 0.25 µM to 1 µM of Dorsomorphin or LDN193189 or DMH-1 till day 8 (D8) (Figure 3:1A). On D8, EBs were harvested and gene expression was analysed at the mRNA level by QRT-PCR and at protein levels by immunocytochemistry (Figure 3:1.B). The neuroectodermal fate was analysed by measuring the expression of neuroectodermal markers PAX6, SOX2 and NESTIN and pluripotency maker OCT4. In parallel, the presence of neural crest cells was analysed by measuring markers- SLUG and P75 (Jiang *et al.* 2009) and the presence of epidermis cells was analysed by measuring CK18

*Pax6* was first detected at E8.5-E9.5 neuroectoderm during mice development (Stoykova and Gruss 1994). PAX6 was co-expressed in SOX2 positive cells at E18 mice and Carnegie stage 8-9 human foetal samples, when the neural plate began to form. This expression was retained at E21 mice/ Carnegie stage 10 human foetal samples in pseudo multi-layered closing neural tube (Zhang *et al.* 2010; Onorati *et al.* 2014). PAX6 was demonstrated to be necessary and sufficient for early neuroectoderm specification from hESCs (Zhang *et al.* 2010). PAX6 over expression

enhanced neuroectoderm specification, whereas, PAX6 knock-down blocked the differentiation into neuroectoderm and this effect was not rescued by dual SMAD inhibition by SB431542 and Noggin (Zhang *et al.* 2010). Thus, PAX6 is possibly an intrinsic crucial downstream effector of neural inducers. PAX6 isoforms Pax6a and Pax6 were shown to bind to promoters of pluripotent genes such as Oct4 and Nanog and repressed their function. Pax6a was shown to occupy the promoters of neural genes and activated their expression (Zhang *et al.* 2010). Thus, PAX6 acts as a key inductive signal for neuroectoderm fate. SOX2 is a transcription factor, expressed in presumptive neuroectoderm (Kishi *et al.* 2000; Zhang *et al.* 2010; Onorati *et al.* 2014). In *Xenopus* ectoderm, overexpression of dominant negative Sox2 (dnSox2) mRNA inhibited formation of CNS and neural crest cells (Kishi *et al.* 2000). In vertebrate CNS, SOX2 functions by maintaining neural progenitor (NPCs) identity. Constitutive expression of SOX2 inhibited neuronal differentiation and maintained NPC characteristics, while SOX2 inhibition induced NPC exit from cell cycle and early onset of neuronal differentiation (Graham *et al.* 2003). SOX2 is also one of the core factors of hPSC pluripotency and has been demonstrated to govern ESC specification to neuroectoderm by repressing differentiation into other lineages (Thomson *et al.* 2011). As ESCs differentiated both Oct4 and Sox2 expression fell initially and then were differentially regulated. Neuroectoderm cells were marked by induction of Sox2 and downregulation of Oct4 while, downregulation of Sox2 and induction of Oct4 marked mesoendodermal cells (Thomson *et al.* 2011). Nestin expression was first observed at E7.5 neuroectoderm. Upon neuronal differentiation and maturation, its expression was downregulated. During P19 NPCs differentiation and in developing chick neural tube, Sox2 was found to bind to Nestin enhancers and regulated its expression (Jin *et al.* 2009). PAX6, SOX2 and NESTIN were used as markers of neuroectoderm in this study.

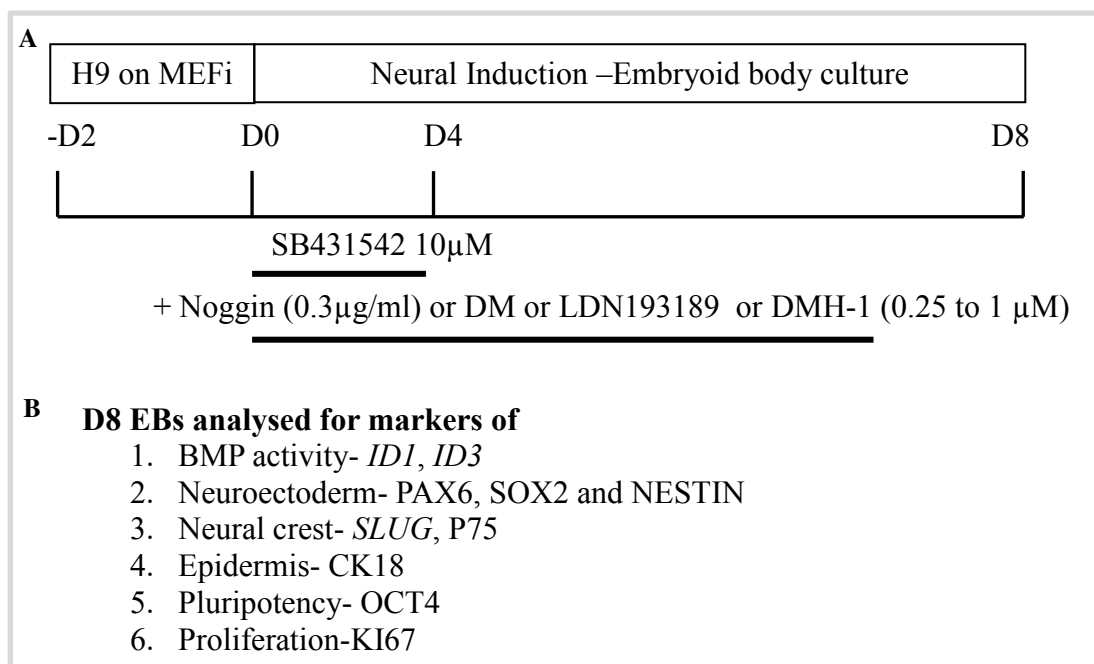


Figure 3:1 A) Neural induction culture regime. H9s grown on MEFis were lifted and plated as suspension cultures in medium supplemented with SB431542 till D4 and either noggin or Dorsomorphin (DM) or LDN193189 or DMH-1 till D8. B) Markers analysed on D8 EBs harvested to determine neural commitment

## 3.4 Results

### 3.4.1 Small molecule mediated inhibition of induced BMP activity

For the application of small molecule BMP inhibitors in hPSC neural induction, their effectiveness in the inhibition of BMP activity was first assessed in H9 hESCs. Undifferentiated H9 cells were pre-treated for an hour, with increasing concentrations of either BMP inhibitors- Dorsomorphin , LDN193189 and DMH-1 (all at 0.25 µM, 0.5 µM and 1µM) or 0.1% Ethanol (vehicle, as negative control) or 300ng/ml of Noggin (positive control). Following stimulation with 2ng/ml of BMP4 for another 1 hour, the samples were lysed and subjected to western blot to analyse the level of BMP-induced SMAD1/5/8 phosphorylation (P-SMAD1/5/8) as well as βactin, as loading control.

Western blot analysis (Figure 3:2) demonstrated no SMAD1/5/8 phosphorylation in untreated H9 cells without any treatment (lane 1) and its strong induction by BMP4 treatment (lane 2). In cultures stimulated with BMP4 (lane 2-13), pre-treatment with Noggin effectively blocked this induction (lane 3), whereas, vehicle only treatment had no effect (lane 4). Pre-treatment with Dorsomorphin (lane 5-7) or LDN193189 (lane 8-10) or DMH-1 (lane 11-13) attenuated P-SMAD1/5/8 in a dose-dependent manner. The intensity of bands was quantified using image J software. P-SMAD1/5/8 intensity of each treatment was determined by measuring the ratio of P-

SMAD1/5/8 and  $\beta$ -actin. The relative intensity percentage normalised to maximum response signal ie, BMP4 alone treatment was then plotted (Figure 3:2). This analysis generated a dose-response pattern of small molecules in blocking BMP induced P-SMAD1/5/8.

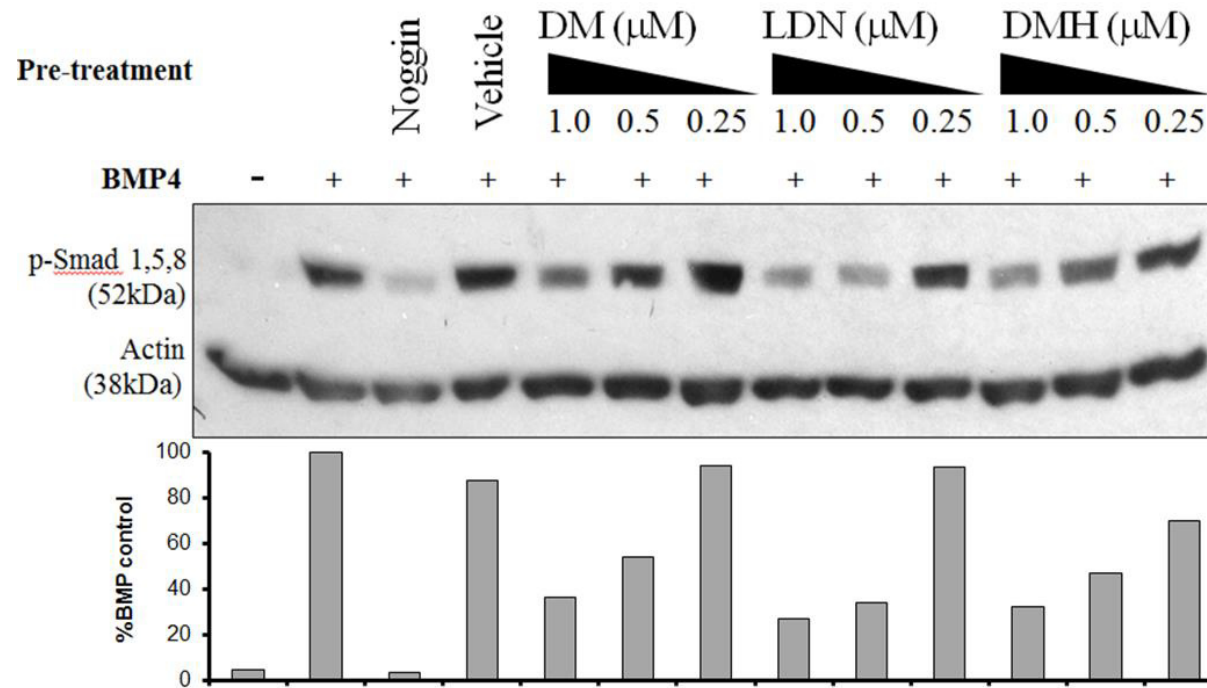


Figure 3:2 Attenuation of BMP4 induced phosphorylation of SMAD1/5/8 in undifferentiated H9 cells by small molecules- Western blot analysis of P-SMAD1/5/8 in H9 cells pre-treated with vehicle or Noggin (300ng/ml) or increasing concentrations of small molecules Dorsomorphin (DM) or LDN193189 (LDN) or DMH-1 and then stimulated with BMP4 (2ng/ml). 30 $\mu$ g of total proteins were loaded into each lane.  $\beta$ Actin was the loading control. Band intensity of PSMAD1/5/8 signal was quantified with ImageJ software. Y axis in the graph represents relative intensity percentage normalised to maximum response signal generated by BMP4 treatment (=100%) without Noggin or small molecules pre-treatment

### 3.4.2 QRT-PCR characterization of small molecule mediated inhibition of endogenous BMP activity during H9 neural induction

Next, the effectiveness of small molecule in blockade of endogenous BMP signalling during neural induction (Figure 3:1) was analysed. At D8, the expression levels of *ID1* and *ID3*, direct transcriptional targets of BMP signalling (Yang *et al.* 2008) was analysed by QRT-PCR. The expression levels normalised to reference gene  $\beta$ -actin (see appendix Table 3.1 for  $\Delta Cq$ ) The fold change determined relative to untreated only control (=1),  $2^{-\Delta\Delta Cq}$  was plotted (Figure 3:3).

A similar level of *ID1* and *ID3* expression were seen in untreated (*ID1*=1.0; *ID3*=1.0) and SB431542 treated cultures (*ID1*=0.9; *ID3*=1.1) (Figure 3:3A and C). Addition of Noggin decreased the expression (*ID1*=0.4; *ID3*=0.3) compared with SB431542 alone (Figure 3:3 B and D). Substituting Dorsomorphin or LDN193189 or DMH-1, for Noggin resulted in an increased inhibition of both *ID1* and *ID3* levels (Figure 3:3 B and D). Dorsomorphin treatment at 0.25 $\mu$ M (*ID1*= 0.3; *ID3* = 0.1), 0.5 $\mu$ M (*ID1*= 0.2; *ID3*= 0.3) and 1.0 $\mu$ M (*ID1*= 0.3; *ID3*= 0.3) reduced the expression levels compared to SB431542 alone. Similarly, LDN193189 treatment at 0.25 $\mu$ M (*ID1*=0.0; *ID3*=0.1), 0.5 $\mu$ M (*ID1*=0.0; *ID3*=0.1) and 1.0 $\mu$ M (*ID1*=0.0; *ID3*=0.1) and DMH-1 treatment at 0.25 $\mu$ M (*ID1*=0.1; *ID3*=0.2), 0.5 $\mu$ M (*ID1*=0.1; *ID3*=0.2) and 1.0 $\mu$ M (*ID1*=0.1; *ID3*=0.2) inhibited the expression, compared with SB431542 alone. Within Dorsomorphin group, LDN193189 group or DMH-1 group, addition of increasing concentrations from 0.25 $\mu$ M to 1.0 $\mu$ M did not appear to result in an increased inhibition and the levels seen from 0.25 $\mu$ M to 1.0 $\mu$ M were comparable. LDN193189 treatment appeared to result in lower expression levels than Dorsomorphin, DMH-1 or Noggin treatments. However, further experimental would be needed to obtain a statistical significance.

### 3.4.3 QRT-PCR characterization of neural induction

To investigate whether the inhibition of endogenous BMP signalling by Noggin or small molecules enhance neural induction, the expression of neuroectodermal marker *PAX6*, neural crest marker *SLUG* and pluripotency marker *OCT4* were analysed in day 8 EBs (see appendix Table 3.2 for  $\Delta Cq$ ). The fold change determined relative to untreated or SB431542 alone (=1) was plotted

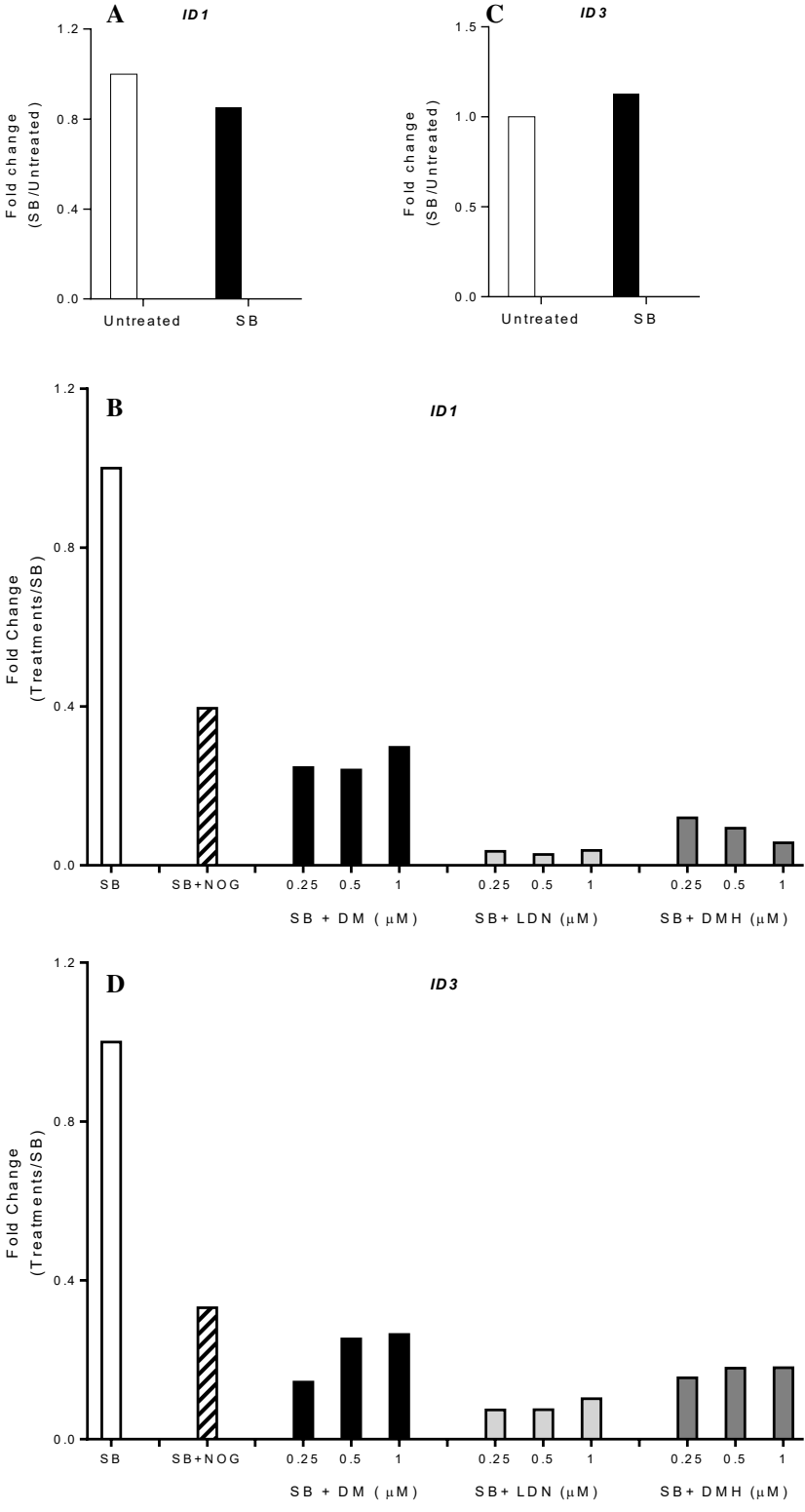


Figure 3:3 Modulation of endogenous BMP signalling by Noggin or small molecules during H9 differentiation- *ID1* expression A) Untreated vs SB431542 (SB) treatment and B) SB431542 vs treatment groups- Dorsomorphin (DM), LDN193189 (LDN) and DMH-1 (DMH). *ID3* expression C) Untreated vs SB431542 treatment and D) SB431542 vs treatment groups The expression levels were normalised to endogenous  $\beta$ -actin. Yaxis in the graph represents expression levels relative to untreated or SB431542 only treated i.e.,  $2^{-\Delta\Delta Cq} = 1$

*PAX6* expression was significantly increased in cultures treated with SB431542 ( $3.4 \pm 0.5$ ) compared with untreated cultures ( $1.0 \pm 0.1$ ) ( $t_4=6.7$ ,  $p<0.001$ ) (Figure 3:4 A). Addition of Noggin ( $2.3 \pm 0.2$ ) or small molecules in combination with SB431542, further significantly increased the expression level compared with SB431542 only treatment ( $1.00 \pm 0.1$ ) ( $F_{10,21}=8.5$ , Dunnett's multiple comparison,  $p<0.0001$ ) (Figure 3:4.B). SB431542+Dorsomorphin treatment at  $0.25 \mu\text{M}$  ( $2.1 \pm 0.2$ ),  $0.5 \mu\text{M}$  ( $3.1 \pm 0.2$ ) and  $1.0 \mu\text{M}$  ( $3.1 \pm 0.4$ ) yielded similar expression levels. SB431542+LDN193189 treatments also showed similar expression levels at  $0.25 \mu\text{M}$  ( $3.2 \pm 0.3$ ),  $0.5 \mu\text{M}$  ( $3.3 \pm 0.3$ ) and  $1.0 \mu\text{M}$  ( $3.1 \pm 0.6$ ). Similarly, SB431542+DMH-1 enhanced *PAX6* expression levels at  $0.25 \mu\text{M}$  ( $3.5 \pm 0.5$ ),  $0.5 \mu\text{M}$  ( $3.8 \pm 0.3$ ) and  $1.0 \mu\text{M}$  ( $3.4 \pm 0.7$ ), compared with SB431542. There was no significant difference in expression level in response to increasing concentrations from  $0.25 \mu\text{M}$  to  $1.0 \mu\text{M}$  of small molecules and among Noggin, Dorsomorphin or LDN193189 or DMH-1 treatment groups.

*SLUG* expression was significantly decreased in cultures treated with SB431542 ( $0.3 \pm 0.1$ ) compared with untreated cultures ( $1.0 \pm 0.1$ ) ( $t_4=5.3$ ,  $p<0.01$ ) (Figure 3:5 A). Addition of Noggin ( $1.3 \pm 0.3$ ) or small molecules in combination with SB431542, did not significantly alter the expression levels ( $F_{10,19}=1.5$ ,  $p=n.s$ ) (Figure 3:5.B). SB431542+Dorsomorphin treatment at  $0.25 \mu\text{M}$  ( $1.0 \pm 0.1$ ),  $0.5 \mu\text{M}$  ( $1.2 \pm 0.1$ ) and  $1.0 \mu\text{M}$  ( $0.9 \pm 0.1$ ) yielded similar expression levels. SB431542+LDN193189 treatments at  $0.25 \mu\text{M}$  ( $0.6 \pm 0.1$ ),  $0.5 \mu\text{M}$  ( $0.6 \pm 0.1$ ) and  $1.0 \mu\text{M}$  ( $0.9 \pm 0.3$ ) also did not differ significantly. Similarly, SB431542+DMH-1 treatment did not have any effect on the expression levels at  $0.25 \mu\text{M}$  ( $0.7 \pm 0.1$ ),  $0.5 \mu\text{M}$  ( $0.8 \pm 0.0$ ) and  $1.0 \mu\text{M}$  ( $0.8 \pm 0.2$ ). There was no significant difference in expression level in increasing concentrations from  $0.25 \mu\text{M}$  to  $1.0 \mu\text{M}$  of small molecules and among Noggin, Dorsomorphin or LDN193189 or DMH-1 treatment groups.

QRT-PCR of *OCT4* generated very weak signal in all day8 EBs. Thus, no further analysis was performed.

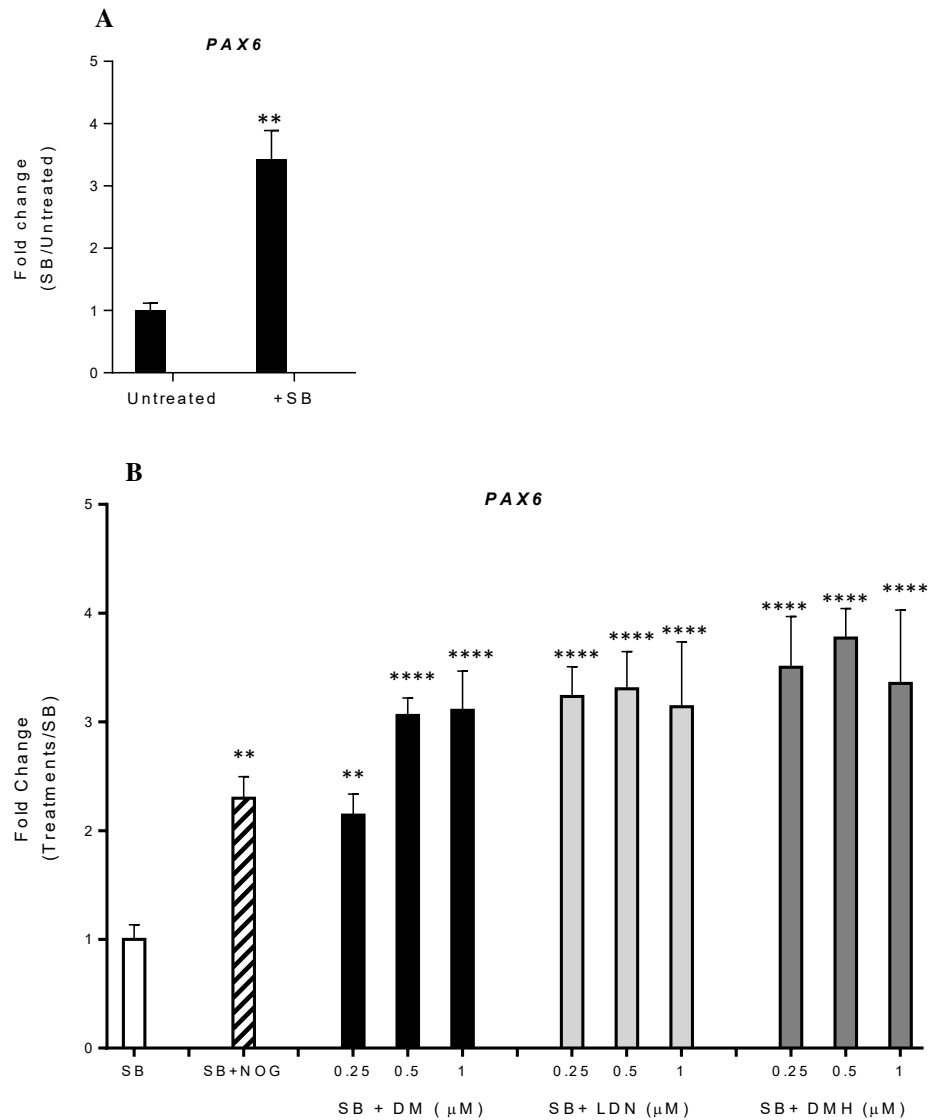


Figure 3:4 Effect of dual SMAD inhibition by SB431542 and either Noggin or small molecules on induction of neuroectoderm marker *PAX6*. A) Untreated vs SB431542 (SB) treatment and (B) SB431542 vs treatment groups- Dorsomorphin (DM), LDN193189 (LDN) and DMH-1 (DMH). The expression levels were normalised to endogenous  $\beta$ -actin. Y axis in the graph represents expression levels relative to untreated or SB431542 only treated (ie,  $2^{-\Delta\Delta Cq} = 1$ ). Data represented as mean  $\pm$  SEM, of 3 different experiment replicates. One way ANOVA with Dunnett's multiple comparison test was used to determine level of significance. \*\*\*\* $p < 0.0001$ , \*\* $p < 0.01$ .

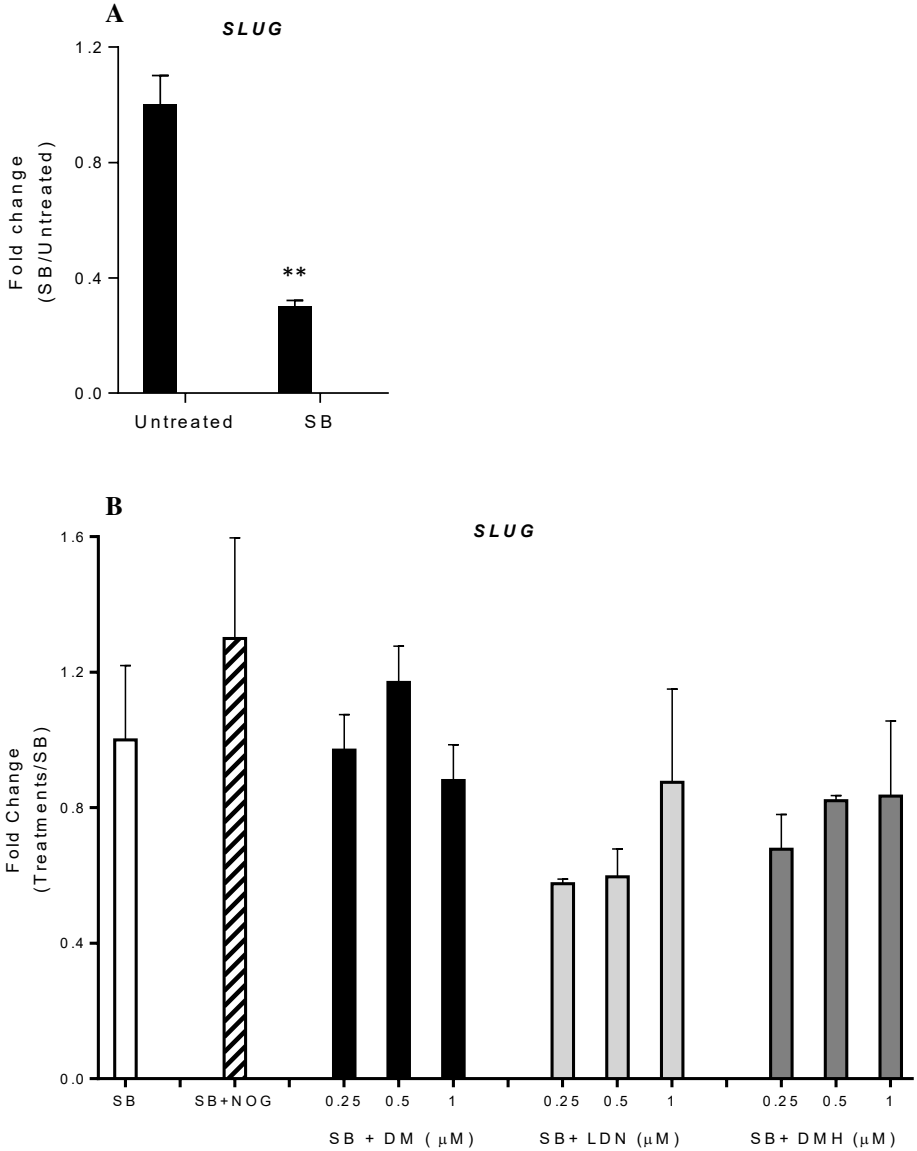


Figure 3:5 Effect of dual SMAD inhibition by SB431542 and either Noggin or small molecules on induction of neuroectoderm marker *SLUG*. A) Untreated vs SB431542 (SB) treatment and B) SB431542 vs treatment groups- Dorsomorphin (DM), LDN193189 (LDN) and DMH-1 (DMH). The expression levels were normalised to endogenous  $\beta$ -actin. Yaxis in the graph represents expression levels relative to untreated or SB431542 only treated (ie,  $2^{-\Delta\Delta Cq} = 1$ ). Data represented as mean  $\pm$  SEM, of 3 different experiment replicates, N=2 for DMH-1 group biological replicates. \*\*p < 0.01

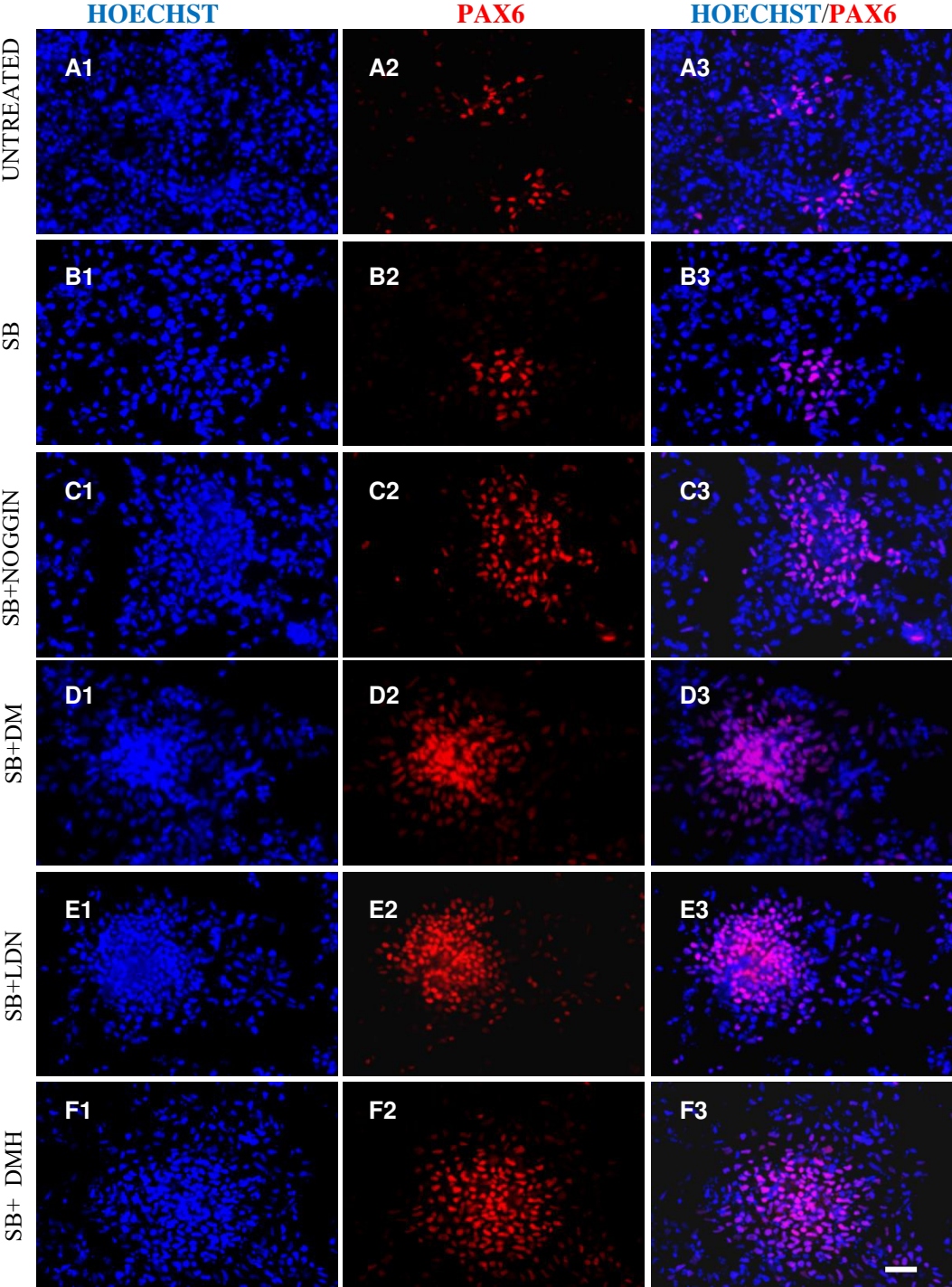
### 3.4.4 Immunocytochemistry characterization of neural induction

To further characterize the neural specification, immunocytochemistry analysis was performed. The highest dose of each small molecule (with minimal cytotoxicity) was taken. Day 8 EBs cultured in the presence of vehicle, SB431542, SB431542+Noggin, SB431542+Dorsomorphin at 1.0 $\mu$ M, SB431542+LDN193189 at 0.5 $\mu$ M and SB431542+DMH-1 at 1 $\mu$ M were enzymatically (using accutase) dissociated into single cells and plated. Cultures were then immuno-stained for neuroectodermal markers- PAX6, SOX2 and NESTIN. The immunofluorescence signal was quantified and represented as percentage of Hoechst positive cells.

PAX6 expression was localized to the nucleus (Figure 3:6). The proportion of PAX6 immuno-positive cells was higher following dual inhibition of SMAD signalling. There was a smaller increase in SB431542 only treatment (25.5 $\pm$ 3.7%) when compared with untreated (15.3 $\pm$ 3.3%) control. Noggin or small molecules in combination with SB431542, resulted in higher PAX6 expression, but the proportion of PAX6<sup>+</sup> cells in SB431542+Noggin (60.8 $\pm$ 2.0%), SB431542+Dorsomorphin (66.9 $\pm$ 3.9%), SB431542+LDN193189 (77.0 $\pm$ 3.2%) or SB431542+DMH-1 (65.7 $\pm$ 0.7%) treated cultures were comparable.

SOX2 expression was localized in the nucleus (Figure 3:7). The proportion of SOX2 immuno-positive cells in untreated (85.1 $\pm$ 4.0%), SB431542 (80.3 $\pm$ 1.2%), SB431542+Noggin (84.0 $\pm$ 1.4%), SB431542+Dorsomorphin (83.6 $\pm$ 1.0%), SB431542+LDN193189 (85.4 $\pm$ 5.1%) or SB431542+DMH-1 (80.0 $\pm$ 1.2%) were comparable.

NESTIN immunoreactivity was present in the cell soma and extended to the neuronal like projections (Figure 3:8). The proportion of NESTIN immuno-positive cells was significantly higher following SB431542 treatment or dual SMAD inhibition (no statistical test was performed as only N=1 was performed). The percentage of NESTIN immuno-positive cells in untreated, SB431542, SB431542+Noggin, SB431542+Dorsomorphin, SB431542+LDN193189 and SB431542+DMH-1 respectively, were found to be 33.5 $\pm$ 7.10%, 90.8 $\pm$ 2.5%, 94.4 $\pm$ 3.0%, 91.6 $\pm$ 1.6%, 91.0 $\pm$ 3.1% and 93.2 $\pm$ 5.1%.



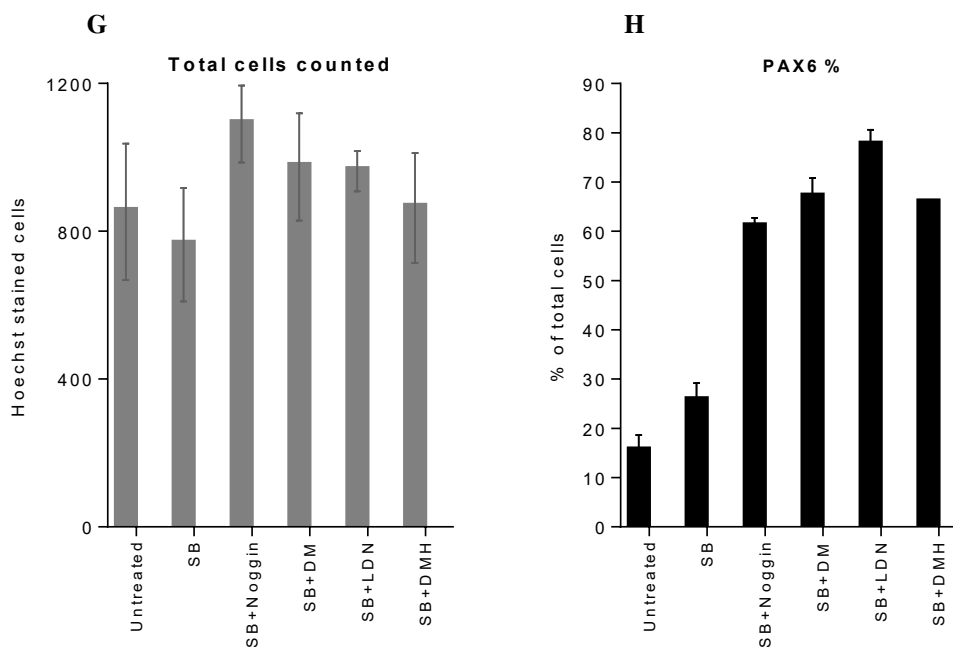
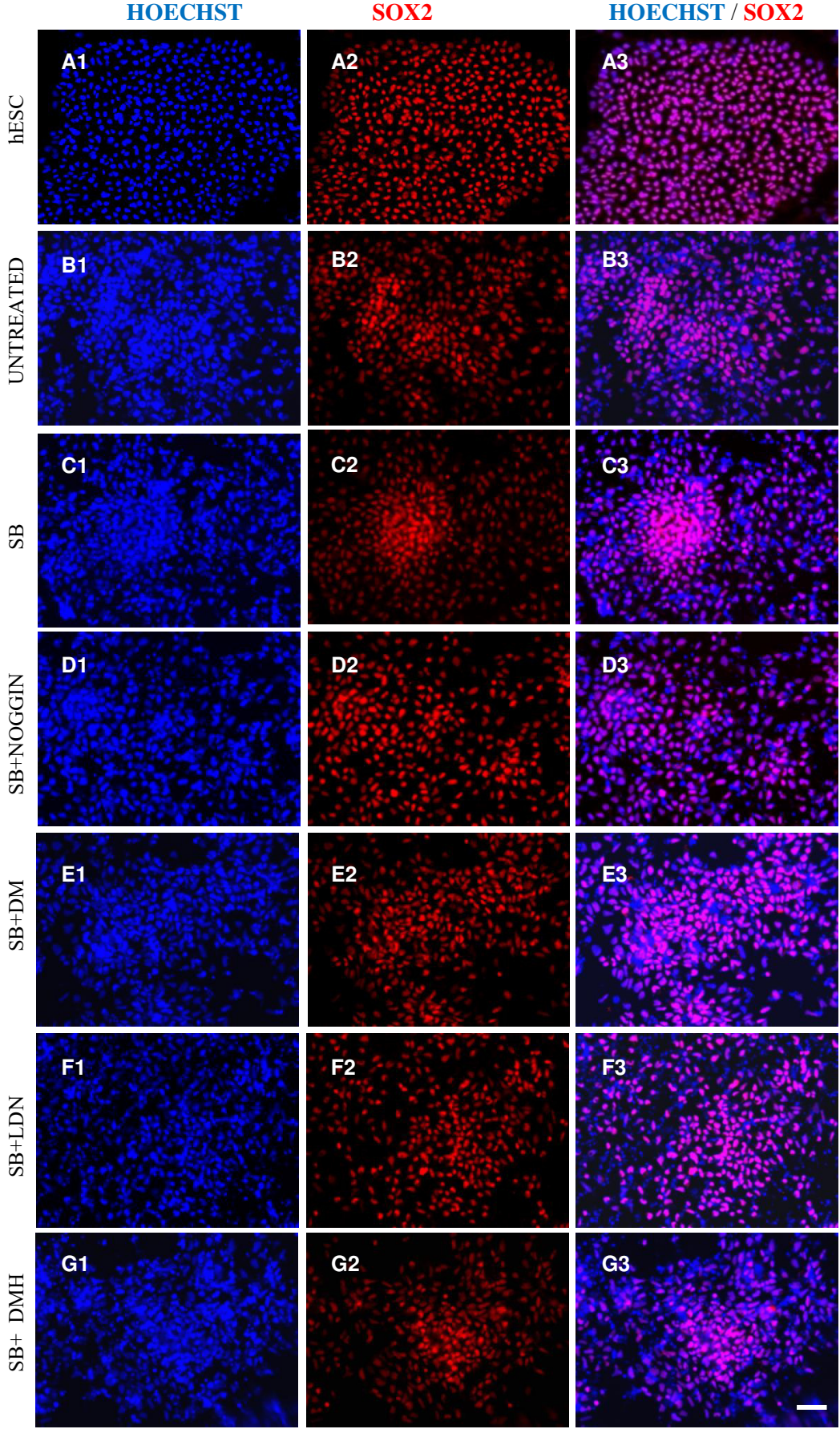


Figure 3:6 Fluorescent immunocytochemistry analysis of PAX6 in D8 cultures. D8 EBs were generated in the absence or in the presence of BMP inhibitors. EBs were then dissociated, replated as single cells onto PLL coated coverslips and fixed on the same day for immunocytochemistry analysis. Cells were immunostained for PAX6 (red) and counter stained for Hoechst nuclear stain (blue). Representative images are given- (A1-F1) of Hoechst stained cells, (A2-F2) PAX6 stained cells and (A3-F3) Hoechst /PAX6 merge, generated in the presence of (A1-A3) no treatment, (B1-B3) SB431542 (SB), (C1-C3) SB431542 + Noggin at 300ng/ml, (D1-D3) SB431542 + Dorsomorphin (DM) at 1.0 $\mu$ M, (E1-E3) SB431542 + LDN193189 (LDN) at 0.5 $\mu$ M and (F1-F3) SB431542 + DMH-1 at 1.0 $\mu$ M.. Scale bar for all images in bottom right image = 100 $\mu$ m. Multiple fields/coverslips were imaged. Graphs represent (G) the number of Hoechst-stained nuclei counted for each treatment and (H) proportion of PAX6 as % of total nuclei. Data represented as mean  $\pm$  SEM of 2 different experiment replicates



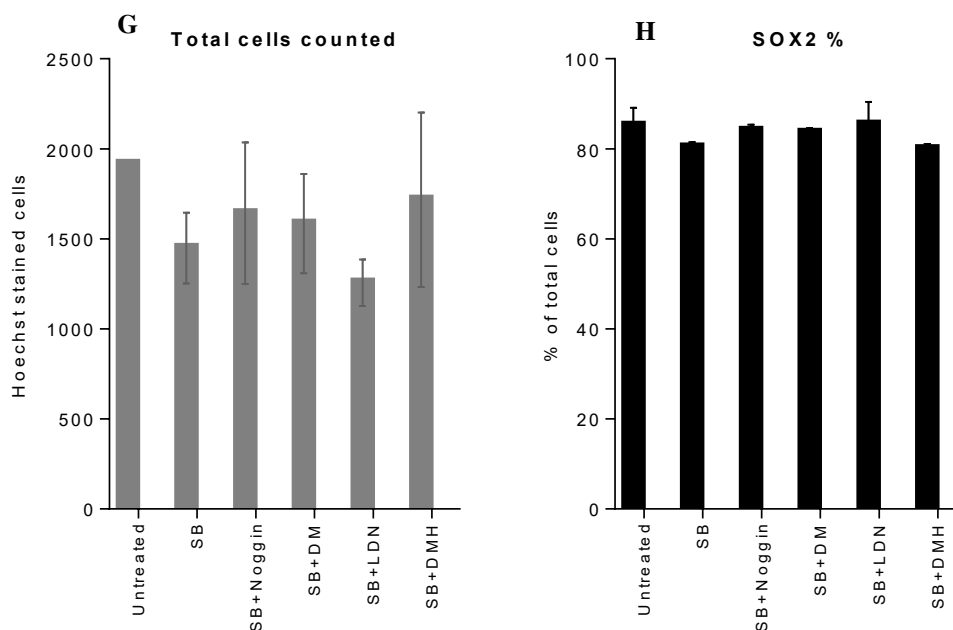
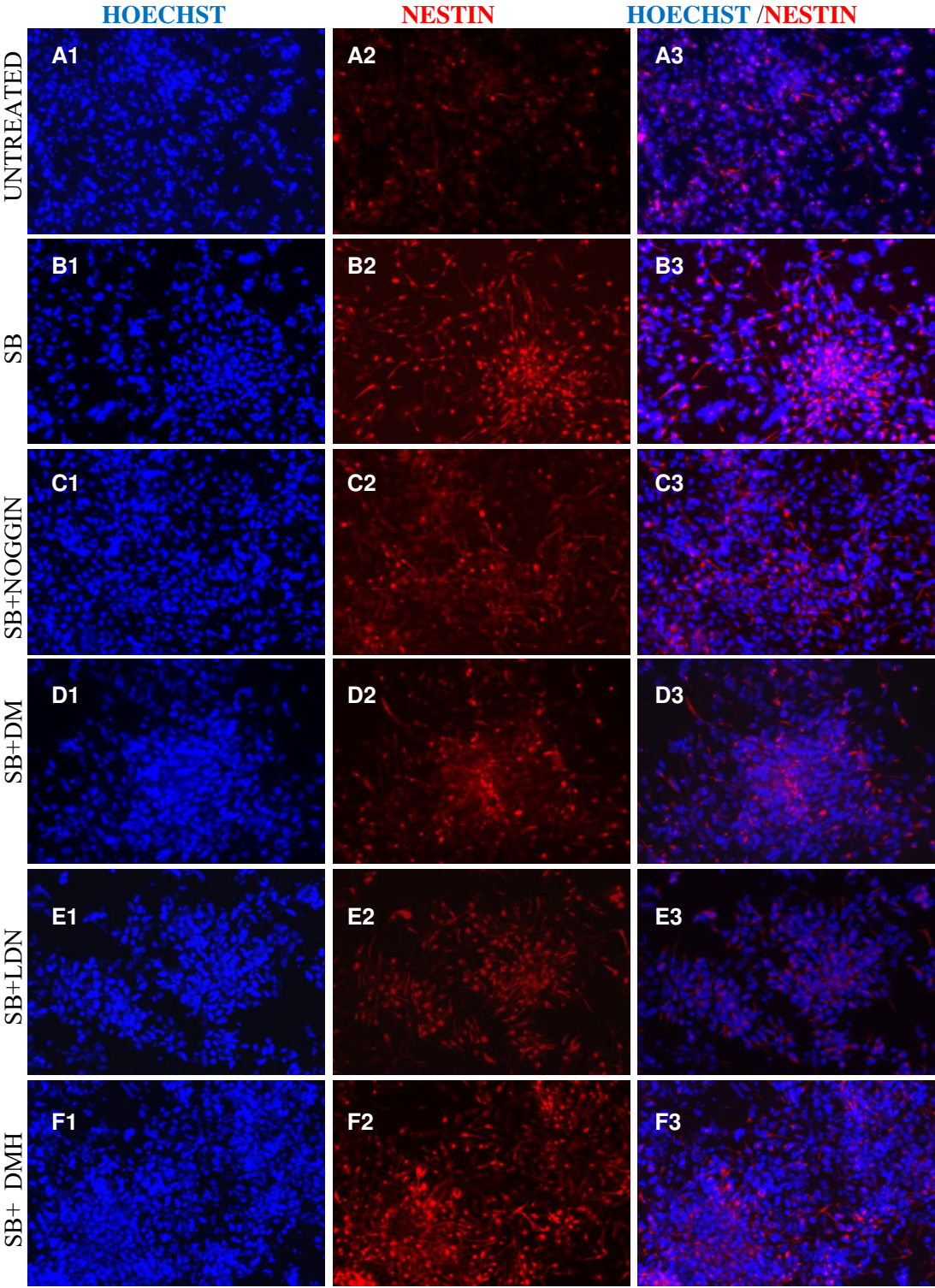


Figure 3:7 Fluorescent immunocytochemistry analysis of SOX2 in D8 cultures. D8 EBs were generated in the absence or in the presence of BMP inhibitors. EBs were then dissociated, re-plated as single cells onto PLL coated coverslips and fixed on the same day for immunocytochemistry analysis. Cells were immunostained for SOX2 (red) and counter stained for Hoechst nuclear stain (blue). Representative images are given- (A1-F1) of Hoechst stained cells, (A2-F2) SOX2 stained cells and (A3-F3) Hoechst/SOX2 merge, (A1-A3) undifferentiated hESC (D0) and D8 EBs generated in the presence of (B1-B3) no treatment, (C1-C3) SB431542 (SB), (D1-D3) SB431542 + Noggin at 300ng/ml, (E1-E3) SB431542 + Dorsomorphin (DM) at 1.0 $\mu$ M, (F1-F3) SB431542 + LDN193189 (LDN) at 0.5 $\mu$ M and (G1-G3) SB431542 + DMH-1 at 1.0 $\mu$ M. Scale bar for all images in bottom right image = 100 $\mu$ m. Multiple fields/coverslips were imaged. Graphs represent (G) the number of Hoechst-stained nuclei counted for each treatment and (H) proportion of SOX2 as % of total nuclei. Data represented as mean  $\pm$  SEM, N=2 biological replicates.



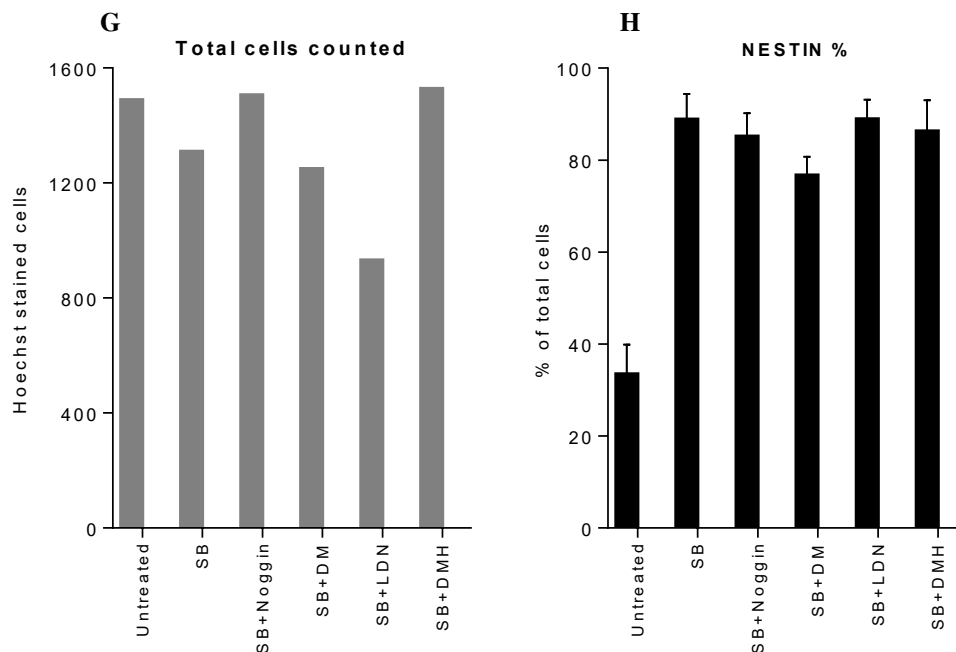


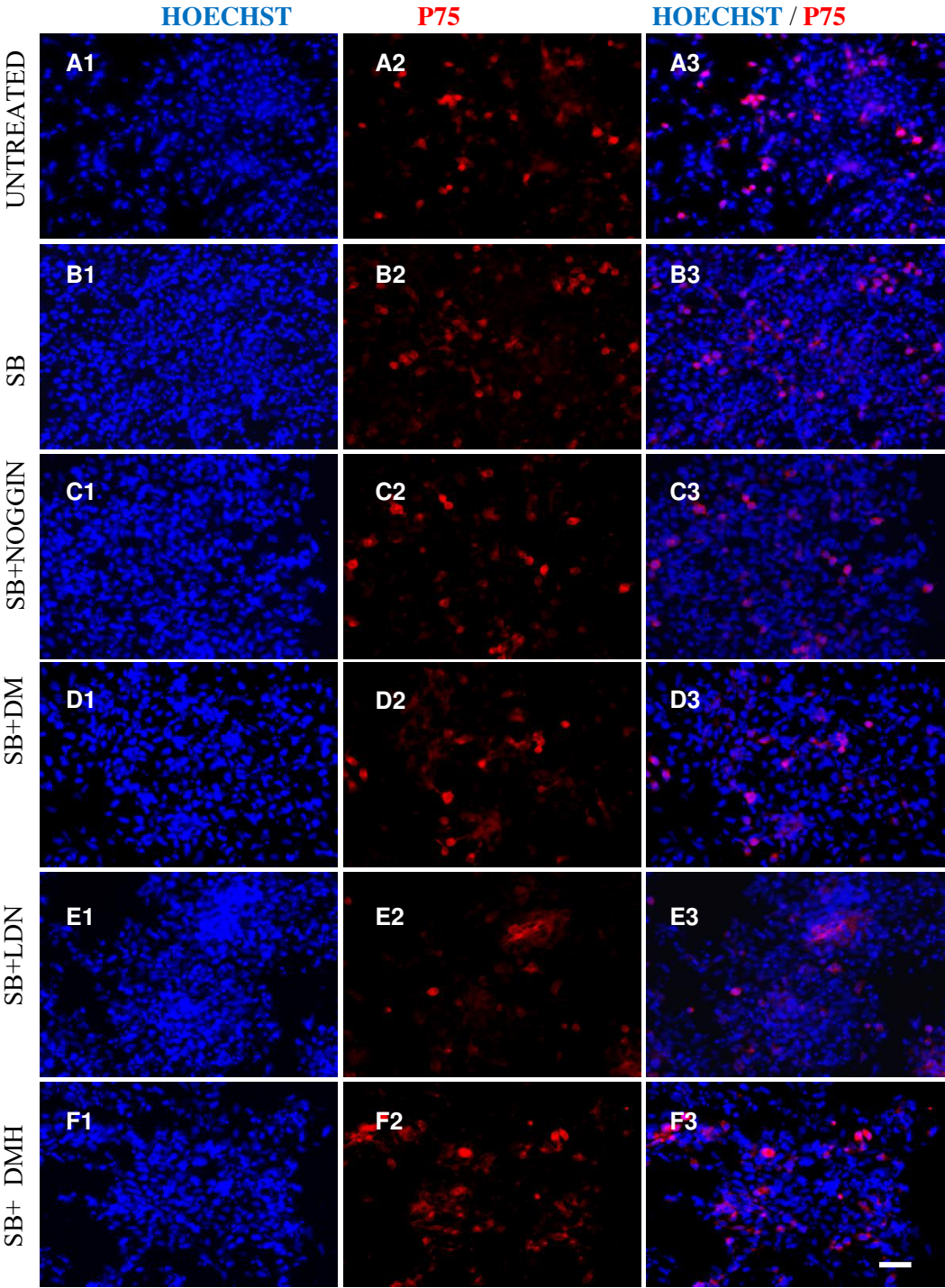
Figure 3:8 Fluorescent immunocytochemistry analysis of NESTIN in D8 cultures. D8 EBs were generated in the absence or in the presence of BMP inhibitors. EBs were then dissociated, re-plated as single cells onto PLL coated coverslips and fixed on the same day for immunocytochemistry analysis. Cells were immunostained for NESTIN (red) and counter stained for Hoechst nuclear stain (blue). Representative images are given- (A1-F1) of Hoechst stained cells, (A2-F2) V stained cells and (A3-F3) Hoechst/NESTIN merge, generated in the presence of (A1-A3) no treatment, (B1-B3) SB431542 (SB), (C1-C3) SB431542 + Noggin at 300ng/ml, (D1-D3) SB431542 + Dorsomorphin (DM) at 1.0 $\mu$ M, (E1-E3) SB431542 + LDN193189 (LDN) at 0.5 $\mu$ M and (F1-F3) SB431542 + DMH-1 at 1.0 $\mu$ M.. Scale bar for all images in bottom right image=100 $\mu$ m. Multiple fields/coverslips were imaged. Graphs represent (G) the number of Hoechst-stained nuclei counted for each treatment and (H) proportion of NESTIN as % of total nuclei. Data represented as mean  $\pm$  SD, N=1, experiment replicates

In parallel to the neuroectodermal markers, the neural crest marker P75 and epidermal marker Cytokeratin 18 (CK18) were analysed (no statistical test was performed as only N=1 was performed). P75 expression was localized on surface of cells (Figure 3:9) and quantification revealed a similar proportion of positive cells across untreated control and treatment samples. P75% in untreated, SB431542, SB431542+Noggin, SB431542+Dorsomorphin, SB431542+LDN193189 and SB431542+DMH-1 respectively, were found to be  $10.2 \pm 2.2\%$ ,  $13.2 \pm 2.8\%$ ,  $9.2 \pm 0.9\%$ ,  $11.5 \pm 3.7\%$ ,  $13.6 \pm 2.1\%$  and  $14.7 \pm 2.5\%$ .

CK18 expression was localized in the cytoplasm (Figure 3:10). Quantification of the filamentous CK18 protein was problematic, however of the total population, CK18<sup>+</sup> region was negligible.

The amount of proliferative neural precursors in the differentiating EBs were analysed by immunocytochemistry for KI67 (MKI67), a marker of cells in the all the phases of cell cycle (G1, S, G2, and mitosis) was performed. The proportion of KI67 immuno-positive cells was determined as the percentage of total nuclei (KI67%) (figure 3.11). There was no difference in KI67% between vehicle or treatment group. The immuno-positive cells in vehicle, SB431542, SB431542+Noggin, SB431542+Dorsomorphin, SB431542+LDN193189 and SB431542+DMH-1 respectively, were found to be  $44.4 \pm 2.9\%$ ,  $54.4 \pm 3.7\%$ ,  $45.9 \pm 7.2\%$ ,  $50.9 \pm 7.1\%$ ,  $44.6 \pm 8.4\%$  and  $45.3 \pm 3.8\%$ .

Finally, the amount of OCT4 immunoreactive cells were analysed. There was no expression in any of the D8 EBs, whereas the undifferentiated hESCs stained highly OCT4<sup>+</sup> (figure 3.12).



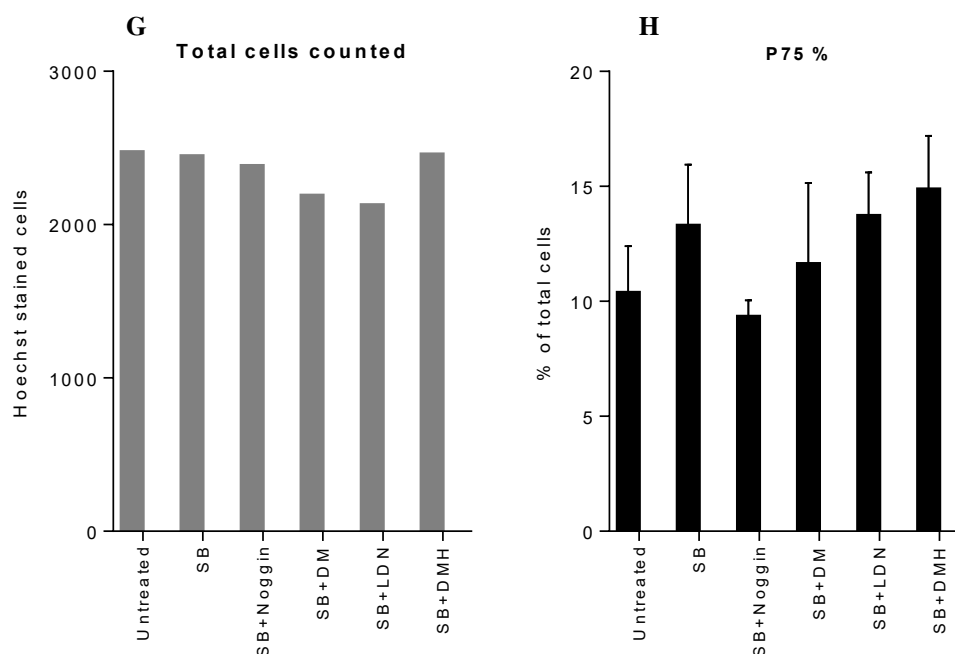


Figure 3:9 Fluorescent immunocytochemistry analysis of P75 in D8 cultures. D8 EBs were generated in the absence or in the presence of BMP inhibitors. EBs were then dissociated, replated as single cells onto PLL coated coverslips and fixed on the same day for immunocytochemistry analysis. Cells were immunostained for P75 (red) and counter stained for Hoechst nuclear stain (blue). Representative images are given- (A1-A3) no treatment, (B1-B3) SB431542 (SB), (C1-C3) SB431542 + Noggin at 300ng/ml, (D1-D3) SB431542 + Dorsomorphin (DM) at 1.0 $\mu$ M, (E1-E3) SB431542 + LDN193189 (LDN) at 0.5 $\mu$ M and (F1-F3) SB431542 + DMH-1 at 1.0 $\mu$ M.. Scale bar for all images in bottom right image=100 $\mu$ m. Multiple fields/coverslips were imaged. Graphs represent (G) the number of Hoechst-stained nuclei counted for each treatment and (H) proportion of P75 as % of total nuclei. Data represented as mean  $\pm$  SD, N=1, experiment replicates

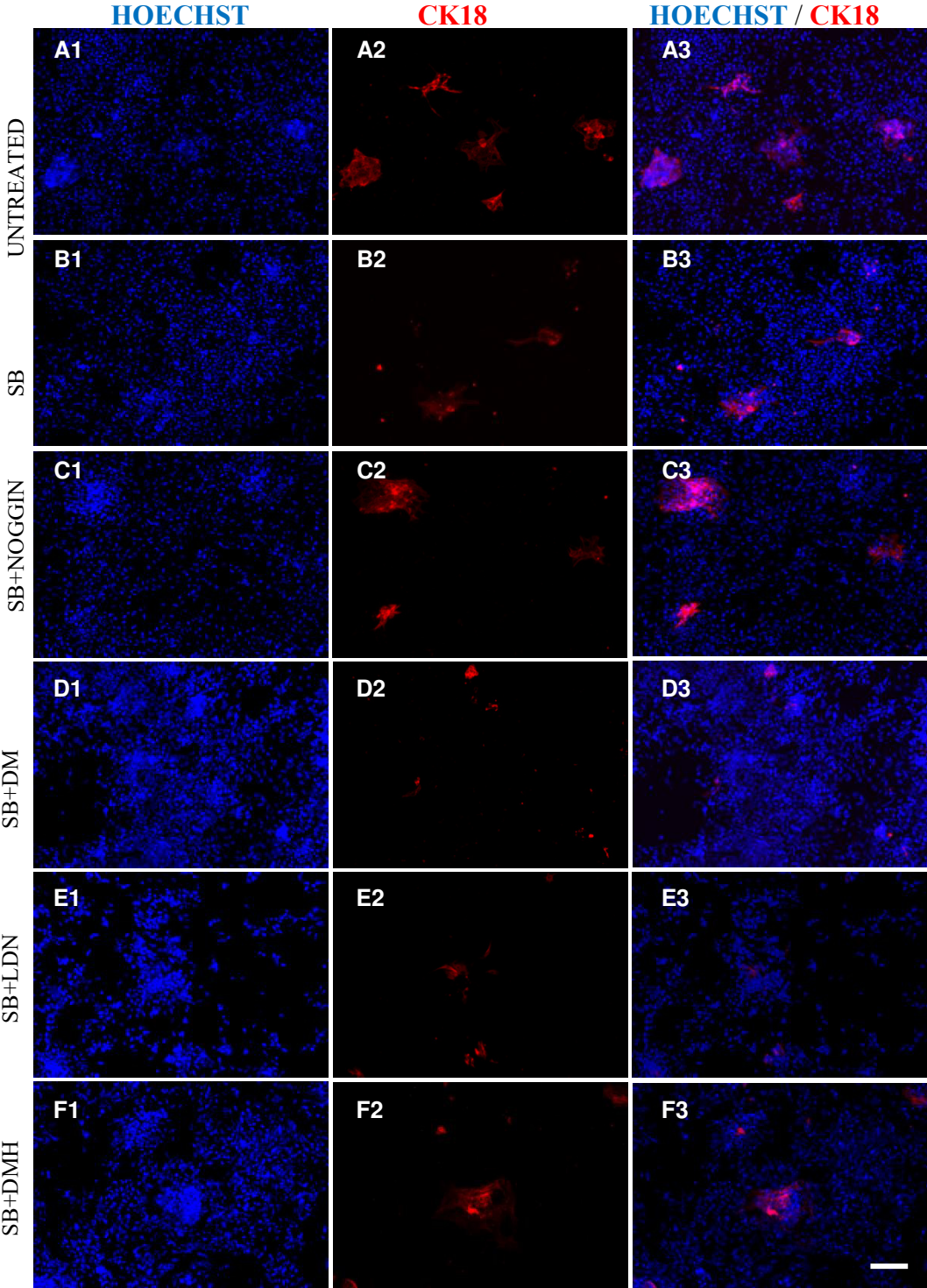
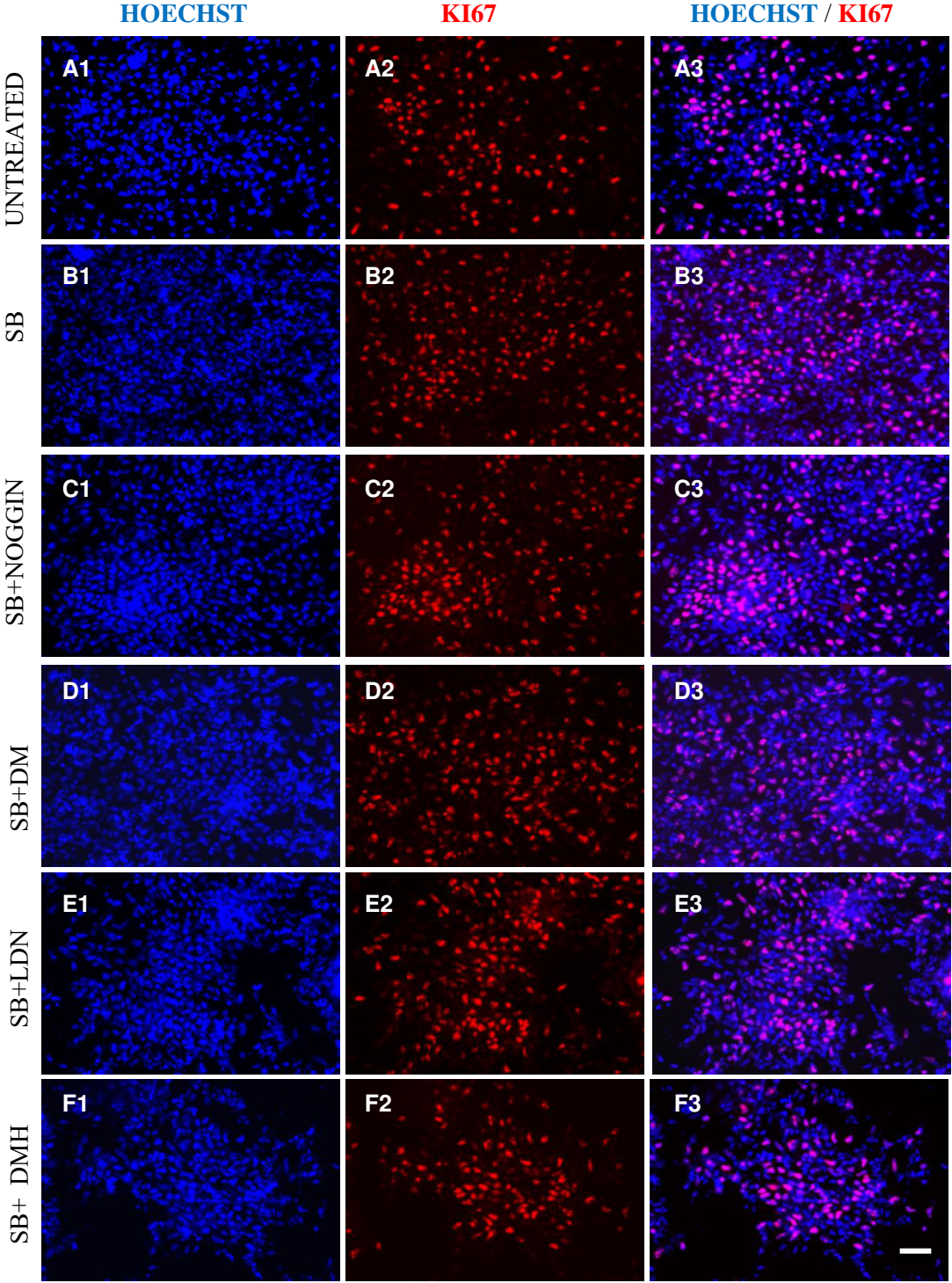


Figure 3:10 Fluorescent immunocytochemistry analysis of CK18 in D8 cultures. D8 EBs were generated in the absence or in the presence of BMP inhibitors. EBs were then dissociated, re-plated as single cells onto PLL coated coverslips and fixed on the same day for immunocytochemistry analysis. Cells were immunostained for CK18 (red) and counter stained for Hoechst nuclear stain (blue). Representative images are given- (A1-F1) of Hoechst stained cells, (A2-F2) CK18 stained cells and (A3-F3) Hoechst/CK18 merge, generated in the presence of (A1-A3) no treatment, (B1-B3) SB431542 (SB), (C1-C3) SB431542 + Noggin at 300ng/ml, (D1-D3) SB431542 + Dorsomorphin (DM) at 1.0µM, (E1-E3) SB431542 + LDN193189 (LDN) at 0.5µM and (F1-F3) SB431542 + DMH-1 at 1.0µM. Scale bar for all images in bottom right image = 200µm.



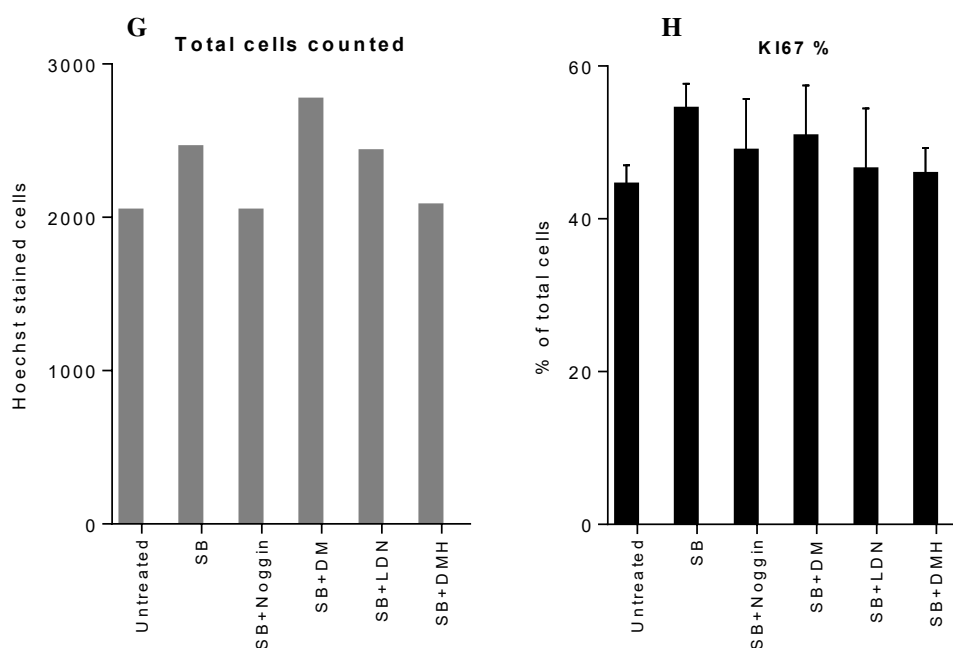


Figure 3:11 Fluorescent immunocytochemistry analysis of KI67 in D8 cultures. D8 EBs were generated in the absence or in the presence of BMP inhibitors. EBs were then dissociated, replated as single cells onto PLL coated coverslips and fixed on the same day for immunocytochemistry analysis. Cells were immunostained for KI67 (red) and counter stained for Hoechst nuclear stain (blue). Representative images are given- (A1-F1) of Hoechst stained cells, (A2-F2) KI67 stained cells and (A3-F3) Hoechst/KI67 merge, generated in the presence of (A1-A3) no treatment, (B1-B3) SB431542 (SB), (C1-C3) SB431542 + Noggin at 300ng/ml, (D1-D3) SB431542 + Dorsomorphin (DM) at 1.0 $\mu$ M, (E1-E3) SB431542 + LDN193189 (LDN) at 0.5 $\mu$ M and (F1-F3) SB431542 + DMH-1 at 1.0 $\mu$ M. Scale bar for all images in bottom right image=100 $\mu$ m. Multiple fields/coverslips were imaged. Graphs represent (G) the number of Hoechst-stained nuclei counted for each treatment and (H) proportion of KI67 as % of total nuclei. Data represented as mean  $\pm$  SD, N=1 experiment replicates

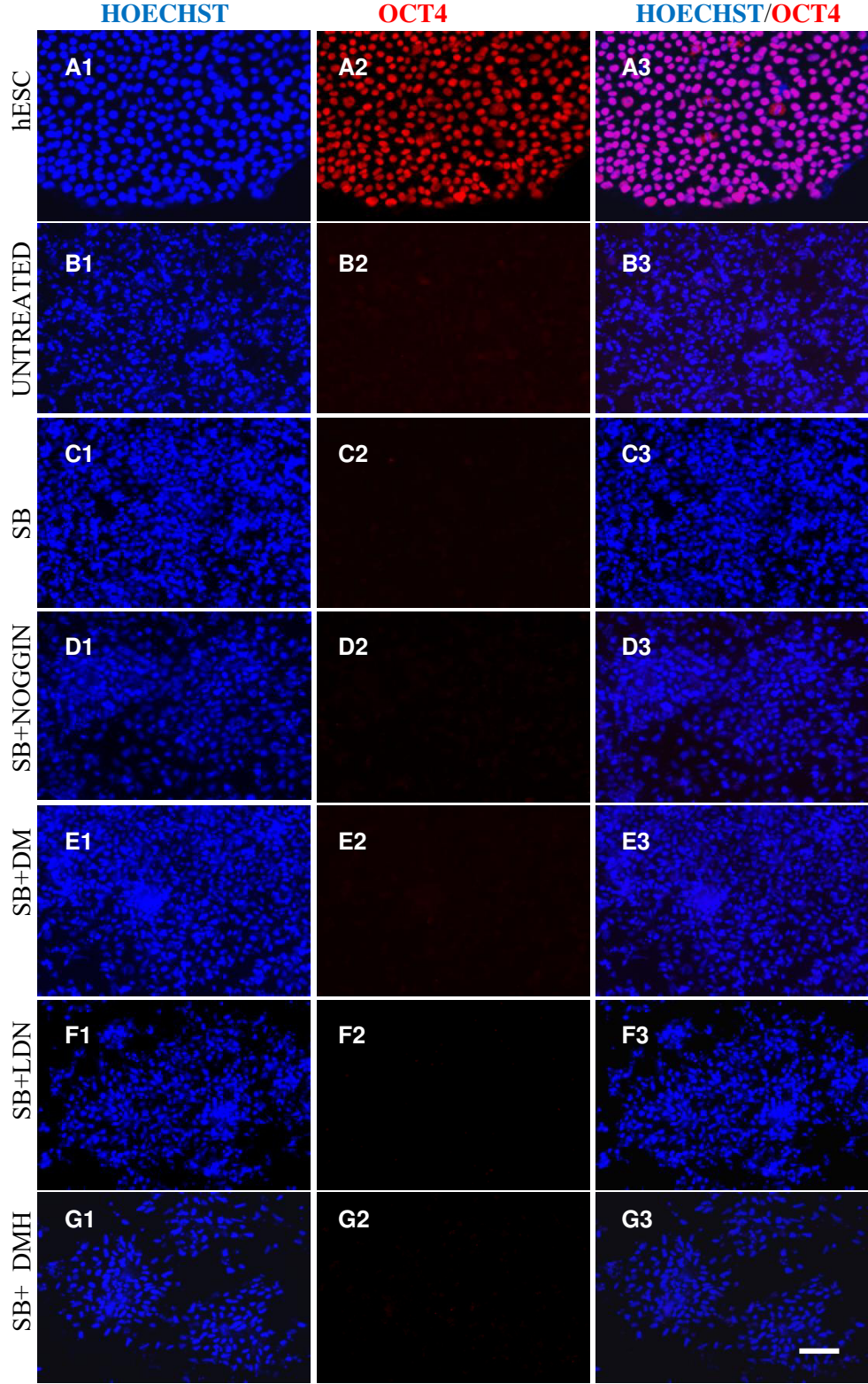


Figure 3:12 13Fluorescent immunocytochemistry analysis of OCT4 in D8 cultures. D8 EBs were generated in the absence or in the presence of BMP inhibitors. EBs were then dissociated, re-plated as single cells onto PLL coated coverslips and fixed on the same day for immunocytochemistry analysis. Cells were immunostained for OCT4 (red) and counter stained for Hoechst nuclear stain (blue). Multiple fields/coverslips were imaged. Representative images are given- (A1-A3) undifferentiated hESC (D0) and D8 EBs generated in the presence of (B1-B3) no treatment, (C1-C3) SB431542 (SB), (D1-D3) SB431542 + Noggin at 300ng/ml, (E1-E3) SB431542 + Dorsomorphin (DM) at 1.0µM, (F1-F3) SB431542 + LDN193189 (LDN) at 0.5µM and (G1-G3) SB431542 + DMH-1 at 1.0µM. Scale bar for all images in bottom right image = 100µm

### 3.5 Discussion

Neural induction of hPSCs requires an exit from the pluripotent stem cell stage and differentiation into neuroectoderm bypassing differentiation into other germ layers and other ectodermal cell types. As described in the introduction, TGF- $\beta$ /nodal/Activin signalling via SMAD2/3 maintains hPSC pluripotency (Xiao *et al.* 2006; Xu *et al.* 2008; Vallier *et al.* 2009). Previous reports showed that inhibition of SMAD2/3 signalling by SB431542 reduced OCT4 and NANOG expression and induced differentiation into NESTIN<sup>+</sup> SOX1<sup>+</sup> neuroectoderm fate (Smith *et al.* 2008) as well as trophoblast fate (Chambers *et al.* 2009; Morizane *et al.* 2011). Trophoblast fate was initiated by BMP mediated SMAD1/5/8 signalling; supplementation of BMP4 induced hPSC conversion to trophoblast (Xu *et al.* 2002) whereas, supplementation of Noggin blocked this differentiation (Xu *et al.* 2002; Chambers *et al.* 2009). TGF- $\beta$ /nodal/Activin and BMP signalling also initiated hPSC mesoderm, endoderm and extra-embryonic endoderm differentiation (Pera *et al.* 2004; Sumi *et al.* 2008). Supplementation of Noggin suppressed this non-neural differentiation and enhanced neural differentiation (Pera *et al.* 2004; Itsykson *et al.* 2005). Later, the concomitant inhibition of SMAD2/3 and SMAD1/5/8 by SB431542 and Noggin was reported to be more effective than SB431542 or Noggin alone treatments. It resulted in highly efficient neuroectodermal conversion of hPSCs by downregulating pluripotency and suppressing differentiation towards, trophoblast, mesoderm and endoderm (Chambers *et al.* 2009). This strategy of dual-SMAD inhibition was applied to an EB based culture to investigate the effect of small molecule BMP inhibitors in my study (figure 3.1).

#### 3.5.1 Effect of BMP inhibitors on neuroectodermal and pluripotency markers

The main result of this study was the demonstration that inhibition of BMP signalling promoted PAX6, but not SOX2 and NESTIN expression, under the culture conditions used. At the protein level, the untreated control cultures contained ~15% PAX6<sup>+</sup>, 85% SOX2<sup>+</sup> and 34% NESTIN<sup>+</sup> cells, indicative of default acquisition of neural identity under the culture conditions used. SB431542 only treatment enhanced PAX6 mRNA expression (3 fold), but resulted in a comparable percentage of PAX6<sup>+</sup> (~26%) and SOX2<sup>+</sup> (~81%) and strongly induced NESTIN<sup>+</sup> (90%). This data was consistent with the previous reports; SB431542 alone treatment in an

adherent culture caused only a slight increase in PAX6 protein (Zhou *et al.* 2010; Surmacz *et al.* 2012) and in an EB based culture, upregulated NESTIN expression and resulted in marginally high but not significantly different SOX1 expression (Smith *et al.* 2008; Morizane *et al.* 2011). Addition of Noggin in combination with SB431542, further enhanced PAX6 expression at both mRNA (2.3 fold) and protein levels (~60% PAX6<sup>+</sup>), but not SOX2 (~84%) and NESTIN (~94%) proteins. This data on PAX6 was consistent with the previously reported hESC monolayer based dual-SMAD inhibition by SB431542 and Noggin, in which, combined treatment for 11 days yielded >80% PAX6<sup>+</sup> cells, compared with <10% when SB431542 or Noggin was used alone (Chambers *et al.* 2009). The difference in PAX6% obtained in my study can be attributed to the discrepancies between the culture conditions and concentration of Noggin used. Temporal analysis of gene expression in their study revealed SOX1 as the earliest marker, preceding PAX6. Only one time point was analysed in my study. Based on the induction of PAX6 which was shown to be a definitive human neuroectoderm fate determinant (Zhang *et al.* 2010), it could be concluded that compared with no treatment or SB431542 alone treatment, dual SMAD inhibition by SB431542 and Noggin in my study efficiently induced neuroectodermal fate in hESCs.

Substituting Dorsomorphin or LDN193189 or DMH-1 for Noggin had a comparable effect. However, no dose dependent effect of small molecules was seen on PAX6 mRNA levels. At all the doses -0.25, 0.5 and 1.0 $\mu$ M, all the 3 small molecules induced around 3-4 fold increase in PAX6 expression. EBs generated using the highest tolerable dose (with minimal cytotoxicity as monitored under phase contrast microscope. Dorsomorphin at 5 $\mu$ m and LDN193189 above 1 $\mu$ M were cytotoxic) - Dorsomorphin at 1 $\mu$ M, LDN193189 at 0.5 $\mu$ M and DMH-1 at 1 $\mu$ M yielded 67%, 77% and 66% PAX6, respectively and the difference was not statistically significant. The same cultures also showed 80-85% SOX2 and 90-93% NESTIN expression. At the time of my study, use of these small molecules to replace Noggin was a novel concept and during the period of my study, similar studies were reported, supporting the dual-SMAD inhibition strategy for efficient neural induction. Dorsomorphin alone treatment dose dependently (0.1 to 5 $\mu$ M) induced PAX6, SOX1 and NESTIN expression and reduced trophoblast markers, indicating that Dorsomorphin by itself permissively supported neural induction (Kim *et al.*

2010; Morizane *et al.* 2011). Although decreased, considerable expression of markers of pluripotency, mesoderm and endoderm were still detectable in those cultures. Simultaneous treatment with SB431542 and Dorsomorphin effectively reduced those markers and highly enriched neural markers (Kim *et al.* 2010; Morizane *et al.* 2011). LDN193189 was shown to be a more potent and efficient inducer of PAX6<sup>+</sup> cells than Dorsomorphin; under monolayer culture for 8 days, SB431542+LDN193189 (1 $\mu$ M) treatment induced ~80% PAX6 in comparison to ~60% PAX6 with SB431542+Dorsomorphin (5 $\mu$ M) +Noggin (50ng/ml). The dose-response curve demonstrated PAX6 induction with an EC50=4.84nm (Surmacz *et al.* 2012). The efficacy of DMH-1 on neural induction has been reported. Comparing SB431542+Noggin (500ng/ml) or SB431542+DMH-1 (0.5 $\mu$ M) in a monolayer based protocol showed similar level induction of PAX6 at both protein and mRNA levels (Neely *et al.* 2012). In their study, induction of SOX1 preceded PAX6 expression as previously reported by Chambers *et al.* (2009). Interestingly, temporal analysis of gene expression revealed a differential regulation of SOX1 at mRNA and protein levels; while both Noggin and DMH-1 treatment upregulated SOX1 by day3, its expression was downregulated by day 5-7 in the presence of DMH-1, whereas it remained elevated in the presence of Noggin. Protein analysis revealed Noggin and DMH-1 dose dependent increase of SOX1 expression, but not on PAX6 expression (Neely *et al.* 2012). DMH-1 at 5 $\mu$ M and Noggin at 500ng/ml generated a comparable SOX1 expression level even though the SOX1% varied between the cell lines used (Neely *et al.* 2012).

Small molecule dose-dependent effect was seen on the inhibition of BMP-induced phosphorylation of SMAD1/5/8 signalling in undifferentiated hESCs. Therefore, all the doses were tested for neural induction to analyse a dose-dependent effect. Due to technical difficulties in obtaining enough protein from D8 EBs to be analysed by western blotting, inhibition of BMP signalling was analysed by QRT-PCR of *ID1* and *ID3*. At D8, all the 3 doses tested, equally inhibited BMP signalling, explaining the comparable PAX6 transcript level achieved by small molecules treatment. As mentioned, Dorsomorphin, LDN193189 and DMH-1 act by inhibiting BMP type I receptors. Dorsomorphin at IC<sub>50</sub> = 0.47 $\mu$ M (Yu *et al.* 2008) and LDN193189 at IC<sub>50</sub> = 5 nM and 30 nM inhibited ALK2 and ALK3 receptors respectively (Cuny *et al.* 2008). DMH-1 at IC<sub>50</sub> = 108 nM inhibited ALK2 receptors

specifically (Hao *et al.* 2010). Including doses above and below IC values of small molecules on BMP inhibition in this study, would have revealed an optimal dose in PAX6 induction. This would also determine the most effective small molecule as well as minimise the possible off target effects. Both Dorsomorphin and LDN193189, but not DMH-1 was shown to have off-target effects against VEGF, PDGFR $\beta$  and BMP mediated non-SMAD signalling such as p38, MAPK, Akt and ERK1/2 (Hao *et al.* 2010; Boergermann *et al.* 2010; Vogt *et al.* 2011). There is also need for caution, when comparing the different protocols to analyse the effect of addition of BMP inhibitors on neural gene expression. Any discrepancies between dual-SMAD inhibitions studies discussed above, may also be attributed to the cell lines used and the many variable factors of the neutralizing cultures as outlined in table 4.

Table 7 Comparison of dual-SMAD inhibition protocols

Reference	Basal medium composition	Culture method	Noggin /Small molecules
My study (2010-2013 lab work)	Advanced DMEM/F-12+1%L-Glutamine (2mM)+ Lipid concentrate+ Insulin+ Transferrin+ $\beta$ -mercaptoethanol	EB- 8 days	SB431542431542 (10 $\mu$ M) Dorsomorphin(0.25 -1 $\mu$ M) LDN193189 (0.25 -1 $\mu$ M) DMH1 (0.25 - 1 $\mu$ M)
Chambers <i>et al.</i> 2009	knockout serum replacement media for 5 days then in increasing amounts of N2 media (25%, 50%, 75%) was added to the knockout serum replacement medium every 2 days	MS5 feeder or monolayer-7 days	SB431542431542 (10 $\mu$ M) Noggin (500ng/ml)
Kim <i>et al.</i> 2010	DMEM/F12 medium+ 20% KSR+, 1x non-essential amino acid+ 0.1mMbeta-mercaptoethanol	EB -10 days	SB431542431542 (10 $\mu$ M) Dorsomorphin (0.1 -5 $\mu$ M) Noggin (1000/ml)
Morizane <i>et al.</i> 2011	DMEM/Ham'sF12+ 5% KSR + 2 mM L-glutamine + and MEM nonessential amino acid solution	PA6 feeders or EB -14 days	SB431542431542 (10 $\mu$ M) Dorsomorphin (0.02 -20 $\mu$ M) Noggin (300ng/ml)

Surmacz <i>et al.</i> 2012	Knockout DMEM+ 20% KSR	Monolayer – 8 days	SB431542431542 (10 $\mu$ M) LDN193189 (0.001 -1 $\mu$ M) Dorsomorphin (5 $\mu$ M) Noggin (50ng/ml)
Neely <i>et al.</i> 2012	Knockout DMEM/F12+ 15% KSR, glutamax+ penicillin/streptomycin + nonessential amino acids+ 55 $\mu$ M $\beta$ -mercaptoethanol. And then in 25% N2-medium (DMEM/F12, N2 supplement, and high D-glucose at a final concentration of 4.5 g/L	Monolayer – 7 days	SB431542431542 (10 $\mu$ M) DMH-1 (0.5-10 $\mu$ M) Noggin (50-500ng/ml)

Concomitant with the induction of neural markers, there was loss of OCT4 in all the D8 EBs including the untreated control. At the mRNA level, negligible signals were generated. Similarly, at the protein level D8 EBs showed no expression, whereas undifferentiated hESCs were almost 100% OCT4<sup>+</sup>. ESC neuroectoderm commitment has been shown to be marked by Sox2 expression and downregulation of Oct4 (Thomson *et al.* 2011). Here, undifferentiated hESCs were SOX2<sup>+</sup>/OCT4<sup>+</sup> and all D8 EBs were SOX2<sup>+</sup>/OCT4<sup>-</sup>. As mentioned above, during dual-SMAD inhibition, SB431542 treatment effectively downregulated pluripotency markers OCT4 and NANOG (Chambers *et al.* 2009; Kim *et al.* 2010; Morizane *et al.* 2011). The expression of comparable proportion of SOX2 in all D8 EBs, indicated that, under this specific culture condition used in my study, OCT4 downregulation and SOX2 expression occurred independently of SB431542 and BMP inhibitors. This expression pattern can also be attributed to the inherent differentiation propensity of the hESC line used.

### 3.5.2 Effect of BMP inhibitors on neural crest and epidermal markers

Both neuroectoderm and neural crest cells are derived from the ectoderm. Generation of neural crest cells was examined in the culture by measuring P75 and *SLUG* expression. The presence of neural crest cells was evident by the expression 10-15% P75<sup>+</sup> cells in all D8 EBs. SB431542 alone or in combination with BMP inhibitors did not seem to alter the expression levels. It should be noted that the

experiment was not replicated to determine a statistical significance. Analysis of *SLUG* mRNA showed significant downregulation by SB431542 treatment compared with untreated. However, addition of Noggin or small molecules did not alter the expression level. Generation of neural crest cells had been reported previously in dual-SMAD inhibition protocols as a by-product. Although the culture yielded high proportion of PAX6<sup>+</sup> cells, neural crest markers were expressed in PAX6<sup>-</sup> cells (Elkabetz *et al.* 2008; Chambers *et al.* 2009; Kreitzer *et al.* 2013). The initial cell plating density seemed to play a critical role in SB431542 + Noggin or SB431542 + LDN193189 monolayer based differentiation; high plating densities led to near-exclusive generation of PAX6<sup>+</sup> cells whereas, low plating densities promoted generation of neural crest cells (Chambers *et al.* 2009; Kreitzer *et al.* 2013). Role of other signalling pathways such as WNT signalling has been demonstrated in neural crest development. Activation of WNT signalling combined with dual-SMAD inhibition was able to divert neuroectoderm fate towards neural crest fate. This was evident by the inhibition of PAX6 and SOX2 and marked increase in *SLUG* mRNA and P75 expression (Menendez *et al.* 2012).

Generation of the non-neural ectoderm derivative, epidermis was analysed in the cultures using CK18 antibody. D8 EBs contained low proportion of CK18<sup>+</sup> cells. The experiments were not replicated to determine statistical significance among the treatments. Though appeared to be negligible, this may indicate a low level endogenous BMP activity in these cultures. Supplementation of exogenous BMPs has been shown to efficiently drive hESC stromal co-culture or EB based ectodermal differentiation towards an epidermal fate (Aberdam *et al.* 2008).

Finally, the presence of 45-50% KI67<sup>+</sup> cells confirmed that EBs contained actively proliferating progenitors. BMP inhibition did not alter the proportion. Thus, dual-SMAD inhibition permits generation of neural progenitors that can be expanded and patterned to generate different neuronal types. Dual-SMAD inhibition strategy along with temporal integration of other developmental pathways has permitted the derivation of cortical (Shi *et al.* 2012), striatal (DelliCarri *et al.* 2013; Nicoleau *et al.* 2013; Arber *et al.* 2015), and midbrain neurons (Kriks *et al.* 2011; Kirkeby *et al.* 2012) from hPSCs.

In conclusion, hESCs were differentiated into neural lineage cells using an EB based protocol. The basal medium used in the study, showed neutralizing

effect as evidenced by the induction of PAX6, SOX2 and NESTIN and downregulation of OCT4. Addition of SB431542 enhanced NESTIN and PAX6. Addition of Noggin or Dorsomorphin or LDN193189 or DMH-1 in combination with SB431542, highly enhanced PAX6 transcript and PAX6 protein. Although a dose-dependent effect on inhibition of induced BMP activity was demonstrated by Dorsomorphin, LDN193189 and DMH-1 at the undifferentiated hESC stage, at D8 all the doses of small molecules equally inhibited BMP signalling. This resulted in a comparable induction of PAX6. Effect of Noggin and small molecule BMP inhibitors were comparable. The differentiated cultures were heterogeneous and contained low proportion of neural crest and epidermis cells.

# 4 Investigation of small molecule mediated WNT antagonism on hPSC telencephalon specification

## 4.1 Aim

To analyse the effect of WNT antagonism on telencephalon induction from hPSCs, utilizing the small molecule WNT inhibitors- IWR1 and KY02111

## 4.2 Background

Evidences from early patterning studies on animal models have demonstrated the role of WNT antagonism on telencephalon induction and specification. In early embryos, WNT proteins are expressed in the primitive streak at the posterior side. WNT antagonists such as Cer1 and Dkk1 expressed in signalling centres AVE and AME, act by repressing posterior signals and thereby enhance anterior neural fate specification (Belo *et al.* 1997; Kimura *et al.* 2000; Kemp *et al.* 2005). Simultaneous inhibition of WNT and BMP signalling by over expression of antagonists induced a complete secondary axis (Glinka *et al.* 1997; Glinka *et al.* 1998), while targeted deletion of Dkk1 lead to anterior truncations (Mukhopadhyay *et al.* 2001; Barco Barrantes *et al.* 2003). As telencephalon developed (E11.5-E16.5), WNT signalling was shown to be active in the pallium but not in the subpallium (Backman *et al.* 2005). Inhibition of WNT signalling resulted in the repression of dorsal markers and in the ectopic expansion of ventral markers, while the activation of WNT signalling in the subpallium resulted in the ectopic expansion of dorsal markers indicating the role played by WNT signalling in dorsal telencephalon (Gunhaga *et al.* 2003; Backman *et al.* 2005).

*In vitro*, in the absence of patterning signals, the default identity of neuroectodermal cells derived from hPSCs using stromal co-culture, serum free EB method or dual SMAD inhibition, has been reported as FOXG1<sup>+</sup> anterior fate (Pankratz *et al.* 2007; Elkabetz *et al.* 2008; Chambers *et al.* 2009; Neely *et al.* 2012; Delli Carri *et al.* 2013). hPSC differentiation protocols have employed the expensive recombinant protein DKK1 for efficient induction of FOXG1<sup>+</sup> cells (Watanabe *et al.* 2007; Li *et al.* 2009; Zhang *et al.* 2010; DelliCarri *et al.* 2013; Nicoleau *et al.* 2013). In

the absence of any morphogens, these FOXP1<sup>+</sup> cells mostly adopted PAX6<sup>+</sup> dorsal telencephalon identity (Chambers *et al.* 2009; Li *et al.* 2009; Nicoleau *et al.* 2013).

In this chapter, I investigated the effect of WNT antagonism by small molecule inhibitors IWR1 and KY02111 during hPSC neural differentiation. IWR1 acts by inhibiting Tankyrase1 and 2 and promotes  $\beta$ -catenin destruction complex (Chen *et al.* 2009; Huang *et al.* 2009). KY02111 acts in a manner distinct from IWR1, possibly by acting downstream of GSK3 $\beta$  and APC in  $\beta$ -catenin destruction complex (Minami *et al.* 2012).

### 4.3 Experimental design

The effect of WNT antagonism on hPSC-derived neuroectoderm specification towards a telencephalic fate was studied. Neuroectoderm cultures were generated using the SMADi strategy described in the previous chapter. Initially, the effect of IWR1 on the inhibition of induced as well as endogenous WNT activity was assessed in neuroectoderm progenitors generated using dual-SMAD inhibition (SB431542+LDN193189) EB protocol (Figure 4:2.A and Figure 4:3A). EB cultures often needed disrupting using a pipette due to their clustering together. This resulted in heterogeneous sized EBs as well as in low yield of neuroectoderm progenitors. Hence, the SB431542+LDN193189 protocol was adapted to a monolayer protocol (Figure 4:1.A). Pluripotent hPSCs were grown on matrigel in mTeSR1 medium. On D0, mTeSR1 was replaced with neural induction medium containing 10 $\mu$ M SB431542 till D8 and LDN193189 till D16 (in the modified protocol, the inhibition of BMP signaling was continued until D16. After re-plating on D8, the concentration of LDN193189 was reduced to 0.25 $\mu$ M due to cytotoxicity at higher concentration). Three sets of experiments were performed. 1) IWR1 was added at D0 and cultures were analysed at D8 and D16, time points representative of initial neural induction phase and subsequent telencephalon induction and specification phase. 2) Time point addition of WNT inhibitors was examined by addition of IWR1 at either D0 or D8 and cultures were analysed at D16. 3) Dose response was performed by addition of IWR1 or KY02111 (at 0.1, 1 and 10  $\mu$ M) at D0. Cultures were harvested and were analysed by QRT-PCR and/or immunocytochemistry on D16. Telencephalon induction and D/V specification were assessed by measuring the expression of FOXP1, PAX6, GSX2 and DLX2. The best dose of each IWR1 and KY02111 were further characterized using

high-throughput QRT-PCR array, for specific markers of CNS, pluripotency and other germ layers as outlined in Figure 4:1.C.

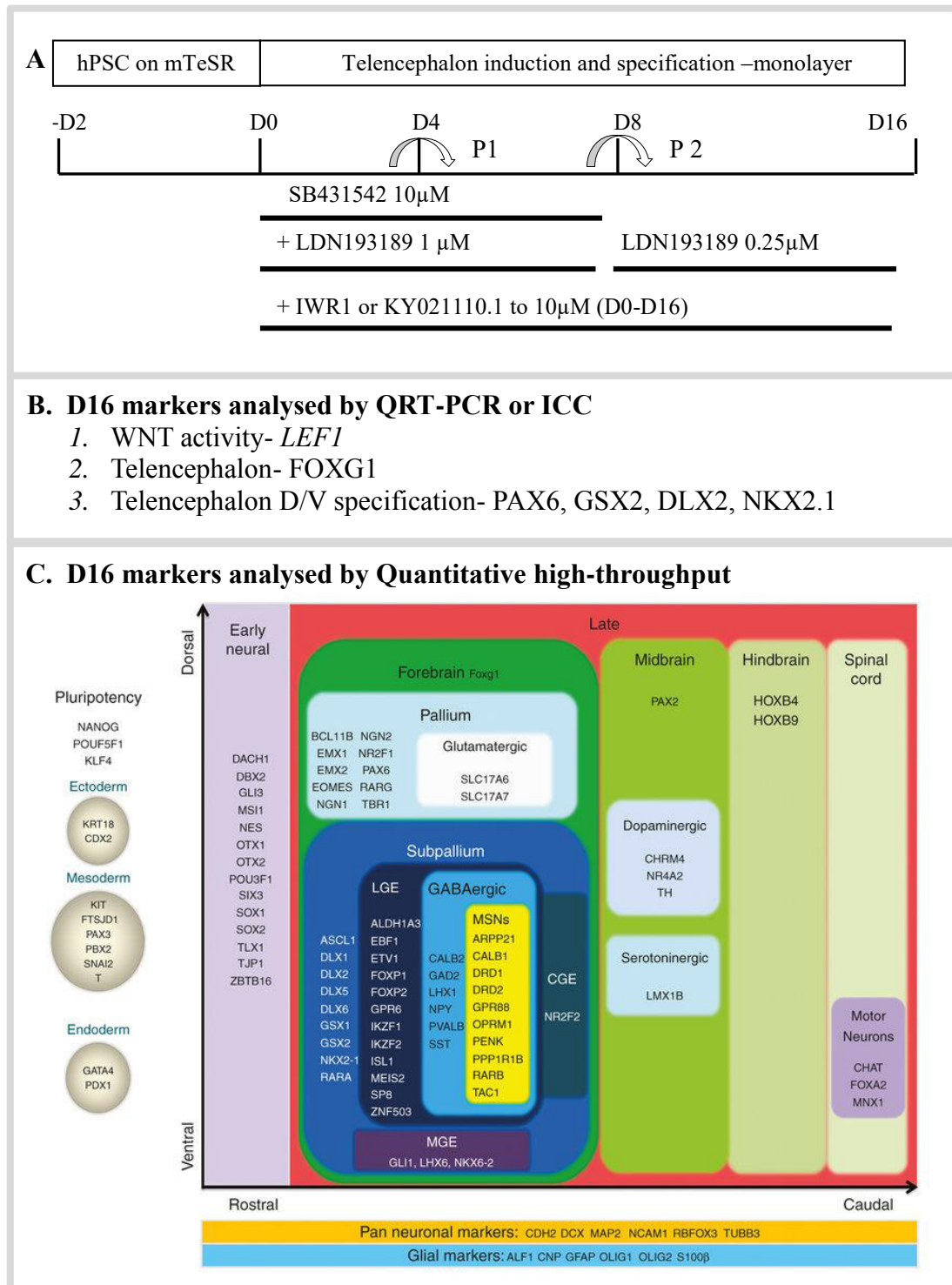


Figure 4:1 A) Cell culture regime for hPSC telencephalon induction. H9s were grown in mTeSR1 on matrigel coated plates. On D0, mTeSR1 was replaced with medium containing SB431542 till D8, LDN193189 til D16 and IWR1 till D16. Cultures were re-plated at 1:2 ratio on D4 and again on D8 and maintained til D16 on matrigel coated plates B) Markers analysed by QRT PCR and/or ICC on D16. C) Markers analysed by quantitative high -throughput array on D16 (figure taken from Straccia et al. 2015). The X-axis and Y-axis represent the rostro-caudal and dorso-ventral axis of human brain development. Left panel shows early neural genes. Bottom panel shows general neuronal and glial gene markers. Far left shows markers of pluripotency, ectoderm, mesoderm and endoderm

## 4.4 Results

### 4.4.1 Effect of IWR1 on inhibition of induced WNT activity

To analyse the modulation of WNT activity, H9 neural progenitors were generated using the dual-SMADi EB protocol. D8 EBs were dissociated and plated as single cells in basal media (Figure 4:2.A). To determine an optimal dose to elicit an acute WNT response in the culture, a pilot assay was performed on D12 with 25 to 200ng/ml WNT3a for 20 hours along with an untreated control. Analysis of immediate WNT signalling target *LEF1* was analysed by QRT-PCR (see appendix table 4.1 for  $\Delta Cq$ ). The fold change over control '0'ng/ml for 25, 20, 100 and 200ng/ml WNT3a treatment was 1.08, 1.18, 1.36 and 1.48 respectively (Figure 4:2.B). WNT 3a at 100ng/ml was used in later studies to elicit WNT activity in cultures.

To analyse the effect of IWR1 on the inhibition of WNT activity, the cultures were pre-treated with 0.0001 to 10 $\mu$ M of IWR1 for 2 hours followed by the addition of WNT3a. The cultures harvested after 12 hours were analysed for *LEF1* expression (see appendix table 4.1 for  $\Delta Cq$ ). Fold change over '0'  $\mu$ M IWR1 was plotted (Figure 4:2 C). ANOVA revealed a significant dose dependent inhibition by IWR1 pre-treatment compared with WNT3a only treatment ( $F_{4,10}=4.9$ ,  $p=0.02$ ). Dunnett's multiple comparisons test confirmed no significant difference at 0.001 $\mu$ M ( $0.7\pm 0.1$ ) and 0.1 $\mu$ M ( $0.9\pm 0.1$ ) and significantly lower expression at 1 $\mu$ M ( $0.6\pm 0.1$ ) and 10 $\mu$ M ( $0.6\pm 0.1$ ).

### 4.4.2 Effect of IWR1 on inhibition of endogenous WNT activity

Next, the effect of IWR1 on inhibition of endogenous WNT signalling was analysed. D8 EBs plated as single cells were cultured in the presence of 0.001 to 10 $\mu$ M IWR1 from D8 to D16 (Figure 4:3.A). At D16, cultures were analysed for the expression of *LEF1*. A high degree of cell death was observed at 10 $\mu$ M and hence was eliminated from the analysis (see appendix table 4.1 for  $\Delta Cq$ ). ANOVA showed a significant a dose-dependent inhibition of *LEF1* ( $F_{4,10}=15.0$ ,  $p=0.0003$ ) (Figure 4:3.B). Dunnett's multiple comparisons test confirmed significantly lower *LEF1* expression at 0.1 $\mu$ M ( $0.4\pm 0.1$ ) and 1 $\mu$ M ( $0.4\pm 0.0$ ) of IWR1 compared to that of untreated control ( $1.0\pm 0.1$ ). At lower concentration of 0.001 $\mu$ M ( $1.1\pm 0.1$ ) and 0.01 $\mu$ M ( $0.8\pm 0.5$ ) there was no statistical significance compared to control.

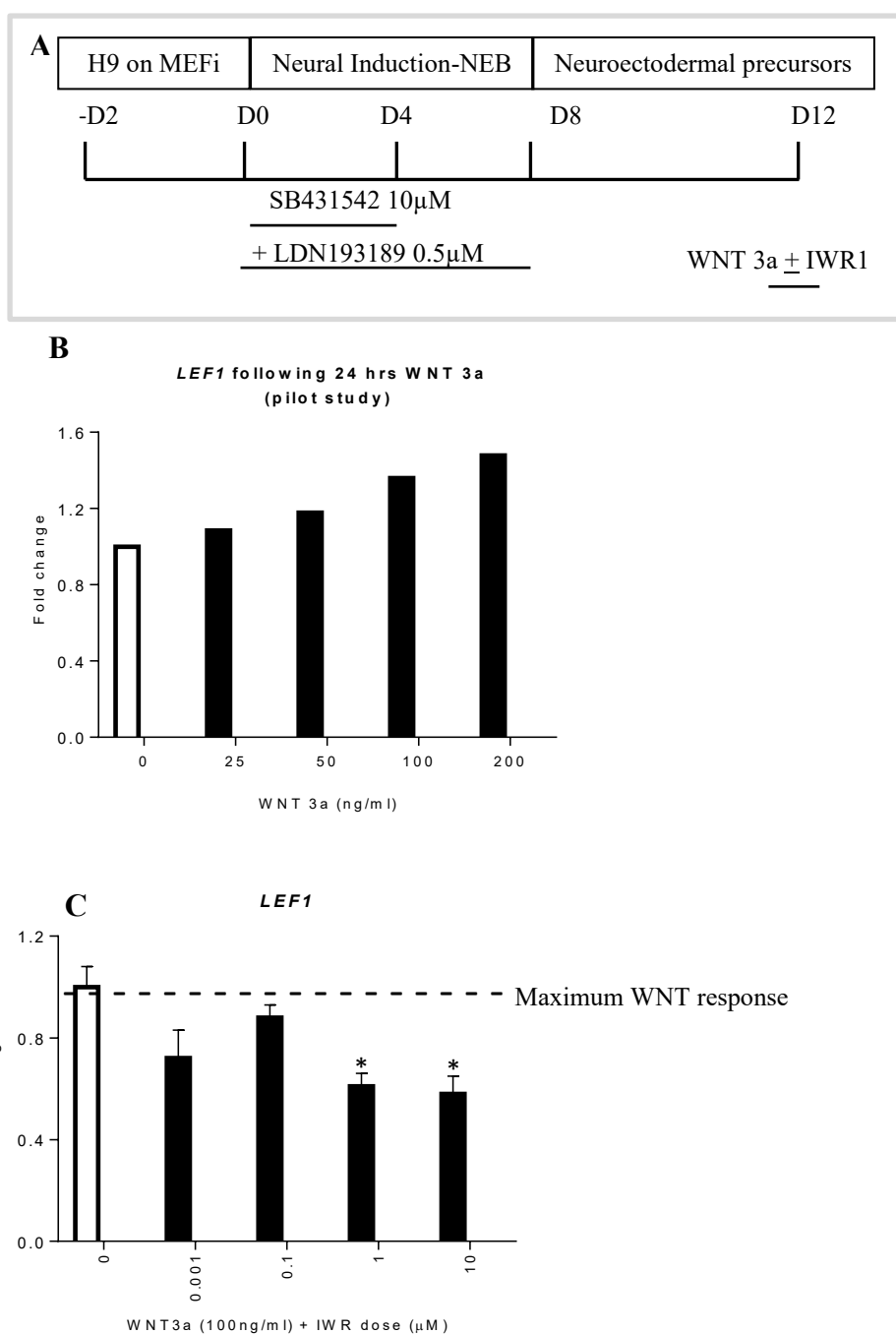


Figure 4:2 Modulation of WNT activity by WNT3a and IWR1 in day 12 neural progenitors- A) Cell culture regime. D8 EBs were plate as monolayer onto PLL coated plates. On D12 neural progenitors were treated with 0 to 200ng/ml for WNT3a or pre-treated with IWR1 for 2 hours followed by addition of 100ng/ml WNT 3a for the experiments. B) Dose dependent induction of *LEF1* by WNT3a after 20 hours (n=1, pilot study). C) Dose dependent inhibition of *LEF1* by IWR1. Dotted line indicates the maximal response elicited by 100ng/ml WNT3a treatment. Data represented as mean  $\pm$  S.E.M, N= 3, experiment replicates . \* P = 0.02

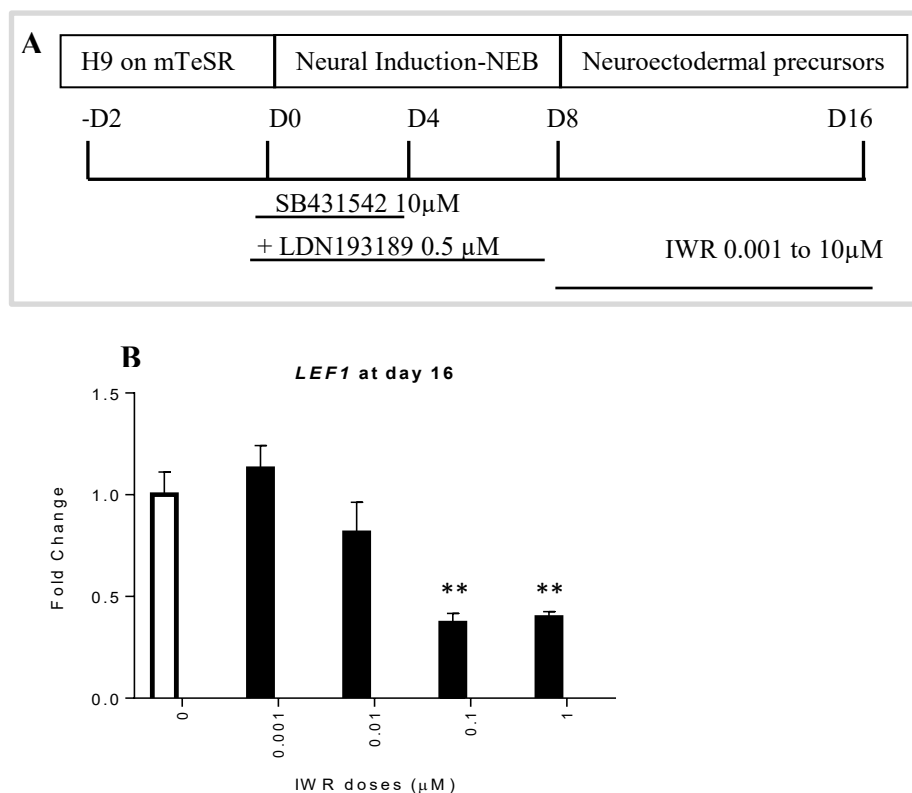


Figure 4:3 Modulation of endogenous WNT activity by IWR1. A) Cell culture regime. D8 NEBs plated as monolayer onto PLL coated plates were treated with 0.001 to 10 $\mu$ M IWR1 till D16. B) Dose dependent inhibition of *LEF1* by IWR1 on D16. Data represented as mean  $\pm$  S.E.M, N= 3, experiment replicates set in parallel. \*\* P < 0.0

#### 4.4.3 Effect of IWR1 on telencephalon induction - time point analysis

Please note that from this point onwards, throughout this thesis, monolayer based protocol (referred as SMADi- hereafter) outlined in Figure 4:3 was used.

First, to determine the time point for analysing the impact of WNT antagonism on telencephalon induction, IWR1 at 1.5 $\mu$ M was added to neural induction cultures from D0 (Note- this experiment was performed on 34D6 iPSC line). The samples were harvested at D8 and D16. The expression levels of neuroectoderm makers- *PAX6* and *SLUG* and telencephalon marker *FOXG1* were monitored by QRT-PCR. As no 'untreated' control was included in the study, the expression normalised to the reference gene GAPDH ( $2^{-\Delta Cq}$ ) was plotted (see appendix table 4.2 for  $\Delta Cq$ ), instead of fold change over untreated control ( $2^{-\Delta\Delta Cq}$ ) (Figure 4:4). Analysis of *PAX6* expression revealed no significant difference between D8 (41.5 $\pm$ 11.3) and D16 (43.5 $\pm$ 10.6) ( $t_4=0.1$ , p=n.s) (Figure 4:4.A). *SLUG* expression showed slightly lower but not significantly different expression between D8 (2.0 $\pm$ 0.4) and D16 (0.8 $\pm$ 0.3) ( $t_4=2.0$ , p=n.s) (Figure 4:4.B). There was significant induction of *FOXG1* at D16 (394.1 $\pm$ 95.8) compared to D8 (42.1 $\pm$  20.3) ( $t_4=4.8$ , p=0.009) (Figure 4:4.C).

Next, to analyse whether WNT antagonism specifies telencephalon during the initial phase of neural induction, two time points for the addition of IWR1 to SMADi-monolayer cultures were considered. IWR1 was added to the neural induction cultures either at D0 or D8. *FOXG1* expression was analysed at day 16 by high-throughput QRT-PCR (see appendix table 4.3 for  $\Delta Cq$ ). The fold change expression over untreated control was plotted. As the experiments were performed on N=2, no statistical tests were performed. However, a high fold induction of *FOXG1* was evident in cultures treated with IWR1 from D0 (Figure 4:5). Thus, for further analysis, D0 addition was used and samples were analysed at D16.

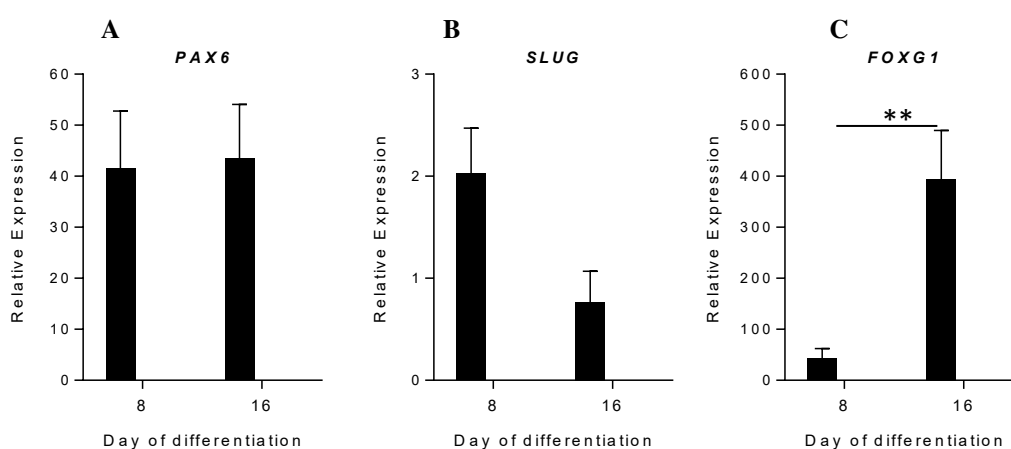


Figure 4:4 Monitoring telencephalon induction on monolayer based protocol. Monolayer differentiation of 34D6 iPSC was performed as in figure 4.3.1. Samples were analysed at D8 and D16. Fold change expression levels of (A) *PAX6*, (B) *SLUG* (C) *FOXG1* at D8 and D16 analysed by QRT-PCR. Data represented as mean  $\pm$  S.E.M, N=3, experiment replicates set in parallel. \*\* P < 0.01

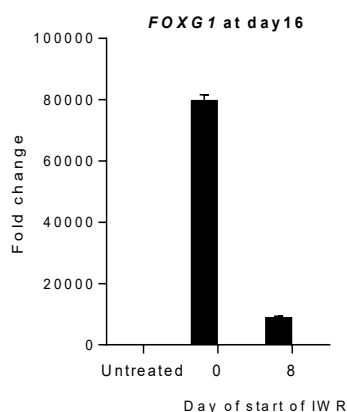


Figure 4:5 Effect of time point addition of IWR1 on *FOXG1*. Monolayer differentiation of H9 ESC was performed as in figure 4.3.1. IWR1 was added at either D0 or D8. Samples were analysed at D16. Fold change over untreated (no IWR1) was plotted. Data represented as mean  $\pm$  S.E.M, N=2, experiment replicates set in parallel.

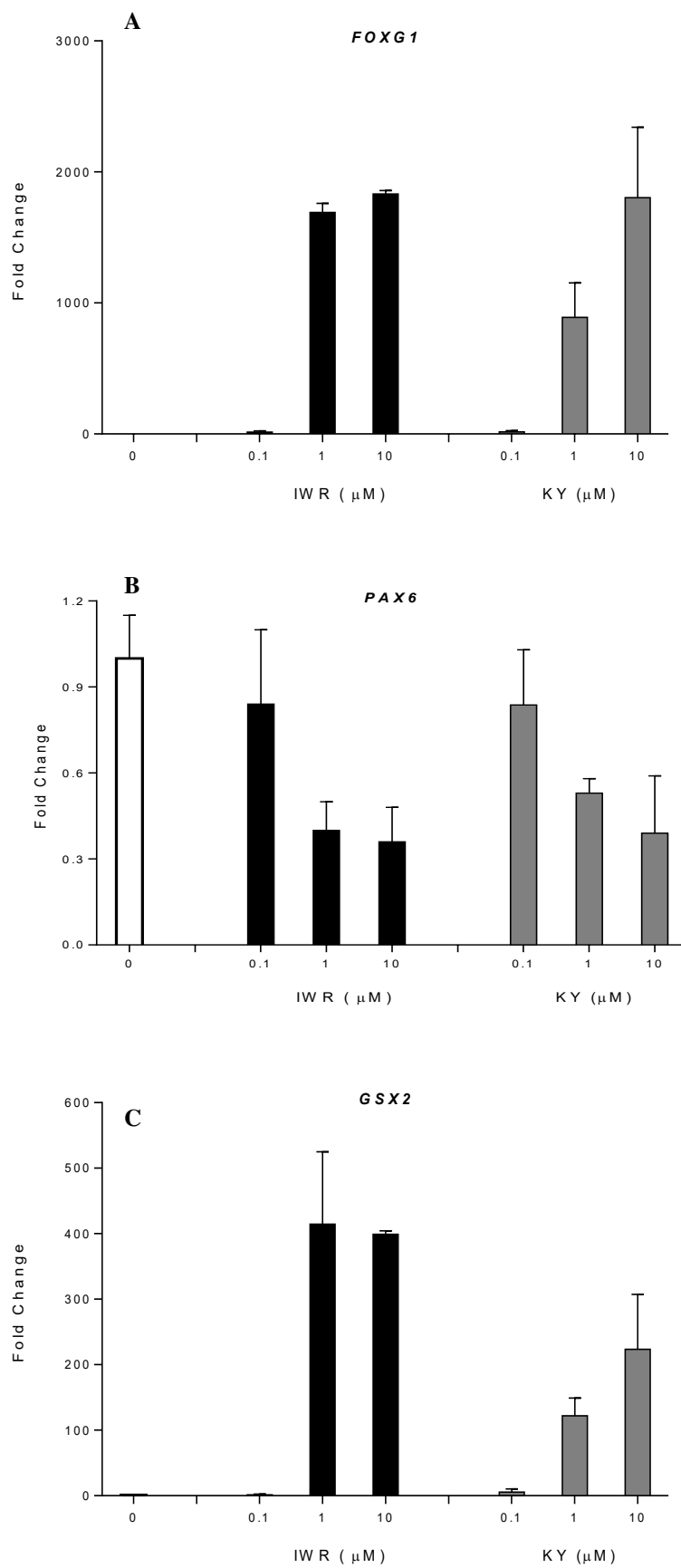
#### 4.4.4 QRT-PCR characterization of WNT inhibitors mediated telencephalon induction and specification

To investigate further whether the D0 addition of WNT inhibitors enhances the telencephalon induction and specification, IWR1 or KY02111 was added at concentrations ranging from 0 to 10 $\mu$ M. The cultures were analysed at D16 for the expression of *FOXG1*, *PAX6*, *GSX2* and *DLX2* (see appendix table 4.4 for  $\Delta$ Cq). Fold change over '0' treatment was plotted. Note that the dose-response experiments were performed only twice, ie, N=2. To avoid giving any misleading P values while interpreting data, no statistical tests were performed. The experiments were repeated with the best dose of both IWR1 and KY02111 and was further analysed by high-throughput QRT-PCR for N=3, discussed later.

There was a marked increase in *FOXG1* expression in a dose-dependent manner by the IWR1 or KY02111 treatment (Figure 4:6. A). The high concentrations of IWR1 1 $\mu$ M (1690.1 $\pm$ 70.3) and 10 $\mu$ M (1832.2 $\pm$ 26.5) yielded a similar expression level which was markedly higher than the level seen at low concentrations of 0.1 $\mu$ M (14.3 $\pm$ 8.4) or '0' control (1.0 $\pm$ 0.8). KY02111 at 10 $\mu$ M (1830.4 $\pm$ 538.3) showed the highest expression level. At 1 $\mu$ M (890.8 $\pm$ 262.6) the expression level was lower than that seen at 10 $\mu$ M but higher than that seen at 0.1 $\mu$ M (15.3 $\pm$  9.5) or '0' treatment.

The expression of *PAX6* was downregulated upon IWR1 or KY02111 treatment (Figure 4:6.B). IWR1 at 1 $\mu$ M (0.4 $\pm$ 0.1) and 10 $\mu$ M (0.4 $\pm$ 0.1) yielded a similar expression level that was lower than that seen at 0.1 $\mu$ M (0.8 $\pm$ 0.3) or '0' control (1.0 $\pm$ 0.2). KY02111 at 10 $\mu$ M (0.4 $\pm$ 0.2) and 1 $\mu$ M (0.5 $\pm$ 0.1) showed an expression level lower than 0.1 $\mu$ M (0.8 $\pm$  0.2) or '0' treatment.

Concomitantly, the expression of *GSX2* was upregulated by IWR1 or KY02111 treatment in a dose dependent manner (Figure 4:6.C). IWR1 at 1 $\mu$ M (414.5 $\pm$ 110.7) and 10 $\mu$ M (399.0 $\pm$ 5.5) yielded higher expression levels than that seen at 0.1 $\mu$ M (1.3 $\pm$  1.3) or '0' untreated control (1.0 $\pm$ 0.4). KY02111 at 10 $\mu$ M (223.5 $\pm$  83.8) and 1 $\mu$ M (122.2 $\pm$ 26.9) showed higher expression levels than that seen at 0.1 $\mu$ M (5.4 $\pm$ 4.8) or '0' treatment. Similarly, IWR1 or KY02111 dose-dependently upregulated *DLX2* expression (Figure 4:6.D). IWR1 at 1 $\mu$ M (145.8 $\pm$ 57.2) and 10 $\mu$ M (72.5 $\pm$ 18.2) yielded higher expression level than that observed at 0.1 $\mu$ M (0.4 $\pm$ 0.1) or '0' treatment (1.0 $\pm$ 0.0). Among KY02111 treatment group, 10 $\mu$ M (91.8 $\pm$ 26.9) yielded the highest expression levels than 1 $\mu$ M (9.7 $\pm$ 4.7), 0.1 $\mu$ M (1.3 $\pm$  1.3) or '0' control.



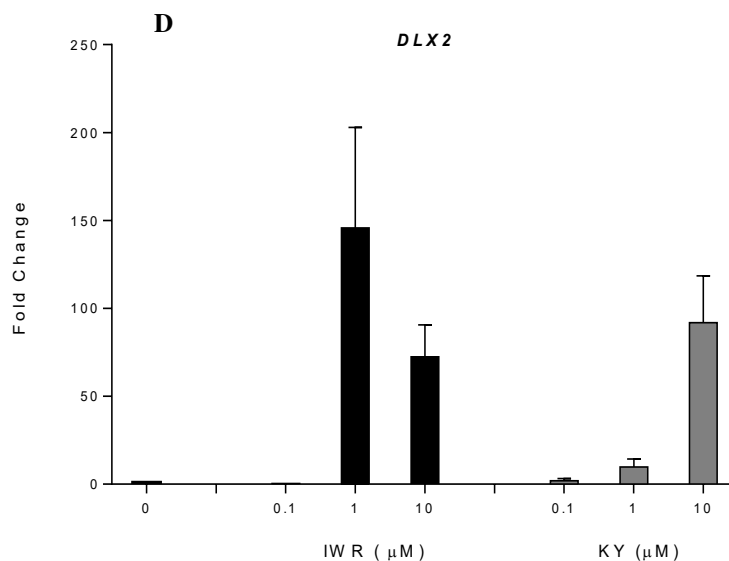


Figure 4:6 Effect of WNT inhibitors on telencephalon induction and specification. IWR1 and KY02111 dose-dependent fold change expression of A) *FOXG1*, B) *PAX6*, C) *GSX2* and D) *DLX2*. Data represented as mean  $\pm$  S.E.M, N= 2, experiment replicates

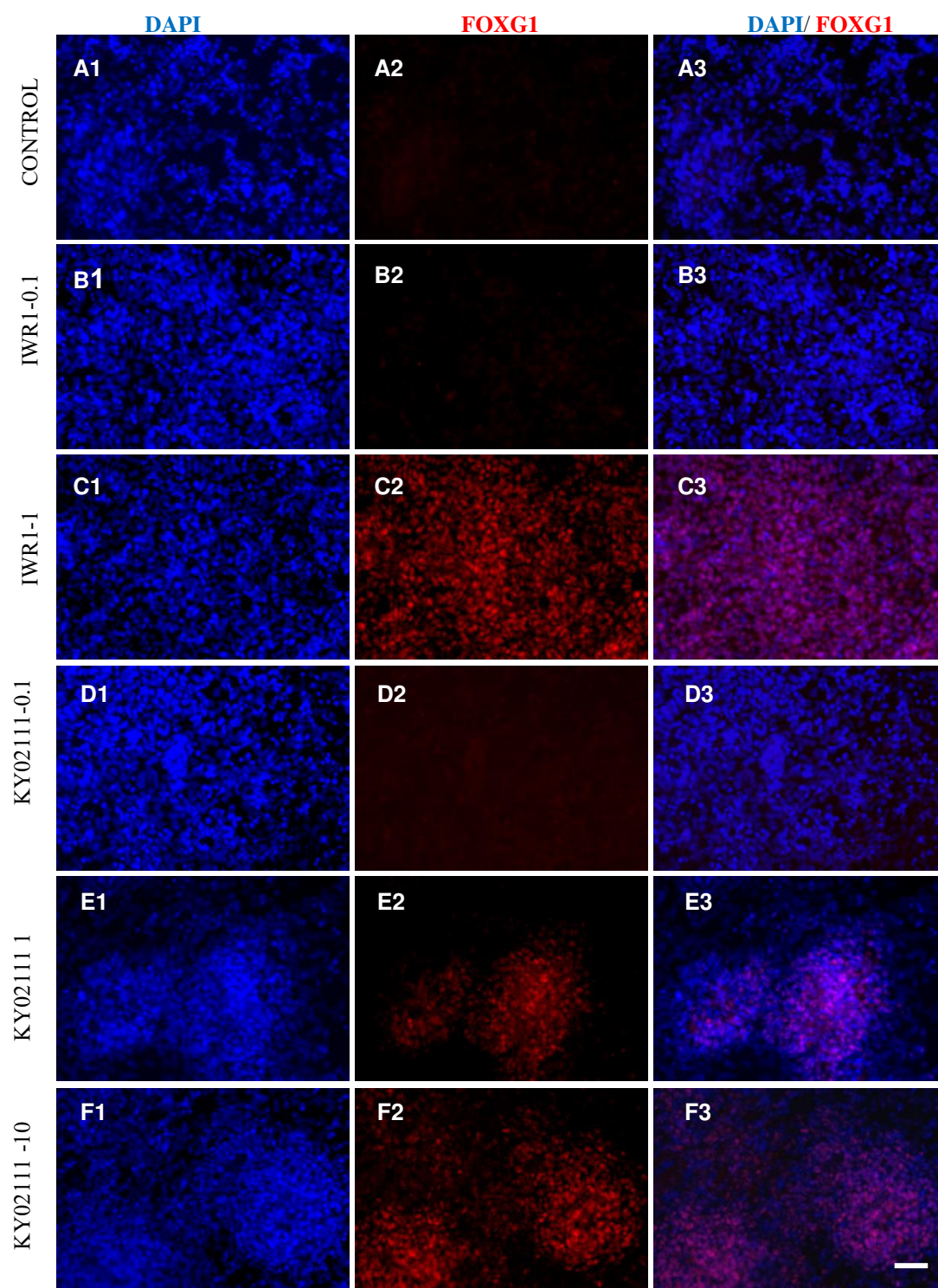
#### 4.4.5 Immunocytochemistry characterization of WNT inhibitor mediated telencephalon induction and specification

To characterize telencephalon induction and specification at the protein level, immunocytochemistry analysis was performed. D16 cultures generated in the presence of IWR1, KY02111 or '0' control treatment (0.1% DMSO) were re-plated onto matrigel coated cover slips and fixed on the same day. Cultures were then immuno-stained for *FOXG1*, *PAX6*, *GSX2* and *NKX2.1*. The immunofluorescence signal was quantified and represented as percentage of DAPI positive cells.

*FOXG1* expression was localized to the nucleus (Figure 4:7). The proportion of *FOXG1* immuno-positive cells was higher following WNT inhibition when compared to control. A dose-dependent effect of IWR1 and KY02111 on *FOXG1* induction was observed. Control ( $5.0 \pm 3.7\%$ ),  $0.1 \mu\text{M}$  IWR ( $1.8 \pm 1.2\%$ ) and  $0.1 \mu\text{M}$  KY02111 ( $1.5 \pm 0.2\%$ ) yielded negligible expression. There was a higher induction at  $1.0 \mu\text{M}$  IWR1 ( $92.0 \pm 3.9\%$ ). KY02111 at  $1 \mu\text{M}$  ( $35.2 \pm 10.0\%$ ) and  $10 \mu\text{M}$  ( $75.5 \pm 5.8\%$ ) also gave a higher yield than control treatment

Further, telencephalon D/V specification was assessed in control as well as IWR1- $1 \mu\text{M}$  and KY02111- $10 \mu\text{M}$  treated cultures that gave the highest *FOXG1* yield. The control cultures showed almost uniform *PAX6* signal intensity whereas a gradient in intensity was observed in cultures treated with IWR1 or KY02111 (Figure 4:8).

Both high and low intensity signals were combined to quantify the total PAX6%. The number of PAX6<sup>+</sup> cells was decreased by IWR1 (77.4±2.8%) and KY02111 treatment (74.5±2.0%) when compared with control (90.5±1.1%) (Figure 4:8.E). Interestingly, the nuclear PAX6 intensity was also decreased by IWR1 (0.4±0.0) and KY02111 (0.3±0.1) compared with the signal detected in control (1) (Figure 4:8.F). Similar to PAX6 expression, GSX2 expression intensity induced by the WNT inhibitors was seen as a gradient, with cultures containing high intensity and low intensity GSX2-positive cells as well as clear GSX2-negative cells (Figure 4:9). Both high intensity and low intensity signals were combined to quantify the total percentage of GSX2<sup>+</sup> cells. Please note that whilst quantifying PAX6 and GSX signals using cell profiler software, the stringent threshold intensity applied to eliminate any background may have excluded some low intensity positive cells. The proportion of GSX2 cells in IWR1 (69.2±2.5%) or KY02111 (49.2±1.5%) treated cultures was higher than in control treatment (0%) (Figure 4:9.E). The proportion of NKX2.1 immunopositive cells in IWR1 (7.3±1.1%) or KY02111 (8.2±0.8%) treated cultures higher than that in control (0%) (Figure 4:10).



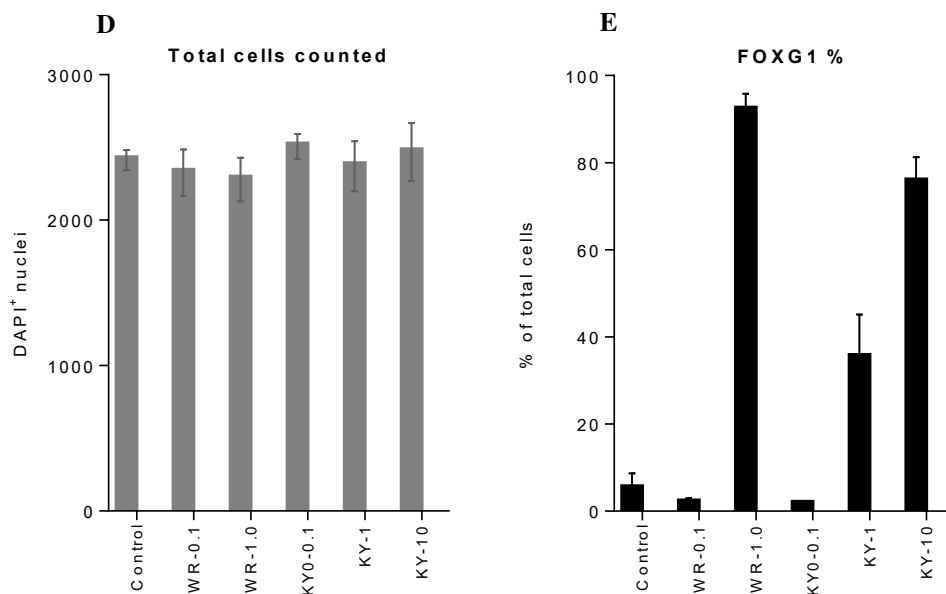


Figure 4:7 Fluorescent immunocytochemistry analysis of FOXG1 in D16 monolayer cultures. D16 progenitors were generated in the absence or in the presence of WNT inhibitors on matrigel coated plates. Cultures were re-plated onto matrigel coated coverslips and fixed on the same day. Cells were immunostained for FOXG1 (red) and counter stained for DAPI nuclear stain (blue). Representative images are given- A1-F1) DAPI stained cells, A2-F2) FOXG1 stained cells A3-F3) DAPI/FOXG1 merge, generated in the presence of A1-A3) no treatment, B1-B3) IWR1 at 0.1 $\mu$ M, C1-C3) IWR1 at 1.0 $\mu$ M, D1-D3) KY02111 at 0.1 $\mu$ M, E1-E3) KY02111 at 1.0 $\mu$ M and E1-E3) KY02111 at 10.0 $\mu$ M. Scale bar for all images in bottom right image= 100 $\mu$ m. Multiple fields/coverslips were imaged. Graphs represent D) the total amount of DAPI-positive nuclei counted for each treatment and E) proportion of FOXG1 as % of DAPI nuclei. Data represented as mean  $\pm$  S.E.M, N=2, experiment replicates set in parallel

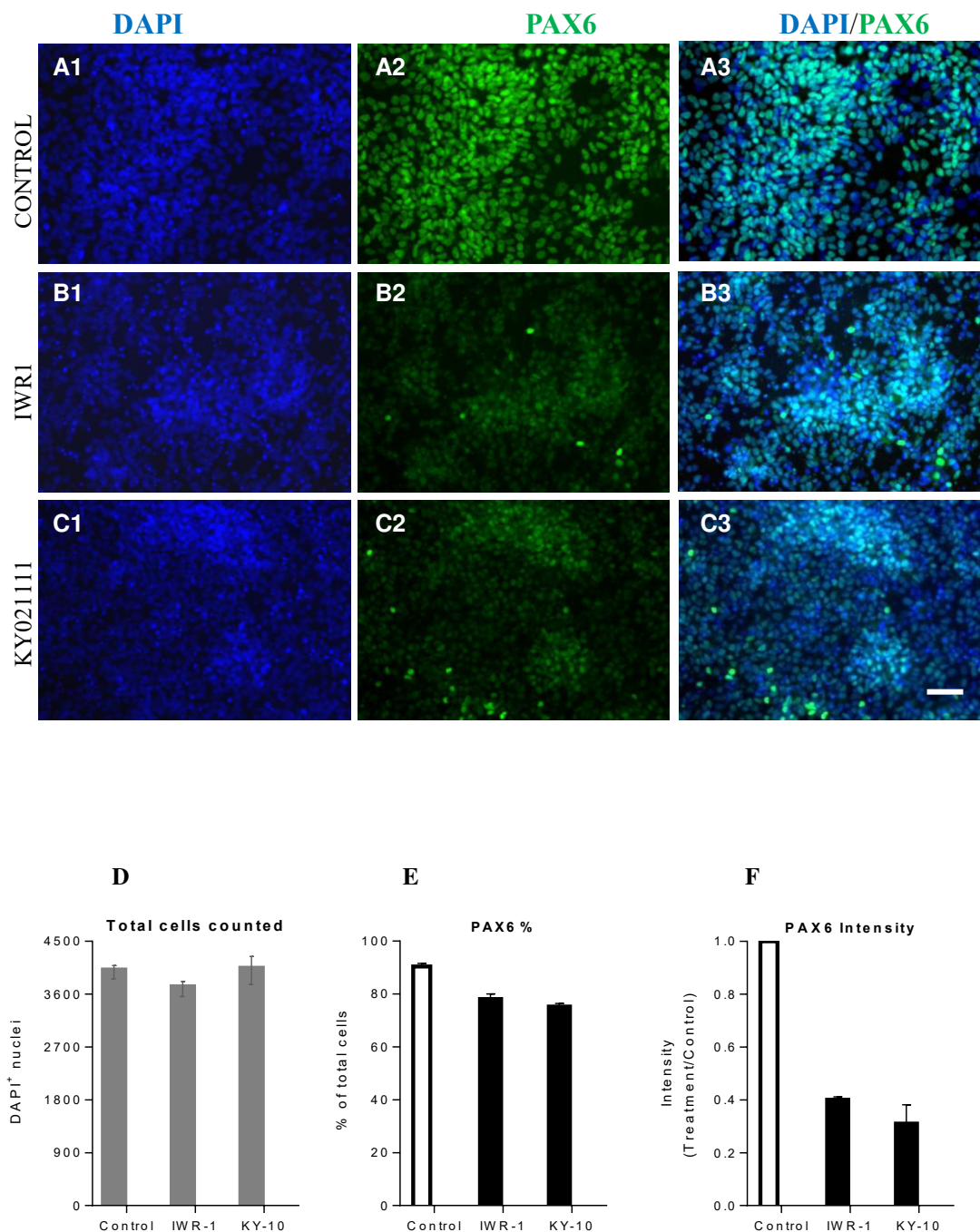


Figure 4:8 Fluorescent immunocytochemistry analysis of PAX6 in D16 monolayer cultures. D16 progenitors were generated in the absence or in the presence of WNT inhibitors on matrigel coated plates. Cultures were re-plated onto matrigel coated coverslips and fixed on the same day. Cells were immunostained for PAX6 (green) and counter stained for DAPI nuclear stain (blue). Representative images are given- A1-A3) DAPI stained cells, A2-C2) PAX6 stained cells and A3-C3) DAPI/PAX6 merge, generated in the presence of A1-A3) no treatment, B1-B3) IWR1 at 1.0 $\mu$ M and C1-C3) KY02111 at 10.0 $\mu$ M. Scale bar for all images in bottom right image= 100 $\mu$ m. Multiple fields/coverslips were imaged. Graphs represent D) the total amount of DAPI-positive nuclei counted for each treatment. E) Proportion of PAX6 as % of DAPI nuclei. F) PAX6 intensity of positive cells, normalized to intensity in control culture. Data represented as mean  $\pm$  S.E.M, N=2, experiment replicates set in parallel

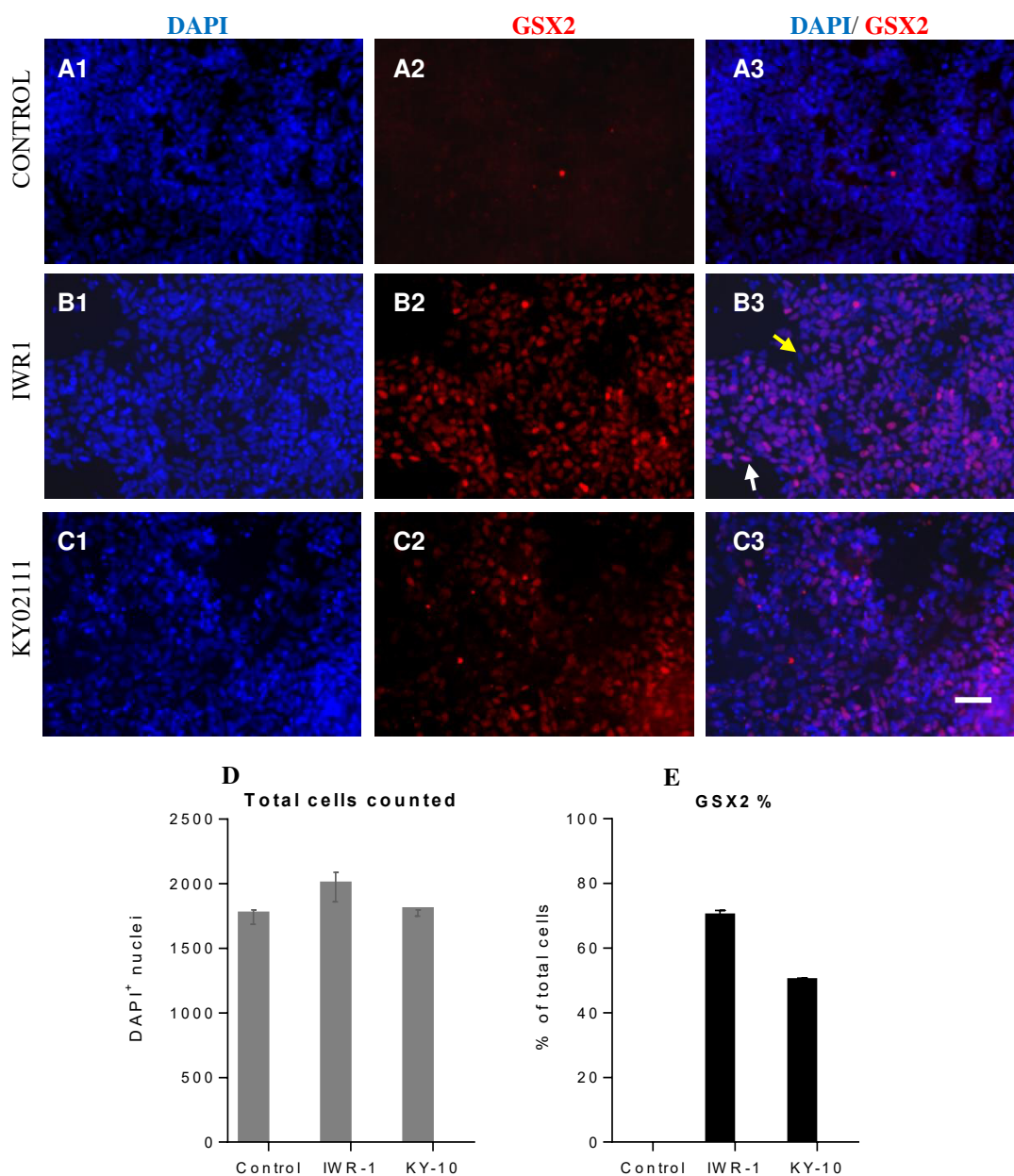


Figure 4:9 Fluorescent immunocytochemistry analysis of GSX2 in D16 monolayer cultures. D16 progenitors were generated in the absence or in the presence of WNT inhibitors on matrigel coated plates. Cultures were re-plated onto matrigel coated coverslips and fixed on the same day. Cells were immunostained for GSX2 (red) and counter stained for DAPI nuclear stain (blue). Representative images are given- A1-C1) DAPI stained cells, A2-C2) GSX2 stained cells and A3-C3) DAPI/GSX2 merge, generated in the presence of A1-A3) no treatment, B1-B3) IWR1 at 1.0 $\mu$ M and C1-C3) KY02111 at 10.0 $\mu$ M. Yellow arrow points towards clear negative cells and white arrow points towards high intensity cells. Scale bar for all images in bottom right image= 100 $\mu$ m. Multiple fields/coverslips were imaged. Graphs represent D) the total amount of DAPI-positive nuclei counted for each treatment and E) proportion of GSX2 as % of DAPI nuclei. Data represented as mean  $\pm$  S.E.M, N=2, experiment replicates set in parallel

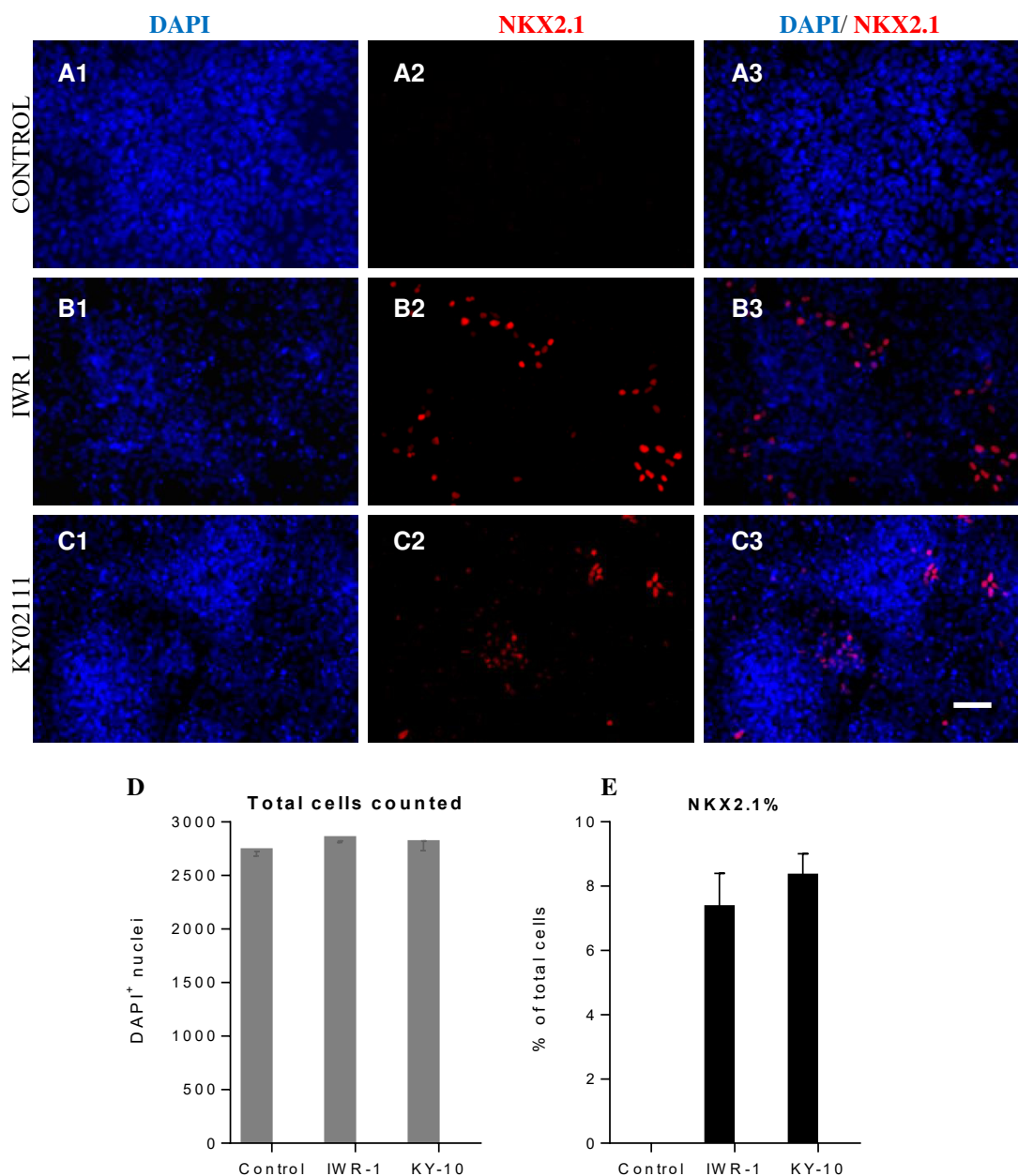


Figure 4:10 Fluorescent immunocytochemistry analysis of NKX2.1 in D16 monolayer cultures. D16 progenitors were generated in the absence or in the presence of WNT inhibitors on matrigel coated plates. Cultures were re-plated onto matrigel coated coverslips and fixed on the same day. Cells were immunostained for NKX2.1 (red) and counter stained for DAPI nuclear stain (blue). Representative images are given- A1-A3) DAPI stained cells, A2-C2) NKX2.1 stained cells and A3-C3) DAPI/NKX2.1 merge, generated in the presence of A1-A3) no treatment, B1-B3) IWR1 at 1.0 $\mu$ M and C1-C3) KY02111 at 10.0 $\mu$ M. Scale bar for all images in bottom right image= 100 $\mu$ m. Multiple fields/coverslips were imaged. Graphs represent D) the total amount of DAPI-positive nuclei counted for each treatment and E) proportion of NKX2.1 as % of DAPI nuclei. Data represented as mean  $\pm$  S.E.M, N=2, experiment replicates set in parallel

#### 4.4.6 High- through put QRT-PCR characterization of IWR1 or KY02111 mediated telencephalon differentiation

For a detailed characterization of progenitor identity, samples treated with IWR1 at 1 $\mu$ M or KY02111 at 10 $\mu$ M and control were subjected to high through put QRT-PCR analysis. As outlined in Figure 4:1, this assay permitted the analysis of different markers of neuroectoderm, A-P axis, telencephalon, pallium, subpallium, LGE, MGE, CGE, neurons and glia as well as reference genes. For the assay analysis,  $\Delta Cq > 12$  for both treatment groups and control was taken as low or negligible expression and is not shown here. The low  $\Delta Cq$  indicates high gene expression. This assay analysis software assigns a  $\Delta Cq = 14.5$  as a cut off value for no expression. The fold change in gene expression was plotted as the ratio of normalized gene expression of IWR1 or KY02111 treated samples to control (see appendix table 4.5 for  $\Delta Cq$  of all makers analysed).

##### 4.4.6.1 Neuroectodermal markers

Neuroectodermal markers *SOX2*, *SOX1* and *NES* (NESTIN) were analysed. Analysis of *SOX2* expression showed no significant difference between untreated control (1.0 $\pm$ 0.2) and IWR1 treated (1.9 $\pm$ 0.4) or KY02111 treated (1.0 $\pm$ 0.1) cultures ( $F_{2,6}=0.9$ ,  $p=n.s$ ) (Figure 4:11.A). Analysis of *SOX1* expression showed no significant difference between untreated control (1.0 $\pm$ 0.1) and IWR1 treated (2.8 $\pm$ 1.4) or KY02111 treated (1.9 $\pm$ 0.5) cultures ( $F_{2,6}=0.3$ ,  $p=n.s$ ) (Figure 4:11.B). Analysis of *NES* expression showed no significant difference between untreated control (1.0 $\pm$ 0.1) and IWR1 treated (1.0 $\pm$  0.1) or KY02111 treated (0.8 $\pm$  0.1) cultures ( $F_{2,6}=0.9$ ,  $p=n.s$ ) (Figure 4:11.C).

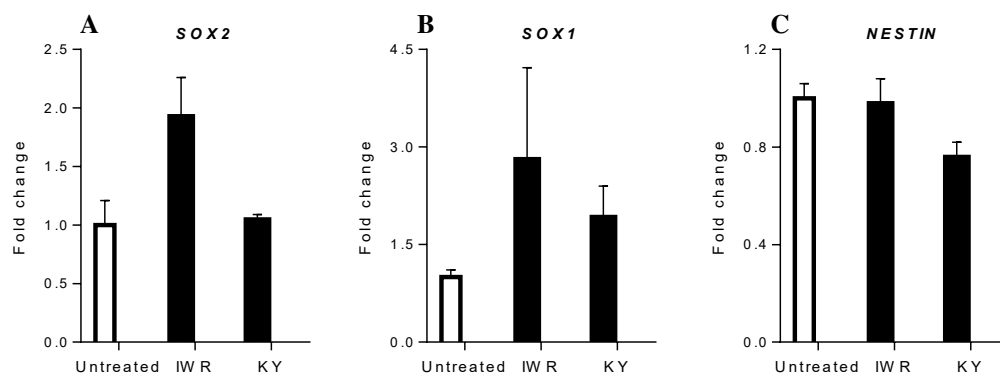


Figure 4:11 Effect of WNT inhibitors on neuroectodermal markers- Fold change expression of A) *SOX2* B) *SOX1* and C) *NES*. Data represented as mean  $\pm$  S.E.M, of 3 different experiments

## 4.4.6.2 Anterior neural tube markers

The expression of markers of anterior neural tube- *FOXP1*, *SIX3*, *OTX2* and *LMX1B* was analysed. Analysis of *FOXP1* showed significant increase in expression by IWR1 ( $459.0 \pm 95.0$ ) or KY02111 treatment ( $142.1 \pm 20.5$ ) compared to control ( $1.0 \pm 0.5$ ) and there was no significant difference between IWR1 and KY02111 treatments ( $F_{2,6}=27.5$ ,  $p=0.001$ ) (Figure 4:12.A). Similarly, analysis of *SIX3* showed significant increase by IWR1 ( $10.7 \pm 2.5$ ) or KY02111 treatment ( $9.6 \pm 0.6$ ) compared to control ( $1.0 \pm 0.7$ ) and there was no significant difference between IWR1 and KY02111 treatments ( $F_{2,6}=12.7$ ,  $p=0.007$ ) (Figure 4:12.B). Analysis of *OTX2* showed no significant difference between untreated control ( $1.0 \pm 0.2$ ) and IWR1 treated ( $1.0 \pm 0.1$ ) or KY02111 treated ( $1.9 \pm 1.6$ ) cultures ( $F_{2,6}=0.20$ ,  $p=n.s$ ) (Figure 4:12.C). Analysis of *LMX1A* showed significant decrease upon IWR1 ( $0.0 \pm 0.0$ ) or KY02111 ( $0.0 \pm 0.0$ ) treatment compared to control ( $1.0 \pm 0.2$ ) and there was no difference between IWR1 or KY02111 treatments ( $F_{2,5}=18.4$ ,  $p=0.003$ ) (Figure 4:12.D).

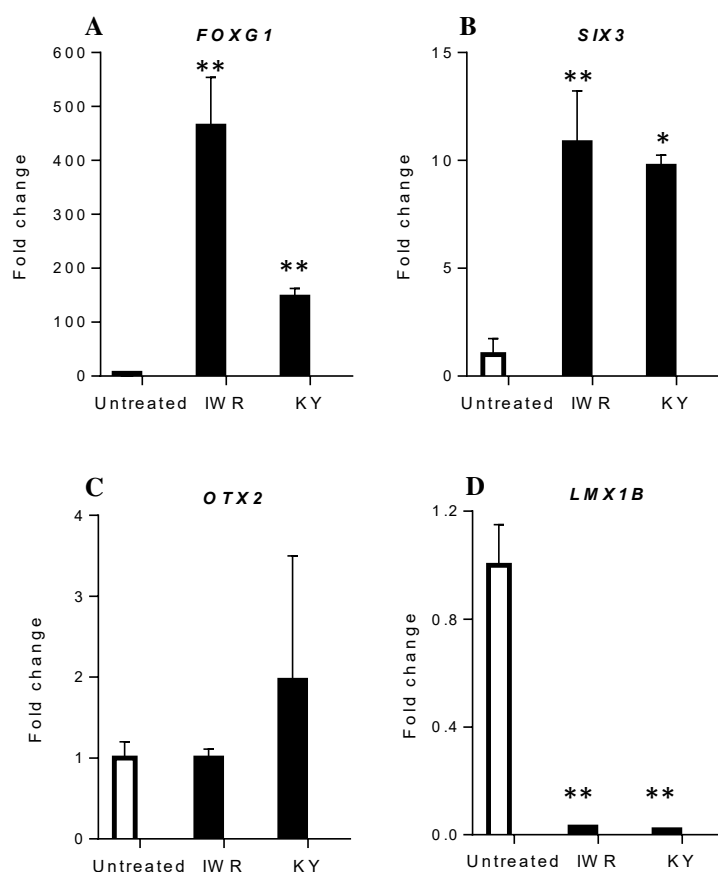


Figure 4:12 Effect of WNT inhibitors on anterior markers. Fold change expression of A) *FOXG1*, B) *SIX3*, C) *OTX2* and D) *LMX1B*. Data represented as mean  $\pm$  S.E.M, of 3 different experiments. \*\* $p < 0.01$  ANOVA, Dunnett's multiple comparisons test

#### 4.4.6.3 Pallial markers

The expression of *PAX6*, *EMX2* and *TBR1* was analysed. *PAX6* expression was not significantly different between control ( $1.0 \pm 0.2$ ) and IWR1 ( $0.6 \pm 0.1$ ) or KY02111 treated ( $0.6 \pm 0.4$ ) cultures ( $F_{2,6}=1.0$ ,  $p=n.s$ ) (Figure 4:13 A). Analysis of *EMX2* showed no significant difference in the expression levels between control ( $1.0 \pm 0.7$ ) and IWR1 ( $6.2 \pm 1.5$ ) and KY02111 ( $2.3 \pm 1.7$ ) treatments ( $F_{2,6}=1.4$ ,  $p=n.s$ ) (Figure 4:13.B). Analysis of *TBR1* showed significant increase in expression by IWR1 ( $32.2 \pm 5.1$ ) or KY02111 ( $19.8 \pm 2.3$ ) treatments compared to control ( $1.0 \pm 0.4$ ) and there was no difference between IWR1 and KY02111 treatments ( $F_{2,6}=35.3$ ,  $p=0.000$ ) (Figure 4:13.C).

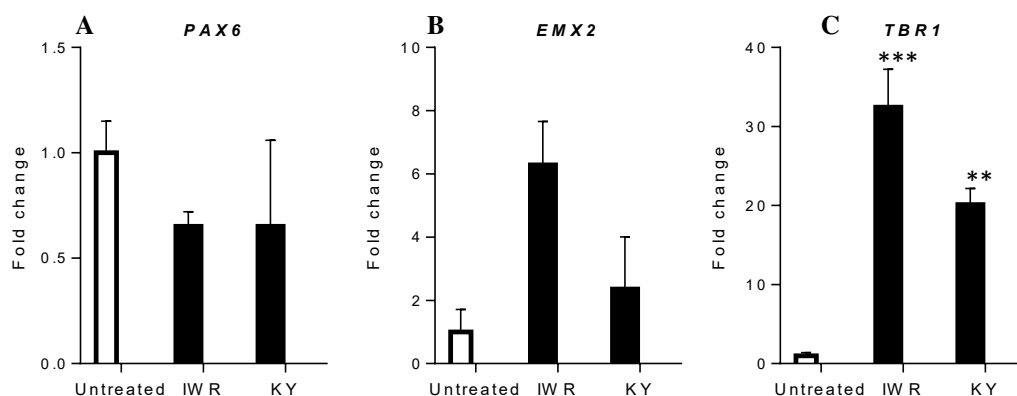


Figure 4:13 Effect of WNT inhibitors on pallial markers. Fold change expression of A) *PAX6*, B) *EMX2* and C) *TBR1*. Data represented as mean  $\pm$  S.E.M of 3 different experiments. \*\* $p < 0.01$ , \*\*\* $p < 0.001$  ANOVA, Dunnett's multiple comparisons test

#### 4.4.6.4 Sub-pallial markers

The expression of *GSX2*, *GSX1*, *DLX2*, *DLX1*, *DLX5*, and *ASCL1* was analysed. Analysis of *GSX2* showed significant increase in expression by IWR1 ( $2232.8 \pm 438.0$ ) or KY02111 treatment ( $418.3 \pm 157.3$ ) compared to control ( $1.0 \pm 0.2$ ) and there was also a significant difference between IWR1 and KY02111 treatments ( $F_{2,6}=126.0$ ,  $P < 0.0001$ ) (Figure 4:14.A). Analysis of *GSX1* showed no significant difference in the expression levels by IWR1 ( $1.6 \pm 0.4$ ) or KY02111 ( $0.7 \pm 0.1$ ) treatments compared to control ( $1.0 \pm 0.0$ ) ( $F_{2,6}=3.5$ ,  $p=n.s$ ) (Figure 4:14.B). Analysis of *ASCL1* showed no significant difference in the expression levels by IWR1 ( $2.9 \pm 1.3$ ) or KY02111 treatment ( $1.5 \pm 1.0$ ) compared to control ( $1.0 \pm 0.12$ ) ( $F_{2,6}=0.7$ ,  $p=n.s$ ) (Figure 4:14.C). Analysis of *DLX2* showed significant increase in expression by IWR1 ( $418.5 \pm 57.3$ ) or KY02111 treatment ( $53.4 \pm 24.1$ ) compared to control ( $1.0 \pm 0.2$ ) and there was also a significant difference between IWR1 and KY02111 treatments

( $F_{2,6}=42.1$ ,  $p=0.000$ ) (Figure 4:14.D). Analysis of *DLX1* showed significant increase in expression by IWR1 ( $167.6 \pm 59.2$ ) or KY02111 treatment ( $121.3 \pm 79.4$ ) compared to control ( $1.0 \pm 0.2$ ) and there was no significant difference between IWR1 and KY02111 treatments ( $F_{2,6}=28.1$ ,  $p=0.001$ ) (Figure 4:14.E). Analysis of *DLX5* showed significant increase in expression by IWR1 ( $1110.8 \pm 166.56$ ) or KY02111 treatment ( $161.0 \pm 41.5$ ) compared to control ( $1.0 \pm 0.2$ ) and there was also a significant difference between IWR1 and KY02111 treatments ( $F_{2,4}=328.5$ ,  $p < 0.0001$ ) (Figure 4:14.F).

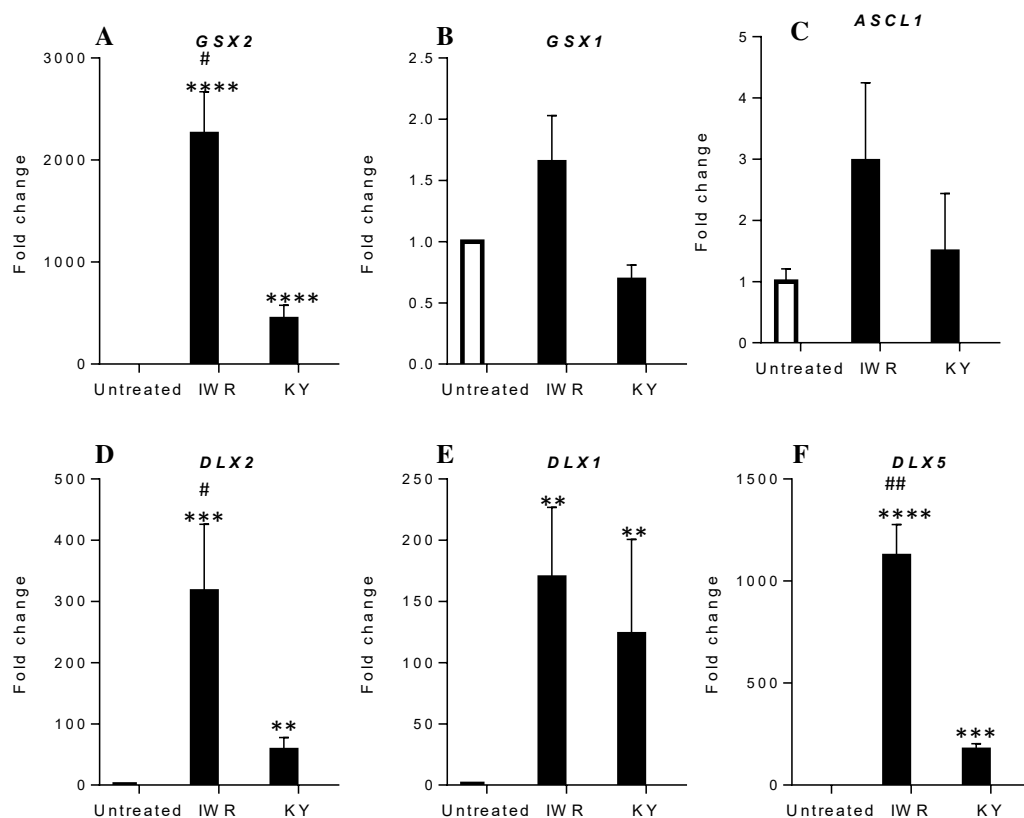


Figure 4:14 Effect of WNT inhibitors on subpallial markers. Fold change expression of A) *GSX2*, B) *GSX1*, C) *ASCL1* D) *DLX2*, E) *DLX1* and E) *DLX5*. Data represented as mean  $\pm$  S.E.M, of 3 different experiments. \* denotes significance control vs treatments and # denotes significance IWR1 vs KY02111. #p < 0.05, \*\*p < 0.01, \*\*\*p < 0.001, \*\*\*\*p < 0.0001 ANOVA, Dunnett's multiple comparisons test

#### 4.4.6.5 LGE markers

The expression of *MEIS2*, *SP8*, *ISL1*, *FOXP1*, *EBF1* and *IKZF2* was analysed. Analysis of *MEIS2* showed significant increase in the expression levels by IWR1 ( $7.8 \pm 0.8$ ) compared to KY02111 treatment ( $2.0 \pm 0.4$ ) or control ( $1.0 \pm 0.2$ ) ( $F_{2,6}=32.7$ ,  $p=0.000$ ) (Figure 4:15 A). Analysis of *SP8* showed no significant difference in the expression levels by IWR1 ( $1.9 \pm 0.1$ ) or KY02111 ( $2.0 \pm 0.6$ ) treatment compared to control ( $1.0 \pm 0.1$ ) ( $F_{2,6}=2.83$ ,  $p=n.s$ ) (Figure 4:15.B). Similar to *MEIS2* expression, analysis of *ISL1* showed significant increase in the expression levels by

IWR1 ( $13.1 \pm 4.8$ ) compared to KY02111 treatment ( $1.9 \pm 0.9$ ) or control ( $1.0 \pm 0.1$ ) ( $F_{2,6}=26.3$ ,  $p=0.005$ ) (Figure 4:15.C). Analysis of *FOXP1* showed no significant difference in the expression levels by IWR1 ( $1.0 \pm 0.3$ ) or KY02111 ( $0.9 \pm 0.1$ ) treatment compared to control ( $1.0 \pm 0.1$ ) ( $F_{2,6}=0.74$ ,  $p=n.s$ ) (Figure 4:15.D). Analysis of *EBF1* showed no significant difference in the expression levels by IWR1 ( $1.8 \pm 0.5$ ) or KY02111 ( $1.3 \pm 0.3$ ) treatment compared to control ( $1.0 \pm 0.1$ ) ( $F_{2,6}=0.9$ ,  $p=n.s$ ) (Figure 4:15.E).

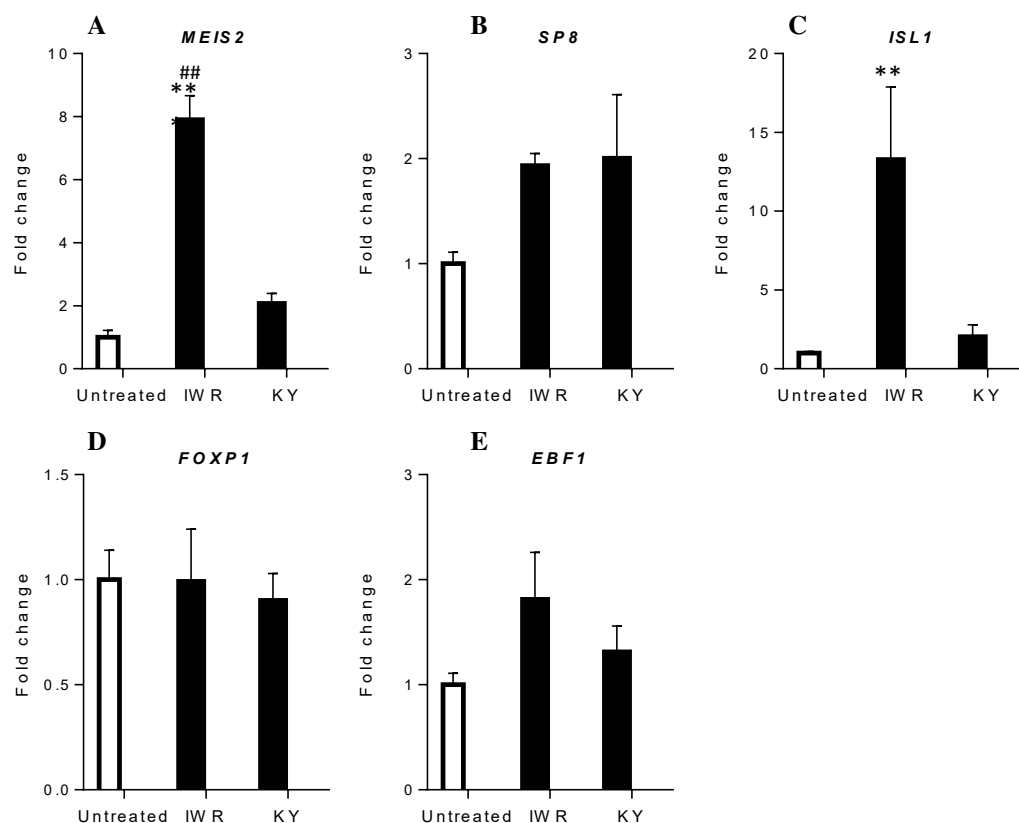


Figure 4:15 Effect of WNT inhibitors on subpallial markers. Fold change expression of A) *MEIS2*, B) *SP8*, C) *ISL1*, D) *FOXP1*, and E) *EBF1*. Data represented as mean  $\pm$  S.E.M, of 3 different experiments \* denotes significance control vs treatments and # denotes significance IWR1 vs KY02111. ###/\*\*/\*\*\* $p < 0.01$ , \*\*\* $p < 0.001$  ANOVA, Dunnett's multiple comparisons test

#### 4.4.6.6 MGE markers

The expression of *NKX2.1*, *LHX6* and *NKX6.2* was analysed. Analysis of *NKX2.1* showed significant increase in expression by IWR1 ( $215.2 \pm 127.1$ ) or KY02111 treatment ( $84.1 \pm 43.7$ ) compared to control ( $1.0 \pm 0.2$ ) and there was no significant difference between IWR1 and KY02111 treatments ( $F_{2,4}=25.3$ ,  $p=0.005$ ) (Figure 4:16.A). Analysis of *LHX6* showed significant increase in the expression levels by IWR1 ( $167.6 \pm 12.3$ ) compared to KY02111 treatment ( $10.0 \pm 7.1$ ) or control

( $1.0 \pm 0.2$ ) ( $F_{2,6}=18.7$ ,  $p=0.004$ ) (Figure 4:16.B). Analysis of *NKX6.2* showed significant increase in the expression levels by IWR1 ( $10.8 \pm 5.8$ ) and KY02111 treatment ( $20.7 \pm 7.1$ ) compared to control ( $1.0 \pm 0.2$ ) and there was no significant difference between IWR1 and KY02111 treatments ( $F_{2,6}=14.4$ ,  $p=0.008$ ) (Figure 4:16.C).

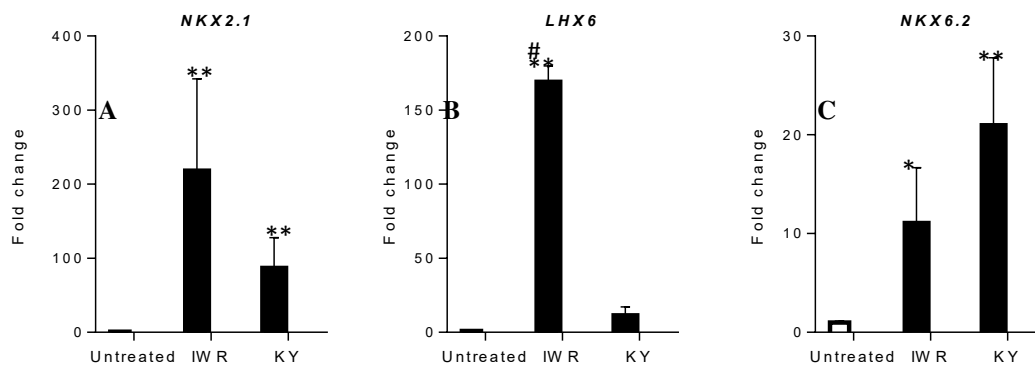


Figure 4:16 Effect of WNT inhibitors on MGE markers Fold change expression of A) *NKX2.1* B) *LHX6* and C) *NKX6.2*. Data represented as mean  $\pm$  S.E.M, of 3 different experiments. \* denotes significance control vs treatments and # denotes significance IWR1 vs KY02111. #  $p < 0.05$ , \*\* $p < 0.01$  ANOVA, Dunnett's multiple comparisons test

#### 4.4.6.7 Neuronal markers

The expression of *NCAM1*, *CDH2* (N-CADHERIN), *TUBB3*, *MAP2* and *DCX* was analysed. Analysis of *NCAM1* expression showed no significant difference between untreated control ( $1.0 \pm 0.1$ ) and IWR1 treated ( $2.0 \pm 0.3$ ) or KY02111 treated ( $1.4 \pm 0.5$ ) cultures ( $F_{2,6}=2.3$ ,  $p=n.s$ ) (Figure 4:17.A). Analysis of *CDH2* expression showed no difference between control ( $1.0 \pm 0.0$ ) and IWR1 treated ( $0.8 \pm 0.1$ ) cultures, but significant decrease by KY02111 treatment ( $0.5 \pm 0.1$ ) ( $F_{2,6}=16.3$ ,  $p=0.004$ ) (Figure 4:17.B). Analysis of *TUBB3* showed significant increase in the expression levels by IWR1 ( $3.7 \pm 0.7$ ) and KY02111 treatment ( $1.9 \pm 0.1$ ) compared to control ( $1.0 \pm 0.2$ ) and there was also a significant difference between IWR1 and KY02111 treatments ( $F_{2,6}=19.2$ ,  $p=0.003$ ) (Figure 4:17.C). Analysis of *MAP2* showed significant decrease in the expression levels by KY02111 treatment ( $0.5 \pm 0.1$ ) compared to IWR1 ( $1.2 \pm 0.3$ ) and control ( $1.0 \pm 0.1$ ) ( $F_{2,6}=5.2$ ,  $p=0.05$ ) (Figure 4:17.D). Analysis of *DCX* showed significant increase in the expression levels by IWR1 ( $12.5 \pm 3.0$ ) compared to KY02111 ( $0.8 \pm 0.2$ ) treatment or control ( $1.0 \pm 0.2$ ) ( $F_{2,5}=35.4$ ,  $p=0.001$ ) (Figure 4:17.E).

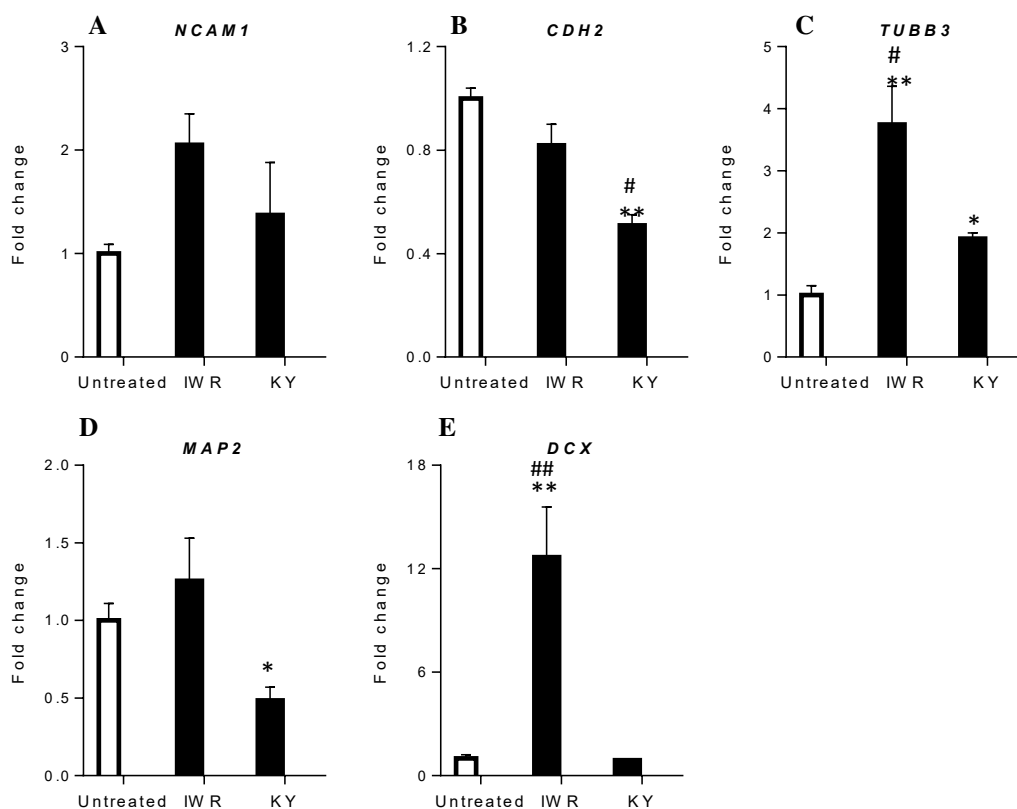


Figure 4:17 Effect of WNT inhibitors on neuronal markers. Fold change expression of A) *NCAM1*, B) *CDH2*, C) *TUBB3*, D) *MAP2* and E) *DCX*. Data represented as mean  $\pm$  S.E.M of 3 different experiments. \* denotes significance control vs treatments and # denotes significance IWR1 vs KY02111. #/\*  $p < 0.05$ , \*\* $p < 0.01$  ANOVA, Dunnett's multiple comparisons test

## 4.5 Discussion

The effect of WNT antagonism on telencephalon specification of hPSCs was studied in this chapter. Initially, WNT inhibitor IWR1 was employed to analyse its effect on the inhibition of the WNT pathway transcriptional target *LEF1*, induced by exogenous WNT3a or endogenous WNT signalling. This demonstrated a dose dependent effect. Next, the dual-SMADi EB protocol described in the previous chapter was adapted to a monolayer culture and used to analyse the effect of small molecule WNT inhibitors- IWR1 and KY02111 on telencephalon induction and specification.

### 4.5.1 Effect of WNT inhibitors on telencephalon induction

The main result of this study was the demonstration that inhibition of WNT signalling efficiently induced telencephalon markers. During hPSC neural differentiation using stromal co-culture, a serum free method or dual-SMAD inhibition, the default identity acquired has been described as anterior neural fate (Pankratz *et al.* 2007; Elkabetz *et al.* 2008; Chambers *et al.* 2009; Li *et al.* 2009; Delli Carri *et al.* 2013). In this study, the feeder-free monolayer dual-SMADi neural

induction cultures in the absence of WNT inhibitors generated < 5% FOXG1<sup>+</sup> cells. The inhibition of WNT signalling in combination with dual-SMADi promoted the induction of *FOXG1* in the majority of the cells by D16 of differentiation. Addition of IWR1 from both D0 and D8 upregulated *FOXG1* expression. High fold induction resulted from D0 addition. Next, IWR1 and KY02111 D0 addition dose-response experiments were performed. The cell responses to both IWR1 and KY02111 was found to be dose dependent. Of the dose range 0.1 to 10µM tested, at least 1µM of IWR1 or KY02111 was needed for *FOXG1* mRNA induction. Cultures treated with IWR1 at 1µM yielded ~ 90% FOXG1<sup>+</sup> cells. Cultures treated with KY02111 at 1µM and 10µM yielded ~35% and ~76% FOXG1<sup>+</sup> cells respectively, suggesting that IWR1 is more potent than KY02111 at low dose. These data complemented findings in animal models where inhibition of WNT signalling has been shown to be required for inducing anterior neural structures (Belo *et al.* 1997; Glinka *et al.* 1997; Glinka *et al.* 1998; Kimura *et al.* 2000; Mukhopadhyay *et al.* 2001; Houart *et al.* 2002; Barco Barrantes *et al.* 2003; Kemp *et al.* 2005). The results here demonstrated that not the absence of WNT agonists, but the active inhibition of endogenous WNT-signalling, induced the telencephalon identity. Inhibition of WNT signalling by DKK1 at 100-500ng/ml has been previously reported to enhance hPSC telencephalon specification. In the presence of DKK1, D35 neurogenic EB cultures yielded ~ 34% FOXG1<sup>+</sup> cells (Watanabe *et al.* 2007) and D10-D15 monolayer cultures yielded ~ 58-64% FOXG1<sup>+</sup> cells (DelliCarri *et al.* 2013; Nicoleau *et al.* 2013). The high yield of FOXG1 70- 90% obtained here, through KY02111 or IWR1 mediated monolayer differentiation makes it an attractive model over DKK1 mediated hPSC differentiation. A similar small molecule based study was published during the period of my research utilizing XAV-939, another TNKS inhibitor (Huang *et al.* 2009). XAV-939 was also able to replace DKK1 and dose-dependently induced the expression of FOXG1. At 1µM, XAV-939 yielded ~85% FOXG1<sup>+</sup> cells (Nicoleau *et al.* 2013).

Further analysis of mRNA expression of cultures treated with IWR1 at 1µM and KY02111 at 10µM was carried out. WNT inhibition influenced the expression of anterior neural tube markers *SIX3*, *OTX2* and *LMX1B*. Both IWR1 and KY02111 upregulated the expression of *SIX3*. However, had no effect on *OTX2*, a maker that is initially expressed in the anterior neuroectoderm and is later restricted to the diencephalon and mesencephalon (Larsen *et al.* 2010; Onorati *et al.* 2014). Interestingly, addition of IWR1 or KY02111 downregulated *LMX1B*, a marker

expressed posterior to the diencephalon. Thus, demonstrating that WNT antagonism during hPSC dual-SMADi neural induction specifically enhanced the telencephalon identity. Recently, IWR1 at 10 $\mu$ M treatment during mESC differentiation was reported to enhance *Foxg1* and *Six3* and downregulate midbrain markers (Bertacchi *et al.* 2015). Both IWR1 or KY02111 treatment had no effect on neuroectodermal markers *SOX2*, *SOX1* and *NESTIN*. This was in line with observations seen with WNT inhibitor XAV-939 + SHH mediated hPSC differentiation (Nicoleau *et al.* 2013). XAV-939 treatment dose dependently increased the expression of *SIX3* and showed no effect on *SOX2*, *NESTIN* and *OTX2* as well as downregulated *LMX1A* (Nicoleau *et al.* 2013).

#### 4.5.2 Effect of WNT inhibitors on telencephalon D/V specification

The study demonstrated that inhibition of WNT signalling coaxed hPSC neuroectoderm specification towards a ventral telencephalon fate. Previous hPSC differentiation studies have reported that under chemically defined conditions without exogenous morphogens, *FOXG1*<sup>+</sup> cells predominantly adopted dorsal telencephalon progenitor identity, which upon terminal differentiation generated cortical neurons (Watanabe *et al.* 2007; Li *et al.* 2009; Shi *et al.* 2012; Lupo *et al.* 2013). This was attributed to the endogenous WNT/ $\beta$ -catenin signalling; the expression of WNT proteins and frizzled proteins was detected during hPSC and mESC *in vitro* neural differentiation (Li *et al.* 2009; Bertacchi *et al.* 2015). This was consistent with the *in vivo* role of this pathway during pallial development (Gunhaga *et al.* 2003; Backman *et al.* 2005). In my study, analysis of *PAX6* showed that, at the transcript level both IWR1 and KY02111 treatment showed a similar trend, with decrease in the expression levels upon increasing the concentration. However, this result was not statistically significant. At the protein level, the control cultures yielded ~90% *PAX6*<sup>+</sup>/*FOXG1*<sup>-</sup> progenitors. The proportion of *PAX6*<sup>+</sup> cells was decreased by IWR1-1 $\mu$ M and KY02111-10  $\mu$ M which yielded 76% and 74% respectively. Interestingly, there was also a decreased *PAX6* signal intensity. Previously, it had been demonstrated that exposure to WNT antagonist soluble Frz8 blocked the generation of *Pax6*<sup>+</sup> cells in chick embryo explants (Gunhaga *et al.* 2003). Similarly, DKK1 treatment decreased *Pax6*<sup>+</sup> cells during serum free EB method of mESC differentiation (Watanabe *et al.* 2005). Conversely, treatment with WNT proteins during an appropriate temporal window during hPSC and mESC differentiation enhanced dorsal telencephalon markers expression (Li *et al.* 2009; Watanabe *et al.* 2005). In the presence of SHH

signalling, DKK or XAV-939 treatment dose dependently was shown to decrease the PAX6 amount and nuclear intensity during hPSC differentiation (Nicoleau *et al.* 2013). The change in PAX6 expression seen in my study indicated that inhibition of endogenous WNT signalling may suppress its expression. However, the upregulation of *EMX2* and *TBR1*, by IWR1-1 $\mu$ M or KY02111-10  $\mu$ M treatment suggested the initiation of cortical neurogenesis in the culture. The proportions of *EMX2*<sup>+</sup> or *TBR1*<sup>+</sup> or *TBR2*<sup>+</sup> immunoreactive cells were not assessed in my study. This would have revealed the yield of cortical progenitors/neurons in the culture. PAX6 is an early neuroectoderm marker, which is later restricted to dorsal telencephalon (cortex). During cortical neurogenesis, radial glia cells located in the VZ asymmetrically divide to form neuron and intermediate progenitor that translocate to SVZ. In the SVZ, they symmetrically divide to form either progenitors or post-mitotic neurons. The transition from radial glia to intermediate progenitors located in SVZ that produce only neurons was associated with downregulation of Pax6 and upregulation of Tbr2. The subsequent transition to post mitotic neurons was marked by upregulation of Tbr1 and downregulation of Tbr2 (Englund *et al.* 2005). Furthermore, IWR1 or KY02111 upregulated early neurogenesis in the progenitors as seen by increased *TUBB3* and *DCX*, markers of immature neurons. WNT signalling gradient activity determined the cell identity during cortical development. Initiation of neurogenesis was dependent on gradual weakening of WNT signalling (Machon *et al.* 2007). Thus, WNT inhibition by IWR1 and KY02111 treatment may have initiated cortical neurogenesis in some telencephalon progenitors. Recently it was reported during mESC differentiation that synergistic action of IWR1 and Dorsomorphin upregulated the time specific expression of *Emx2* and *Tbr1* in Pax6<sup>+</sup>/Foxg1<sup>+</sup> cells. Furthermore, global gene expression profile comparison of these progenitors to isocortex and ventral telencephalon, revealed a dorsal telencephalon identity (Bertacchi *et al.* 2015). Previous studies reported that during hPSC differentiation, WNT inhibitors did not abrogate dorsal telencephalon markers in the absence of ventralizing SHH signalling in neural progenitors (Li *et al.* 2009; Watanabe *et al.* 2005; Nicoleau *et al.* 2013). This suggested that default cortical specification of hPSC and mESC derived telencephalon progenitors could take place even when Wnt/ $\beta$ -catenin was inactive. In the presence of exogenous SHH signalling, WNT inhibition strongly sensitized hPSC derived telencephalon progenitors to ventral telencephalic fate (Watanabe *et al.* 2007; Li *et al.* 2009; Zhang *et al.* 2010; Delli Carri *et al.* 2013; Nicoleau *et al.* 2013).

Concomitantly, IWR1 and KY02111 treatment substantially increased the ventral transcripts *GSX2* and *DLX2*, in a dose dependent manner. At the protein level, IWR1-1 $\mu$ M and KY02111-10  $\mu$ M induced 69% and 49% *GSX2*<sup>+</sup> cells respectively. The cultures also contained 7-8% *NKX2.1*<sup>+</sup> cells. Furthermore, a ventral identity was revealed by high-throughput QRT-PCR as seen by upregulation of *DLX1*, *DLX5*, *ISL1*, LGE marker *MEIS2* and MGE markers- *NKX2.1*, *NKX6.2* and *LHX6*. A similar data on the ventralizing activity of WNT inhibition by XAV-939 has been reported in which, XAV-939 treatment did not alter the expression of *EMX1*, but dose dependently increased *GSX2* and *NKX2.1* (Nicoleau *et al.* 2013). However, XAV-939 alone yielded only 30% *GSX2*<sup>+</sup> and 5% *NKX2.1*<sup>+</sup> cells, whereas in combination with SHH resulted in 60% *GSX2*<sup>+</sup> and 80% *NKX2.1*<sup>+</sup> cells (Nicoleau *et al.* 2013). Activation of endogenous SHH signalling, although weakly has been reported during hPSC frizzled8 mediated anterior neuroectoderm differentiation (Lupo *et al.* 2013). The ventral markers *GLI1* and *NKX2.1* were upregulated whereas *EMX1* was not detectable in these cultures. Previous studies have shown that the inhibition of HH pathway prevented *NKX2.1* but did not activate *EMX1* and *TBR2* suggesting that suppression of endogenous SHH activity did not enhance dorsal markers (Lupo *et al.* 2013; Nicoleau *et al.* 2013). As mentioned above, activation of WNT signalling was shown to upregulate *PAX6*, *EMX1* and *GLI3* and decrease *Nkx2.1*<sup>+</sup> and *Gsx2*<sup>+</sup> cells among *Foxg1*<sup>+</sup> cells (Li *et al.* 2009; Watanabe *et al.* 2005).

Collectively, previous hPSC differentiation studies indicated that activation of WNT signalling promoted dorsal telencephalon markers and decreased ventral markers (Li *et al.* 2009). The endogenous WNT signalling via upregulation of truncated *GLI3* (which is a repressor of SHH signalling) contributed to the default dorsal identity (Li *et al.* 2009). Treatment with *DKK1* had little effect on repression of *PAX6* or induction of *NKX2.1*, but significantly decreased *GLI3* (Li *et al.* 2009). WNT inhibitors did not abrogate dorsal markers in the absence of SHH (Li *et al.* 2009; Nicoleau *et al.* 2013) and promoted ventral telencephalon identity in the presence of SHH (Watanabe *et al.* 2007; Li *et al.* 2009; Zhang *et al.* 2010; Delli Carri *et al.* 2013; Nicoleau *et al.* 2013). This was partially through downregulation of truncated *GLI3* and upregulation of full length *GLI3* (Li *et al.* 2009). Thus, WNT and SHH signalling through *GLI3* regulated hPSC D/V telencephalon specification. The role of *GLI3* and SHH in D/V specification was in line with the observations in mice. Absence of *GLI3* in *Gli3*<sup>-/-</sup> mutants caused loss of dorsal markers and expansion of ventral markers and

absence of SHH in *Shh*<sup>-/-</sup> mutants greatly diminished the expression of ventral markers (Rallu *et al.* 2002). Interestingly, *Gli3*<sup>-/-</sup>/*Shh*<sup>-/-</sup> double mutants showed normal D/V patterning suggesting that ventral repression of GLI3 by SHH and conversely dorsal repression of SHH by GLI3 (Rallu *et al.* 2002). In addition, this study also supported the idea of SHH-independent pathways in telencephalon D/V patterning. In my study WNT inhibition by IWR1 or KY02111 in combination with BMP inhibition by LDN193189 efficiently directed hPSC differentiation towards an intermediate telencephalon -like fate. The IWR1 protocol developed here was used by Straccia *et al.* (2015) for hPSCs differentiation. Time point high-throughput array and comparison to WGE and adult striatum samples revealed that D16 DLX1<sup>+</sup> samples were similar to 7-9 weeks WGE than striatum. By D28 samples were close to adult striatum (Straccia *et al.* 2015). My study for the first time thus possibly demonstrated SHH-independent LGE-like specification of hPSCs. It would be interesting to analyse in detail the precise role of BMP inhibition in this process. (In the next chapter in this thesis, I studied the effect of SHH signalling in combination with WNT and BMP inhibition).

In conclusion, dual-SMADi induced PAX6<sup>+</sup> neuroectoderm cells. On this ground, inhibition of canonical WNT signaling by IWR1 or KY02111 dose dependently induced a FOXG1<sup>+</sup> telencephalon fate. In the absence of any ventralizing signals, WNT inhibition by IWR1 and KY02111 decreased PAX6 expression and increased sub-pallial markers as well as neuronal makers. IWR1 seemed to be more potent than KY02111 at 1 $\mu$ M. The study demonstrated a novel SHH-independent method for hPSC *in vitro* differentiation towards a sub-pallial fate.

# 5 Investigation of effect of HH and Activin signalling on hPSC ventral telencephalon specification

## 5.1 Aim

To analyse the effect of a) HH signalling, utilizing the small molecule SHH agonists - Purmorphamine and SAG and b) Activin signalling on hPSC ventral telencephalon specification

## 5.2 Background

During telencephalon development, *Shh* is expressed initially expressed by the prechordal plate, at E9 in the ventral telencephalon (which becomes subdivided into LGE, MGE and CGE) and by E12.5 in MGE MZ (Shimamura *et al.* 1995; Stamatakis *et al.* 2005; Yu *et al.* 2009). Analysis of *Shh* mutants demonstrated that early ablation of Hh signalling between E8.5 and E10 resulted in loss of ventral telencephalon patterning with failure to specify cell types originating from ventral GEs (Chiang *et al.* 1996; Fuccillo *et al.* 2004). In contrast, later *Shh* ablation between E10 and E12 maintained grossly normal telencephalon patterning, although a deficit in the production of oligodendrocytes and MGE derived cortical interneurons was seen (Machold *et al.* 2003; Xu *et al.* 2005). Recombinant SHH induced *Nkx2.1* expression in rat E9.5 explants, but not in E11.5 explants. Instead there was repression of dorsal markers *Emx1* and *Tbr1* and induction of *Dlx2*, *Isl1/2* and *Ikaros* expression indicative of LGE/striatal identity (Kohtz *et al.* 1998). Ectopic activation of Shh signalling in E8.5-E10.5 mouse telencephalon resulted in induction of *Gsx2* and *Dlx2* throughout neocortex with concomitant repression of dorsal markers (Rallu *et al.* 2002). In zebrafish ventral telencephalon, inhibition of HH signalling by cyclopamine suppressed *dlx2* and *nkx2.1* at neural plate stage (bud/2ss) and there was no effect when cyclopamine was provided at later 8ss stage (Danesin *et al.* 2009). Collectively, the developmental studies have demonstrated a temporal requirement of SHH for the subregional specification within ventral telencephalon.

During hPSC differentiation, SHH alone or in combination with WNT inhibitors has been reported to promote ventral telencephalon specification in a

temporal and dose-dependent manner. An early exposure to high concentration of SHH from day 9 of stromal-mediated neural induction or from day 1 of SB+Noggin dual-SMADi neural induction, induced FOXA2<sup>+</sup> floor plate fate and repressed FOXG1<sup>+</sup> telencephalon fate via repression of the WNT inhibitor DKK1 (Fasano *et al.* 2010). Late SHH exposure from day 7 or 12 had no effect on FOXG1 or OTX2 but induced ventralization (Fasano *et al.* 2010; Ma *et al.* 2012). Addition of SHH from day 12 to 26 during hPSC monolayer differentiation and from day 3 to 12 during mESC EB-based differentiation (compared with from day 5 or 6 addition) dose-dependently induced ventral markers at the expense of dorsal markers (Danjo *et al.* 2011; Ma *et al.* 2012). The highest doses of SHH (30nM or 500-1000ng/ml) induced NKX2.1<sup>+</sup> MGE identity, moderate dose (10nM or 200ng/ml) induced MEIS2, MASH1 and GSX2 indicative of LGE identity and there was concomitant dose-dependent reduction of PAX6 (Danjo *et al.* 2011; Ma *et al.* 2012). Exposure of these LGE-like progenitors (generated using 10nM SHH) to 30nM Shh from day 9 to 12 inhibited LGE identity and induced MGE and CGE identity (Danjo *et al.* 2011). Similarly, in the presence of WNT inhibitors (and dual-SMADi or stromal or EB based neural induction), addition of SHH from day 4 or 10, did not alter *FOXG1* but dose-dependently upregulated *GSX2*, *DLX2*, *ASCL1* and *NKX2.1* (Watanabe *et al.* 2007; Aubry *et al.* 2008; Li *et al.* 2009; DelliCarri *et al.* 2013; Nicoleau *et al.* 2013). Conflicting results have been reported on the timing of SHH pathway activation for induction of MGE, employing dual-SMADi and WNT inhibition. During hPSC-derived NKX2.1:GFP<sup>+</sup> cells differentiation, early SHH exposure (days 2-18) repressed FOXG1, further late phase exposure (6-18, 10-18) did not alter FOXG1, but enhanced OLIG2, the late phase 10-18 exposure resulted in the highest yield as well as induced *NKX6.2* (both are markers of MGE-derived cortical interneurons) (Maroof *et al.* 2013). However, an early SHH activation alone from day 0 or in combination with FGF signalling has been reported to highly induce MGE fate, judged by the expression of NKX2.1, OLIG2, DLX2 and FOXG1 (Nicholas *et al.* 2014; Kim *et al.* 2014). SHH signalling in conjunction with FGF signalling has been shown to modulate MGE vs CGE fate specification (Danjo *et al.* 2011; Kim *et al.* 2014).

Activin A (referred to as Activin) is a member of TGF- $\beta$  family. Activin subunits, receptors and its effector protein Smad2 are expressed in the developing

LGE (Feijen *et al.* 1994; Maira *et al.* 2010). Smad proteins have been shown to co-express and physically interact with Dlx transcription factors and plays a role in telencephalic GABAergic neuron development (Maira *et al.* 2010). During mESC and hPSC differentiation, Activin was shown to act independently of SHH signalling and induced ventralization, specifically CGE or LGE identity (Cambray *et al.* 2012; Arber *et al.* 2015). Dual-SMADi neural induction followed by an early exposure to Activin from day 9 to 18 induced LGE identity whereas a late exposure from day 20 to 27 induced CGE identity (Cambray *et al.* 2012; Arber *et al.* 2015). In their studies, during the early time window, SHH dose-dependently induced *NKX2.1*, *GSX2*, *DLX2* and *LHX8* (a marker of MGE derived interneurons) whereas Activin treatment (at 25ng/ml) led to the upregulation of pan-ventral markers as well as LGE specific markers *FOXP2*, *NOLZ1* and *CTIP2* (Arber *et al.* 2015). During the late exposure window, Activin enhanced progenitor differentiation and induced CGE- derived GABAergic Calretinin<sup>+</sup> (~75%) interneurons that migrate to the cortex (Cambray *et al.* 2012). Activin was found to mediate its patterning effects by inhibiting Hh signalling in a Gli3 dependent manner as well as by enhancing the pro-neurogenic retinoic acid signalling (Cambray *et al.* 2012). Furthermore, it was suggested that Activin mediated CGE fate specification might involve Fgf15, a direct target of Activin pathway in ESCs (Cambray *et al.* 2012).

In this chapter, I investigated the effect of SHH signalling by known small molecule agonists Purmorphamine and SAG. Purmorphamine binds and activates SMO and upregulates Hh pathway down-stream members Gli1 and Patched (Sinha and Chen 2006). SAG also acts by binding to SMO but inhibits Hh signalling at higher concentrations above 1 $\mu$ M (Chen *et al.* 2002). In parallel, Activin at 20ng/ml was employed. At the time of this study, Arber *et al.* 2015 was not published. The experiments were set up based on the manuscript provided and personal communications.

### 5.3 Experimental design

The effect of Purmorphamine, SAG or Activin on telencephalon ventral patterning was analysed in combination with BMP and WNT signalling inhibition. Telencephalic progenitors from 2 cell lines- H9 (ESC) and 34D6 (iPSC) were generated using monolayer based culture dual-SMADi+ IWR1 described in Figure

5.1. Modulation of the HH or Activin pathway was achieved during D8 to D16 of differentiation by the addition of Purmorphamine (at 0.1, 0.5 and 1 $\mu$ M) or SAG (at 0.001, 0.01 and 0.1 $\mu$ M) or Activin at 20ng/ml. At D16, the cultures were analysed by QRT-PCR and/or immunocytochemistry for D/V markers described previously in this thesis- PAX6, GSX2, DLX2, DLX5 and NKX2.1. The characterization of mRNA expression in detail was performed by high-throughput QRT-PCR array.

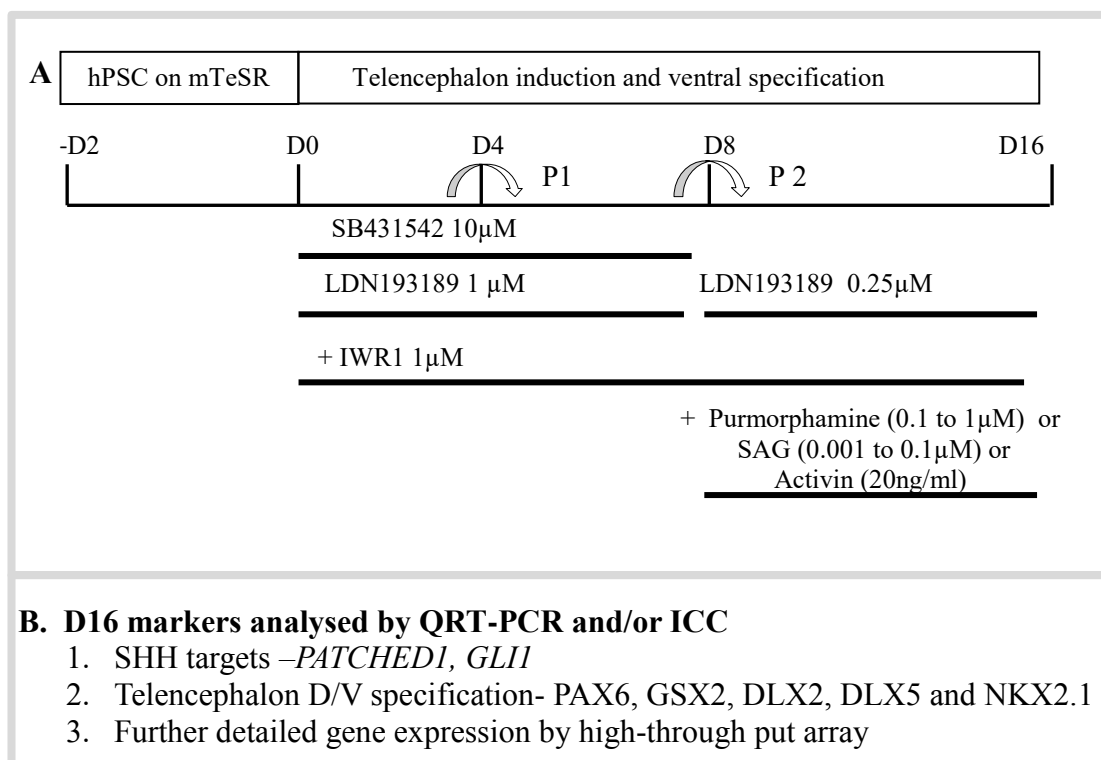


Figure 5:1 Cell culture regime for hPSC telencephalon induction and ventral specification. hPSCs were grown in mTeSR1 on matrigel coated plates. On D0, mTeSR1 was replaced with neural induction medium containing dual-SMAD inhibitors and WNT inhibitor IWR1 for the time window shown above. Cultures were re-plated at 1:2 ratio on D4 and again on D8 and maintained till D16 on matrigel coated plates. Activin or SHH agonists Purmorphamine or SAG were added to cultures from D8 to D16. B) Markers analysed by QRT PCR and/or ICC on D16.

## 5.4 Results

### 5.4.1 Modulation of HH signalling by Purmorphamine and SAG during hPSC differentiation.

Initially, the modulation of HH signalling by Purmorphamine and SAG was analysed by measuring the expression levels of SHH targets- *PATCHED1* and *GLII*. The experiments were performed in 2 experiment replicates and no statistical analysis were performed (see appendix table 5.1 for  $\Delta$ Cq). Fold change over ‘0’ treatment control was plotted. There was a marked increase in *PATCHED1* by Purmorphamine and SAG treatment in a dose-dependent manner (Figure 5.2.A).

Purmorphamine at 0.1, 0.5 and 1  $\mu\text{M}$  treatment yielded fold change of  $2.4 \pm 0.6$ ,  $8.7 \pm 2.3$  and  $18.5 \pm 5.7$  respectively when compared to IWR1 control cultures ( $1.0 \pm 0.7$ ). SAG at 0.001, 0.01 and 0.1  $\mu\text{M}$  treatment yielded fold change of  $0.7 \pm 0.0$ ,  $1.0 \pm 0.3$  and  $6.1 \pm 2.3$  respectively. Similarly, *GLII* expression was upregulated by Purmorphamine and SAG treatment in a dose-dependent manner (Figure 5.2B). Purmorphamine at 0.1, 0.5 and 1  $\mu\text{M}$  treatment yielded fold change of  $0.6 \pm 0.1$ ,  $2.10 \pm 2.1$  and  $42.0 \pm 0.0$  respectively when compared to control ( $1.0 \pm 0.0$ ). At least 0.1  $\mu\text{M}$  of SAG was required to upregulate *GLII* expression, which gave fold change of  $12.1 \pm 3.3$  over IWR-1 control.

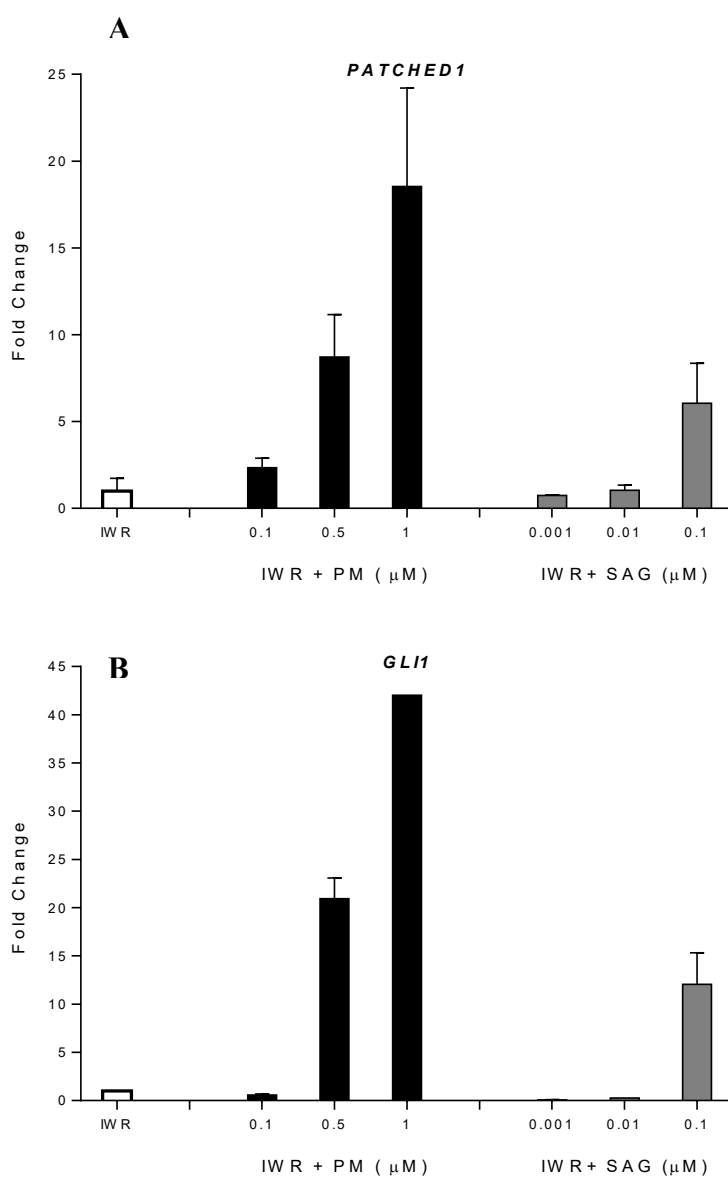


Figure 5:2 Modulation of HH activity by Purmorphamine and SAG in H9 day 16 neural progenitors- Neural progenitors were treated with either Purmorphamine (PM) (0.1 to 1  $\mu\text{M}$ ) or SAG (0.001 to 0.1  $\mu\text{M}$ ) from D8 to D16. Dose-dependent induction of A) *PATCHED1* and B) *GLII* by

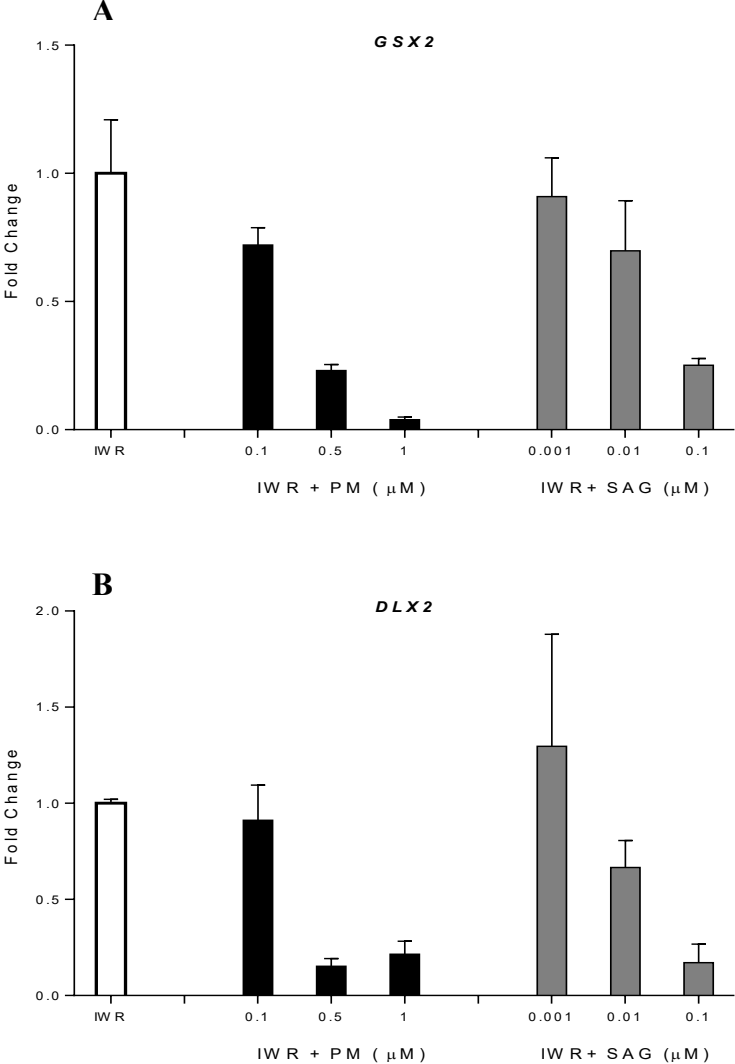
Purmorphamine and SAG analysed by QRT-PCR. Data represented as mean  $\pm$  S.E.M, N=2. experiment replicates set in parallel

#### 5.4.2 QRT-PCR characterization of Purmorphamine or SAG mediated ventral telencephalon specification

To investigate whether the addition of SHH agonists enhances ventral telencephalon specification, D16 cultures were analysed for the expression of ventral markers *GSX2*, *DLX2*, *DLX5* and *NKX2.1* (see appendix table 5.2 for  $\Delta$ Cq). Fold change over '0' treatment was plotted. Note that the dose response experiments were performed only twice, ie, N=2 and no statistical tests were performed. The experiments was further analysed by high-through put QRT-PCR array for N=3, discussed later.

There was a marked decrease in *GSX2* expression in a dose-dependent manner by the Purmorphamine or SAG treatment (Figure 5.3.A). Compared with control (1.0 $\pm$ 0.2), Purmorphamine at 0.1 $\mu$ M showed a similar expression (0.9 $\pm$ 0.2), at 0.5 $\mu$ M caused a decrease (0.2 $\pm$ 0.0) and at 1 $\mu$ M markedly reduced the expression level (0.1 $\pm$ 0.0). SAG at 0.001 $\mu$ M (0.9 $\pm$ 0.2) and 0.01 $\mu$ M (0.7 $\pm$ 0.2) showed an expression level comparable to control and at 0.1 $\mu$ M resulted in reduced expression (0.3 $\pm$ 0.0). *DLX2* expression showed a similar trend (Figure 5.3.B). Purmorphamine at 0.1 $\mu$ M (0.9 $\pm$ 0.2) gave an expression level similar to control (1.0 $\pm$ 0.0) and the high concentrations of 0.5 $\mu$ M (0.2 $\pm$ 0.0) and 1 $\mu$ M (0.2 $\pm$ 0.6) yielded low expression levels. SAG at 0.001 $\mu$ M (0.9 $\pm$ 0.2) gave an expression level of similar to control, at 0.01 $\mu$ M resulted in a smaller reduction (0.7 $\pm$ 0.1) and at 0.1 $\mu$ M, gave the lowest expression level (0.2 $\pm$ 0.1). Similar to *GSX2* and *DLX2* expression, *DLX5* expression was also found to be downregulated in a dose-dependent manner (Figure 5.3.C). Compared with control (1.0 $\pm$ 0.0), Purmorphamine at 0.1 $\mu$ M (0.6 $\pm$ 0.2) showed a decreased expression level and at 0.5  $\mu$ M (0.0 $\pm$ 0.00 and 1 $\mu$ M (0.1 $\pm$ 0.0) caused a marked reduction. SAG at 0.001 $\mu$ M (1.0 $\pm$ 0.0) gave an expression level similar to control, at 0.01 $\mu$ M resulted in a reduction (0.3 $\pm$ 0.1) and at 0.1 $\mu$ M further reduced the expression level (0.0 $\pm$ 0.0). The expression of *NKX2.1* was upregulated by Purmorphamine or SAG treatment in a dose-dependent manner (Figure 5.3 D). Compared with control (1.0 $\pm$ 0.2), Purmorphamine at 0.1 $\mu$ M showed a similar expression level (1.5 $\pm$ 0.1), at 0.5 $\mu$ M caused a smaller increase (9.7 $\pm$ 4.2) and at 1 $\mu$ M yielded the highest expression level (774.6 $\pm$ 82.5). SAG at 0.001 (1.8 $\pm$ 0.1) and

0.01 $\mu$ M (1.3 $\pm$ 0.0) showed an expression level similar to control and at 0.1 $\mu$ M resulted in an increase (24.0 $\pm$ 13.2).



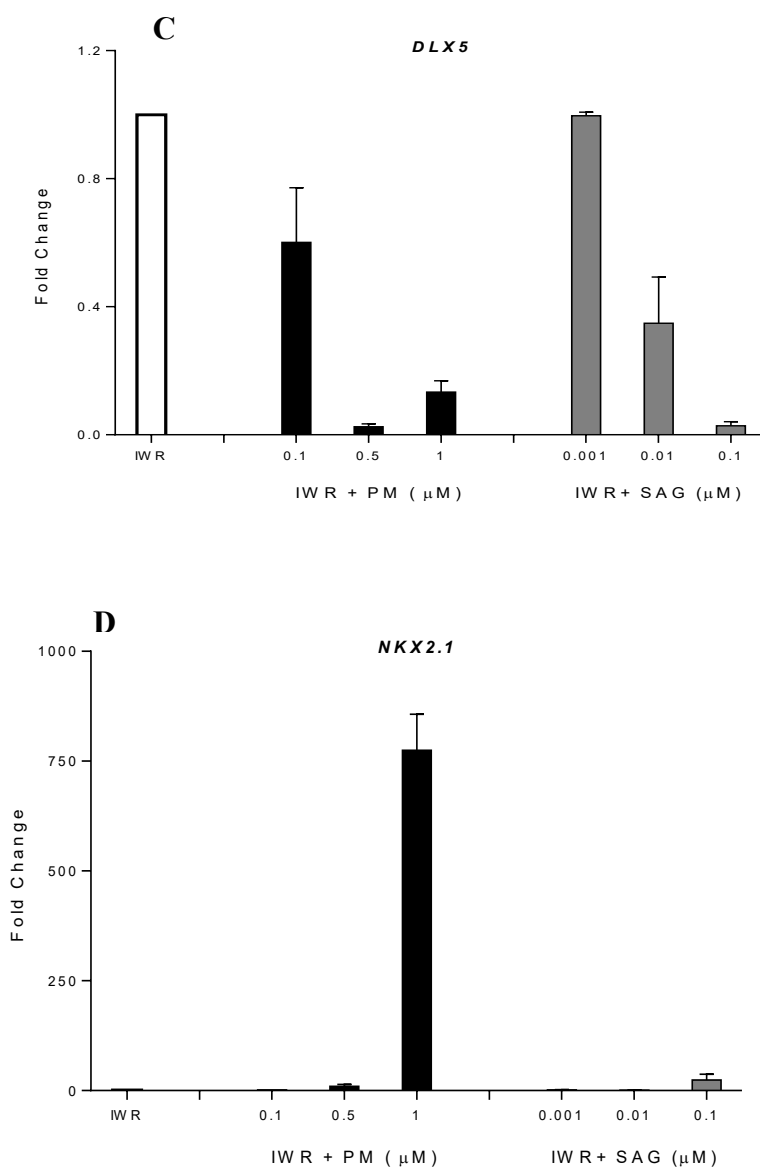


Figure 5:3 Effect of Purmorphamine and SAG on ventral telencephalon markers analysed by QRT-PCR during H9 differentiation. Purmorphamine (PM) and SAG dose-dependent downregulation of A) GSX2, B) DLX2 and C) DLX5 and up-regulation of D) NKX2.1 . Data represented as mean  $\pm$  S.E.M, N= 2.experiment replicates set in parallel

#### 5.4.3 Immunocytochemistry characterization of Purmorphamine or Activin mediated ventral telencephalon specification of H9 ESCs and 34D6 iPSCs

To characterize ventral telencephalon specification at the protein level, immunocytochemistry analysis was performed. D16 cultures generated in the presence of Purmorphamine (0.1 to  $1\mu\text{M}$  in H9 and 0.5 and  $1\mu\text{M}$  in 34D6) or Activin

(at 20ng/ml in 34D6 only) or '0' control treatment were re-plated onto matrigel coated cover slips and fixed on the same day. Cultures were immuno-stained for PAX6, GSX2 and NKX2.1. The immunofluorescence signal was quantified and represented as percentage of DAPI positive cells.

PAX6 and NKX2.1 expression were localized to the nucleus. Purmorphamine treatment dose-dependently reduced the proportion of PAX6 and increased the proportion of NKX2.1 immunoreactive cells in H9s (Figure 5.4). IWR1 alone (66.7%), IWR1+0.1 $\mu$ M Purmorphamine (69.1%) and IWR1+0.5 $\mu$ M Purmorphamine (59.8%) treatments showed a similar percentage of PAX6<sup>+</sup> cells and the proportion was reduced by IWR1+1.0 $\mu$ M Purmorphamine (27.0%) treatment. IWR1 (5.9%) and IWR1+0.1 $\mu$ M Purmorphamine (6.2%) treatments showed a similar number of NKX2.1<sup>+</sup> cells. The proportion of NKX2.1<sup>+</sup> cells was slightly increased by IWR1+0.5 $\mu$ M Purmorphamine (15.4%) treatment and highly increased by IWR1+1.0 $\mu$ M Purmorphamine (70.0%). Interestingly, 34D6 cultures showed low number of PAX6<sup>+</sup> (3.2-7.0%) under all the conditions (Figure 5.5). The proportion of NKX2.1<sup>+</sup> in IWR1 (9.1 $\pm$ 0.1%) cultures were slightly increased by IWR1+0.5 $\mu$ M Purmorphamine (21.0 $\pm$ 3.6%) treatment and highly increased by IWR1+1.0 $\mu$ M Purmorphamine (45.2 $\pm$  1.0%) IWR1+Activin cultures showed negligible amount of PAX6<sup>+</sup> or NKX2.1<sup>+</sup> cells.

GSX2 expression was localized to the nucleus. During H9 differentiation, IWR1 (66.6 $\pm$ 2.8%), IWR1+0.1 $\mu$ M Purmorphamine (69.9 $\pm$ 1.7%) and IWR1+0.5 $\mu$ M Purmorphamine (68.5 $\pm$ 7.1%) treatments showed a similar proportion of GSX2 immunoreactive cells. The number of GSX2<sup>+</sup> was reduced by IWR1+1.0 $\mu$ M Purmorphamine (43.7 $\pm$ 0.8%) treatment (Figure 5:6). During 34D6 differentiation GSX2/CTIP2 double immunostaining was performed. IWR1 (60.1 $\pm$ 0.5%) and IWR1+0.5 $\mu$ M Purmorphamine (50.9 $\pm$ 8.0%) showed a comparable proportion of GSX2<sup>+</sup> cells. The number of GSX2<sup>+</sup> was reduced by IWR1+1.0 $\mu$ M Purmorphamine (24.0 $\pm$ 1.1%) treatment. GSX2 immunoreactive cells were reduced in IWR1+Activin cultures (31.5 $\pm$ 1.7%) and there was concomitant induction of CTIP2 (53.4%) (Figure 5.7). There was no co-location of GSX2 and CTIP2.

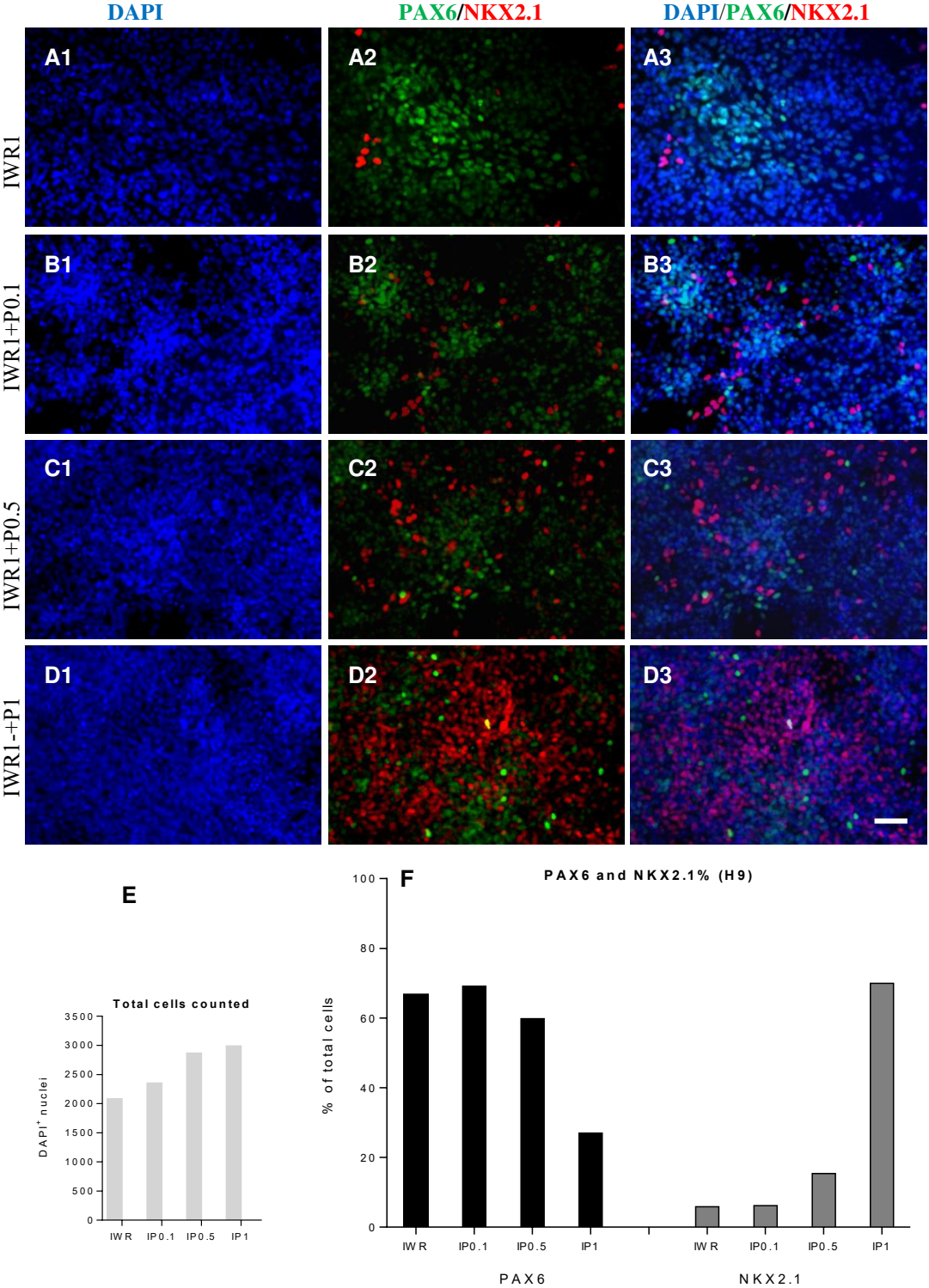


Figure 5:4 Fluorescent immunocytochemistry analysis of PAX6 and NKX2.1 in H9 D16 monolayer cultures. D16 progenitors generated in the absence or presence of Purmorphamine (IP) on matrigel coated plates were re-plated as single cell onto matrigel coated coverslips and fixed on the same day. Cells were double-immunostained for PAX6 (green), NKX2.1 (red) and counter stained for DAPI nuclear stain (blue). Representative images are given- A1-C1) DAPI stained cells, A2-C2) PAX6/NKX2.1 stained cells and A3-C3) DAPI/ PAX6/NKX2.1 merge, generated in the presence of A1-A3) no Purmorphamine B1-B3) Purmorphamine at 0.1 $\mu$ M, C1-C3) Purmorphamine at 0.5 $\mu$ M and D1-D3) Purmorphamine at 1.0 $\mu$ M. Scale bar for all images in bottom right image= 100 $\mu$ m. Multiple fields/coverslips were imaged. Graphs represent E) the total amount of DAPI-positive nuclei counted for each treatment and F) proportion of PAX6 and NKX2.1 as % of DAPI nuclei. Data represented as mean, N=1, experiment replicates

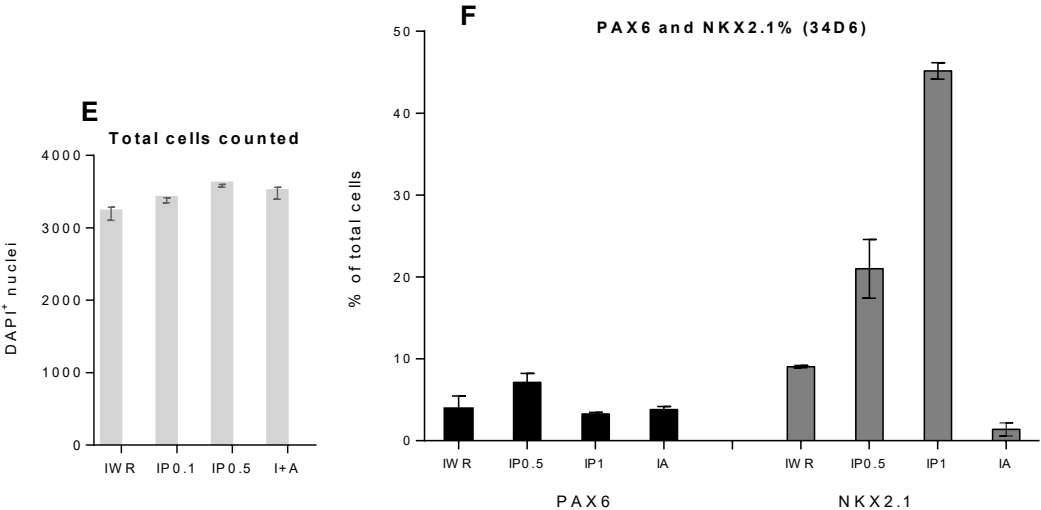
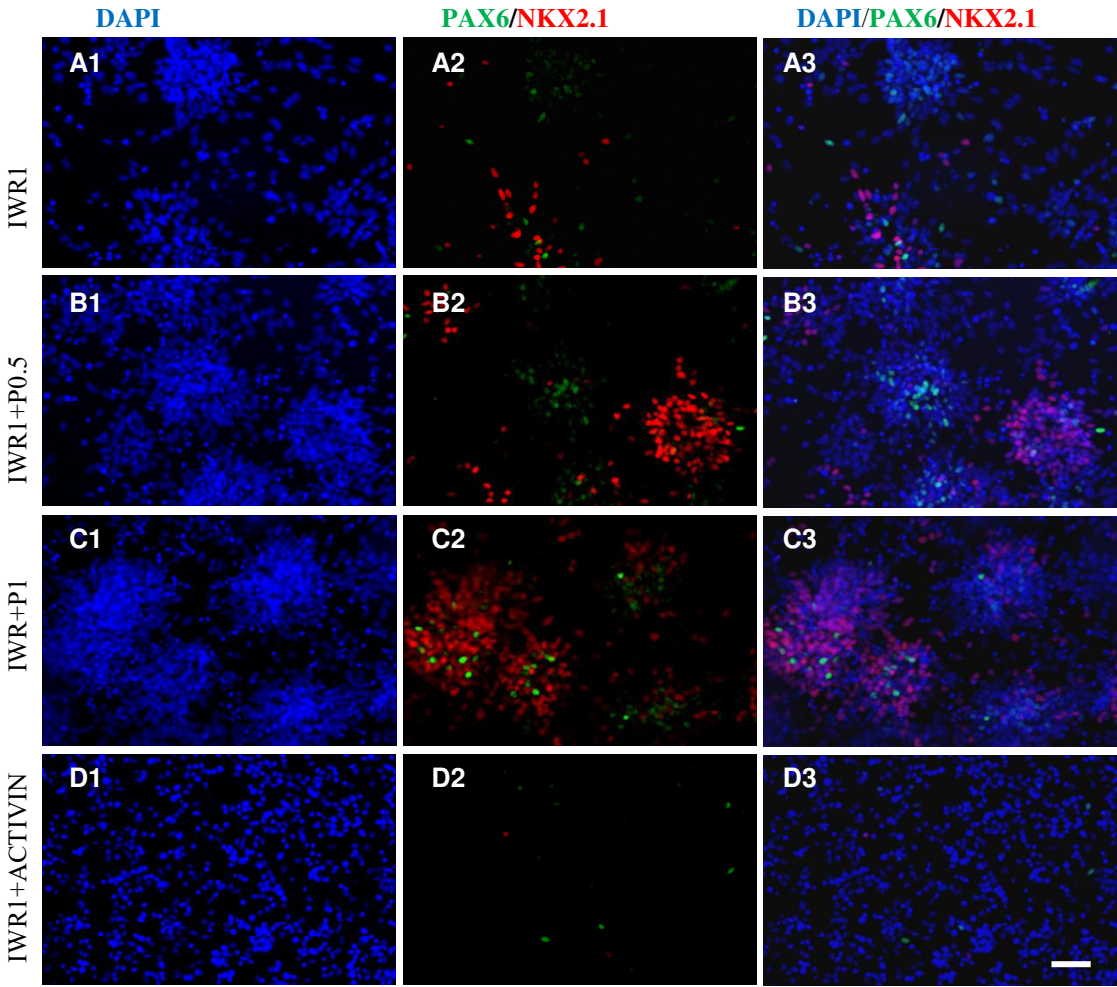


Figure 5:5 Fluorescent immunocytochemistry analysis of PAX6 and NKX2.1 in 34D6 D16 monolayer cultures. D16 progenitors generated in the absence or presence of Purmorphamine (IP) or Activin (IA) on matrigel coated plates were re-plated as single cell onto matrigel coated coverslips and fixed on the same day. Cells were double-immunostained for PAX6 (green), NKX2.1 (red) and counter stained for DAPI nuclear stain (blue). Representative images are given-A1-C1) DAPI stained cells, A2-C2) PAX6/NKX2.1 stained cells and A3-C3) DAPI/PAX6/NKX2.1 merge, generated in the presence of A1-A3) no Purmorphamine B1-B3) Purmorphamine at 0.5µM, C1-C3) Purmorphamine at 1µM and D1-D3) Activin at 20ng/ml. Scale bar for all images in bottom right image=100µm. Multiple fields/coverslips were imaged. Graphs represent E) the total amount of DAPI-positive nuclei counted for each treatment and F) proportion of PAX6 and NKX2.1 as % of DAPI nuclei. Data represented as mean±S.E.M, N=2, experiment replicates set in parallel

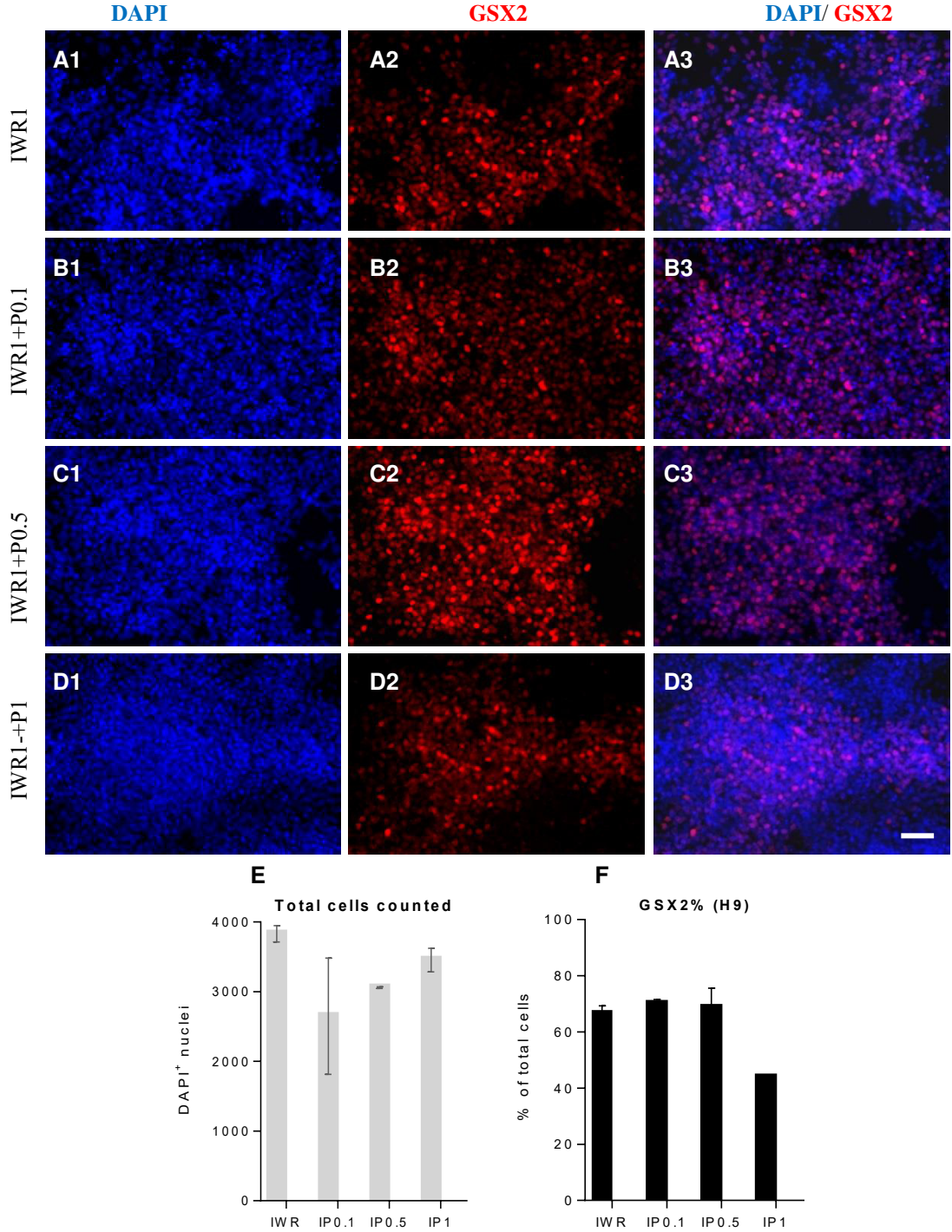


Figure 5:6 Fluorescent immunocytochemistry analysis of GSX2 in H9 D16 monolayer cultures. D16 progenitors generated in the absence or presence of Purmorphamine (IP) on matrigel coated plates were re-plated as single cell onto matrigel coated coverslips and fixed on the same day. Cells were double-immunostained for GSX2 (red) and counter stained for DAPI nuclear stain (blue). Representative images are given- A1-A3) DAPI stained cells, A2-C2) GSX2stained cells and A3-C3) DAPI/ GSX2 merge, generated in the presence of A1-A3) no Purmorphamine B1-B3) Purmorphamine at 0.1 $\mu$ M, C1-C3) Purmorphamine at 0.5 $\mu$ M and D1-D3) Purmorphamine at 1.0 $\mu$ M. Scale bar for all images in bottom right image= 100 $\mu$ m. Multiple fields/coverslips were imaged. Graphs represent E) the total amount of DAPI-positive nuclei counted for each treatment and F) proportion of GSX2 as % of DAPI nuclei. Data represented as mean, as mean $\pm$ S.E.M, N=2, experiment replicates set in parallel

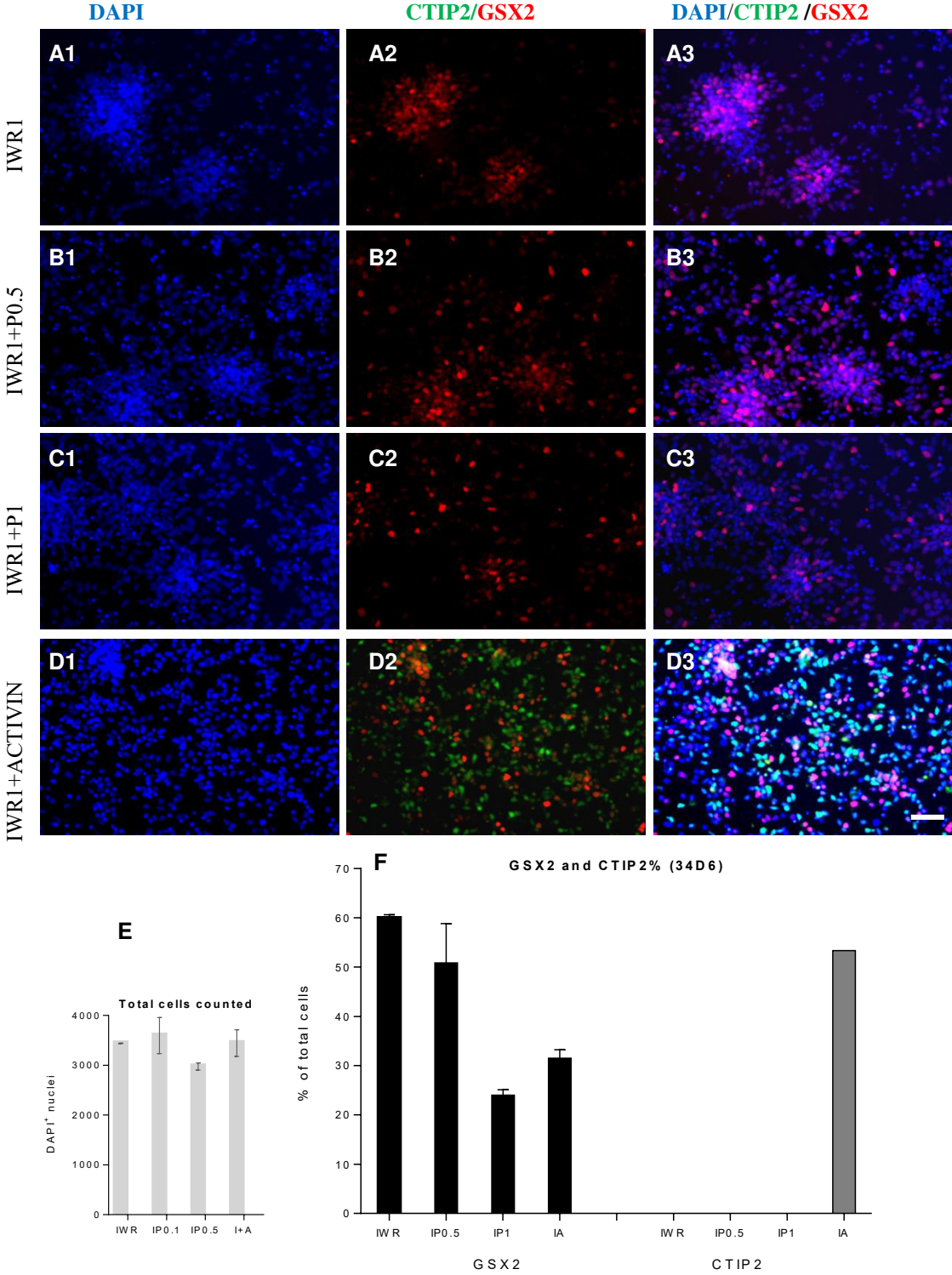


Figure 5:7 Fluorescent immunocytochemistry analysis of GSX2 and CTIP2 in 34D6 D16 monolayer cultures. D16 progenitors generated in the absence or presence of Purmorphamine (IP) or Activin (IA) on matrigel coated plates were re-plated as single cell onto matrigel coated coverslips and fixed on the same day. Cells were double-immunostained for CTIP2 (green), GSX2 (red) and counter stained for DAPI nuclear stain (blue). Representative images are given- A1-C1) DAPI stained cells, A2-C2) GSX2/CTIP2 stained cells and A3-C3) DAPI/CTIP2/GSX2 merge, generated in the presence of A1-A3) no Purmorphamine B1-B3) Purmorphamine at 0.5µM, C1-C3) Purmorphamine at 1.0µM and D1-D3) Activin at 20ng/ml. Scale bar for all images in bottom right image= 100µm. Multiple fields/coverslips were imaged. Graphs represent E) the total amount of DAPI-positive nuclei counted

for each treatment and F) proportion of GSX2 and CTIP2 as % of DAPI nuclei. Data represented as mean±S.E.M, N=2, experiment replicates set in parallel. N=1 for CTIP2

#### 5.4.4 High-through put QRT-PCR characterization of Purmorphamine or Activin mediated ventral telencephalon specification of H9 ESC and 34D6 iPSCs

For a detailed characterization, D16 samples were subjected to high-through put QRT-PCR analysis. H9 samples included cultures treated with 0.5µM or 1µM Purmorphamine or 20ng/ml Activin and control. 34D6 samples included cultures treated with 0.3µM or 1µM Purmorphamine and control. As explained in the previous chapter, high-throughput array permitted the analysis of a number of different markers of neuroectoderm, A-P axis, telencephalon, pallium, subpallium, LGE, MGE, CGE, neurons and glia as well as reference genes. See appendix table 5.3. for  $\Delta Cq$  values For the analysis,  $\Delta Cq > 12$  for both treatment groups and control was taken as low or negligible expression and was not shown here. The fold change in gene expression was plotted as the ratio of normalized gene expression of treatment samples to control. One way ANOVA with Dunnett's multiple test was used to determine the statistical significance. (Notes- (1) Both Purmorphamine and Activin data was shown on the same graph. However, Activin treatment being N=2 was excluded from the statistical analysis. (2) The analysis software automatically assigned a high Cq value for no signal, resulting in a high  $\Delta Cq$  value for the gene of interest. If two out of the 3 samples showed similar  $\Delta Cq$  values, this automatically assigned value was excluded in this analysis shown here).

##### 5.4.4.1 Analysis of neuroectodermal markers

Neuroectodermal markers *SOX2*, *SOX1* and *NES* were analysed

H9 differentiation- Analysis of *SOX2* expression showed no significant difference between untreated control (1.0±0.2) and 0.5µM (1.9±0.8) or 1µM treated (2.5±0.7) cultures ( $F_{2,6}=1.4$ ,  $p=n.s$ ). Activin treatment (1.1±0.1) yielded an expression level similar to that of control (Figure 5:8.A). Analysis of *SOX1* expression showed no significant difference between untreated control (1.0±0.2) and 0.5µM (0.5±0.1) or 1µM treated (0.4±0.0.1) cultures ( $F_{2,6}=4.4$ ,  $p=n.s$ ). Expression level in Activin treatment (1.3±0.0) was comparable to control (Figure 5:8.B). Analysis of *NES* expression showed no significant difference between untreated control (1.0±0.1) and 0.5µM (1.3±0.4) or 1µM treated (0.8±0.20) cultures ( $F_{2,6}=0.6$ ,

p=n.s) Expression levels in Activin treatment ( $1.16 \pm 0.20$ ) was comparable to control (Figure 5:8.C).

34D6 differentiation- Analysis of *SOX2* expression showed no significant difference between untreated control ( $1.0 \pm 0.5$ ) and  $0.3 \mu\text{M}$  ( $1.0 \pm 0.5$ ) or  $1 \mu\text{M}$  treated ( $1.7 \pm 0.7$ ) cultures ( $F_{2,6}=0.3$ , p=n.s) (Figure 5:8 D). Analysis of *SOX1* expression showed a decreased expression level by  $0.3 \mu\text{M}$  ( $0.4 \pm 0.1$ ) or  $1 \mu\text{M}$  treatment ( $0.3 \pm 0.2$ ) that was not significantly different from untreated control ( $1.0 \pm 0.0$ ) ( $F_{2,6}=1.9$ , p=n.s) (Figure 5:8.E). Analysis of *NES* expression showed no significant difference between untreated control ( $1.0 \pm 0.4$ ) and  $0.3 \mu\text{M}$  ( $1.2 \pm 0.2$ ) or  $1 \mu\text{M}$  treatment ( $1.3 \pm 0.4$ ) ( $F_{2,6}=2.9$ , p=n.s) (Figure 5:8.F).

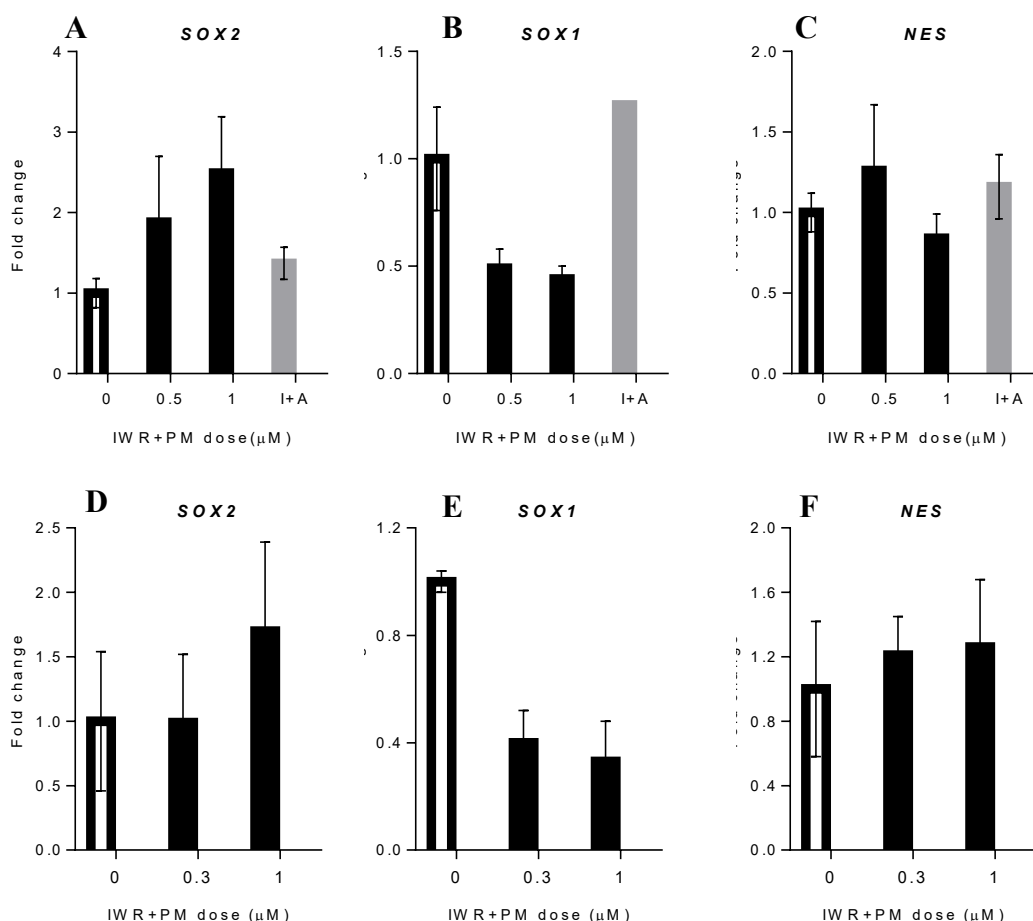


Figure 5:8 Effect of Purmorphamine or Activin treatment on neuroectodermal markers at D16- Fold change expression of *SOX2*, *SOX1* and *NES* in A-C) H9 ESC-derived and D-F) 34D6 iPSC-derived D16 progenitors. Data represented as mean  $\pm$  S.E.M, N=3 except for I+A (IWR1+Activin) N=2. (N= experiment replicates, independent experiments for H9 and experiments set in parallel for 34D6)

#### 5.4.4.2 Analysis of anterior or floor plate markers

The expression of markers of anterior *FOXG1*, *SIX3* and *OTX2* and floor plate marker *FOXA2* was analysed.

H9 differentiation- Analysis of *FOXG1* showed no significant difference in the expression levels by 0.5 $\mu$ M (1.1 $\pm$ 0.0) or 1.0 $\mu$ M Purmorphamine treatment (0.7 $\pm$ 0.3) compared to control (1.0 $\pm$ 0.2) ( $F_{2,6}=0.3$ ,  $p=n.s.$ ). Activin treatment maintained a comparable expression level (1.1 $\pm$ 0.1) (Figure 5:9 A). Analysis of *SIX3* showed no significant difference by 0.5 $\mu$ M (1.1 $\pm$ 0.0) or 1.0 $\mu$ M Purmorphamine treatment (0.7 $\pm$ 0.2) compared to control (1.0 $\pm$ 0.2) ( $F_{2,6}=1.8$ ,  $p=n.s.$ ) Activin treatment resulted in a comparable expression level (1.0 $\pm$ 0.4) (Figure 5:9 B). *OTX2* showed no significant difference between untreated control (1.0 $\pm$ 0.2) and 0.5 $\mu$ M treated (0.9 $\pm$ 0.1) or 1.0 $\mu$ M Purmorphamine treated (1.6 $\pm$ 0.7) cultures ( $F_{2,6}=0.1$ ,  $p=n.s.$ ). Activin (0.2 $\pm$ 0.0) treatment seemed to have decreased the expression level (Figure 5:9 C). Analysis of *FOXA2* showed induction only in 1.0 $\mu$ M Purmorphamine treated cultures (31.2 $\pm$ 11.1), compared with untreated control (1.0 $\pm$ 0.3) or 0.5 $\mu$ M treated (0.9 $\pm$ 0.5) (Figure 5:9.D). No statistical analysis was performed as in both control and Purmorphamine 0.5 $\mu$ M treatment, no transcript was detected and the automatically assigned value was used for the fold change calculation. No transcript was detected in Activin treatment.

34D6 differentiation- Analysis of *FOXG1* showed no significant difference in the expression levels by 0.3 $\mu$ M (0.8 $\pm$ 0.3) or 1.0 $\mu$ M Purmorphamine treatment (1.2 $\pm$ 0.5) compared to control (1.0 $\pm$ 0.5) ( $F_{2,6}=0.1$ ,  $p=n.s.$ ) (Figure 5:9.E). Analysis of *SIX3* showed no significant difference by 0.3 $\mu$ M (0.6 $\pm$ 0.1) or 1.0 $\mu$ M treatment (0.5 $\pm$ 0.0) compared to control (1.0 $\pm$ 0.2) ( $F_{2,6}=0.7$ ,  $p=n.s.$ ) (Figure 5:9.F). Analysis of *OTX2* showed no significant difference between untreated control (1.0 $\pm$ 0.5) and 0.3 $\mu$ M treated (0.8 $\pm$ 0.3) or 1.0 $\mu$ M treated (0.8 $\pm$ 0.4) cultures ( $F_{2,6}=0.0$ ,  $p=n.s.$ ) (Figure 5:9.G). Analysis of *FOXA2* showed induction only in 1.0 $\mu$ M treated cultures (56.2 $\pm$ 0.0), compared with untreated control (1.0 $\pm$ 0.2) or 0.5 $\mu$ M treated (0.8 $\pm$ 0.2) (Figure 5:9.H). No statistical analysis was performed as in both control and Purmorphamine 0.3 $\mu$ M treatment, no transcript was detected and the automatically assigned value was used for the fold change calculation.

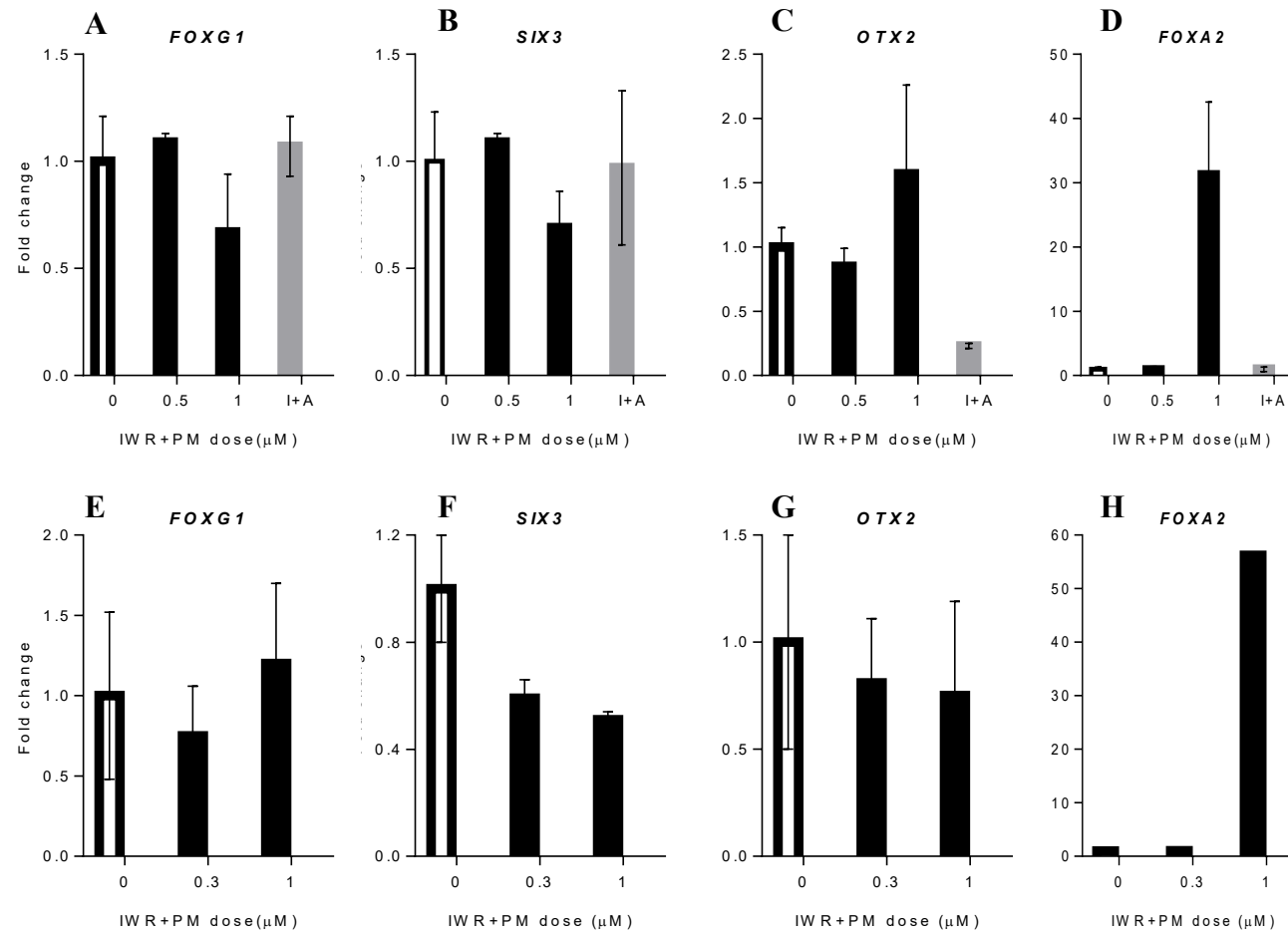


Figure 5:9 Effect of Purmorphamine or Activin treatment on anterior or floor plate markers at D16- Fold change expression of *FOXG1*, *SIX3*, *OTX2* and *FOXA2* in A-D) H9 ESC-derived and E-H) 34D6 iPSC-derived D16 progenitors. Data represented as mean  $\pm$  S.E.M, N=3 except for I+A (IWR1+Activin) N=2. (N= experiment replicates, independent experiments for H9 and experiments set in parallel for 34D6)

#### 5.4.4.3 Analysis of dorsal markers

The expression of *PAX6*, *EMX2*, *TBR2*, *TBR1* and *GLI3* was analysed.

H9 differentiation- *PAX6* expression did not differ by 0.5 $\mu$ M (1.5 $\pm$ 0.3) treatment, but was significantly decreased by 1 $\mu$ M (0.3 $\pm$ 0.0) treatment when compared with control (1.0 $\pm$ 0.1) ( $F_{2,6}=24.8$ ,  $p=0.006$ ). Activin treatment resulted in marked reduction (0.1 $\pm$ 0.0) (Figure 5:10 A). Analysis of *EMX2* showed no significant difference in the expression between control (1.0 $\pm$ 0.2) and 0.5 $\mu$ M (1.1 $\pm$ 0.6) or 1.0 $\mu$ M (0.6 $\pm$ 0.3) treatments ( $F_{2,6}=0.7$ ,  $p=n.s$ ). Activin treatment decreased *EMX2* expression (0.3 $\pm$ 0.2) (Figure 5:10 .B). Analysis of *TBR2* showed no significant difference in the expression levels between control (1.0 $\pm$ 0.6) and 0.5 $\mu$ M (1.2 $\pm$ 0.0) or 1.0 $\mu$ M (0.5 $\pm$ 0.2) treatments ( $F_{2,6}=0.7$ ,  $p=n.s$ ), whereas Activin treatment effectively decreased its expression (0.0 $\pm$ 0.0) (Figure 5:10.C). *TBR1* expression was not significantly different by 0.5 $\mu$ M treatment (0.4 $\pm$ 0.1) but significantly decreased by 1 $\mu$ M (0.2 $\pm$ 0.1) treatment when compared with control (1.0 $\pm$ 0.3) ( $F_{2,6}=4.9$ ,  $p=0.05$ ). *TBR1* expression was found to be decreased by Activin treatment (0.1 $\pm$ 0.1) (Figure 5:10 D). *GLI3* expression was not significantly different by 0.5 $\mu$ M treatment (0.6 $\pm$ 0.2) but significantly decreased by 1 $\mu$ M (0.3 $\pm$ 0.1) treatment when compared with control (1.0 $\pm$ 0.1) ( $F_{2,6}=10.4$ ,  $p=0.01$ ). *GLI3* expression was found to be decreased by Activin treatment (0.3 $\pm$ 0.2) (Figure 5:10.E).

34D6 differentiation- *PAX6* expression did not alter significantly at 0.3 $\mu$ M (0.4 $\pm$ 0.2), but was significantly decreased by 1 $\mu$ M (0.0 $\pm$ 0.0) treatment when compared to control (1.0 $\pm$ 0.4) ( $F_{2,6}=16.1$ ,  $p=0.004$ ) (Figure 5:10.F). Analysis of *EMX2* showed no significant difference in the expression levels between control (1.0 $\pm$ 0.0) and 0.3 $\mu$ M (0.4 $\pm$ 0.2), but a significant decrease at 1.0 $\mu$ M (0.0 $\pm$  0.0) ( $F_{2,6}=10.4$ ,  $p=0.01$ ) (Figure 5:10.G). *TBR2* expression was not significantly different at 0.3 $\mu$ M (0.4 $\pm$ 0.4) or 1.0 $\mu$ M (0.2 $\pm$ 0.2) treatments when compared with control (1.0 $\pm$ 0.3) ( $F_{2,6}=1.8$ ,  $p=n.s$ ). (Figure 5:10.H). *TBR1* expression was significant decreased by 0.3 $\mu$ M (0.1 $\pm$ 0.1) or 1.0 $\mu$ M (0.0 $\pm$ 0.0) treatments compared to control (1.0 $\pm$ 0.3) ( $F_{2,6}=13.0$ ,  $p=0.006$ ) (Figure 5:10.I). *GLI3* expression was no significantly different at 0.3 $\mu$ M (0.4 $\pm$ 0.1) or 1.0 $\mu$ M (0.3 $\pm$ 0.2) treatments compared to control (1.0 $\pm$ 0.3) ( $F_{2,6}=2.8$ ,  $p=n.s$ ) (Figure 5:10.J).

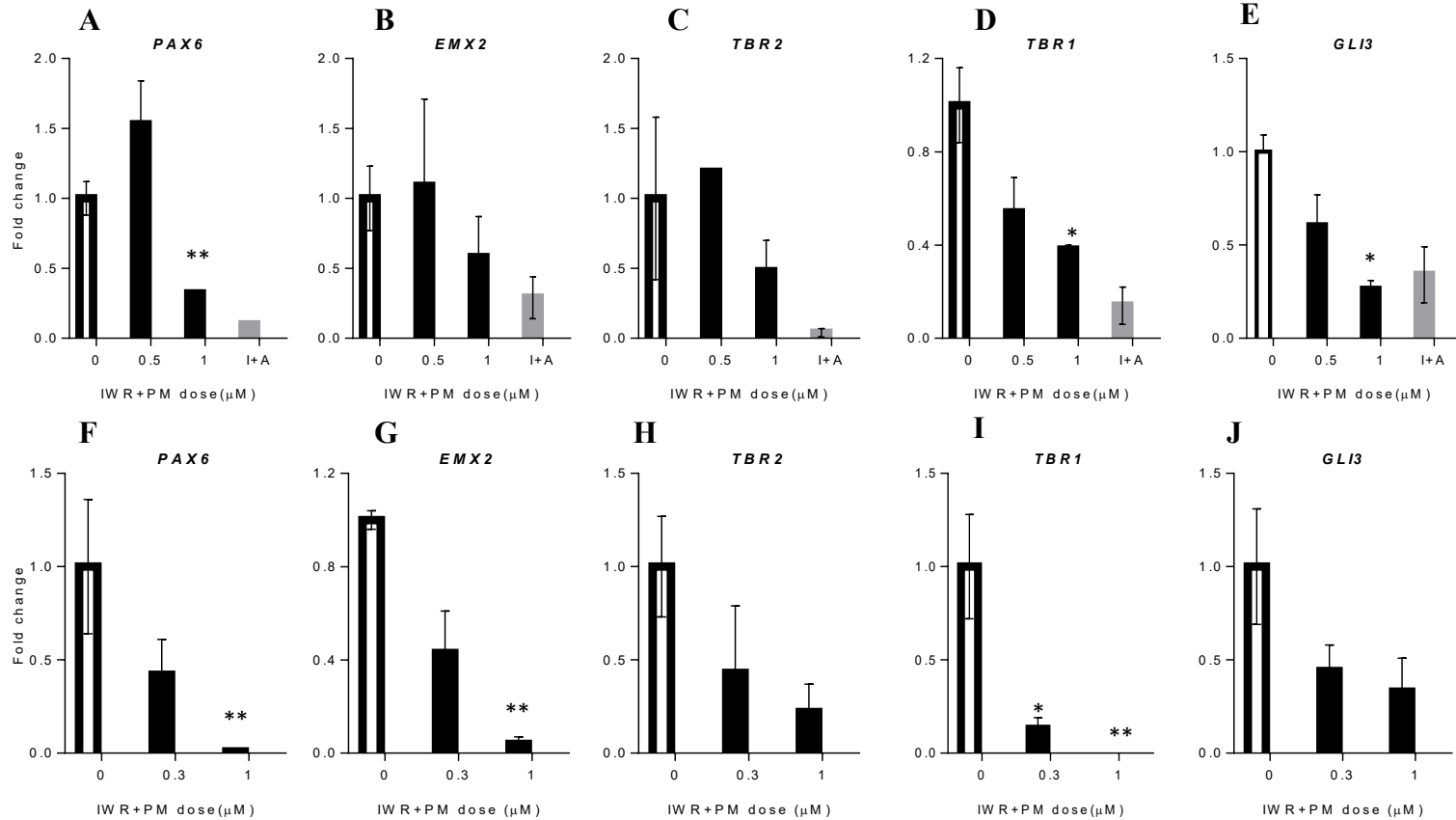


Figure 5:10 Effect of Purmorphamine or Activin treatment on pallial markers at D16- Fold change expression of *PAX6*, *EMX2*, *TBR2*, *TBR1* and *GLI3* in A-E) H9 ESC- derived and F-J) 34D6 iPSC-derived D16 progenitors. Data represented as mean  $\pm$  S.E.M, N=3 except for I+A (IWR1+Activin) N=2. (N= experiment replicates, independent experiments for H9 and experiments set in parallel for 34D6)

#### 5.4.4.4 Analysis of ventral markers

The expression of *GSX2*, *GSX1*, *DLX2*, *DLX1*, *DLX5*, *ASCL1* and *NKX2.1* was analysed.

H9 differentiation- Analysis of *GSX2* showed significant decrease in the expression levels by 1 $\mu$ M (0.1 $\pm$ 0.0) compared to 0.5 $\mu$ M treatment (0.4 $\pm$ 0.1) or control (1.0 $\pm$ 0.2) and there was no significant difference between 0.5 $\mu$ M and control ( $F_{2,6}=27.8$ ,  $p=0.0009$ ). Activin treatment (0.7 $\pm$ 0.2) yielded an expression level comparable to control (Figure 5:11.A). Analysis of *GSX1* showed no significant difference in the expression levels by 0.5 $\mu$ M (1.5 $\pm$ 1.4) or 1 $\mu$ M (1.3 $\pm$ 0.3) treatments compared to control (1.0 $\pm$ 0.3) ( $F_{2,6}=1.0$ ,  $p=n.s$ ). The expression level in Activin was comparable to control (Figure 5:11.B). Analysis of *DLX2* showed significant decrease in the expression levels by 0.5 $\mu$ M (0.2 $\pm$ 0.0) or 1 $\mu$ M treatment (0.1 $\pm$ 0.0) compared to control (1.0 $\pm$ 0.1) ( $F_{2,5}=14.7$ ,  $p=0.005$ ). Activin treatment led to increased expression (3.6 $\pm$ 0.5) (Figure 5:11.C). Analysis of *DLX1* showed no significant difference in the expression levels by 0.5 $\mu$ M (0.5 $\pm$ 0.1) or 1 $\mu$ M treatment (0.4 $\pm$ 0.3) compared to control (1.0 $\pm$ 0.4) ( $F_{2,6}=0.5$ ,  $p=n.s$ ). An increased expression was resulted by Activin treatment (3.9 $\pm$ 0.0) (Figure 5:11.D). Analysis of *DLX5* showed significant decrease in expression by 0.5 $\mu$ M (0.1 $\pm$ 0.1) or 1 $\mu$ M treatment (0.1 $\pm$ 0.0) compared to control (1.0 $\pm$ 0.2) ( $F_{2,5}=8.3$ ,  $p=0.04$ ). Activin treatment seemed to have resulted in an increase (2.1 $\pm$ 0.0) (Figure 5:11.E). Analysis of *ASCL1* showed no significant difference in the expression levels by 0.5 $\mu$ M (0.6 $\pm$ 0.2) or 1 $\mu$ M treatment (1.0 $\pm$ 0.4) compared to control (1.0 $\pm$ 0.5) ( $F_{2,6}=0.4$ ,  $p=n.s$ ), whereas Activin treatment (2.5 $\pm$ 0.1) upregulated the expression (Figure 5:11F).

34D6 differentiation- Analysis of *GSX2* showed no significant difference in the expression levels by 0.3 $\mu$ M (0.6 $\pm$ 0.3) treatment and a lower but not statistically significant decrease by 1 $\mu$ M treatment (0.4 $\pm$ 0.0) compared to control (1.0 $\pm$ 0.5) ( $F_{2,6}=0.4$ ,  $p=n.s$ ) (Figure 5:11.G). Analysis of *GSX1* showed no significant difference in the expression levels by 0.3 $\mu$ M (1.3 $\pm$ 0.3) or 1 $\mu$ M (2.3 $\pm$ 0.8) treatments compared to control (1.0 $\pm$ 0.2) ( $F_{2,6}=1.6$ ,  $p=n.s$ ) (Figure 5:11.H). Analysis of *DLX2* showed no significant difference in the expression levels by 0.3 $\mu$ M (0.4 $\pm$ 0.2) or 1 $\mu$ M treatment (0.6 $\pm$ 0.3) compared to control (1.0 $\pm$ 0.4) ( $F_{2,6}=0.2$ ,  $p=n.s$ ) (Figure 5:11.I). Analysis of *DLX1* showed no significant difference in the expression levels by 0.3 $\mu$ M (0.5 $\pm$ 0.2) or 1 $\mu$ M treatment (0.4 $\pm$ 0.2) compared to control (1.0 $\pm$ 0.5) ( $F_{2,6}=0.5$ ,  $p=n.s$ ) (Figure

5:11J). Analysis of *DLX5* showed no significant difference in expression by 0.3 $\mu$ M (0.4 $\pm$ 0.1) or 1 $\mu$ M treatment (0.4 $\pm$ 0.2) compared to control (1.0 $\pm$ 0.3) ( $F_{2,6}=0.3$ ,  $p=n.s$ ) (Figure 5:11.K). Analysis of *ASCL1* showed no significant difference in the expression levels by 0.3 $\mu$ M (0.8 $\pm$ 0.2) or 1 $\mu$ M treatment (0.9 $\pm$ 0.5) compared to control (1.0 $\pm$ 0.5) ( $F_{2,6}=0.2$ ,  $p=n.s$ ) (Figure 5:11.L).

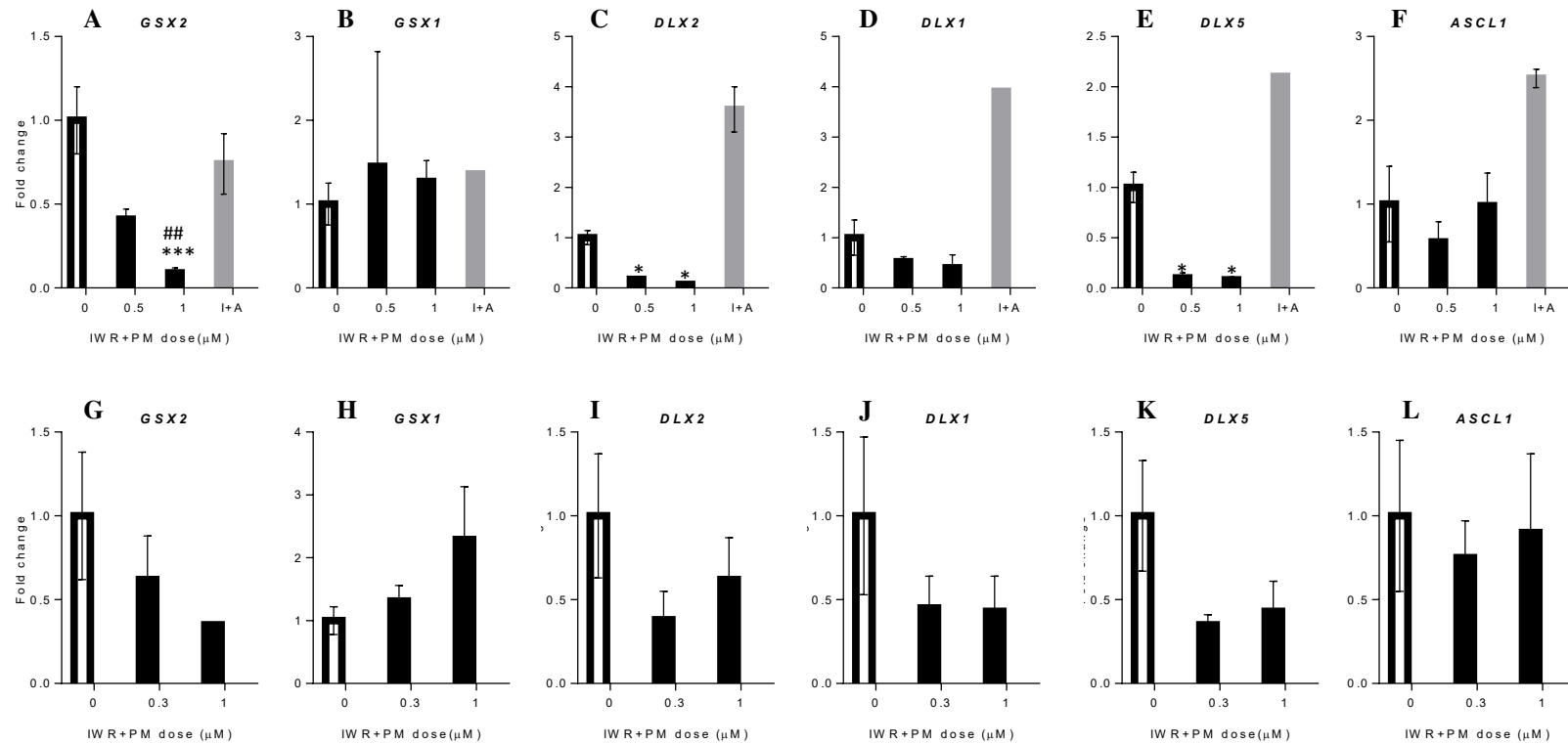


Figure 5:11 Effect of Purmorphamine or Activin treatment on pallial markers at D16- Fold change expression of *GSX2*, *GSX1*, *DLX2*, *DLX1*, *DLX5* and *ASCL1* in A-F) H9 ESC-derived and G-L) 34D6 iPSC-derived D16 progenitors. Data represented as mean  $\pm$  S.E.M, N=3 except for I+A (IWR1+Activin) N=2. (N= experiment replicates, independent experiments for H9 and experiments set in parallel for 34D6)

#### 5.4.4.5 Analysis of LGE markers

The expression of *MEIS2*, *SP8*, *ISLI*, *FOXP1* and *EBF1* was analysed.

H9 differentiation- Analysis of *MEIS2* showed significant decrease in the expression levels by 0.5 $\mu$ M (0.4 $\pm$ 0.1) or 1 $\mu$ M treatment (0.3 $\pm$ 0.0) compared to control (1.0 $\pm$ 0.1) ( $F_{2,6}$ =25.4,  $p$ =0.001). Activin treatment (2.5 $\pm$ 0.8) yielded increased expression level (Figure 5:12.A). Analysis of *SP8* showed no significant difference in the expression levels by 0.5 $\mu$ M (1.1 $\pm$ 0.2) or 1 $\mu$ M (0.7 $\pm$ 0.2) treatment compared to control (1.0 $\pm$ 0.1) ( $F_{2,6}$ =1.2,  $p$ =n.s). A decrease in the expression was seen by Activin treatment (0.3 $\pm$ 0.1) (Figure 5:12.B). Similar to *MEIS2* expression, analysis of *ISLI* showed a significant decrease in the expression level by 0.5 $\mu$ M (0.1 $\pm$ 0.0) or 1 $\mu$ M treatment (0.1 $\pm$ 0.0) compared with control (1.0 $\pm$ 0.4) ( $F_{2,4}$ =23.6,  $p$ =0.006). Activin treatment (3.6 $\pm$ 1.3) resulted in increased expression (Figure 5:12.C). Analysis of *FOXP1* showed no significant difference in the expression levels by 0.5 $\mu$ M (1.0 $\pm$ 0.1) or 1 $\mu$ M treatment (0.8 $\pm$ 0.1) compared to control (1.0 $\pm$ 0.3) ( $F_{2,6}$ =1.4,  $p$ =n.s). An increased expression level was seen in Activin treatment (2.2 $\pm$ 0.3) (Figure 5:12.D). Analysis of *EBF1* showed no significant difference in the expression levels by 0.5 $\mu$ M (0.9 $\pm$ 0.6) or 1 $\mu$ M treatment (0.8 $\pm$ 0.5) compared to control (1.0 $\pm$ 0.3) ( $F_{2,6}$ =0.9,  $p$ =n.s). Activin treatment (15.2 $\pm$ 6.8) led to increased expression (Figure 5:12.E).

34D6 differentiation- Analysis of *MEIS2* showed low, but not statistically significant difference in the expression level by 0.3 $\mu$ M (0.5 $\pm$ 0.1) or 1 $\mu$ M treatment (0.3 $\pm$ 0.1) compared to control (1.0 $\pm$ 0.1) ( $F_{2,6}$ =0.7,  $p$ =n.s) (Figure 5:12.F). Analysis of *SP8* showed no significant difference in the expression levels by 0.3 $\mu$ M (0.5 $\pm$ 0.1) or 1 $\mu$ M (0.7 $\pm$ 0.4) treatment compared to control (1.0 $\pm$ 0.2) ( $F_{2,6}$ =1.2,  $p$ =n.s) (Figure 5:12.G). Analysis of *ISLI* showed no significant difference in the expression levels 0.3 $\mu$ M (0.4 $\pm$ 0.1) or 1 $\mu$ M treatment (0.5 $\pm$ 0.1) compared to control (1.0 $\pm$ 0.2) ( $F_{2,6}$ =0.4,  $p$ =n.s) (Figure 5:12H). Analysis of *FOXP1* showed no significant difference in the expression levels by 0.3 $\mu$ M (0.8 $\pm$ 0.2) or 1 $\mu$ M treatment (0.5 $\pm$ 0.0) compared to control (1.0 $\pm$ 0.0) ( $F_{2,6}$ =0.4,  $p$ =n.s) (Figure 5:12I). Analysis of *EBF1* showed a low but not statistically significant expression by 0.3 $\mu$ M (0.2 $\pm$ 0.1) treatment and significantly lower expression by 1 $\mu$ M treatment (0.1 $\pm$ 0.0) compared with control (1.0 $\pm$ 0.5) ( $F_{2,6}$ =7.2,  $p$ =0.03) (Figure 5:12.J).

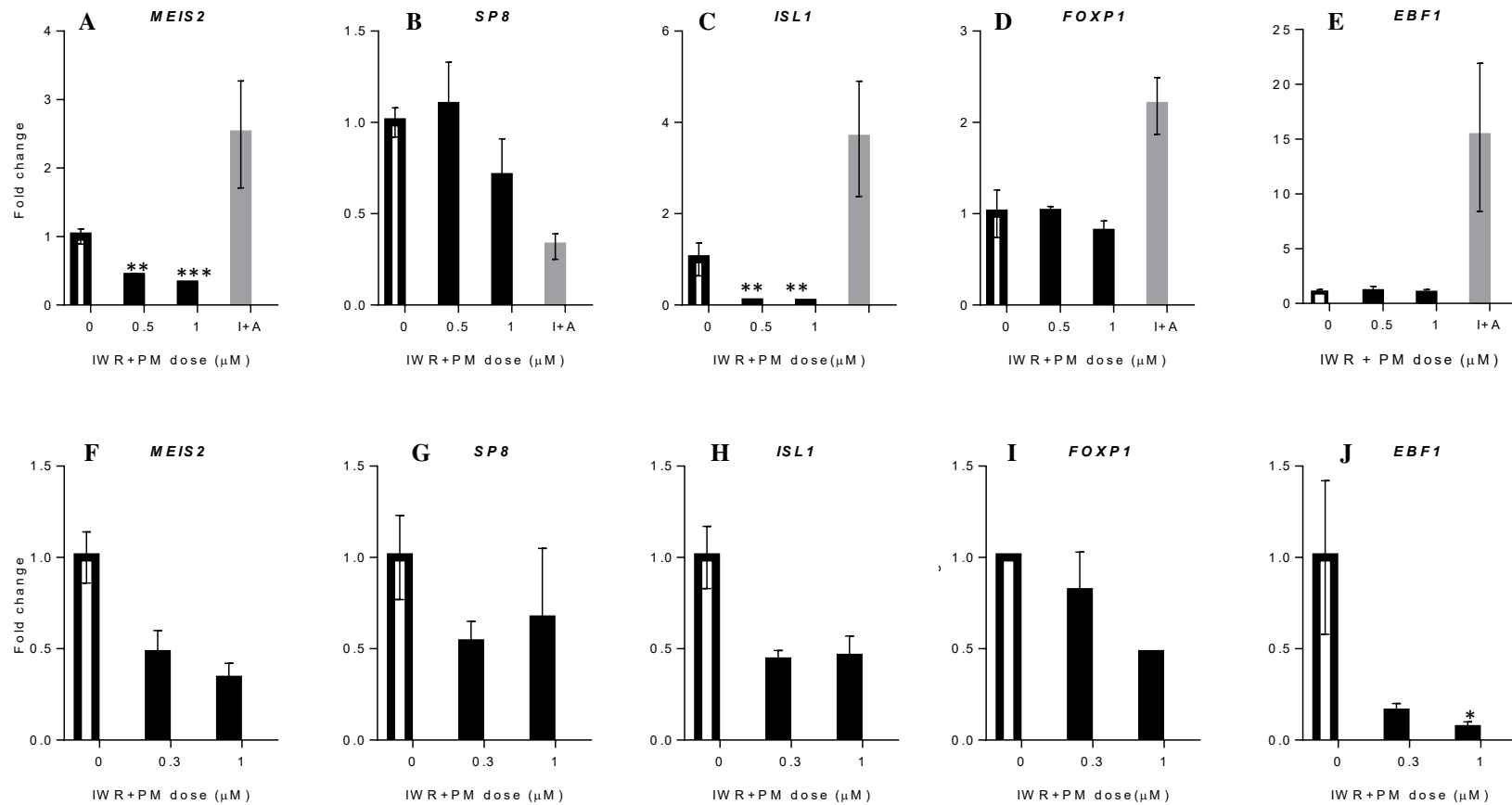


Figure 5:12 Effect of Purmorphamine or Activin treatment on pallial markers at D16- Fold change expression of *MESI2*, *SP8*, *ISL1*, *FOXP1* and *EBF1* in A-E) H9 ESC- derived and F-J) 34D6 iPSC-derived D16 progenitors. Data represented as mean  $\pm$  S.E.M, N=3 except for I+A (IWR1+Activin) N=2. (N= experiment replicates, independent experiments for H9 and experiments set in parallel for 34D6)

#### 5.4.4.6 Analysis of striatal neuronal markers

The expression of *NOLZI*, *GPR6*, *TAC1*, *NPY* and *SST* notably upregulated by Activin treatment is shown here. Purmorphamine treatment and control yielded either very low level or no detectable transcripts. Hence only H9 data is shown here (Figure 5:13). No statistical analysis was performed.

Analysis of *NOLZI* showed a comparable level expression by 0.5 $\mu$ M (1.8 $\pm$ 1.2) or 1 $\mu$ M (3.1 $\pm$ 1.3) Purmorphamine or control (1.0 $\pm$ 0.1) treatment, whereas Activin (30.2 $\pm$ 12.0) treatment showed elevated expression (Figure 5:13.A). There was no detectable level expression of *GPR6* transcript in 0.5 $\mu$ M or 1 $\mu$ M Purmorphamine treatment. Activin (72.9 $\pm$ 11.9) treatment yielded high level expression, when compared with control (1.0 $\pm$ 0.5) (Figure 5:13.B). Analysis of *TAC1* showed a similar level expression by 0.5 $\mu$ M (0.9 $\pm$ 0.0) and reduced expression by 1 $\mu$ M (0.2 $\pm$ 0.1) Purmorphamine treatment when compared with control (1.0 $\pm$ 0.4), whereas Activin (76.2 $\pm$ 22.4) treatment yielded higher expression (Figure 5:13.C). There was no detectable level expression of *NPY* transcript in 0.5 $\mu$ M or 1 $\mu$ M Purmorphamine treatment and Activin treatment (456.1 $\pm$ 141.9) induced higher level expression, when compared with control (1.0 $\pm$ 0.1) (Figure 5:13 D). Analysis of *SST* showed increased expression by 0.5 $\mu$ M (5.5 $\pm$ 0.1) or 1 $\mu$ M (5.1 $\pm$ 0.4) Purmorphamine treatment when compared with control (1.0 $\pm$ 0.2). Activin (56.3 $\pm$ 17.9) treatment showed higher expression (Figure 5:13.E).

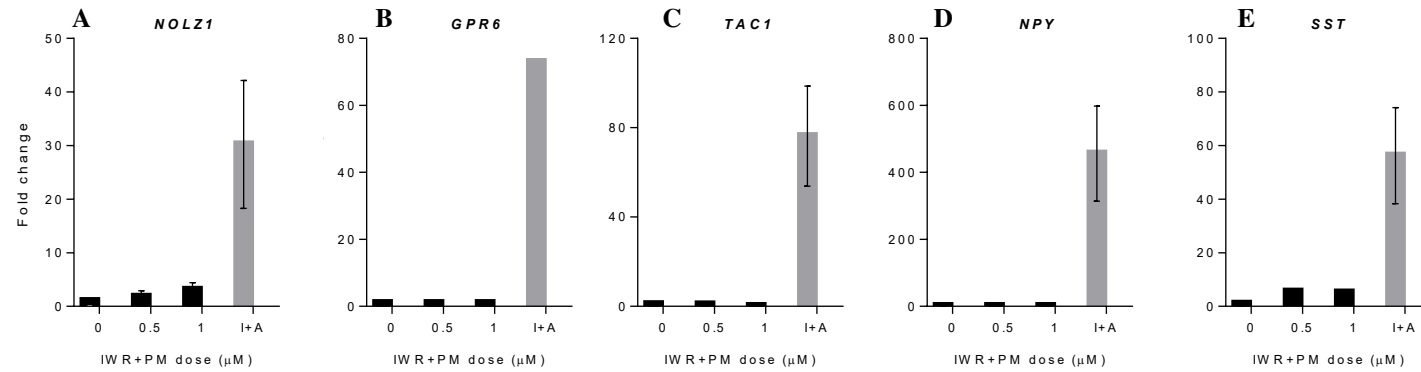


Figure 5:13 Effect of Purmorphamine or Activin treatment on pallial markers at D16- Fold change expression of A)*NOLZ1*, B)*GPR6*, C)*TAC1*, D)*NPY* and E)*SST* in H9 ESC-derived D16 progenitors. Data represented as mean  $\pm$  S.E.M, N=3 except for I+A (IWR1+Activin) N=2. (N= experiment replicates, independent experiments for H9

#### 5.4.4.7 Analysis of MGE markers

The expression of *GLI*, *NKX2.1*, *NKX6.2* and *LHX6* was analysed.

H9 differentiation- Analysis of *GLII* showed significant increase in the expression levels by 0.5 $\mu$ M (35.6 $\pm$ 12.2) or 1 $\mu$ M treatment (111.3 $\pm$ 12.9) compared to control (1.0 $\pm$ 0.3) ( $F_{2,6}$ =31.8,  $p$ =0.006). An increased expression was seen by Activin treatment (22.7 $\pm$ 8.3) (Figure 5:14 A). Analysis of *NKX6.2* showed significant increase in the expression levels by 0.5 $\mu$ M (9.0 $\pm$ 2.7) and 1 $\mu$ M treatment (12.8 $\pm$ 0.2) compared to control (1.0 $\pm$ 0.5) ( $F_{2,6}$ =15.7,  $p$ =0.007) (Figure 5:14 B). Activin treatment (17.1 $\pm$ 0.0) also led to increased expression level. Out of the 3 replicates analysed, 2 sets of Purmorphamine treatments did not generate any signals for *LHX6*. Data for the remaining experiment was plotted. There was an upregulation of *LHX6* by 0.5 $\mu$ M (4.7 $\pm$ 0.0) and 1 $\mu$ M (3.1 $\pm$ 0.0) treatment, compared with control (1.0 $\pm$ 0.1) (Figure 5:14 C). Analysis of *NKX2.1* showed significant increase in expression by 1 $\mu$ M treatment (30.8 $\pm$ 6.8) compared to control (1.0 $\pm$ 0.8) and there was no significant difference between 0.5 $\mu$ M treatment (0.7 $\pm$ 0.4) and control ( $F_{2,6}$ =6.2,  $p$ =0.03). Activin treatment (5.6 $\pm$ 3.3) caused an increase in the expression (Figure 5:14.D).

34D6 differentiation- Analysis of *GLII* showed increased, but not statistically different expression by 0.3 $\mu$ M (1.9 $\pm$ 0.2) or 1 $\mu$ M treatment (5.2 $\pm$ 2.2) compared to control (1.0 $\pm$ 0.4) ( $F_{2,6}$ =1.2,  $p$ =n.s) (Figure 5:14.E). Analysis of *NKX6.2* showed comparable expression between control (1.0 $\pm$ 0.2) and by 0.3 $\mu$ M (0.5 $\pm$ 0.4) and an increased but not statistically significant different expression by 1 $\mu$ M treatment (2.2 $\pm$ 0.2) ( $F_{2,6}$ =2.1,  $p$ =n.s) (Figure 5:14.F). Analysis of *LHX6* showed significant increase in the expression by 0.3 $\mu$ M (11.0 $\pm$ 1.5) or 1 $\mu$ M treatment (7.8 $\pm$ 0.7) compared to control (1.0 $\pm$ 0.2) ( $F_{2,6}$ =8.8,  $p$ =0.02) (Figure 5:14G). Analysis of *NKX2.1* showed significant increase in expression by 1 $\mu$ M treatment (8.0 $\pm$ 0.7) compared to control (1.0 $\pm$ 0.5) and there was no significant difference between 0.3 $\mu$ M treatment (2.4 $\pm$ 1.1) and control ( $F_{2,6}$ =4.7,  $p$ =0.05) (Figure 5:14.H).

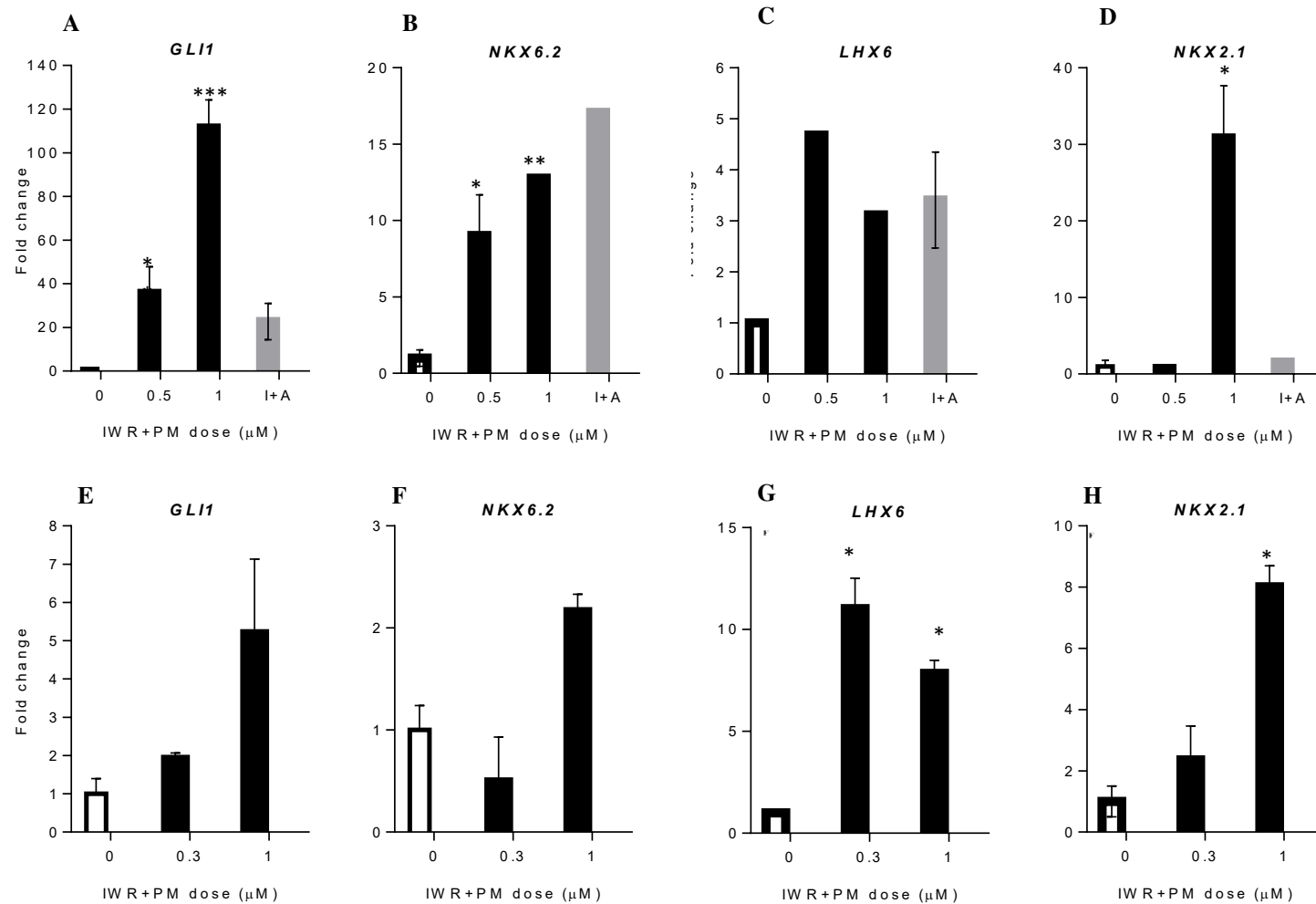


Figure 5:14 Effect of Purmorphamine or Activin treatment on pallial markers at D16- Fold change expression of *GLI1*, *NKX6.2*, *LHX6* and *NKX2.1* in A-D) H9 ESC- derived and E-H) 34D6 iPSC-derived D16 progenitors. Data represented as mean  $\pm$  S.E.M, N=3 except for I+A (IWR+PM dose in  $\mu$ M) (N= experiment replicates, independent experiments for H9 and experiments set in parallel for 34D6). Graph C-shown for N=1

#### 5.4.4.8 Analysis of neuronal/glial markers

The expression of *TUBB3*, *MAP2*, *DCX* and *OLIG2* was analysed. One way ANOVA and Dunnett's multiple comparison test was performed to determine the statistical significance.

H9 differentiation- Analysis of *TUBB3* showed no significant difference in the expression levels by 0.5 $\mu$ M (0.7 $\pm$ 0.2) or 1 $\mu$ M treatment (0.5 $\pm$ 0.0) compared to control (1.0 $\pm$ 0.2) ( $F_{2,6}=3.5$ ,  $p=n.s$ ). Activin treatment resulted in an increase in the expression (2.5 $\pm$ 0.3) (Figure 5:15.A). Analysis of *MAP2* showed no significant difference in the expression levels by 0.5 $\mu$ M (0.5 $\pm$ 0.1) or 1 $\mu$ M (0.5 $\pm$ 0.1) treatment or control (1.0 $\pm$ 0.2) ( $F_{2,6}=3.0$ ,  $p=n.s$ ). Activin treatment did not greatly alter the expression level (1.8 $\pm$ 0.8) (Figure 5:15.B). Analysis of *DCX* showed no significant difference in the expression levels by 0.5 $\mu$ M (0.8 $\pm$ 0.3) or 1 $\mu$ M (1.3 $\pm$ 0.6) treatment or control (1.0 $\pm$ 0.2) ( $F_{2,6}=0.3$ ,  $p=0.001$ ). Activin treatment resulted in an increased expression (3.3 $\pm$ 0.3) (Figure 5:15.C). Analysis of *OLIG2* showed no significant difference in the expression by 0.5 $\mu$ M (2.7 $\pm$ 1.4), but resulted in a significant increase by 1 $\mu$ M (7.7 $\pm$ 3.5) treatment, when compared with control (1.0 $\pm$ 0.0) ( $F_{2,5}=5.6$ ,  $p=0.05$ ). An increased expression was seen in Activin treated culture (4.4 $\pm$ 1.4) (Figure 5:15.D).

34D6 differentiation- Analysis of *TUBB3* showed no significant difference in the expression levels by 0.3 $\mu$ M (0.8 $\pm$ 0.1) or 1 $\mu$ M treatment (0.7 $\pm$ 0.0) compared to control (1.0 $\pm$ 0.2) ( $F_{2,6}=0.3$ ,  $p=n.s$ ) (Figure 5:15.E). Analysis of *MAP2* showed no significant difference in the expression levels by 0.3 $\mu$ M (0.9 $\pm$ 0.3) or 1 $\mu$ M (0.6 $\pm$ 0.1) treatment compared to control (1.0 $\pm$ 0.3) ( $F_{2,6}=0.1$ ,  $p=n.s$ ) (Figure 5:15.F). Analysis of *DCX* showed no significant difference in the expression levels by 0.3 $\mu$ M (1.2 $\pm$ 0.5) or 1 $\mu$ M (1.2 $\pm$ 0.5) treatment or control (1.0 $\pm$ 0.2) ( $F_{2,6}=0.28$ ,  $p=n.s$ ) (Figure 5:15.G). Analysis of *OLIG2* showed an increase in the expression by 1 $\mu$ M (4.7 $\pm$ 0.8) compared to 0.3 $\mu$ M (2.2 $\pm$ 0.2) or control (1.0 $\pm$ 0.4) ( $F_{2,5}=5.6$ ,  $p=0.05$ ) (Figure 5:15.H).

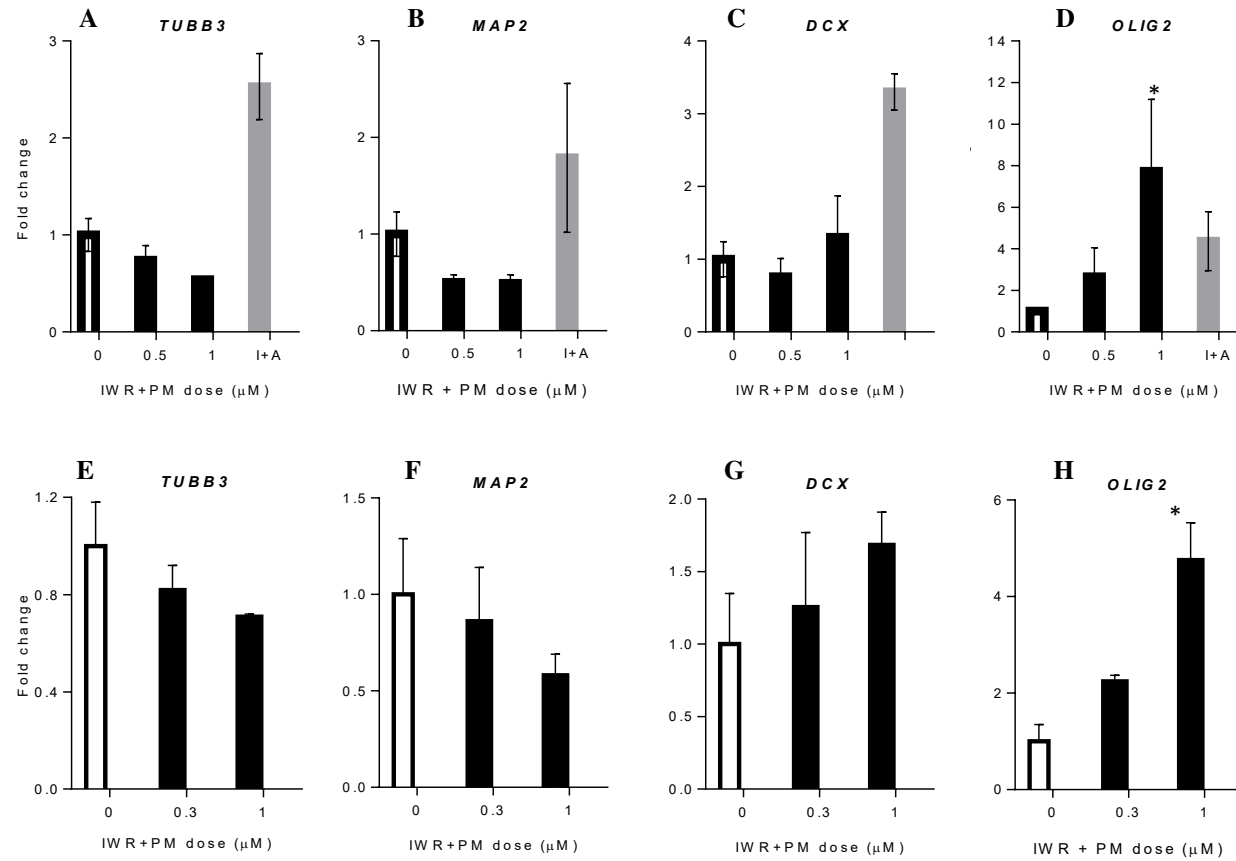


Figure 5:15 Effect of Purmorphamine or Activin treatment on neuronal and glial markers at D16- Fold change expression of *TUBB3*, *MAP2*, *DCX* and *OLIG2* in A-D) H9 ESC-derived and E-H) 34D6 iPSC-derived D16 progenitors. Data represented as mean  $\pm$  S.E.M, N=3 except for I+A (IWR-1+Activin) N=2. (N= experiment replicates, independent staggered experiments for H9 and experiments set in parallel for 34D6)

## 5.5 Discussion

The effect of SHH signalling and Activin signalling on ventral telencephalon fate specification of hPSCs was studied in this chapter. During monolayer dual-SMADi+ WNT inhibition (SB431542+ LDN193189+IWR1) 16 days differentiation protocol, SHH agonists or Activin treatment was started at D8. Initially, known SHH agonists Purmorphamine and SAG were employed during H9 differentiation to analyse their effect on the activation of SHH pathway transcriptional targets *PATCHED1* and *GLI1*. Both Purmorphamine and SAG demonstrated a dose-dependent effect. Following this, the differentiation was characterized in detail. Activin at 20ng/ml was employed in parallel from D8 to D16 to analyse its effect on neural patterning. The culture conditions in terms of integration of developmental pathways differed from Cambrey *et al.* (2012) and Arber *et al.* (2015) in that in this study, Activin was employed in combination with both BMP and WNT inhibition.

### 5.5.1 Effect of SHH agonists or activin on dorsal and ventral markers

The main result of this study was that under the culture conditions used and the time point analysed, high SHH pathway activation partially inhibited pan-ventral and some LGE markers but potentially induced MGE interneuron transcripts, whereas, Activin signalling appeared to specifically enhance LGE markers and striatal transcripts. Furthermore, both SHH signalling and activin signalling downregulated dorsal transcripts (Note- Preliminary data on Activin treatment from 2 experiments was shown. Experiments were not replicated again and hence the statistical significance was not determined. Also, note that mRNA expression was analysed in H9 ESC line and the protein expression was analysed in 34D6 iPSC line).

The role of SHH signalling in ventral telencephalon patterning via repression of *GLI3R* is well established (Rallu *et al.* 2002; Corbin *et al.* 2003; Li *et al.* 2009). In agreement with this, supplementation of recombinant SHH alone or in combination with WNT inhibitor has been reported to induce LGE or MGE identity at the expense of dorsal fate during mESC and hPSC differentiation (Aubry *et al.* 2008; Danjo *et al.* 2011; Ma *et al.* 2012; Li *et al.* 2009; 1.Delli Carri *et al.* 2013; Nicoleau *et al.* 2013). In these studies, SHH dose-dependently upregulated ventral markers *GSX2*, *DLX2*, *ASCL1*, *MES12* and *NKX2.1* and downregulated dorsal

markers *PAX6*, *EMX2*, *EMX1* and *TBR2*. A similar patterning was also achieved by Purmorphamine treatment at 0.65 $\mu$ M (Ma *et al.* 2012). The preliminary data (N=2) on the effect of SHH pathway activation during H9 differentiation in my study was surprising. Both Purmorphamine and SAG dose-dependently down-regulated pan-ventral markers *GSX2*, *DLX2*, *DLX5*. There was a dose-dependent upregulation of *NKX2.1*, in line with other studies. Only the high dose of Purmorphamine at 1 $\mu$ M induced *NKX2.1*. Protein level characterization of Purmorphamine dose-response by immunocytochemistry for *PAX6*, *NKX2.1* and *GSX2* on H9 (N=1) and 34D6 lines (N=2) showed some differences. *PAX6*<sup>low</sup>/*GSX2*<sup>+</sup>/*NKX2.1*<sup>+</sup> cell fate in both lines indicated acquisition of ventral identity by the highest dose of Purmorphamine. Down regulation of *GSX2* expression indicated a partial inhibition rather than a complete blockade of expression by high SHH activation. High-throughput QRT-PCR analysis of H9 and 34D6 samples (N=3 for both) showed significant reduction of *PAX6*, *TBR1* and *GLI3* in H9s and *PAX6*, *TBR1* and *EMX2* in 34D6s by 1 $\mu$ M Purmorphamine. Despite the different level of statistical significance obtained in the two cell lines, this observation was in line with the reports on negative regulation of dorsal markers by recombinant SHH during hPSC differentiation (Aubry *et al.* 2008; Danjo *et al.* 2011; Ma *et al.* 2012; Li *et al.* 2009; Delli Carri *et al.* 2013; Nicoleau *et al.* 2013). Analysis of pan-ventral markers confirmed H9 preliminary QRT-PCR and immunocytochemistry data and demonstrated significant downregulation of *GSX2*, *DLX2*, *DLX1* and *DLX5* by 1 $\mu$ M treatment. At 0.5 $\mu$ M, there was reduction of *DLX2* and *DLX5*. 34D6 differentiation although not statistically significant showed a similar trend as in H9, as seen by the low transcript levels in Purmorphamine treatment groups compared to control. This might suggest an inhibition of these transcripts by Purmorphamine. It might also be possible that activation of SHH signalling during D8-D16 temporal window, did not modulate the expression of these genes. This observation contrasted the above mentioned studies where supplementation of recombinant SHH was found to enhance ventral markers at the expense of dorsal markers (Aubry *et al.* 2008; Danjo *et al.* 2011; Ma *et al.* 2012; Li *et al.* 2009; Delli Carri *et al.* 2013; Nicoleau *et al.* 2013). The significant down regulation of LGE markers *MEIS2* and *ISL1* by 0.5  $\mu$ M and 1 $\mu$ M Purmorphamine treatment in H9s and the reduced but not statistically significant expression of these transcripts in 34D6s suggested inhibition of LGE identity. The concomitant upregulation of MGE makers *GLI*, *NKX2.1*, *NKX6.2*, *LHX6* and *OLIG2* in both cell

lines indicated that SHH pathway activation during D8-D16 temporal window in this study, enhanced MGE fate. A similar effect of SHH pathway activation on inhibition of LGE fate and induction of MGE fate has been reported in mESC differentiation (Danjo *et al.* 2011). In their study, early Shh treatment at 10nM from D3 enhanced Gsx2 but continued Shh treatment from D9 with higher concentration of 30nM Shh or 100nM SAG inhibited Gsx2, LGE/striatal markers Nolz1, Ctip2 and induced Nkx2.1 and Lhx6 (Danjo *et al.* 2011). The control treatment in my study highly induced GSX2 (as well as other ventral markers as seen in the previous chapter and as reported in Straccia *et al.* (2015)). At this context of ventral patterning and regional specification, high SHH activation by Purmorphamine at 0.5-1 $\mu$ M may have enhanced the ventral most, ie, MGE fate specification. During hPSC differentiation, (using combined and temporal integration of dual-SMADi+ WNT inhibition) SAG addition (from D0) was found to induce MGE derived interneurons (Kim *et al.* 2014). SAG at 10nM and 100nM induced similar level ISL1 and at 100nM highly induced NKX2.1 indicating that high SHH activation induced MGE fate at the expense of LGE fate.

One plausible explanation for inhibition of LGE character, comes from the role played by NKX2.1 and SHH signalling in interneuron specification (Xu *et al.* 2010). Nkx2.1 which is induced by SHH act in a temporal manner. Nkx2.1 first induced around E9.5 in the mouse was required for MGE formation; *Nkx2.1* null mutants showed severely reduced MGE (Sussel *et al.* 1999; Corbin *et al.* 2003). Shh via Gli3 repression established initial D/V patterning between E9-E12.5 (Rallu *et al.* 2002; Chiang *et al.* 1996; Fuccillo *et al.* 2004) and maintained Nkx2.1 expression by Gli-3 independent mechanism until E14 into neurogenesis (Xu *et al.* 2005; Gulacsi and Anderson 2006). Retroviral mediated activation of Shh at E8.5-E10.5 resulted in induction of Nkx2.1 in LGE and Gsx2 and Dlx2 throughout neocortex (Rallu *et al.* 2002). From E9.5-12.5 Nkx2.1 was required for mainly MGE fate specification and for repressing LGE/CGE identity. Loss of *Nkx2.1* in conditional knock outs at E9.5-10.5 showed MGE conversion to LGE and at E12.5 showed conversion to CGE (Sussel *et al.* 1999; Butt *et al.* 2008). In support of this, *Nkx2.1* was found to positively regulate MGE cortical interneuron markers *Lhx6*, *Lhx7* and *Shh* and repress LGE and CGE markers (Elias *et al.* 2008). Shh signalling confers cortical interneuron identity in ventral progenitors (Xu *et al.* 2005; Xu *et al.* 2010). The cortical interneurons predominantly arise from MGE and CGE. Nkx2.1<sup>+</sup> and Nkx6.2<sup>+</sup> MGE progenitors

give rise to Somatostatin (SS) or Parvalbumin (PV) positive early interneurons, which contribute to about 65% of total cortical interneurons and Gsx2<sup>+</sup> CGE progenitors give to Calretinin positive bipolar late interneurons (Xu *et al.* 2010). During interneuron specification, down regulation of SHH signalling was found to convert some MGE progenitors into CGE fate whereas, high concentration of SHH signalling prevented this re-specification of MGE progenitors by repressing Gsx2 and maintaining Nkx2.1, which function to specify PV and SS fate (Xu *et al.* 2010). FGF signalling has also been implicated in this process. During interneuron specification of mESCs and hPSCs, high SHH activation along with supplementation of FGF8 significantly enhanced MGE fate at the expense of CGE fate whereas supplementation of FGF15/19 enhanced CGE fate (Danjo *et al.* 2011; Kim *et al.* 2014). In mice development, repression of Gsx2 do not affect Nkx2.1 mediated MGE induction and specification. Gsx2 functions to establish LGE/CGE identity by positively regulating genes such as *Dlx1* *Dlx2* and *Ascl1* while repressing of dorsal fate via cross-repression of Pax6 (Szucsik *et al.* 1997; Corbin *et al.* 2000; Yun *et al.* 2001). *Gsx2*<sup>-/-</sup> mutants and *Gsx2;Dlx1/2* compound mutants showed aberrant LGE/CGE development, while MGE was preserved including the expression of *Nkx2.1*, *Nkx6.2*, *Olig2* and *Lhx6* (Sussel *et al.* 1999; Long *et al.* 2009; Wang *et al.* 2013). The control culture conditions of this study, yielded ventral or an intermediate telencephalic like progenitors as shown in the previous chapter. Under this condition, high SHH activation by Purmorphamine is likely to have favoured MGE neurogenesis and partially repressed LGE/CGE identity. The expression of markers such as DLX2, DLX5, MEIS2, FOXP1, ISL1, NKX6.2 and LHX6 is to be determined at the protein level to quantify the LGE vs MGE fate acquired by these D16 progenitors. (In the next chapter, terminal differentiation of these progenitors was carried out and was analysed for striatal phenotype). It is also to be determined whether pushing SHH activation temporal window forward and including low concentration of Purmorphamine would influence LGE vs MGE fate specification.

The preliminary data on Activin treatment in H9 showed downregulation of dorsal markers *PAX6*, *EMX2*, *TBR2* and *TBR1* and upregulation of ventral markers *DLX2*, *DLX1*, *DLX5* and *ASCL1*. This was in line with the observations in Cambray *et al.* (2012) and Arber *et al.*(2015). The increased expression of LGE specific transcripts- *MEIS2*, *ISL1*, *FOXP1* and *EBF1*- and striatal markers-*NOLZI*, *GPR6*, *TAC1*, *NPY* and *SST*- suggested that Activin treatment induced LGE progenitors

maturation towards striatal phenotype. Interestingly, Activin treatment also appeared to have increased MGE interneuron markers *GLI1*, *NKX6.2* and *LHX6*. This was in contrast to what was reported in Cambray *et al.* (2012) and Arber *et al.* (2015), where Activin treatment via *GLI3* inhibited SHH signalling and in turn inhibited *GLI1*, *NKX2.1* and *LHX6*. The discrepancy can be attributed to culture conditions and remnant endogenous SHH signalling, however, until further experimental repeats are carried out, no conclusion can be drawn. Also, the expression of these markers at the protein level is to be determined. Analysis of PAX6, NKX2.1, GSX2 and CTIP in 34D6 D16 progenitors showed negligible amount of PAX6 and NKX2.1. The cultures contained ~32% GSX2<sup>+</sup> and ~54% CTIP2<sup>+</sup> cells. The proportion of GSX2<sup>+</sup> cells were lower compared to IWR1 treatment (~60%) and there was no co-localization of these markers. Mutually exclusive expression of GSX2 and CTIP2 has been reported in human foetal striatal samples (Onorati *et al.* 2014). Thus the preliminary data in both H9 and 34D6 showed that Activin treatment induced LGE/striatal fate in agreement with previous studies.

### 5.5.2 Effect of SHH agonists or Activin on neuroectodermal, anterior and neuronal markers

Purmorphamine doses or Activin treatment did not alter anterior markers *FOXG1*, *SIX3* and *OTX2*, indicating that D8 addition in this study did not influence telencephalon induction. Early addition of SHH has been reported to repress *FOXG1* and induced floor plate maker *FOXA2* (Fasano *et al.* 2010). Interestingly, *DKK1* inhibited *FOXA2* and induced *FOXG1* (Fasano *et al.* 2010). The highest dose of Purmorphamine appeared to have induced *FOXA2*, however, there low levels of transcript ( $\Delta Cq = 7.68$  in H9 and 8.20 in 34D6) compared to high levels of *FOXG1* ( $\Delta Cq = \sim 1$  in both H9 and 34D6). Purmorphamine or Activin treatment did not alter neuroectodermal markers *SOX2*, *SOX1* and *NES*. During hPSC differentiation, exogenous SHH has been shown to promote *NESTIN* expression whereas Activin or cyclopamine inhibited its expression and promoted  $\beta$ -tubulin (Cambray *et al.* 2012). Purmorphamine treatment did not alter the expression of neuronal markers *TUBB3*, *MAP2* and *DCX*. However, Activin treatment appeared to have resulted in upregulation indicating that Activin promoted differentiation of progenitors. This was in agreement with the previous study (Cambray *et al.* 2012).

In summary, at the context of both BMP and WNT pathway inhibition, activation of SHH signalling by Purmorphamine treatment in a dose-dependent manner, appeared to inhibit pan-ventral and LGE markers but enhanced MGE interneuron markers, whereas Activin treatment specifically enhanced LGE/striatal neuronal markers.

## 5.6 Limitations of the methods in the chapter

The QRT-PCR data was as plotted as fold change ie, ratio of normalized gene expression of treatments to control. When comparing the level of expression of different transcripts, the  $\Delta Cq$  values have to be taken into account. Also, this method accounts for the total cell population and needs to be performed in conjunction with immunocytochemistry quantification to obtain the overall level of expression of markers. Protein level analysis could also be performed by flow cytometry, however, could be problematic, as it requires high number of cells and optimization.

## 6 Characterization of *in vitro* neuronal differentiation: Looking for striatal markers

### 6.1 Aim

To analyse the striatal specification of hPSC derived telencephalon progenitors upon terminal differentiation

### 6.2 Background

The significance and quality of small molecule-mediated telencephalon progenitor specification of hPSCs, relies on the strength of this commitment during terminal neuronal differentiation. Various studies have shown that hPSC-derived LGE-like progenitors patterned with DKK1+SHH or SHH alone produced GABAergic DARPP32<sup>+</sup> MSNs upon *in vitro* and *in vivo* neuronal differentiation (Aubry *et al.* 2008; Li *et al.* 2009; Zhang *et al.* 2010; Ma *et al.* 2012; Delli Carri *et al.* 2013; Nicoleau *et al.* 2013). The yield of DARPP-32<sup>+</sup> neurons upon 45-80 days of *in vitro* neuronal differentiation in medium containing BDNF, VPA and cAMP varied between 10-18%. These cultures also contained varied proportions of neuronal markers such as  $\beta$ -tubulin III, MAP2, Synaptophysin and striatal markers such as FOXP1, FOXP2, CTIP2, GABA, GAD67, Calbindin and DRD2 (Aubry *et al.* 2008; Li *et al.* 2009; Zhang *et al.* 2010; Ma *et al.* 2012; Delli Carri *et al.* 2013; Nicoleau *et al.* 2013). Activin patterned progenitors were reported to yield between 20-50% DARPP32 (varied between cell lines) and the cultures contained varied proportions of above mentioned striatal markers (Arber *et al.* 2015). Please refer to Table 1 in chapter 1 for details of the differentiation protocols.

### 6.3 Experimental design

Neural progenitors were generated as described in the previous chapters under five different conditions- L, LI, LIP0.5, LIP1.0 and LIA as shown in Figure 6:1. On D16, the neural progenitors were re-plated onto PDL/matrigel coated coverslip and differentiated for 3 weeks in a defined media developed in our lab (was being formulated at the time of this study and now published Telezhkin *et al.* (2016). The protocol involved sequential use of two media –SCM1 and SCM2, containing BDNF, Ascorbic acid and small molecules to promote neurogenesis, synaptogenesis

and further neuronal maturation. Rapid synchronized neuronal differentiation was achieved in 21 days, by small molecules that mediated the manipulation of signalling pathways, specifically cell cycle exit, inhibition of Notch pathway activation and activation of GABA, CREB and WNT signalling pathway (Telezhkin *et al.* 2016). The transition from neural progenitors to neurons was achieved by promoting the cell cycle exit and inhibiting Notch, by combined use of N-[N-(3,5-Difluorophenacetyl)-L-alanyl]-S-phenylglycine t-butyl ester (DAPT) (a Notch signalling inhibitor targeting  $\gamma$ -secretase, as well as delays G1/S phase) and PD 0332991 (a cyclin dependent kinase 4/6 inhibitor that arrests the cell cycle at G1) (Telezhkin *et al.* 2016). The neuronal maturation was enhanced by inducing and maintaining CREB-phosphorylation and ERK-phosphorylation by addition of BDNF, forskolin (agonist of CREB pathway, adenylate cyclase activator), GABA (300 $\mu$ M) and by raising extracellular  $\text{Ca}^{2+}$  (1.8mM) (Telezhkin *et al.* 2016). GABA receptor stimulation leading to  $\text{Ca}^{2+}$  dependent ERK and CREB phosphorylation regulates neurogenic gene expression. Inclusion of CHIR99021 (presynaptic antagonists of GSK3 $\beta$ ) further enhanced the neuronal excitability (Telezhkin *et al.* 2016).

The original experimental plan included differentiation of both H9 and 34D6 cell lines in parallel. However, H9s was discarded at the progenitor stage due to contamination issues. The 34D6 line was differentiated in N=2, different experiments set in parallel. The D16 progenitors differentiated for 3 weeks in SCM1/2 were analysed by immunocytochemistry for makers of a) striatal phenotype- DARPP32, CTIP2, ISL1, GABA and Calbindin (striatum matrix marker), b) post mitotic neuron- MAP2 and c) Synaptogenesis- Synaptophysin and PSD95. Samples were also collected for analysis by high-throughput QRT-PCR, however the experiments being N=2 needed additional replicates which could not be set up within the timeline. As the interest of the lab was to replicate the protocols in HD-iPSC lines by other members of the research group, these samples remained un-analysed.

Based on the gene expression profile in mouse striatum development, most of the hPSC differentiation studies have reported DARPP32 and DARPP32/CTIP2 co-expression as the definitive markers of MSNs (Aubry *et al.* 2008; Li *et al.* 2009; Zhang *et al.* 2010; Ma *et al.* 2012; 1.Delli Carri *et al.* 2013; Nicoleau *et al.* 2013). Delli Carri *et al.* (2013) and Onorati *et al.* (2014) (which were in manuscript forms at the time of my study and was discussed in the consortium)

reported that at 8-11 weeks of human development, striatal neurons were marked by the co-expression of EBF1, ISL1, FOXP1, FOXP2, CTIP2, DARPP32 and GABA in LGE MZ. At 20 weeks, ISL1 expression was also restricted to a few cells and did not co-express CTIP2, FOXP1 or FOXP2 (Onorati *et al.* 2014). CTIP2<sup>+</sup> cells co-expressed FOXP1, FOXP2 and DARPP-32. At this stage, DARPP32 was also seen in neocortex however co-localization with CTIP2 was rarely seen and lacked GABAergic identity (Onorati *et al.* 2014). Thus in my study, CTIP2/DARPP32 co-localization and GABA expression was analysed for MSN fate commitment. Antibodies against FOXP1, EBF1, NOLZ1, D2 dopamine receptor (DRD2) and Choline acetyl transferase (ChAT) were also tried, however looked non-specific and were excluded. FOXP1 antibody gave inconsistent staining. The other antibodies gave either no signals or intense background staining and needed further optimization.

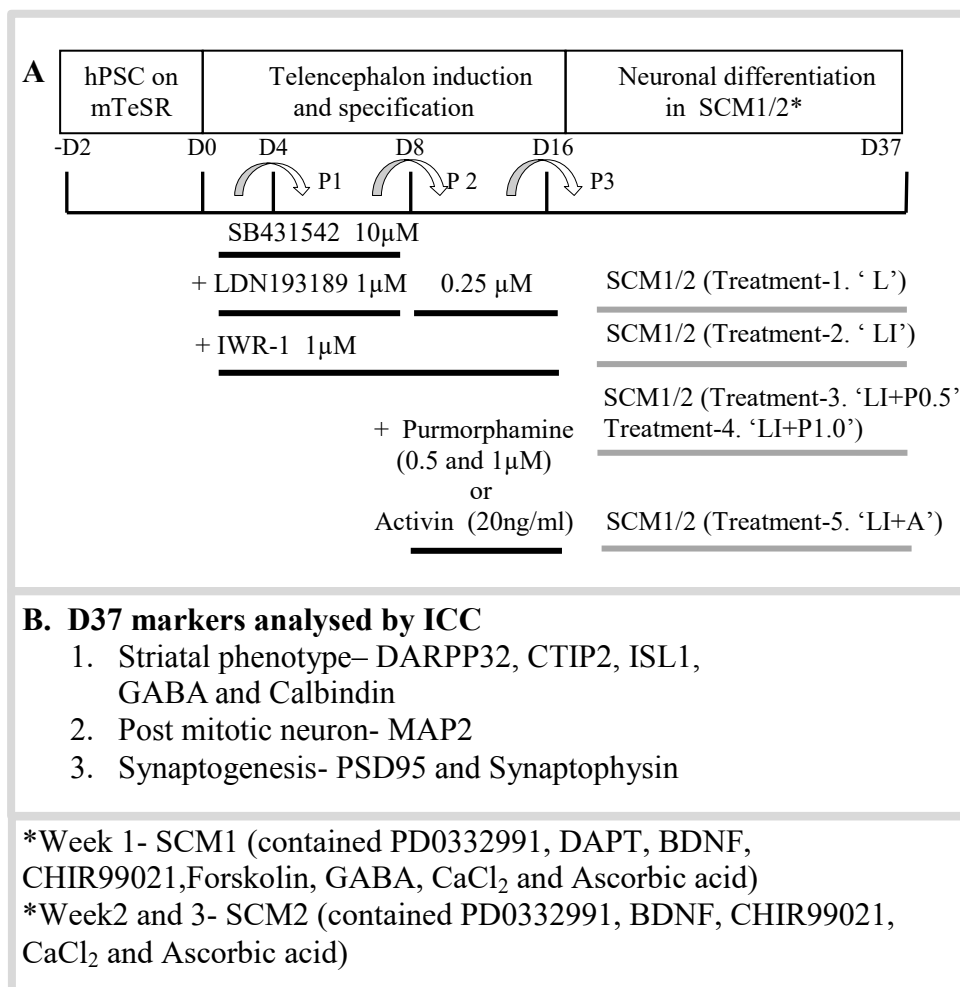


Figure 6:1 A) Cell culture regime. Neural progenitors were generated on matrigel coated plates under the 5 conditions till D16- Treatment 1- L: dual-SMADi, Treatment 2- LI: dual-SMADi+ IWR1, Treatment 3 and 4 -LI+P0.5 or P1.0: dual-SMADi+ IWR1+ Purmorphamine 0.5 or 1 $\mu$ M and Treatment 5- LIA; dual-SMADi+ IWR1+ Activin. Cultures were re-plated at 1:2 ratios on D4 and again on D8 and maintained until D16. On D16, cultures were re-plated at 50K cells onto PDL/matrigel coated coverslips in SCM1/2 media (refer materials and methods for detailed recipe) and differentiated for 3 weeks, ie, till D37. B) On D37, cultures were fixed and analysed for markers of striatum, neurons and synaptogenesis

## 6.4 Results

### 6.4.1 Analysis of striatal differentiation

Striatal neuronal differentiation was analysed by measuring the expression of DARPP32, CTIP2, ISL1, GABA and Calbindin and post mitotic neuronal marker MAP2.

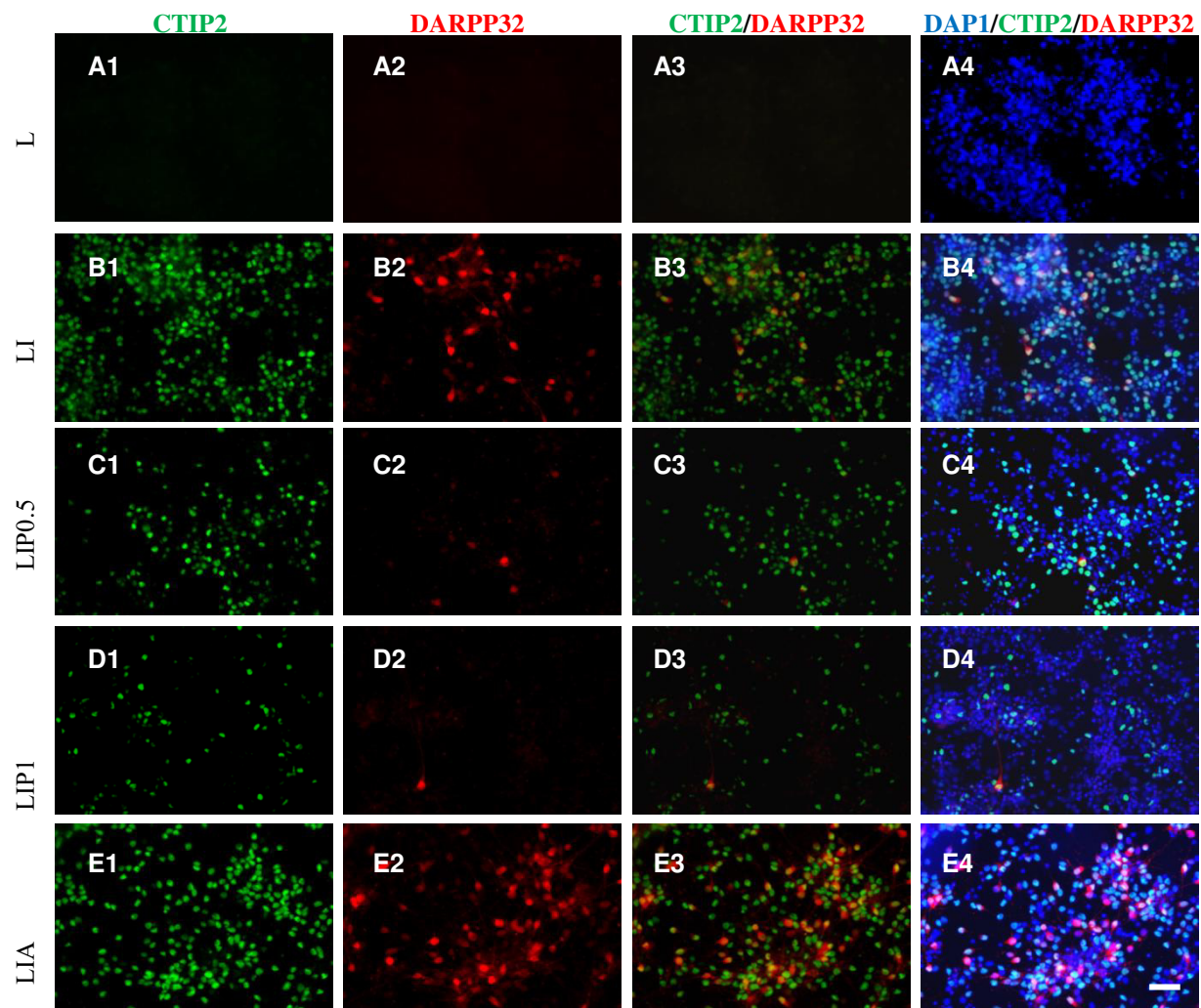
Double immunostaining for DARPP32 and CTIP2 showed their co-localised expression. DARPP32 was localized to cell bodies and CTIP2 was

localized to nucleus (Figure 6:2). There was no expression in 'L' treated cultures. LI treated progenitors generated  $59.6 \pm 4.7\%$  CTIP2 and  $16.3 \pm 0.4\%$  DARPP32. LIP0.5 treated progenitors had lower proportions of both CTIP2<sup>+</sup> ( $31.0 \pm 2.1\%$ ) and DARPP32<sup>+</sup> cells ( $0.6 \pm 0.1\%$ ). Similarly, LIP1.0 treated progenitors generated low proportion of both CTIP2<sup>+</sup> ( $23.4 \pm 0.8\%$ ) and DARPP32<sup>+</sup> cells ( $0.4 \pm 0.0\%$ ). LIA treated progenitors gave  $60.2 \pm 0.4\%$  CTIP2<sup>+</sup> and  $29.7 \pm 0.6\%$  DARPP32<sup>+</sup>. Both LI and LIA treated cultures showed co-localization expression of CTIP2 and DARPP32 in majority of the cells. However, in some DARPP32<sup>+</sup> cells, the intensity of CTIP2 staining was found to be reduced (Figure 6:3)

Double immunostaining of ISL1 and MAP2 showed their co-expression. ISL1 was localized to the nucleus and MAP2 was localized to the soma and axons (Figure 6:4) Under SCM1/2 conditions, the majority of cells, >92% were MAP2<sup>+</sup>, regardless of their different patterning conditions. The proportion of ISL1<sup>+</sup> cells in L, LI, LIP0.5, and LIP1.0 treated cultures was found to be  $7.2 \pm 0.9\%$ ,  $85.1 \pm 0.9\%$ ,  $85.00 \pm 2.4\%$  and  $88.7 \pm 1.6\%$  respectively. The intensity of ISL1 staining was found to be lower in some of the cells in LIA group and it yielded  $60.0 \pm 2.5\%$  ISL1<sup>+</sup> cells.

Calbindin expression was localized to cell bodies and axons (Figure 6:5). The proportion of Calbindin<sup>+</sup> cells in treatment group L, LI, LIP1 and LIA treated cultures was found to be  $4.2 \pm 1.6\%$ ,  $10.8 \pm 1.4\%$ ,  $6.1 \pm 0.6\%$  and  $3.6 \pm 0.2\%$ , respectively.

GABA expression was localized to cell bodies and axons (Figure 6:6). Two fields- field 1 and field 2 per treatment shown for LI, LIP and LIA represented low and high cell density areas of the coverslips, respectively. Quantification of the staining was difficult due to the filamentous nature of staining in high cell density fields.



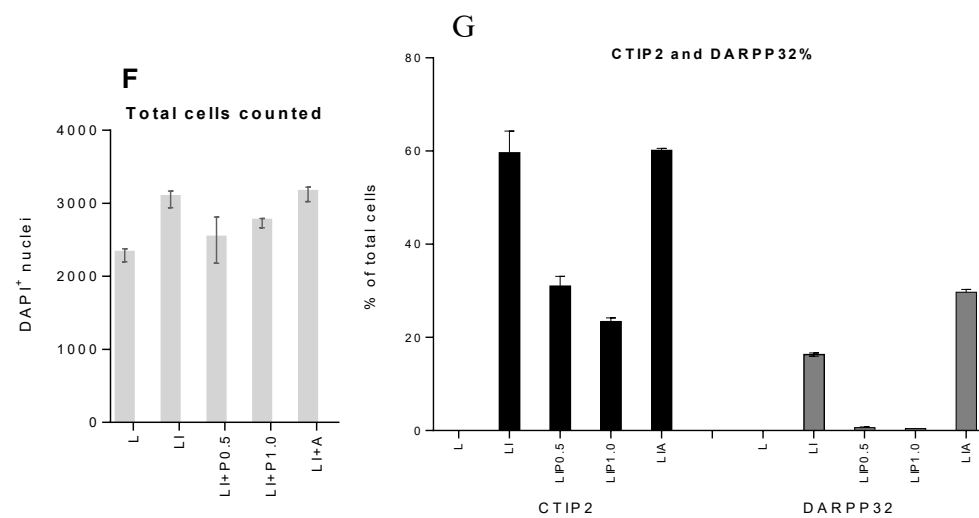


Figure 6:2 Fluorescent immunocytochemistry analysis of CTIP2 and DARPP32 on 34D6-iPSC derived neurons on D37. D16 progenitors generated under different conditions-L, LI, LIP0.5, LIP1 and LIA were differentiated in SCM1/2 for 3 weeks on PDL/matrigel coated coverslips. On D37, cells were double-immunostained for CTIP2 (green), DARPP32 (red) and counter stained for DAPI nuclear stain (blue). Representative images are given- A1-E1) CTIP2 stained cells, A2-E2) DARPP32 stained cells, A3-E3) CTIP2/DARPP32 merge and A4-E3) DAPI/CTIP2/DARPP32 merge. Scale bar for all images in bottom right image= 100 $\mu$ m. Graphs represent F) the total amount of DAPI-positive nuclei counted for each treatment and G) proportion of CTIP2 and DARPP32 positive cells as % of DAPI nuclei. Data represented as mean, N=2, experiments set in parallel

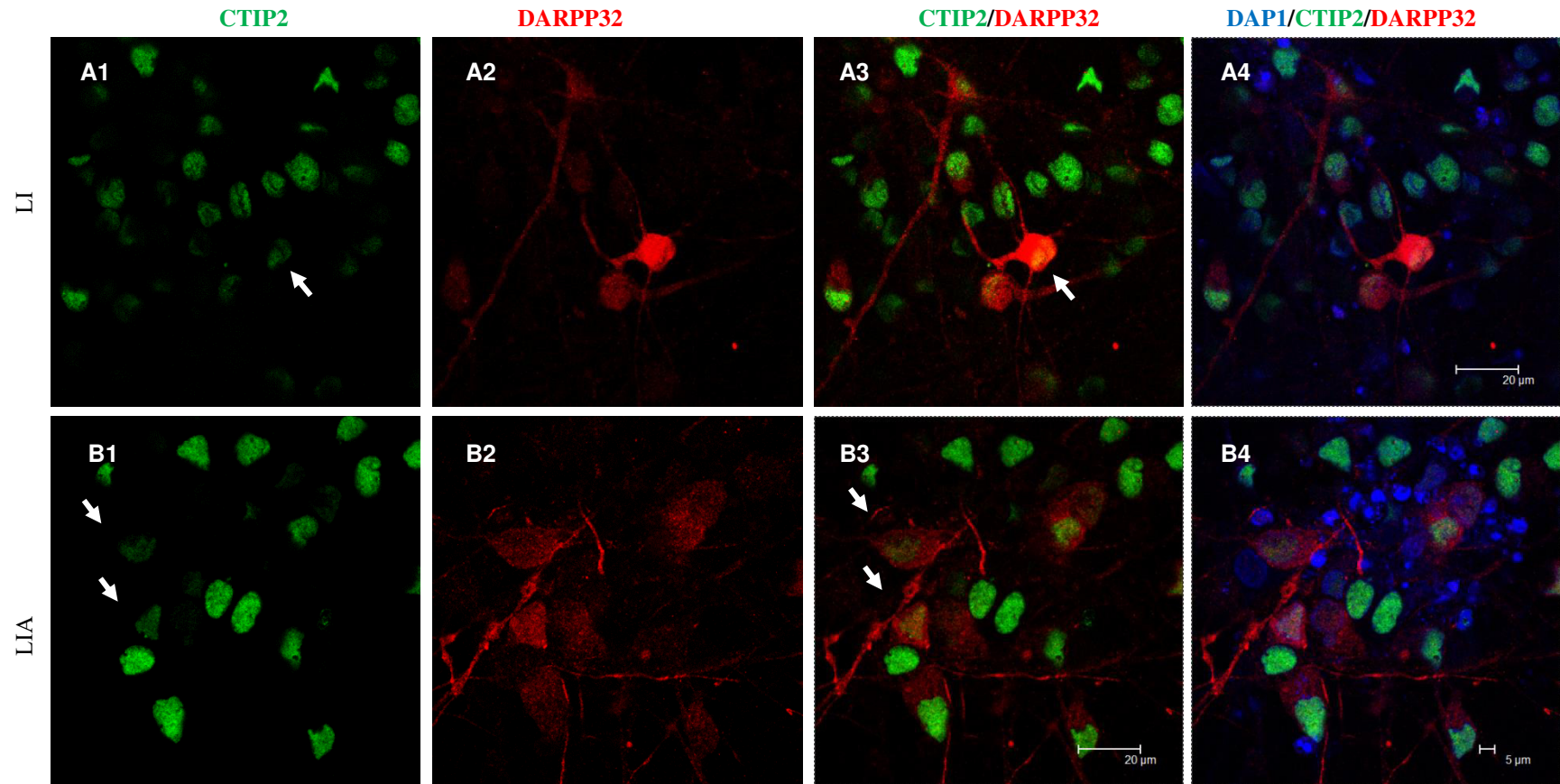
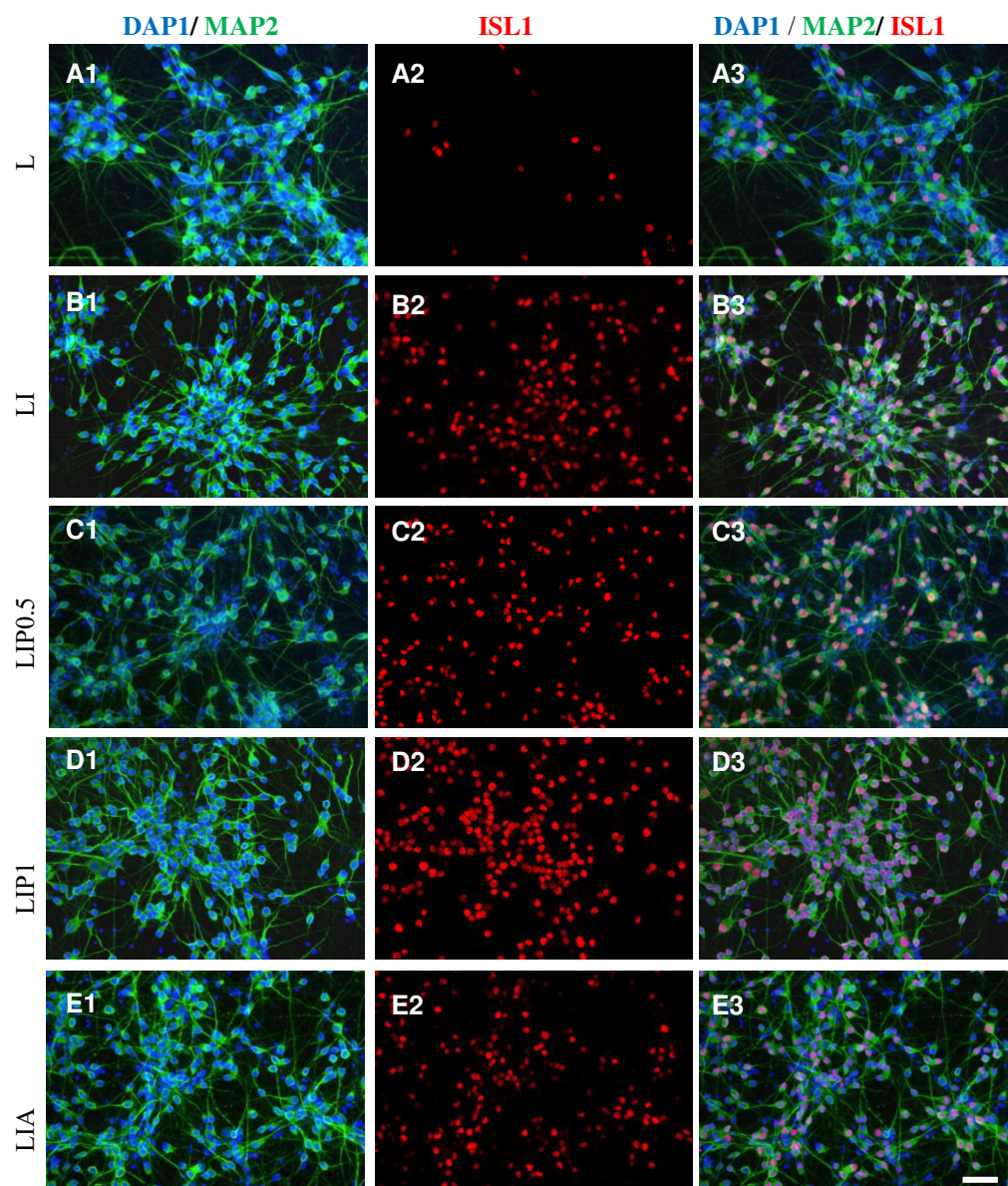


Figure 6:3 Confocal images of fluorescent immunostaining showing weaker CTIP2 expression in some DARPP32 positive neurons. D16 progenitors patterned under conditions- LI and LIA were differentiated in SCM1/2 for 3 weeks on PDL/matrigel coated coverslips. On D37, cells were double-immunostained for CTIP2 (green), DARPP32 (red) and counter stained for DAPI nuclear stain (blue). Representative images are given- A1-B1) CTIP2 stained cells, A2-B2) DARPP32 stained cells, A3-B3) DARPP32/CTIP2 merge and A4-B4) DAPI/DARPP32/CTIP2. White arrows point to weaker CTIP2 expression



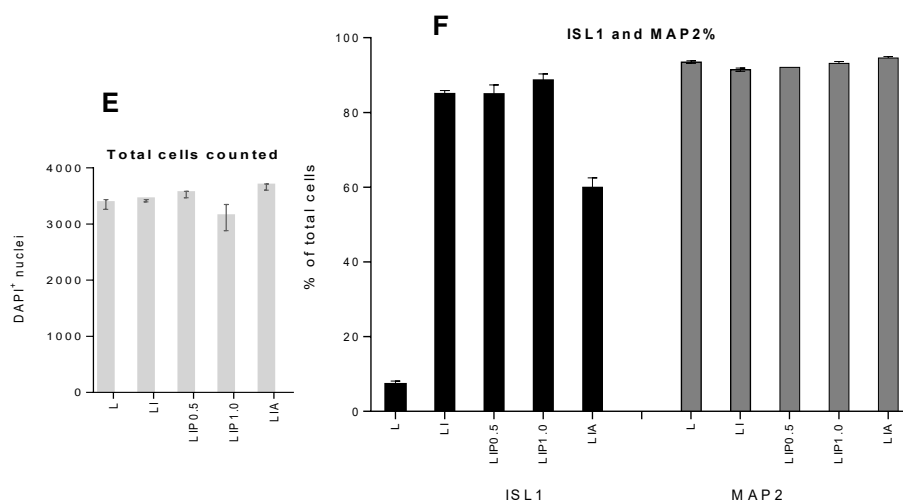


Figure 6:4 Fluorescent immunocytochemistry analysis of MAP2 and ISL1 on 34D6-iPSC derived neurons on D37. D16 progenitors generated under different conditions-L, LI, LIP0.5, LIP1 and LIA were differentiated in SCM1/2 for 3 weeks on PDL/matrigel coated coverslips. On D37, cells were double-immunostained for MAP2 (green), ISL1 (red) and counter stained for DAPI nuclear stain (blue). Representative images are given- A1-E1) DAPI/MAP2 stained cells, A2-E2) ISL1 stained cells and A3-E3) DAPI/MAP2/ISL1 merge. Scale bar for all images in bottom right image= 100 $\mu$ m. Graphs represent F) the total amount of DAPI-positive nuclei counted for each treatment and G) proportion of MAP2 and ISL1 positive cells as % of DAPI nuclei. Data represented as mean, N=2, experiments set in parallel

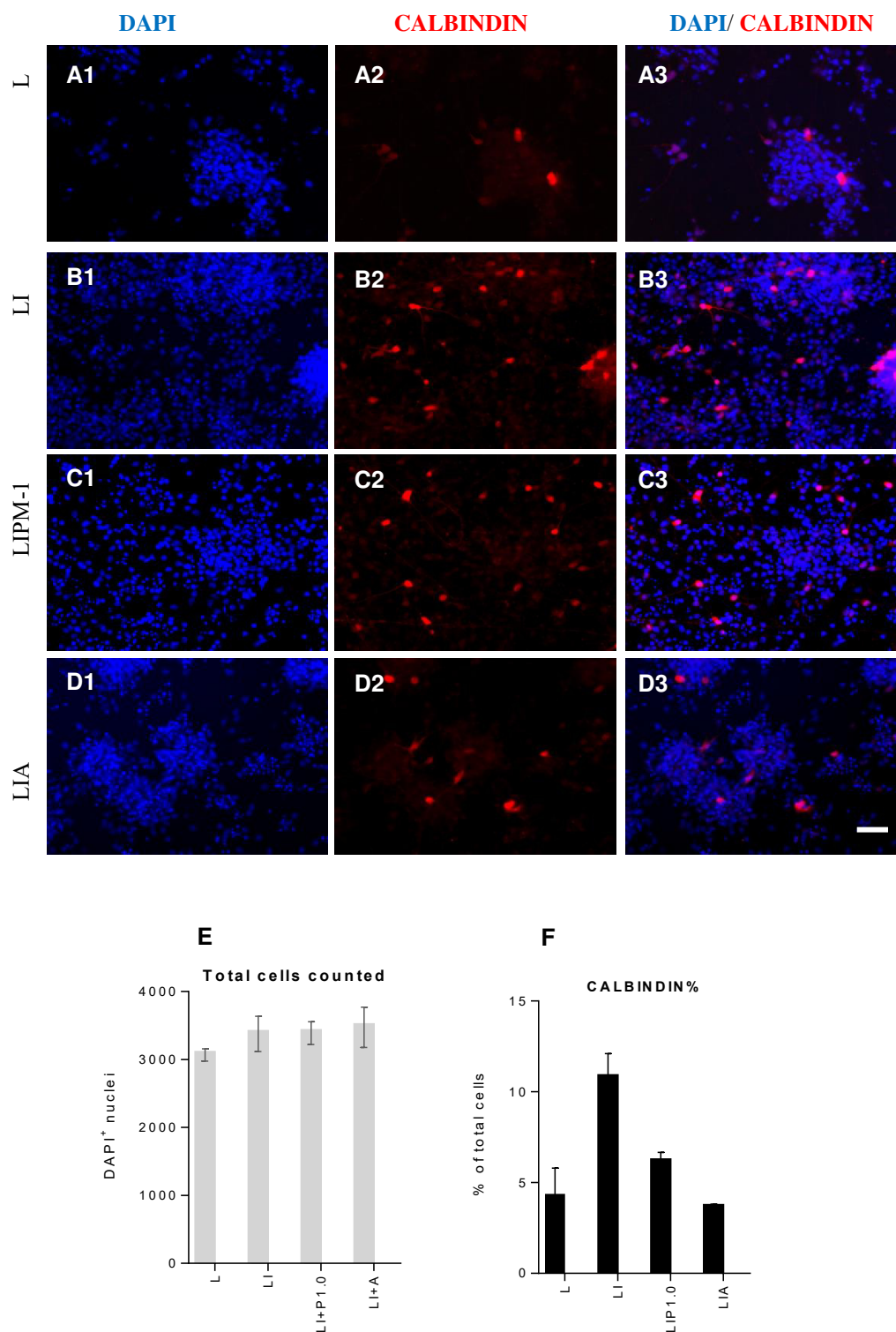


Figure 6:5 Fluorescent immunocytochemistry analysis of Calbindin on 34D6-iPSC derived neurons on D37. D16 progenitors generated under different conditions-L, LI, LIP1 and LIA were differentiated in SCM1/2 for 3 weeks on PDL/matrigel coated coverslips. On D37, cells were immunostained for Calbindin (red) and counter stained for DAPI nuclear stain (blue). Representative images are given- A1-D1) DAPI stained cells, A2-D2) Calbindin stained cells and A3-D3) DAPI/Calbindin merge. Scale bar for all images in bottom right image= 100 $\mu$ m. Graphs represent E) the total amount of DAPI-positive nuclei counted for each treatment and F) proportion of Calbindin positive cells as % of DAPI nuclei. Data represented as mean, N=2, experiments set in parallel.

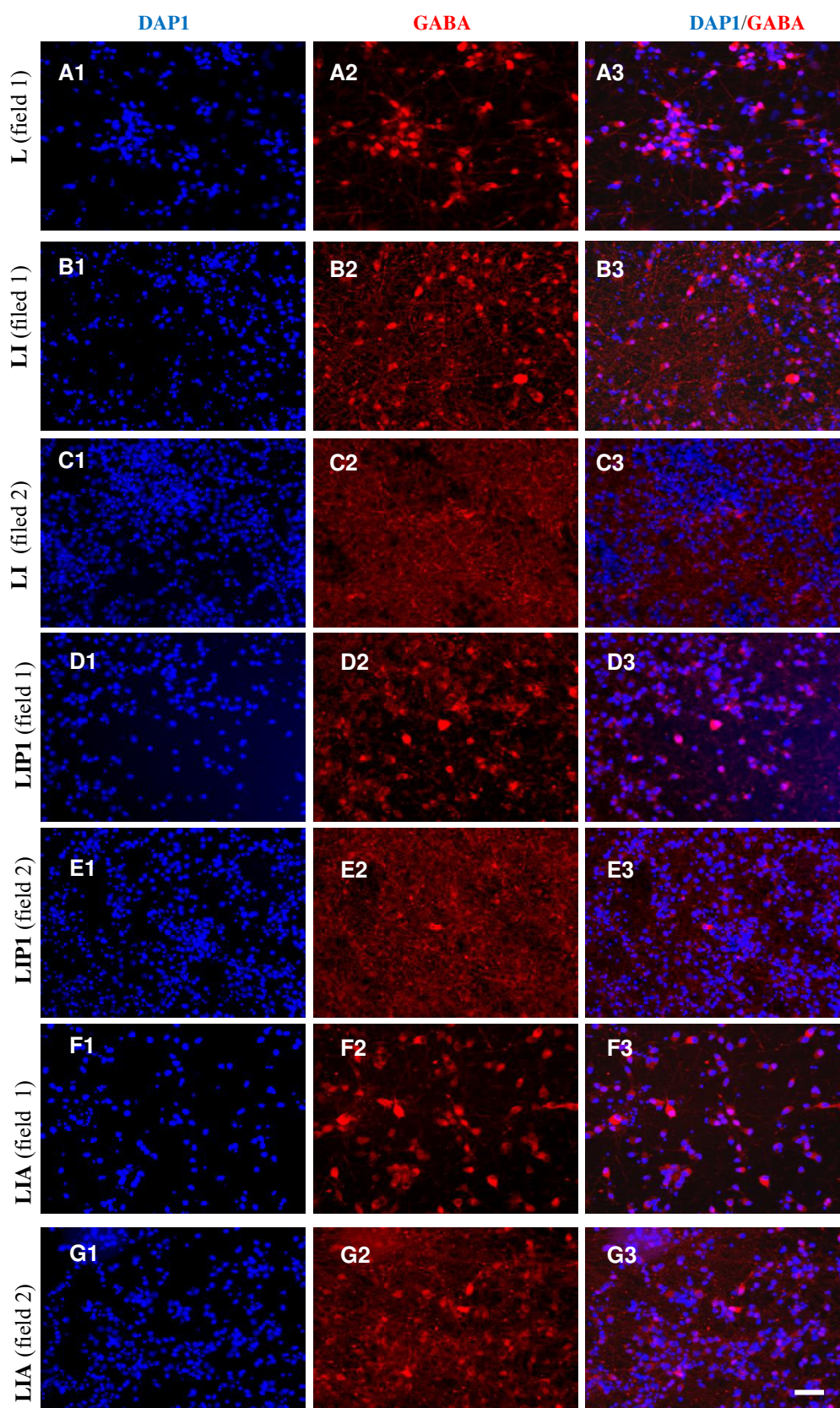


Figure 6:6 Fluorescent immunocytochemistry analysis of GABA on 34D6-iPSC derived neurons on D37. D16 progenitors generated under different conditions-L, LI, LIP1 and LIA were differentiated in SCM1/2 for 3 weeks on PDL/matrigel coated coverslips. On D37, cells were immunostained for GABA (red) and counter stained for DAPI nuclear stain (blue). Representative images are given- A1-G1) DAPI stained cells, A2-G2) GABA stained cells and A3-G3) DAPI/GABA merge. Scale bar for all images in

bottom right image= 100 $\mu$ m. Filed 1 represents low cell density areas and field 2 represents high cell density areas

### 6.4.2 Analysis of pre and post synaptic markers

Synaptogenesis was analysed by double immunostaining for the pre-synaptic marker Synaptophysin and post-synaptic marker PSD95. Synaptophysin was localized to axons and PSD95 was localized to cell bodies and axons (Figure 6:7). Under SCM1/2 conditions, all the treatment groups expressed both markers and there was also their co-registration indicative of pre and post synaptic terminals. This was further confirmed by confocal microscopy (Figure 6:8).

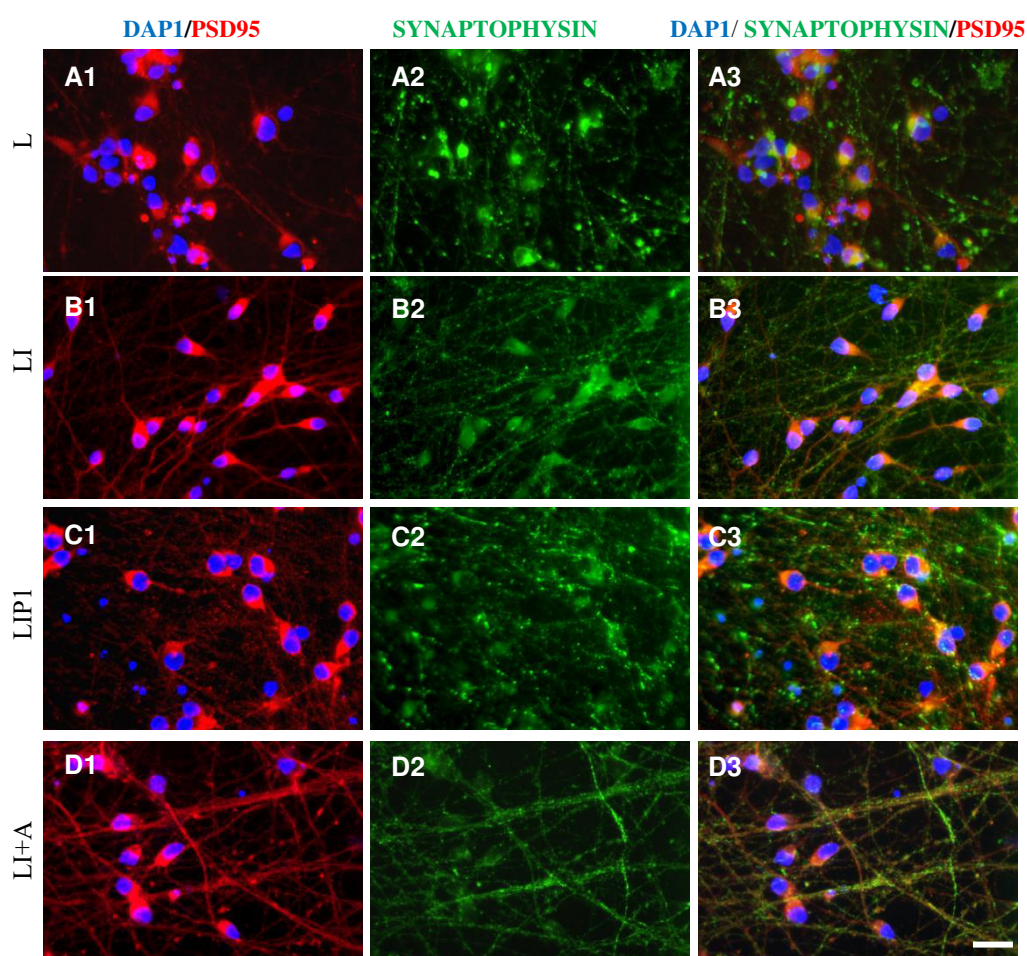


Figure 6:7 Fluorescent immunocytochemistry analysis of Synaptophysin and PSD65 on 34D6-iPSC derived neurons on D37. D16 progenitors generated under different conditions were differentiated in SCM1/2 for 3 weeks on PDL/matrigel coated coverslips. On D37, cells were double-immunostained for PSD95 (red), Synaptophysin (green) and counter stained for DAPI nuclear stain (blue). Representative images are given- A1-D1) DAPI/PSD95stained cells, A2-D2) Synaptophysin stained cells and A3-D3) DAPI/ Synaptophysin/PSD95merge. Scale bar for all images in bottom right image= 50 $\mu$ m.

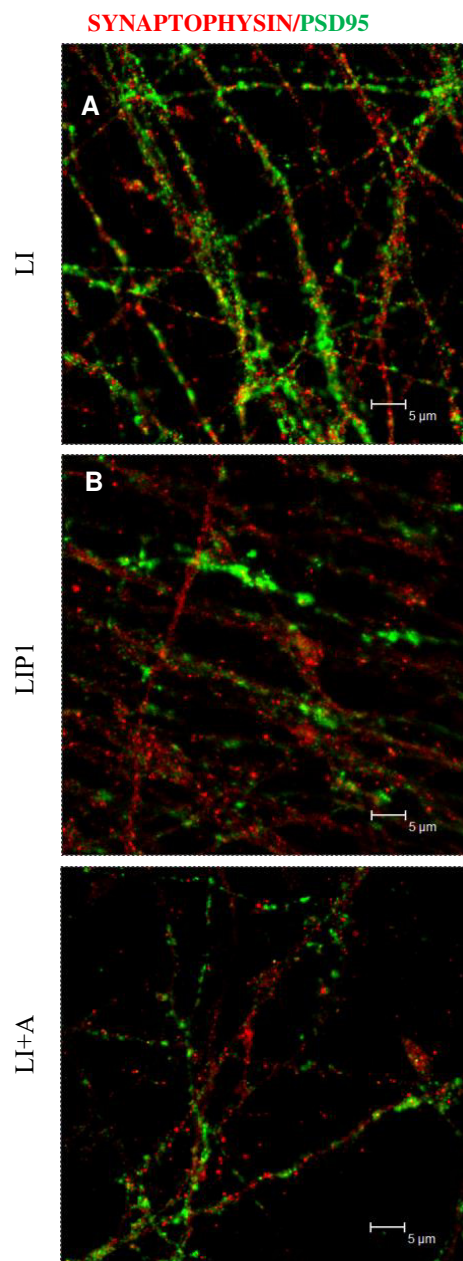


Figure 6:8 Confocal images of fluorescent immunostaining showing co-registration of Synaptophysin and PSD65 on 34D6-iPSC derived neurons. D16 progenitors generated under different conditions A) L, B) LIP1 and C) LIA were differentiated in SCM1/2 for 3 weeks on PDL/matrigel coated coverslips. On D37, cells were double-immunostained for PSD95 (red), Synaptophysin (green). Scale = 5 μm.

## 6.5 Discussion

In this chapter, D16 progenitors generated under different patterning cues, as described in the previous chapters and as outlined in figure 6.1, were analysed for neuronal yield and striatal differentiation, following *in vitro* culture in SCM1/2 for 3 weeks. The analysis of striatal differentiation by immunocytochemistry was limited to the markers- CTIP2, DARPP32, ISL1, Calbindin and GABA against which successful antibodies were available. Neuronal yield and maturation was analysed by measuring the expression of MAP2, Synaptophysin and PSD95.

### 6.5.1 Effect of D16 treatments on generation of DARPP32<sup>+</sup>/CTIP2<sup>+</sup> neurons

The results here confirmed the analyses performed on D16 neural progenitors that indicated LI and LIA treatments as optimal for the production of LGE-like cells. ‘L’ treated cultures yielded 0%CTIP2/0%DARPP32<sup>+</sup> neurons. LI and LIA treated cultures generated 59% CTIP2<sup>+</sup>/16% DARPP32<sup>+</sup> and 60% CTIP2<sup>+</sup>/30% DARPP32<sup>+</sup> neurons, respectively. This indicated that D16 progenitor specification by WNT inhibition enhanced the generation of DARPP32<sup>+</sup> MSN like phenotype and in combination with Activin pathway activation further enhanced their production. LIP0.5 and LIP1.0 treated cultures showed 31% CTIP2/0.64% DARPP32 and 23% CTIP2/0.41% DARPP32, indicating that WNT inhibition in combination with high SHH pathway activation (in the specific temporal window used in this study) inhibited the generation of MSN-like phenotype.

LGE like progenitor specification by application of SHH alone or in combination with WNT inhibitors followed by *in vitro* differentiation for 45-80 days, has been reported to generate 10-18% DARPP32<sup>+</sup> neurons (Aubry *et al.* 2008; Li *et al.* 2009; Zhang *et al.* 2010; Ma *et al.* 2012; 1.Delli Carri *et al.* 2013; Nicoleau *et al.* 2013). Generation of DARPP32<sup>+</sup> neurons (27%) has also been reported from PA6 stromal induced neurogenic embryoid bodies in the absence of any morphogens(Jeon *et al.* 2012). Here, under defined culture conditions, LI patterned progenitors generated a comparable percentage of DARPP32<sup>+</sup> neurons in a short period- just 3 weeks after plating down D16 progenitors ie, on D37. In agreement with other studies (Li *et al.* 2009; Ma *et al.* 2012; Delli Carri *et al.* 2013; Nicoleau *et al.* 2013), there was DARPP32/ CTIP2 co-localisation. There was also a high percentage (60%) of CTIP2<sup>+</sup> cells compared to 14-31% reported by Li *et al.* (2009) and Delli Carri *et al.* (2013).

Interestingly, some of the  $DARPP32^+$  neurons showed decreased CTIP2 intensity, suggesting potential downregulation of CTIP2 upon striatal neuronal maturation. mRNA expression profiling of 7-9 weeks human foetal WGE, cortex and adult striatum by Straccia *et al.* (2015) reported lower *CTIP2* expression in adult striatal samples compared to foetal cortex and WGE samples. *DARPP32* expression displayed the opposite trend, high in adult striatum and low in foetal cortex and WGE. Thus, Straccia *et al.* (2015) hypothesized that CTIP2/*DARPP32* co-localization may be a marker of human foetal MSNs, but not the adult striatum. Temporal mRNA expression profiling of hPSC differentiation using the LI condition (protocol shared in the CHDI consortium) identified a ventral progenitor like phase at D8-D16 and progression towards adult striatal fate at D16-D28, thus the decreased CTIP2 intensity observed in some  $DARPP32^+$  neurons may indicate striatal maturation. Similarly, LIA patterned progenitors also showed CTIP2/*DARPP32* co-localization and decreased CTIP2 intensity in some  $DARPP32^+$  neurons. The higher proportion of  $DARPP32^+$  (30%) obtained was comparable to what was reported (20-50%, varied between cell lines) by Arber *et al.* (2015). In their study, Activin treatment was shown to induce LGE identity by upregulating CTIP2 and the ALK5 inhibitor SB431542 suppressed Activin-induced CTIP2 generation. In chapter 5 preliminary experiments, Activin treatment was observed to induce ~53%  $CTIP2^+$  cells by D16 and at D37 here, a comparable level (60%) was seen. LI only treatment at D16 showed no CTIP2 and at D37 showed 59%  $CTIP2^+$ . Thus, both LI and LIA mediated patterning favoured the generation of  $CTIP2^+$  cells. Activin treatment may have accelerated the striatal neuronal maturation of  $CTIP2^+$  cells as there was no further increase of its expression. In chapter 5, Activin treatment was also observed to result in upregulation of other striatal neuronal makers. mRNA expression and protein level analysis of other striatal markers as well as cortical makers remain to be performed on these LI and LIA treated cultures to identify and quantify the different neural progenitors/neuronal types. Based on the data obtained here, both LI and LIA treatments were being replicated for detailed analysis, in other hPSC lines including HD-iPSCs by other members of the lab at the time of completion of lab work of this thesis. In chapter 5, the results suggested that activation of SHH signalling by Purmorphamine led to potential downregulation of some LGE markers (not consistent with all markers) and upregulation of MGE markers. The reduced proportion of CTIP2 and markedly low amount of *DARPP32* in LIP0.5 and LIP1.0 treated cultures further supported this notion of LGE inhibition by SHH

pathway activation. DKK1+SHH mediated ventral patterning using 200ng/ml of SHH concentration, has been reported to result in down regulation CTIP2 and induction of NKX2.1 at D28 (Nicoleau *et al.* 2013).

### 6.5.2 Effect of D16 treatments on generation of ISL1<sup>+</sup> neurons

Interestingly, a comparable percentage of ISL1<sup>+</sup> neurons (~85%) were seen in LI, LIP0.5 and LIP patterned progenitors and LIA-patterned progenitors generated slightly reduced proportion (60%). L-treated progenitors showed 7% ISL1<sup>+</sup> cells. In mice, LGE expression of *Isl1* has been shown to be essential for the development of striatal neurons of striatonigral pathway (Ehrman *et al.* 2013). *Isl1* shows a spatial and temporal expression pattern during striatum development (Wang and Liu 2001). In rat, *Isl1* protein was first detected around E13 LGE and was expressed in all striatal precursors at E15. During the early phase of differentiation, at E18 striatum, *Isl1* was co-expressed with *Map2*. As differentiation progressed at E20, P0 and by P7, *Isl1* was downregulated and persisted in some cells that co-expressed *ChAT*, indicating cholinergic interneuron specification. *Isl1* expression was sustained throughout development in cholinergic cells. Non-cholinergic precursors that lost *Isl1* expression, expressed *Darpp32* (Wang and Liu 2001). *Isl1* expression was also detected in rat at E13 and E15 MGE and E18 MGE derived globus pallidus cells (Wang and Liu 2001). *Isl1* co-expression with *Nkx2.1* and *Lhx7/8* has been implicated in MGE derived striatal cholinergic interneuron as well as basal forebrain cholinergic projection neuron specification (Fragkouli *et al.* 2009; Cho *et al.* 2014). In human development, ISL1 expressed at 8-11 weeks in all striatal precursors/neurons was restricted to a few cells by week 20 (Onorati *et al.* 2014). Consistent with the *in vivo* data, Delli Carri *et al.* (2013) reported that during DKK1+SHH mediated hPSC striatal specification, *ISL1* mRNA expression peaked at D45 and decreased thereafter. Concomitantly, the expression of *DARPP32* gradually increased from D45 and persisted throughout the differentiation (Delli Carri *et al.* 2013). Here in my study, at D37, the co-expression of ISL1 with MAP2 under all the patterning conditions confirmed the post mitotic neuronal specification. LIA which gave the highest DARPP32 (30%) yield showed a reduction in ISL1<sup>+</sup> (60%) cells, compared to LI (16% DARPP32<sup>+</sup>/85% ISL<sup>+</sup>). The high proportion of ISL1<sup>+</sup> cells indicated striatal-like fate specification by LI and LIA treatments. The high proportion of DARPP32<sup>+</sup> neurons in LIA treated cultures suggested a transition towards a mature striatal phenotype. However, further

experimental replicates and analysis of other striatal makers are required to support this data. A high proportion of ISL1 was also seen in LIP0.5 and LIP1.0 treated cultures. Whether this corresponds to a LGE or MGE fate needs to be determined by analysing the co-expression of MGE markers such as NKX2.1. In chapter 5, compared to LI, Purmorphamine treatment (LIP conditions) was observed to result in downregulation of *ISL1* mRNA in H9 ESC D16 progenitors and a similar but not statistically significant trend was observed in 34D6 iPSC progenitors indicating prevention of upregulation of *ISL1* by SHH pathway activation. However, there was induction of the MGE marker NKX2.1 at the protein level (21-45%) and *GLII*, *NKX2.1*, *NKX6.2* and *LHX6* at the mRNA level. SHH (1000ng/ml) or Purmorphamine (1.5 $\mu$ M) mediated MGE induction and specification to basal forebrain cholinergic neurons has been reported in mESC and hPSCs (Yue *et al.* 2015; Hu *et al.* 2016). These forebrain cholinergic neurons co-expressed ISL1, NKX2.1, OLIG2 and ChAT (Yue *et al.* 2015; Hu *et al.* 2016). The combinatorial activity of *Isl1*, *Lhx6* and *Lhx7* has been reported to mediate MGE progenitors specification towards cholinergic or GABAergic striatal interneuron fate specification (Fragkouli *et al.* 2009) MGE progenitors No conclusion was drawn on the LIP0.5, LIP1 induced cell fate at D37 here, however, downregulation of CTIP2, and DARPP32 as mentioned above suggested potential inhibition of striatal identity. High-throughput QRT-PCR and immunocytochemistry analysis for MGE derived neuronal markers remain to be analysed in these cultures to determine cell identity.

### **6.5.3 Effect of D16 treatments on generation of GABA, Calbindin, Synaptophysin and PSD95**

All the cultures, regardless of the different D16 patterning treatments showed GABA expression and Synaptophysin/PSD95 co-expression indicative of GABAergic neuronal development and synaptogenesis. GABAergic identity of LI patterned progenitors differentiated with SCM1/2 media is now published by Telezhkin *et al.* (2016).

Calbindin-28K, (a calcium binding protein expressed in striatum matrix MSNs as well as in human forebrain cholinergic neurons (Onorati *et al.* 2014; Straccia *et al.* 2015; Geula *et al.* 1993)) positive neurons were present in all culture conditions. L and LIA treatment showed a comparable level (4%), LIP1 had slightly higher proportion (6%) and LI gave the highest yield (11%). Further experimental replicates

are needed to confirm the proportions obtained and determine the statistical significance of the different treatments. In 20 week-human fetal striatum, CTIP2<sup>+</sup> cells displayed GABAergic identity and Calbindin co-expression (Onorati *et al.* 2014). During DKK1+SHH mediated or Activin mediated hPSC striatal specification, and a proportion of CTIP2<sup>+</sup> cells showed Calbindin co-expression (DelliCarri *et al.* 2013; Arber *et al.* 2015). The Calbindin expression seen in my study, need to be analysed by double immunostaining for LGE and MGE markers to determine their striatal vs cholinergic neuronal identity.

In conclusion, SCM1/2 culture conditions promoted efficient neuronal differentiation with GABAergic identity and synaptogenesis as indicated by uniform expression of MAP2, Synaptophysin/ PSD95 and GABA in all the cultures. LI and LIA treatments appeared to be optimal for the production of CTIP2<sup>+</sup>/DARPP32<sup>+</sup> MSN-like phenotype, whereas LIP treatments resulted in the downregulation of these markers. Reduced intensity of CTIP2 in some DARPP32<sup>+</sup> neurons potentially indicated striatal neuronal maturation. LIA gave the highest yield of DARPP32<sup>+</sup> neurons. LI, LIA and LIP treatments also enhanced production of ISL1<sup>+</sup>/MAP2<sup>+</sup> neurons, however, ISL1 immunocytochemistry needs to be analysed in conjunction with further markers to confirm the LGE vs MGE identity. Compared to the other protocols in the literature, the study here, showed the generation of DARPP32<sup>+</sup> neurons in a short period under chemically defined conditions.

## 7 General Discussion

The neural development begins with the induction of neuroectoderm, which in turn gives rise to the neural tube. The neural tube under the influence of instructive signals delineates the anterior-posterior axis and dorso-ventral axis of the CNS. In this thesis, hPSCs were used as a model system to investigate the role of signalling pathways in the neuroectoderm formation, telencephalon development and subsequent regional specification towards a LGE-like fate. At this context, the role of BMP antagonism, WNT antagonism, SHH signalling and Activin pathway was investigated using small molecule agonists or antagonists of the pathways. The thesis aimed at developing chemically defined culture conditions for the optimized production of cell types that are of direct relevance in HD. The aspiration is that it offers a powerful platform not only for understanding human LGE/striatal development but also for *in vitro* HD modelling using hPSCs harbouring mutant *HTT* allele. It may simultaneously permit the identification of target for drug screening as well as provide a renewable cell source for cell-based therapies.

### 7.1 Summary of the results

The current methods for *in vitro* MSN generation includes neural induction using stromal co-culture, embryoid body culture or dual SMAD/BMP inhibition, followed by specification of LGE-like fate using a combination of WNT inhibition and SHH pathway or Activin-A signalling activation (more recent) and finally maturation towards MSNs. A similar paradigm was applied in this thesis using small molecules agonists or antagonists instead of the expensive recombinant proteins as in the other protocols. In chapter 3, in agreement with the other models, dual-SMADi BMP inhibition by Dorsomorphin, LDN193189 and DMH1 in combination with SB431542, together called dual-SMADi, was shown to efficiently induce neuroectoderm markers expression. In chapter 4, dual-SMADi in combination with WNT signalling inhibition by IWR1 and KY02111 from D0 to D16, was found to promote both telencephalic induction and ventral patterning of precursors in a dose-dependent manner. This is the first report of demonstrating the role of WNT antagonism in hPSC telencephalon induction and specification towards a ventral telencephalic fate without the use of any ventralizing molecule. IWR1 at 1 $\mu$ M appeared to be more potent than KY at 1 or 10 $\mu$ M. IWR1 was used for further

experiments (referred to as LI). In chapter 5, dual-SMADi combined with IWR1 mediated WNT inhibition and activation of SHH signalling by Purmorphamine (referred to as LIP) (and SAG, excluded after the preliminary experiments) from D8 to D16, appeared to downregulate or prevent the upregulation pan-ventral and some LGE markers and promoted MGE markers. Whereas, Activin treatment at 20ng/ml from D8 to D16 (preliminary experiments) appeared to specifically enhance LGE/striatal transcripts. In chapter 6, D16 progenitors were plated for terminal differentiation in SCM1/2 media for 3 weeks. Protein level analysis by immunocytochemistry at D37, revealed LI and LIA treatments optimal for the production of DARPP32<sup>+</sup>/CTIP2<sup>+</sup> cells indicative of MSN-like striatal phenotype, LIA treatment was more effective than LI. LIP treatments appeared to inhibit the generation of DARPP32<sup>+</sup>/CTIP2<sup>+</sup> cells.

## 7.2 Small molecules-mediated directed differentiation of hPSCs

Driving the differentiation of hPSCs towards MSN-like phenotype requires the manipulation and timely integration of the developmental signals at the precise level. Many studies have attempted to mimic these developmental cues by applying the expensive recombinant proteins (Watanabe *et al.* 2007; Aubry *et al.* 2008; Li *et al.* 2009; N. Zhang *et al.* 2010; Ma *et al.* 2012; The HD iPSC Consortium 2012; DelliCarri *et al.* 2013).

Despite considerable progress, increasing the efficiency of hPSC differentiation towards MSN fate remains challenging. Moreover, the high cost of recombinant proteins and the use of serum often with batch-to-batch inconsistencies in these protocols are major limitations for culture scale-up. In order to develop a reproducible, efficient and cost effective model system to investigate the developmental mechanisms that govern striatal-like commitment, this thesis (lab work done in 2010-2014 period) attempted to drive hPSC differentiation by the application of inexpensive synthetic known small molecules agonists or antagonists. By varying the dose or duration of small molecule exposure, the developmental pathways could be modulated *in vitro*

### 7.2.1 BMP antagonism promoted PAX6<sup>+</sup> neuroectoderm fate specification

The three main approaches for neural induction in hPSC striatal differentiation protocols are stromal co-culture, embryoid body (EB) culture or dual SMAD/BMP inhibition. MS5 or PA6 mouse stromal cell-derived inducing activity

(SCID) method has the drawback of relying on unidentified factors and the protocol overall takes about 3 weeks *in vitro* (Aubry *et al.* 2008; Jeon *et al.* 2012). hPSC EB culture in neutralizing medium under serum (N. Zhang *et al.* 2010) or serum-free condition with N2 supplement (Joannides *et al.* 2007; Pankratz *et al.* 2007; Ma *et al.* 2012) are cost effective as it does not include growth factors, however, the heterogeneous culture limits the efficiency of neural induction. Integration of developmental cues further refined the culture conditions. Inhibition of Activin/Nodal signalling by SB431542 under defined condition (Smith *et al.* 2008) or inhibition of BMP signalling by Noggin under serum (Pera *et al.* 2004) or serum-free embryoid body culture (Itsykson *et al.* 2005) or MS5 co-culture (Lee *et al.* 2007; Chambers *et al.* 2009) was shown to promote neural induction. The synergistic action of SB431542/Noggin (termed dual-SMADi) under defined conditions, demonstrated by Chambers *et al.* (2009) is advantageous over other culture methods in that it highly enhanced neural induction whilst suppressing the pluripotency and hPSC differentiation towards the other lineages. In chapter 3, dual-SMADi was applied to H9ESC embryoid body culture and the effect of small molecule antagonists of BMP signalling Dorsomorphin, LDN193189 and DMH1 was investigated in combination with SB431542. The strength of the experimental design in this chapter was that all the 3 small molecules as well as Noggin treatment was compared in parallel. The results demonstrated that the inhibition of BMP signalling promoted the induction of definitive neuroectoderm marker PAX6 (X. Zhang *et al.* 2010) at both mRNA and protein level (about 70%) when compared with basal media or SB431542 alone treatment. The effect of Noggin and small molecules was comparable. However, the experiments did not reveal an optimal dose for PAX6 induction. At D8, all the doses 0.25, 0.5 and 1  $\mu$ M tested equally induced PAX6 mRNA expression. Kim *et al.* (2010) and Morizane *et al.* (2011) compared the effect of Noggin or Dorsomorphin, both in combination with SB431542 in an EB based culture. Dose response experiments revealed Dorsomorphin at 2 or 5  $\mu$ M showing a comparable effect to 300 or 1000 ng/ml Noggin (Kim *et al.* 2010; Morizane *et al.* 2011). Surmacz *et al.* (2012) reported high PAX6 induction (~90%) by LDN193189 at 1  $\mu$ M as compared to Dorsomorphin at 5  $\mu$ M and Noggin at 50 ng/ml, all in combination with SB431542 in a monolayer culture system. Further a dose-response curve revealed PAX6 induction by LDN193189 with  $EC_{50}$ =4.84 nM. Chambers *et al.* (2012) reported the application of LDN193189 at 0.1  $\mu$ M thus replacing Noggin (500 ng/ml) in dual-SMADi strategy.

Neely *et al.* (2012) reported a comparable effect of DMH1 at 0.5 $\mu$ M and Noggin 500ng/ml on PAX6 induction in monolayer based dual-SMADi protocol. Kim *et al.* (2010) and Morizane *et al.* (2011) also reported Dorsomorphin dose dependent effect on SOX1 and NESTIN. Neely *et al.* (2012) reported DMH1 dose dependent effect on SOX1, but not on PAX6. Thus optimal dose of small molecules are crucial for expression of genes involved in neuronal lineage specification. The various studies discussed here show the rapid progress in the field of small molecule-mediated differentiation. Collectively, these studies and my study demonstrate that the small molecule BMP inhibitors can replace Noggin. There are discrepancies in the reported effective dose of Dorsomorphin and LDN193189 and it may be attributed to the many variable factors of culture conditions including the cell lines used. However the studies highlighted that LDN193189 is potent than Dorsomorphin or DMH1 at low dose. Recent hPSC striatal differentiation protocols reported dual-SMADi neural induction using LDN193189 at 0.1 $\mu$ M (Nicoleau *et al.* 2013) and in combination with 0.2 $\mu$ M Dorsomorphin (Arber *et al.* 2015). Although a dose dependent effect was not seen on PAX6 in my study at the small molecules doses tested, the study clearly demonstrated that BMP inhibition was critical for PAX6 induction at mRNA and protein level. The effect of basal media, SB431542 alone treatment or in combination with Noggin or small molecules on the down regulation of OCT4 and maintenance of SOX2 was comparable, indicating that basal culture conditions used here favoured neural differentiation. The flaw of the experimental design was that a wide dose range below and above IC<sub>50</sub> values of BMP inhibition by small molecules was not included. This would have determined an effective small molecule and an optimal dose for neural induction and would minimize the possibility of any off target effects.

Although seemingly efficient, the dual-SMADi EB cultures were heterogeneous and contained small percentage of neural crest and epidermis cells. Moreover, EB cultures gave low yield of progenitors. Dual-SMADi using SB431542 and LDN193189 was adapted to a monolayer culture with subtle difference in the exposure time of SB431542 and both dose and exposure time of LDN193189. This protocol was validated by other members in the lab and was used in the rest of the thesis.

### 7.2.2 WNT antagonism promoted FOXG1<sup>+</sup> telencephalic progenitor induction and ventral fate specification

In the absence of any exogenous signals, the default identity of neuroectodermal cells derived using stromal co-culture or serum free EB method or dual-SMADi has been reported to be FOXG1<sup>+</sup> PAX6<sup>+</sup> anterior dorsal fate (Pankratz *et al.* 2007; Elkabetz *et al.* 2008; Chambers *et al.* 2009; Li *et al.* 2009; Neely *et al.* 2012; DelliCarri *et al.* 2013). Various studies have employed WNT inhibitor DKK1 (500ng/ml) to further enhance FOXG1<sup>+</sup> commitment (Watanabe *et al.* 2007; Li *et al.* 2009; N. Zhang *et al.* 2010; DelliCarri *et al.* 2013). In chapter 4, the role of WNT antagonism was analysed during H9 differentiation. The D16 monolayer dual-SMADi (SB431542/LDN193189) cultures yielded >90%PAX6<sup>+</sup>/ $<5\%$ FOXG1<sup>+</sup> cells indicative of neuroectoderm identity. Maroof *et al.* (2013) also reported a similar observation using SB431542/LDN193189. Addition of WNT inhibitors IWR1 and KY02111 to dual-SMADi culture from D0 highly induced FOXG1. IWR1 and KY02111 dose-response effect was observed; IWR1 at 1 $\mu$ M and KY02111 at 10 $\mu$ M yielded 90% and 70% FOXG1<sup>+</sup> cells respectively. This indicated that IWR-1 was more potent than KY02111. This yield was higher than previously reported DKK1-mediated EB (34%) (Watanabe *et al.* 2007) or monolayer based differentiation (58-64%) (DelliCarri *et al.* 2013; Nicoleau *et al.* 2013). Nicoleau *et al.* (2013) and Maroof *et al.* (2013) compared the effect of DKK1 and another small molecule XAV939 (that inhibits WNT pathway in a similar manner to IWR-1) and reported high efficiently FOXG1 induction (85%) by XAV939. IWR1 or KY939 treatments in my study and XAV939 treatment reported in Nicoleau *et al.* (2013) showed no effect on neuroectoderm markers *SOX2*, *NESTIN* and anterior marker *OTX2* suggesting that WNT antagonism combined with dual-SMADi specifically enhanced FOXG1 identity. Further analysis of dorsal and ventral telencephalon markers showed that IWR1 or KY02111 treatments resulted in a smaller decrease in percentage of PAX6<sup>+</sup> cells and lower intensity of PAX6 signal. Previous studies reported that in the absence of ventralizing molecule such as SHH, WNT inhibitors did not abrogate dorsal markers (Li *et al.* 2009; Nicoleau *et al.* 2013). XAV939 in combination with SHH (50ng/ml) (Nicoleau *et al.* 2013) and DKK1 in combination with SHH (Li *et al.* 2009) had an inhibitory effect on PAX6. Detailed analysis by high-throughput QRT-PCR revealed that IWR1 and KY02111 treatment enhanced ventral fate specification as evidenced by the induction of *GSX2*, *DLX2*, *DLX5*, *DLX1*, *MEIS2*, *ISL1*, *NKX2.1*, *LHX6* and *NKX6.2* There was also induction of

post mitotic dorsal maker *TBR1* and neuronal markers *TUBB3* and *DCX*. Temporal analysis of gene expression during dual-SMADi+IWR-1 mediated hPSC differentiation and comparison to human WGE and adult striatum samples by Straccia *et al.* (2015) revealed a ventral fate specification phase at D8-D16 followed by acquisition of WGE identity that was progressing towards adult striatal fate by D16-D28. Thus, my study clearly demonstrated that WNT antagonism enhanced ventral telencephalic fate specification. This is the first report of hPSC ventral fate specification achieved without use of any ventralizing molecules. Nicoleau *et al.* (2013) also highlighted the requirement of WNT antagonism in ventral fate specification, however in their study the ventralizing property of XAV9393 was reduced in the absence of SHH. In my study the effect of WNT inhibitors was analysed in combination with continued BMP inhibition till D16, whereas Nicoleau *et al.* (2013) analysed the effect of XAV939 alone or in combination with SHH, after the withdrawal of BMP inhibitor from the cultures. Despite the difference in the culture conditions, both studies demonstrated that small molecule-mediated WNT antagonism promoted telencephalon induction and regional specification towards a ventral fate. My study presents a cost effective and robust protocol for hPSC LGE-like specification without needing the expensive SHH protein in the culture system.

### **7.2.3 SHH and Activin signalling enhanced MGE-like and LGE-like fate specification respectively**

In chapter 5, the role of SHH signalling by small molecules Purmorphamine and SAG as well as Activin signalling was analysed at the context of concurrent BMP and WNT inhibition (SB431542/LDN193189+IWR1). SHH alone or in combination with DKK1 in an appropriate temporal window during hPSC differentiation has been reported to achieve LGE or MGE specification in SHH dose-dependent manner (Ma *et al.* 2012; Watanabe *et al.* 2007; Aubry *et al.* 2008; Li *et al.* 2009; DelliCarri *et al.* 2013; Nicoleau *et al.* 2013). Following a pilot study (N=2) with Purmorphamine at 0.1, 0.5 and 1 $\mu$ M, the highest doses 0.5 and 1 $\mu$ M that upregulated SHH targets *PATCHED1* and *GLII* was used for further differentiation experiments. Detailed analysis by high-throughput QRT-PCR revealed that Purmorphamine treatment (at 0.5 and 1 $\mu$ M in H9 ESC and 0.3 and 1 $\mu$ M in 34D6 iPSC) during D8-D16 temporal window did not alter anterior markers *FOXG1*, *SIX3* and *OTX2*. In line with other studies, there was Purmorphamine dose-dependent down regulation of dorsal

transcripts *PAX6*, *TBR1* and *GLI3* and upregulation of MGE specific transcripts *GLI1*, *NKX2.1*, *NKX6.2* and *LHX6*. However, pan-ventral and LGE specific markers *GSX2*, *DLX2*, *DLX5*, *ISL1* and *MEIS2* were down regulated in H9 cells. 34D6 cells showed a similar but not statistically significant trend, which may indicate either prevention of upregulation of these transcripts or no modulation of these transcripts by SHH pathway activation during D8-D16 temporal window. H9 cells exposed to Activin instead of Purmorphamine during the same temporal window, showed upregulation of a number of LGE and striatal specific transcripts. This showed during D8-D16 window, the progenitors were responsive to developmental signals and that cell responses to Activin signalling and SHH signalling were different.

Results of Purmorphamine treatment was initially surprising as SHH signalling has been shown to mediate ventral patterning by antagonising GLI3 which mediates the dorsal patterning (Rallu *et al.* 2002; Li *et al.* 2009). Most of the hPSC neural differentiation protocols report a default cortical identity of progenitors (Pankratz *et al.* 2007; Elkabetz *et al.* 2008; Chambers *et al.* 2009; Li *et al.* 2009; Neely *et al.* 2012; DelliCarri *et al.* 2013). A graded ventralizing effect by SHH application has been reported; the highest dose upregulated MGE markers and an optimal dose which enhanced pan-ventral markers *GSX2*, *DLX2*, but not *NKX2.1* qualified for generation of DARPP32<sup>+</sup> MSN-like neurons (Li *et al.* 2009; Ma *et al.* 2012; Nicoleau *et al.* 2013). At this optimal SHH dose, additional WNT inhibition by DKK1 or XAV939 (in a dose-dependent manner) strongly enhanced the ventralization (Li *et al.* 2009; Nicoleau *et al.* 2013). Thus, it can be suggested that SHH rather acts by suppressing the default cortical specification than directly mediating striatal specification. Further support of this notion came from the study by Arber *et al.* (2015); Activin treatment in combination with increasing dose of SHH upregulated MGE markers but did not increase Activin-induced LGE markers. At context of ventralization achieved by WNT inhibition in my study, activation of SHH pathway appeared to have directly enhanced MGE fate at the expense of LGE fate. A similar observation i.e., induction of MGE fate at the expense of LGE/CGE fate has been reported during SHH or SAG- mediated mESC (Danjo *et al.* 2011) and hPSC (Kim *et al.* 2014) specification towards MGE derived cortical interneurons. Both SHH dose and temporal window of exposure played a role in this process (Nicholas *et al.* 2014; Kim *et al.* 2014).

The Activin-induced gene expression patterns were distinct from those induced by Purmorphamine. Arber *et al.* (2015), reported an increase in the number of GSX2<sup>+</sup> and CTIP2<sup>+</sup> cells upon Activin treatment during hPSC differentiation. In contrast, in my study, there was a smaller decrease in GSX2<sup>+</sup> cells by Activin treatment (LIA) in 34D6 iPSC line compared to control (LI). During H9 ESC differentiation, Activin treatment did not appear to alter *GSX2* transcript but preferentially upregulated *DLX* transcripts, GABAergic neuronal transcripts *NPY* and *SST*, LGE transcripts *FOXP1* and *NOLZI* as well as MSN marker *TAC1*. This suggested that Activin treatment at the context of both BMP and WNT inhibition in my study potentially induced a LGE-like or GABAergic neuronal maturation. Support for this notion comes from the study by Maira *et al.* (2010) in which TGF- $\beta$  family proteins through interactions with *Dlx* genes were shown to regulate telencephalic GABAergic neuron development. It would be of interest to analyse if small molecules can replace the function of Activin in our culture system. IDE1 and IDE2 are two small molecules that have been shown to phenocopy the function of Activin during hPSC endoderm differentiation (Borowiak *et al.* 2009).

#### 7.2.4 Patterning effects persist when terminally differentiated into neurons

*In vitro* differentiation of D16 progenitors in SCM1/2 media which has been shown to achieve synchronized neural differentiation (Telezhkin *et al.* 2016) revealed the strength of D16 telencephalic commitment and regional commitment. Both LI and LIA showed DARPP32<sup>+</sup>/CTIP2<sup>+</sup> neurons whilst LIP conditions downregulated the expression of these markers. The comparable proportion of ISL1<sup>+</sup> cells suggested acquisition of ventral fate by LI, LIA and LIP patterning. The data shown is limited and further experiment replicates and analysis of further LGE and MGE are needed to confirm the phenotype achieved. However, compared to all the other protocol utilizing DKK1+SHH, in my study, LGE like fate specification and generation of DARPP32<sup>+</sup> method was achieved in a shortest time. The highly positive GABA, MAP2 and Synaptophysin/PSD95 on D37 neurons regardless of the patterning conditions revealed their GABAergic post mitotic identity and initiation of synaptogenesis in the culture.

### 7.3 Future work and scope of the project

The hPSCs provide a unique model system for investigating the role of developmental pathways. Following neural induction, the progenitors in this study showed distinct cell response to WNT inhibition, SHH pathway activation and Activin pathway activation. Although LI and LIA conditions enhanced LGE-like fate, the yield of DARPP32<sup>+</sup> neurons was still low. Future work is needed to identify the developmental mechanisms that drive LGE-like progenitor differentiation towards MSNs. Although DARPP32 is used as gold standard, further markers of striatal neurons need to be analysed.

The scope of this project is in the application of protocols for *in vitro* disease modelling of HD-iPSC lines. The various hPSC striatal-like specification studies report promising results from *in vivo* engraftment in HD animal models to exploit the potential for cell transplantation applications. The increasing number of studies utilizing small molecules in hPSC differentiation protocols shows the rapid advancement in this field. Small molecules with the desired biological effect could overcome cell-based drug screening hurdles.

# Bibliography

Aasen, T., Raya, A., Barrero, M.J., Garreta, E., Consiglio, A., Gonzalez, F., Vassena, R., *et al.* (2008). Efficient and rapid generation of induced pluripotent stem cells from human keratinocytes. *Nature biotechnology* **26**:1276–84.

Aberdam, E., Barak, E., Rouleau, M., de LaForest, S., Berrih-Aknin, S., Suter, D.M., Krause, K.-H., *et al.* (2008). A pure population of ectodermal cells derived from human embryonic stem cells. *Stem cells* **26**:440–444.

Albin, R.L., Reiner, A., Anderson, K.D., Dure, L.S., Handelin, B., Balfour, R., Whetsell, W.O., *et al.* (1992). Preferential loss of striato-external pallidal projection neurons in presymptomatic Huntington's disease. *Annals of neurology* **31**:425–430.

An, M.C., Zhang, N., Scott, G., Montoro, D., Wittkop, T., Mooney, S., Melov, S., *et al.* (2012). Genetic correction of huntington's disease phenotypes in induced pluripotent stem cells. *Cell Stem Cell* **11**:253–263.

Anderson, G.J. and Darshan, D. (2008). Small-molecule dissection of BMP signaling. *Nature chemical biology* **4**:15–16.

Anderson, K.D. and Reiner, A. (1991). Immunohistochemical localization of DARPP-32 in striatal projection neurons and striatal interneurons: implications for the localization of D1-like dopamine receptors on different types of striatal neurons. *Brain research* **568**:235–243.

Anderson, R.M., Lawrence, A.R., Stottmann, R.W., Bachiller, D. and Klingensmith, J. (2002). Chordin and noggin promote organizing centers of forebrain development in the mouse. *Development* **29**:4975–4987.

Anderson, S.A, Qiu, M., Bulfone, a, Eisenstat, D.D., Meneses, J., Pedersen, R. and Rubenstein, J.L. (1997). Mutations of the homeobox genes *Dlx-1* and *Dlx-2* disrupt the striatal subventricular zone and differentiation of late born striatal neurons. *Neuron* **19**:27–37.

Andrew, S.E., Goldberg, Y.P., Kremer, B., Telenius, H., Theilmann, J., Adam, S., Starr, E., *et al.* (1993). The relationship between trinucleotide (CAG) repeat length and clinical features of Huntington's disease. *Nature genetics* **4**:398–403.

Antonini, A, Leenders, K.L., Spiegel, R., Meier, D., Vontobel, P., Weigell-Weber, M., Sanchez-Pernaute, R., *et al.* (1996). Striatal glucose metabolism and dopamine D2 receptor binding in asymptomatic gene carriers and patients with Huntington's disease. *Brain : a journal of neurology* **119** ( Pt 6):2085–2095.

Arber, C., Precious, S. V., Cambray, S., Risner-Janiczek, J.R., Kelly, C., Noakes, Z., Fjodorova, M., *et al.* (2015). Activin A directs striatal projection neuron differentiation of human pluripotent stem cells. *Development* **142**:1375–1386.

Arrasate, M., Mitra, S., Schweitzer, E.S., Segal, M.R. and Finkbeiner, S. (2004). Inclusion body formation reduces levels of mutant huntingtin and the risk of neuronal death. *Nature* **431**:805–810.

Aubry, L., Bugi, A., Lefort, N., Rousseau, F., Peschanski, M. and Perrier, A.L. (2008). Striatal progenitors derived from human ES cells mature into DARPP32 neurons in vitro and in quinolinic acid-lesioned rats. *Proceedings of the National Academy of Sciences of*

*the United States of America* **105**:16707–12.

Avilion, A.A., Nicolis, S.K., Pevny, L.H., Perez, L., Vivian, N. and Lovell-Badge, R. (2003). Multipotent cell lineages in early mouse development on SOX2 function. *Genes Dev.* **17**:126–140.

Bachiller, D., Klingensmith, J., Kemp, C., Belo, J. a, Anderson, R.M., May, S.R., McMahon, J. a, *et al.* (2000). The organizer factors Chordin and Noggin are required for mouse forebrain development. *Nature* **403**:658–661.

Backman, M., Machon, O., Mygland, L., Van Den Bout, C.J., Zhong, W., Taketo, M.M. and Krauss, S. (2005). Effects of canonical Wnt signaling on dorso-ventral specification of the mouse telencephalon. *Developmental Biology* **279**:155–168.

Bano, D., Zanetti, F., Mende, Y. and Nicotera, P. (2011). Neurodegenerative processes in Huntington's disease. *Cell Death and Disease* **2**:e228.

Barco Barrantes, I. Del, Davidson, G., Gröne, H.J., Westphal, H. and Niehrs, C. (2003). Dkk1 and noggin cooperate in mammalian head induction. *Genes and Development* **17**:2239–2244.

Beal, M.F., Kowall, N.W., Ellison, D.W., Mazurek, M.F., Swartz, K.J. and Martin, J.B. (1986). Replication of the neurochemical characteristics of Huntington's disease by quinolinic acid. *Nature* **321**:168–171.

Becher, M.W., Kotzuk, J. a, Sharp, a H., Davies, S.W., Bates, G.P., Price, D.L. and Ross, C. a (1998). Intranuclear neuronal inclusions in Huntington's disease and dentatorubral and pallidoluyisian atrophy: correlation between the density of inclusions and IT15 CAG triplet repeat length. *Neurobiology of disease* **4**:387–397.

Beddington, R.S.P. (1994). Induction of a second neural axis by the mouse node. **620**:613–620.

Beddington, R.S.P. and Robertson, E.J. (1999). Axis development and early asymmetry in mammals. *Cell* **96**:195–209.

Belo, J.A., Bouwmeester, T., Leyns, L., Kertesz, N., Gallo, M., Follettie, M. and De Robertis, E.M. (1997). Cerberus-like is a secreted factor with neutralizing activity expressed in the anterior primitive endoderm of the mouse gastrula. *Mechanisms of development* **68**:45–57.

Ten Berge, D., Koole, W., Fuerer, C., Fish, M., Eroglu, E. and Nusse, R. (2008). Wnt signaling mediates self-organization and axis formation in embryoid bodies. *Stem Cell* **3**:508–518..

Bertacchi, M., Pandolfini, L., D'Onofrio, M., Brandi, R. and Cremisi, F. (2015). The double inhibition of endogenously produced bmp and wnt factors synergistically triggers dorsal telencephalic differentiation of mouse es cells. *Developmental Neurobiology* **75**:66–79.

Bibb, J. a, Snyder, G.L., Nishi, a, Yan, Z., Meijer, L., Fienberg, a a, Tsai, L.H., *et al.* (1999). Phosphorylation of DARPP-32 by Cdk5 modulates dopamine signalling in neurons. *Nature* **402**:669–671.

Boer, B., Kopp, J., Mallanna, S., Desler, M., Chakravarthy, H., Wilder, P.J., Bernadt, C., *et al.* (2007). Elevating the levels of Sox2 in embryonal carcinoma cells and embryonic stem cells inhibits the expression of Sox2:Oct-3/4 target genes. *Nucleic Acids Research* **35**:1773–1786.

- Boergermann, J.H., Kopf, J., Yu, P.B. and Knaus, P. (2010). Dorsomorphin and LDN-193189 inhibit BMP-mediated Smad, p38 and Akt signalling in C2C12 cells. *International Journal of Biochemistry and Cell Biology* **42**:1802–1807.
- Borlongan, C. V., Theodore, K.K. and Sanberg, P.R. (1997). 3-Nitropropionic acid animal model and Huntington's disease. *Neuroscience & Biobehavioral Reviews* **21**:289–293.
- Borowiak, M., Maehr, R., Chen, S., Chen, A.E., Tang, W., Fox, J., Schreiber, S., *et al.* (2009). Small molecules efficiently direct endodermal differentiation of mouse and human embryonic stem cells *Malgorzata*. **33**:348–358.
- Bourguignon, C., Li, J. and Papalopulu, N. (1998). XBF-1, a winged helix transcription factor with dual activity, has a role in positioning neurogenesis in *Xenopus* competent ectoderm. *Development* **125**:4889–900.
- Boyer, L. a L. a., Lee, T.I.T.I., Cole, M.F.M.F., Johnstone, S.E.S.E., Stuart, S., Zucker, J.P.J.P., Guenther, M.G.M.G., *et al.* (2005). Core Transcriptional Regulatory Circuitry in Human Embryonic Stem Cells. *Cell* **122**:947–956.
- Bradley, C.K., Scott, H.A., Chami, O., Peura, T.T., Dumevska, B., Schmidt, U. and Stojanov, T. (2011). Derivation of Huntington's disease-affected human embryonic stem cell lines. *Stem cells and development* **20**:495–502.
- Brennan, W. a, Bird, E.D. and Aprille, J.R. (1985). Regional mitochondrial respiratory activity in Huntington's disease brain. *Journal of neurochemistry* **44**:1948–1950.
- Browne, S.E., Bowling, a C., MacGarvey, U., Baik, M.J., Berger, S.C., Muqit, M.M., Bird, E.D., *et al.* (1997). Oxidative damage and metabolic dysfunction in Huntington's disease: selective vulnerability of the basal ganglia. *Annals of neurology* **41**:646–653.
- Browne, S.E., Ferrante, R.J. and Beal, M.F. (1999). Oxidative Stress in Huntington's Disease. **9**:147–163.
- Butt, S.J.B., Sousa, V.H., Fuccillo, M. V, Hjerling-leffler, J., Kimura, S. and Fishell, G. (2008). The requirement of Nkx2-1 in the temporal specification of cortical interneuron subtypes. *Neurons* **59**:722–732.
- Butterworth, J., Yates, C.M. and Reynolds, G.P. (1985). Distribution of phosphate-activated glutaminase, succinic dehydrogenase, pyruvate dehydrogenase and gamma-glutamyl transpeptidase in post-mortem brain from Huntington's disease and agonal cases. *Journal of the Neurological Sciences* **67**:161–171.
- Cambrey, S., Arber, C., Little, G., Dougalis, A.G., de Paola, V., Ungless, M. a., Li, M., *et al.* (2012). Activin induces cortical interneuron identity and differentiation in embryonic stem cell-derived telencephalic neural precursors. *Nature Communications* **3**:841.
- Camnasio, S., Carri, A.D., Lombardo, A., Grad, I., Mariotti, C., Castucci, A., Rozell, B., *et al.* (2012). The first reported generation of several induced pluripotent stem cell lines from homozygous and heterozygous Huntington's disease patients demonstrates mutation related enhanced lysosomal activity. *Neurobiol Dis* **46**:41–51.
- Casarosa, S., Fode, C. and Guillemot, F. (1999). Mash1 regulates neurogenesis in the ventral telencephalon. *Development* **126**:525–534.
- Castro, D.S., Martynoga, B., Parras, C., Ramesh, V., Pacary, E., Johnston, C., Drechsel, D., *et al.* (2011). A novel function of the proneural factor Ascl1 in progenitor proliferation identified by genome-wide characterization of its targets. *Genes and Development* **25**:930–945.

- Chae, J.-I., Kim, D.-W., Lee, N., Jeon, Y.-J., Jeon, I., Kwon, J., Kim, J., *et al.* (2012). Quantitative proteomic analysis of induced pluripotent stem cells derived from a human Huntington's disease patient. *The Biochemical journal* **446**:359–71.
- Chambers, S.M., Fasano, C.A., Papapetrou, E.P., Tomishima, M., Sadelain, M. and Studer, L. (2009). Highly efficient neural conversion of human ES and iPS cells by dual inhibition of SMAD signaling. *Nature Biotechnology* **27**:275–280.
- Chambers, S.M., Qi, Y., Mica, Y., Lee, G., Zhang, X., Niu, L., Bilsland, J., *et al.* (2012). Combined small-molecule inhibition accelerates developmental timing and converts human pluripotent stem cells into nociceptors. *Nature Biotechnology* **30**:715–720.
- Chan, A.W.S. (2009). Transgenic primate research paves the path to a better animal model: Are we a step closer to curing inherited human genetic disorders? *Journal of Molecular Cell Biology* **1**:13–14.
- Chang, H.T., Wilson, C.J. and Kitai, S.T. (1982). A Golgi study of rat neostriatal neurons: light microscopic analysis. *The Journal of comparative neurology* **208**:107–126.
- Chatzi, C., Brade, T. and Duester, G. (2011). Retinoic acid functions as a key gabaergic differentiation signal in the basal ganglia. *PLoS Biology* **9**(4).
- Chen, B., Dodge, M.E., Tang, W., Lu, J., Ma, Z., Wei, S., Hao, W., *et al.* (2009). Small molecule-mediated disruption of Wnt-dependent signaling in tissue regeneration and cancer. *Nature chemical biology* **5**:100–107.
- Chen, J.K., Taipale, J., Young, K.E., Maiti, T. and Beachy, P. a (2002). Small molecule modulation of Smoothed activity. *Proceedings of the National Academy of Sciences of the United States of America* **99**:14071–14076.
- Chiang, C., Litingtung, Y., Lee, E., Young, K.E., Corden, J.L., Westphal, H. and Beachy, P. a (1996). Cyclopia and defective axial patterning in mice lacking Sonic hedgehog gene function. *Nature* **383**:407–413.
- Cho, H.H., Cargnin, F., Kim, Y., Lee, B., Kwon, R.J., Nam, H., Shen, R., *et al.* (2014). Isl1 Directly Controls a Cholinergic Neuronal Identity in the Developing Forebrain and Spinal Cord by Forming Cell Type-Specific Complexes. *PLoS Genetics* **10**.
- Cooper, J.K., Schilling, G., Peters, M.F., Herring, W.J., Sharp, A.H., Kaminsky, Z., Masone, J., *et al.* (1998). Truncated N-terminal fragments of huntingtin with expanded glutamine repeats form nuclear and cytoplasmic aggregates in cell culture. *Human Molecular Genetics* **7**:783–790.
- Corbin, J.G., Gaiano, N., Machold, R.P., Langston, a and Fishell, G. (2000). The Gsh2 homeodomain gene controls multiple aspects of telencephalic development. *Development* **127**:5007–5020.
- Corbin, J.G., Rutlin, M., Gaiano, N. and Fishell, G. (2003). Combinatorial function of the homeodomain proteins Nkx2.1 and Gsh2 in ventral telencephalic patterning. *Development* **130**:4895–4906.
- Crossley, P.H., Martinez, S., Ohkubo, Y. and Rubenstein, J.L.R. (2001). Coordinate expression of Fgf8, Otx2, Bmp4, and Shh in the rostral prosencephalon during development of the telencephalic and optic vesicles. *Neuroscience* **108**:183–206.
- Cuny, G., Yu, P., Laha, J., Xing, X., Liu, J., Lai, C., Deng, D., *et al.* (2008) Structure-activity relationship study of bone morphogenetic protein (BMP) signaling inhibitors. *Bioorg med chem Lett* **18**:4388–4392.

- Dalton, S. (2013). Signaling networks in human pluripotent stem cells. *Current Opinion in Cell Biology* **25**:241–246.
- Danesin, C., Peres, J.N., Johansson, M., Snowden, V., Cording, A., Papalopulu, N. and Houart, C. (2009). Integration of Telencephalic Wnt and Hedgehog Signaling Center Activities by Foxg1. *Developmental Cell* **16**:576–587.
- Danjo, T., Eiraku, M., Muguruma, K., Watanabe, K., Kawada, M., Yanagawa, Y., Rubenstein, J.L.R., *et al.* (2011). Subregional Specification of Embryonic Stem Cell-Derived Ventral Telencephalic Tissues by Timed and Combinatory Treatment with Extrinsic Signals. *Journal of Neuroscience* **31**:1919–1933.
- David, L. and Polo, J.M. (2014). Phases of reprogramming. *Stem cell research* **12**:754–761.
- Davies, S.W., Turmaine, M., Cozens, B. a., DiFiglia, M., Sharp, A.H., Ross, C. a., Scherzinger, E., *et al.* (1997). Formation of neuronal intranuclear inclusions underlies the neurological dysfunction in mice transgenic for the HD mutation. *Cell* **90**:537–548.
- DelliCarri, A., Onorati, M., Lelos, M.J., Castiglioni, V., Faedo, A., Menon, R., Camnasio, S., *et al.* (2013). Developmentally coordinated extrinsic signals drive human pluripotent stem cell differentiation toward authentic DARPP-32+ medium-sized spiny neurons. *Development* **15**;140(2):301-12
- Deng, Y.P., Albin, R.L., Penney, J.B., Young, a. B., Anderson, K.D. and Reiner, a. (2004). Differential loss of striatal projection systems in Huntington's disease: A quantitative immunohistochemical study. *Journal of Chemical Neuroanatomy* **27**:143–164.
- DiFiglia, M., Sapp, E., Chase, K., Schwarz, C., Meloni, a, Young, C., Martin, E., *et al.* (1995). Huntingtin is a cytoplasmic protein associated with vesicles in human and rat brain neurons. *Neuron* **14**:1075–1081.
- DiFiglia, M., Sapp, E., Chase, K.O., Davies, S.W., Bates, G.P., Vonsattel, J.P. and Aronin, N. (1997). Aggregation of huntingtin in neuronal intranuclear inclusions and dystrophic neurites in brain. *Science* **277**:1990–3.
- Ding, S. and Schultz, P.G. (2004). A role for chemistry in stem cell biology. *Nature biotechnology* **22**:833–840.
- Dor, Y. and Melton, A.D. (2004). How Important are Adult Stem Cells for Tissue Maintenance? *Cell Cycle* **3**:1104–1106.
- Doria, J.G., Silva, F.R., De Souza, J.M., Vieira, L.B., Carvalho, T.G., Reis, H.J., Pereira, G.S., *et al.* (2013). Metabotropic glutamate receptor 5 positive allosteric modulators are neuroprotective in a mouse model of Huntington's disease. *British Journal of Pharmacology* **169**:909–921.
- Dragatsis, I., Levine, M.S. and Zeitlin, S. (2000). Inactivation of Hdh in the brain and testis results in progressive neurodegeneration and sterility in mice. *Nature genetics* **26**:300–306.
- Du, T., Xu, Q., Ocbina, P.J. and Anderson, S.A. (2008). NKX2.1 specifies cortical interneuron fate by activating Lhx6. *Development* **135**:1559–1567.
- Duyao, M.P., Auerbach, A.B., Ryan, A., Persichetti, F., Barnes, G.T., McNeil, S.M., Ge, P., *et al.* (1995). Inactivation of the mouse Huntington ' s disease gene homolog Hdh. *Science* **269**:407–410.

- Ehrman, L.A., Mu, X., Waclaw, R.R., Yoshida, Y., Vorhees, C. V, Klein, W.H. and Campbell, K. (2013). The LIM homeobox gene *Isl1* is required for the correct development of the striatonigral pathway in the mouse. *Proceedings of the National Academy of Sciences of the United States of America* **110**:E4026-35.
- Eisenstat, D.D., Liu, J.K., Mione, M., Zhong, W., Yu, G., Anderson, S. a., Ghattas, I., *et al.* (1999). DLX-1, DLX-2, and DLX-5 expression define distinct stages of basal forebrain differentiation. *Journal of Comparative Neurology* **414**:217–237.
- El-akabawy, G., Medina, L.M., Jeffries, A., Price, J. and Modo, M. (2011). Purmorphamine Increases DARPP-32 Differentiation in Human Striatal Neural Stem Cells Through the Hedgehog Pathway. *Stem cells and development* **20**:1873–1887.
- Elias, L.A.B., Potter, G.B. and Kriegstein, A.R. (2008). A Time and a Place for Nkx2-1 in Interneuron Specification and Migration. *Neuron* **59**:679–682.
- Elkabetz, Y., Panagiotakos, G., Al Shamy, G., Socci, N.D., Tabar, V. and Studer, L. (2008). Human ES cell-derived neural rosettes reveal a functionally distinct early neural stem cell stage. *Genes and Development* **22**:152–165.
- Englund, C., Fink, A., Charmaine, L., Pham, D., Ray, D.A.M., Bulfone, A., Kowalczyk, T., *et al.* (2005). Pax6, Tbr2, and Tbr1 Are Expressed Sequentially by Radial Glia, Intermediate Progenitor Cells, and Postmitotic Neurons in Developing Neocortex. *Journal of Neuroscience* **25**:247–251.
- Ericson, J., Muhr, J., Placzek, M., Lints, T., Jessel, T.M. and Edlund, T. (1995). Sonic hedgehog induces the differentiation of ventral forebrain neurons: A common signal for ventral patterning within the neural tube. *Cell* **81**:747–756.
- Evans, A.E., Kelly, C., Precious, S.V. and Rosser, A.E. (2012). Molecular regulation of striatal development: a review. *Anatomy Research International* **2012**;2012:106529..
- Evans, M.J. and Kaufman, M.H. (1981). Establishment in culture of pluripotential cells from mouse embryos. *Nature* **292**:154–6.
- Faber, P.W., Alter, J.R., MacDonald, M.E. and Hart, A.C. (1999). Polyglutamine-mediated dysfunction and apoptotic death of a *Caenorhabditis elegans* sensory neuron. *Proceedings of the National Academy of Sciences of the United States of America* **96**:179–84.
- Fasano, C., Chambers, S.M., Lee, G., Tomishima, M.J. and Studer, L. (2010). Efficient Derivation of Functional Floor Plate Tissue from Human Embryonic Stem Cells. *Cell Stem Cell* **6**:336–347.
- Feijen, a, Goumans, M.J. and van den Eijnden-van Raaij, a J. (1994). Expression of activin subunits, activin receptors and follistatin in postimplantation mouse embryos suggests specific developmental functions for different activins. *Development* **120**:3621–3637.
- Fernandez, É., Schiappa, R., Girault, J.A. and Le Novère, N. (2006). DARPP-32 is a robust integrator of dopamine and glutamate signals. *PLoS Computational Biology* **2**:1619–1633.
- Feyoux, M., Bourgois-Rocha, F., Redfern, A., Giles, P., Lefort, N., Aubert, S., Bonnefond, C., *et al.* (2012). Early transcriptional changes linked to naturally occurring Huntington's disease mutations in neural derivatives of human embryonic stem cells. *Human Molecular Genetics* **21**:3883–3895.

- Fode, C., Ma, Q., Casarosa, S., Ang, S.L., Anderson, D.J. and Guillemot, F. (2000). A role for neural determination genes in specifying the dorsoventral identity of telencephalic neurons. *Genes and Development* **14**:67–80.
- Fong, H., Hohenstein, K. a and Donovan, P.J. (2008). Regulation of self-renewal and pluripotency by Sox2 in human embryonic stem cells. *Stem cells* **26**:1931–1938.
- Fragkouli, A., van Wijk, N.V., Lopes, R., Kessar, N. and Pachnis, V. (2009). LIM homeodomain transcription factor-dependent specification of bipotential MGE progenitors into cholinergic and GABAergic striatal interneurons. *Development* **136**:3841–51.
- Fuccillo, M., Rallu, M., McMahon, A.P. and Fishell, G. (2004). Temporal requirement for hedgehog signaling in ventral telencephalic patterning. *Development* **131**:5031–5040.
- Furuta, Y., Piston, D.W. and Hogan, B.L. (1997). Bone morphogenetic proteins (BMPs) as regulators of dorsal forebrain development. *Development* **124**:2203–2212.
- Fusaki, N., Ban, H., Nishiyama, A., Saeki, K. and Hasegawa, M. (2009). Efficient induction of transgene-free human pluripotent stem cells using a vector based on Sendai virus, an RNA virus that does not integrate into the host genome. *Proceedings of the Japan Academy. Series B, Physical and biological sciences* **85**:348–362.
- Gammill, L.S. and Bronner-Fraser, M. (2003). Neural crest specification: migrating into genomics. *Nature reviews. Neuroscience* **4**:795–805.
- Gardner, R.L. and Beddington, R.S. (1988). Multi-lineage ‘stem’ cells in the mammalian embryo. *Journal of cell science. Supplement* **10**:11–27.
- Gerfen, C.R. (1992). The neostriatal mosaic: multiple levels of compartmental organization. *Journal of neural transmission. Supplementum* **36**:43–59.
- Gerfen, C.R. (1989). The neostriatal mosaic: striatal patch-matrix organization is related to cortical lamination. *Science* **246**:385–388.
- Gervais, F.G., Singaraja, R., Xanthoudakis, S., Gutekunst, C.-A., Leavitt, B.R., Metzler, M., Hackam, A.S., *et al.* (2002). Recruitment and activation of caspase-8 by the Huntingtin-interacting protein Hip-1 and a novel partner Hipp1. *Nature cell biology* **4**:95–105.
- Geula, C., Schatz, C.R. and Mesulam, M.M. (1993). Differential localization of naphthylphosphorase and calbindin-D28k within the cholinergic neurons of the basal forebrain, striatum and brainstem in the rat, monkey, baboon and human. *Neuroscience* **54**:461–476.
- Glinka, a, Wu, W., Delius, H., Monaghan, a P., Blumenstock, C. and Niehrs, C. (1998). Dickkopf-1 is a member of a new family of secreted proteins and functions in head induction. *Nature* **391**:357–362.
- Glinka, a, Wu, W., Onichtchouk, D., Blumenstock, C. and Niehrs, C. (1997). Head induction by simultaneous repression of Bmp and Wnt signalling in *Xenopus*. *Nature* **389**:517–519.
- Goldberg, Y., Nicholson, D., Rasper, D., Kalchman, M., Koide, H., Graham, R., Bromm, M., *et al.* (1996). Cleavage of huntingtin by apopain, a proapoptotic cysteine protease, is modulated by the polyglutamine tract. *Nat Genet.* **14**:353–6.
- Golden, J.A., Braciclovic, A., McFadden, K.A., Beesley, J.S., Rubenstein, J.L. and Grinspan, J.B. (1999). Ectopic bone morphogenetic proteins 5 and 4 in the chicken forebrain lead to cyclopia and holoprosencephaly. *Proceedings of the National Academy of*

*Sciences of the United States of America* **96**:2439–44.

Goodrich, L. V, Milenkovic, L., Higgins, K. and Scott, M.P. (1997). Altered neural cell fates and medulloblastoma in mouse patched mutants. *Science* **277**:1109–1113.

Graham, R.K., Deng, Y., Slow, E.J., Haigh, B., Bissada, N., Lu, G., Pearson, J., *et al.* (2006). Cleavage at the Caspase-6 Site Is Required for Neuronal Dysfunction and Degeneration Due to Mutant Huntingtin. *Cell* **125**:1179–1191.

Graham, V., Khudyakov, J., Ellis, P. and Pevny, L. (2003). SOX2 functions to maintain neural progenitor identity. *Neuron* **39**:749–765.

Graveland, G. a, Williams, R.S. and DiFiglia, M. (1985). A Golgi study of the human neostriatum: neurons and afferent fibers. *The Journal of comparative neurology* **234**:317–333.

Gray, M., Shirasaki, D.I., Cepeda, C., André, V.M., Wilburn, B., Lu, X.-H., Tao, J., *et al.* (2008). Full-length human mutant huntingtin with a stable polyglutamine repeat can elicit progressive and selective neuropathogenesis in BACHD mice. *The Journal of neuroscience : the official journal of the Society for Neuroscience* **28**:6182–6195.

Grunz, H. and Tacke, L. (1989). Neural differentiation of *Xenopus laevis* ectoderm takes place after disaggregation and delayed reaggregation without inducer. *Cell differentiation and development* **28**:211–217.

Gu, M., Gash, M. and Mann, V.M. (1996). Mitochondrial Defect in Huntington ' s Disease Caudate Nucleus. *Annals of Neurology*:385–389.

Guidetti, P., Charles, V., Chen, E.Y., Reddy, P.H., Kordower, J.H., Whetsell, W.O., Schwarcz, R., *et al.* (2001). Early degenerative changes in transgenic mice expressing mutant huntingtin involve dendritic abnormalities but no impairment of mitochondrial energy production. *Experimental neurology* **169**:340–350.

Gulacsi, A. a and Anderson, S. a (2008).  $\beta$ -catenin-mediated Wnt signaling regulates neurogenesis in the ventral telencephalon. *Nat Neurosci.* **11**:1383–1391.

Gulacsi, A. and Anderson, S.A. (2006). Shh maintains Nkx2.1 in the MGE by a Gli3-independent mechanism. *Cerebral Cortex* **16**:89–95.

Gunhaga, L., Jessell, T.M. and Edlund, T. (2000). Sonic hedgehog signaling at gastrula stages specifies ventral telencephalic cells in the chick embryo. *Development* **127**:3283–93.

Gunhaga, L., Marklund, M., Sjödal, M., Hsieh, J.-C., Jessell, T.M. and Edlund, T. (2003). Specification of dorsal telencephalic character by sequential Wnt and FGF signaling. *Nature neuroscience* **6**:701–707.

Gusella, J.F., Wexler, N.S., Conneally, P.M., Naylor, S.L., Anderson, M. a, Tanzi, R.E., Watkins, P.C., *et al.* (1983). A polymorphic DNA marker genetically linked to Huntington ' s disease. *Nature* **306**:234–238.

Gutin, G., Fernandes, M., Palazzolo, L., Paek, H., Yu, K., Ornitz, D.M., McConnell, S.K., *et al.* (2006). FGF signalling generates ventral telencephalic cells independently of SHH. *Development* **133**:2937–2946.

Halpain, S., Girault, J. a and Greengard, P. (1990). Activation of NMDA receptors induces dephosphorylation of DARPP-32 in rat striatal slices. *Nature* **343**:369–372.

Han, I., You, M., Kordower H, J., Brady T, S. and Morfini A, G. (2010). Differential

- vulnerability of neurons in Huntington's disease: The role of cell type-specific features. *Journal of neurochemistry* **113**:1073–1091.
- Hanna, J., Saha, K., Pando, B., van Zon, J., Lengner, C.J., Creighton, M.P., van Oudenaarden, A., *et al.* (2009). Direct cell reprogramming is a stochastic process amenable to acceleration. *Nature* **462**:595–601.
- Hao, J., Ho, J.N., Lewis, J. a, Karim, K. a, Daniels, R.N., R, P., Hopkins, C.R., *et al.* (2010). In Vivo Structure Activity Relationship Study of Dorsomorphin Analogs Identifies Selective VEGF and BMP Inhibitors. *Chem Biol* **5**:245–253.
- Hawkins, K., Joy, S. and McKay, T. (2014). Cell signalling pathways underlying induced pluripotent stem cell reprogramming. *World Journal of Stem Cells* **6**:620.
- Hay, D.C., Sutherland, L., Clark, J. and Burdon, T. (2004). Oct-4 knockdown induces similar patterns of endoderm and trophoblast differentiation markers in human and mouse embryonic stem cells. *Stem cells* **22**:225–235.
- Heinsen, H., Strik, M., Bauer, M., Luther, K., Ulmar, G., Gangnus, D., Jungkunz, G., *et al.* (1994). Cortical and striatal neurone number in Huntington's disease. *Acta Neuropathologica* **88**:320–333.
- Heisenberg, C.P., Houart, C., Take-Uchi, M., Rauch, G.J., Young, N., Coutinho, P., Masai, I., *et al.* (2001). A mutation in the Gsk3-binding domain of zebrafish masterblind/Axin1 leads to a fate transformation of telencephalon and eyes to diencephalon. *Genes and Development* **15**:1427–1434.
- Hemmati-Brivanlou, A. and Melton, D. a. (1994). Inhibition of activin receptor signaling promotes neuralization in xenopus. *Cell* **77**:273–281.
- Hemmings, H.C., Greengard, P., Tung, H.Y. and Cohen, P. (1984). DARPP-32, a dopamine-regulated neuronal phosphoprotein, is a potent inhibitor of protein phosphatase-1. *Nature* **310**:503–5.
- Houart, C., Caneparo, L., Heisenberg, C.P., Barth, K.A., Take-Uchi, M. and Wilson, S.W. (2002). Establishment of the telencephalon during gastrulation by local antagonism of Wnt signaling. *Neuron* **35**:255–265.
- Hsieh-Li, H.M., Witte, D.P., Szucsik, J.C., Weinstein, M., Li, H. and Potter, S.S. (1995). Gsh-2, a murine homeobox gene expressed in the developing brain. *Mechanisms of development* **50**:177–186.
- Hu, Y., Qu, Z., Cao, S., Li, Q., Ma, L., Krencik, R., Xu, M., *et al.* (2016). Directed differentiation of basal forebrain cholinergic neurons from human pluripotent stem cells. *Journal of Neuroscience Methods* **266**:42–49.
- Huang, S.-M.A., Mishina, Y.M., Liu, S., Cheung, A., Stegmeier, F., Michaud, G.A., Charlat, O., *et al.* (2009). Tankyrase inhibition stabilizes axin and antagonizes Wnt signalling. *Nature* **461**:614–620.
- Huangfu, D., Maehr, R., Guo, W., Eijkelenboom, A., Snitow, M., Chen, A.E. and Melton, D. a (2008). Induction of pluripotent stem cells by defined factors is greatly improved by small-molecule compounds. *Nature biotechnology* **26**:795–797.
- Huntington's disease collaborative research (1993). A novel gene containing a trinucleotide repeat that is expanded and unstable on Huntington's disease chromosomes. The Huntington's Disease Collaborative Research Group. *Cell* **72**:971–983.

- Hyslop, L., Stojkovic, M., Armstrong, L., Walter, T., Stojkovic, P., Przyborski, S., Herbert, M., *et al.* (2005). Downregulation of NANOG induces differentiation of human embryonic stem cells to extraembryonic lineages. *Stem cells* **23**:1035–1043.
- Itsykson, P., Ilouz, N., Turetsky, T., Goldstein, R.S., Pera, M.F., Fishbein, I., Segal, M., *et al.* (2005). Derivation of neural precursors from human embryonic stem cells in the presence of noggin. *Molecular and Cellular Neuroscience* **30**:24–36.
- Jackson, G.R., Salecker, I., Dong, X., Yao, X., Arnheim, N., Faber, P.W., MacDonald, M.E., *et al.* (1998). Polyglutamine-expanded human huntingtin transgenes induce degeneration of Drosophila photoreceptor neurons. *Neuron* **21**:633–642.
- James, D., Levine, A.J., Besser, D. and Hemmati-Brivanlou, A. (2005). TGFbeta/activin/nodal signaling is necessary for the maintenance of pluripotency in human embryonic stem cells. *Development* **132**:1273–1282.
- Jenkins, B.G., Koroshetz, W.J., Beal, M.F. and Rosen, B.R. (1993). Evidence for impairment of energy metabolism in vivo in Huntington's disease using localized <sup>1</sup>H NMR spectroscopy. *Neurology* **43**:2689–2689.
- Jenkins, B.G., Rosas, H.D., Chen, Y.C., Makabe, T., Myers, R., MacDonald, M., Rosen, B.R., *et al.* (1998). <sup>1</sup>H NMR spectroscopy studies of Huntington's disease: correlations with CAG repeat numbers. *Neurology* **50**:1357–1365.
- Jeon, I., Lee, N., Li, J.Y., Park, I.H., Park, K.S., Moon, J., Shim, S.H., *et al.* (2012). Neuronal properties, in vivo effects, and pathology of a Huntington's disease patient-derived induced pluripotent stem cells. *Stem Cells* **30**:2054–2062.
- Jiang, X., Gwyne, Y., McKeown, S.J., Bronner-Fraser, M., Lutzko, C. and Lawlor, E.R. (2009). Isolation and characterization of neural crest stem cells derived from in vitro-differentiated human embryonic stem cells. *Stem cells and development* **18**:1059–1070.
- Jin, Z., Liu, L., Bian, W., Chen, Y., Xu, G., Cheng, L. and Jing, N. (2009). Different transcription factors regulate nestin gene expression during P19 cell neural differentiation and central nervous system development. *Journal of Biological Chemistry* **284**:8160–8173.
- Joannides, A., Fiore-Hériché, C., Battersby, A., Athauda-Arachchi, P., Bouhon, I., Williams, L., Westmore, K., *et al.* (2007). A Scalable and Defined System for Generating Neural Stem Cells from Human Embryonic Stem Cells. *Stem Cells* **25**:731–737.
- Juopperi, T.A., Kim, W., Chiang, C.-H., Yu, H., Margolis, R.L., Ross, C.A., Ming, G., *et al.* (2012). Astrocytes generated from patient induced pluripotent stem cells recapitulate features of Huntington's disease patient cells. *Molecular Brain* **5**:17.
- Kemp, C., Willems, E., Abdo, S., Lambiv, L. and Leyns, L. (2005). Expression of all Wnt genes and their secreted antagonists during mouse blastocyst and postimplantation development. *Developmental Dynamics* **233**:1064–1075.
- Khokha, M.K., Yeh, J., Grammer, T.C. and Harland, R.M. (2005). Depletion of three BMP antagonists from Spemann's organizer leads to a catastrophic loss of dorsal structures. *Developmental Cell* **8**:401–411.
- Kiecker, C. and Lumsden, A. (2005). Compartments and their boundaries in vertebrate brain development. *Nature Reviews Neuroscience* [Online] **6**:553–564.
- Kim, C.H., Oda, T., Itoh, M., Jiang, D., Artinger, K.B., Chandrasekharappa, S.C., Driever, W., *et al.* (2000). Repressor activity of Headless/Tcf3 is essential for vertebrate head

formation. *Nature* **407**:913–6.

Kim, D., Kim, C.-H., Moon, J.-I., Chung, Y.-G., Chang, M.-Y., Han, B.-S., Ko, S., *et al.* (2009). Generation of human induced pluripotent stem cells by direct delivery of reprogramming proteins. *Cell stem cell* **4**:472–476.

Kim, D.S., Lee, J.S., Leem, J.W., Huh, Y.J., Kim, J.Y., Kim, H.S., Park, I.H., *et al.* (2010). Robust enhancement of neural differentiation from human ES and iPS cells regardless of their innate difference in differentiation propensity. *Stem Cell Reviews and Reports* **6**:270–281.

Kim, J.B., Sebastiano, V., Wu, G., Araúzo-Bravo, M.J., Sasse, P., Gentile, L., Ko, K., *et al.* (2009). Oct4-induced pluripotency in adult neural stem cells. *Cell* **136**:411–9.

Kim, T.-G., Yao, R., Monnell, T., Cho, J.-H., Vasudevan, A., Koh, A., Kumar T, P., *et al.* (2014). Efficient specification of interneurons from human Pluripotent stem cells by dorsoventral and rostrocaudal modulation. *Stem Cells* **32**:1789–1804.

Kimura, C., Yoshinaga, K., Tian, E., Suzuki, M., Aizawa, S. and Matsuo, I. (2000a). Visceral endoderm mediates forebrain development by suppressing posteriorizing signals. *Developmental biology* **225**:304–21.

Kimura, C., Yoshinaga, K., Tian, E., Suzuki, M., Aizawa, S. and Matsuo, I. (2000b). Visceral endoderm mediates forebrain development by suppressing posteriorizing signals. *Developmental biology* **225**:304–321.

Kin, R., Kam, T., Deng, Y., Chen, Y. and Zhao, H. (2012). Retinoic acid synthesis and functions in early embryonic development. *Cell & Bioscience* **2**:11.

Kirkeby, A., Grealish, S., Wolf, D. a., Nelander, J., Wood, J., Lundblad, M., Lindvall, O., *et al.* (2012). Generation of Regionally Specified Neural Progenitors and Functional Neurons from Human Embryonic Stem Cells under Defined Conditions. *Cell Reports* **1**:703–714.

Kishi, M., Mizuseki, K., Sasai, N., Yamazaki, H., Shiota, K., Nakanishi, S. and Sasai, Y. (2000). Requirement of Sox2-mediated signaling for differentiation of early Xenopus neuroectoderm. *Development* **127**:791–800.

Kohtz, J.D., Baker, D.P., Corte, G. and Fishell, G. (1998). Regionalization within the mammalian telencephalon is mediated by changes in responsiveness to Sonic Hedgehog. *Development* **125**:5079–5089.

Komiya, Y. and Habas, R. (2008). Wnt signal transduction pathways. *Organogenesis* **4**:68–75.

Kreitzer, F.R., Salomonis, N., Sheehan, A., Huang, M., Park, J.S., Spindler, M.J., Lizarraga, P., *et al.* (2013). A robust method to derive functional neural crest cells from human pluripotent stem cells. *American journal of stem cells* **2**:119–31.

Kriks, S., Shim, J.-W., Piao, J., Ganat, Y.M., Wakeman, D.R., Xie, Z., Carrillo-Reid, L., *et al.* (2011). Dopamine neurons derived from human ES cells efficiently engraft in animal models of Parkinson’s disease. *Nature* **480**:547–551.

Kroll, T.T. and O’Leary, D.D.M. (2005). Ventralized dorsal telencephalic progenitors in Pax6 mutant mice generate GABA interneurons of a lateral ganglionic eminence fate. *Proceedings of the National Academy of Sciences of the United States of America* **102**:7374–9.

- Kuhl, D.E., Markham, C.H., Metter, E.J., Riege, W.H., Phelps, M.E. and Mazziotta, J.C. (1985). Local cerebral glucose utilization in symptomatic and presymptomatic Huntington's disease. *Research publications - Association for Research in Nervous and Mental Disease* **63**:199–209..
- Kuschel, S., Rütther, U. and Theil, T. (2003). A disrupted balance between Bmp/Wnt and Fgf signaling underlies the ventralization of the Gli3 mutant telencephalon. *Developmental Biology* **260**:484–495.
- Kuwert, T., Boecker, H., Titz, H., Herzog, H., Wang, B.C., Nayak, U., Feinendegen, L.E., *et al.* (1993). Striatal glucose consumption in chorea-free subjects at risk of Huntington's disease. *Journal of Neurology* **241**:31–36.
- Kuwert, T., Lange, H.W., Langen, K.J., Herzog, H., Aulich, a and Feinendegen, L.E. (1990). Cortical and subcortical glucose consumption measured by PET in patients with Huntington's disease. *Brain : a journal of neurology* **113 ( Pt 5)**:1405–1423.
- de la Monte, S.M., Vonsattel, J.P. and Richardson, E.P. (1988). Morphometric demonstration of atrophic changes in the cerebral cortex, white matter, and neostriatum in Huntington's disease. *Journal of neuropathology and experimental neurology* **47**:516–25.
- Langbehn, D.R., Brinkman, R.R., Falush, D., Paulsen, J.S. and Hayden, M.R. (2004). A new model for prediction of the age of onset and penetrance for Huntington's disease based on CAG length. *Clinical Genetics* **65**:267–277.
- Larsen, K.B., Lutterodt, M.C., Møllgård, K. and Møller, M. (2010). Expression of the homeobox genes OTX2 and OTX1 in the early developing human brain. *The journal of histochemistry and cytochemistry : official journal of the Histochemistry Society* **58**:669–678.
- Lee, H., Shamy, G. Al, Elkabetz, Y., Schofield, C.M., Harrision, N.L., Panagiotakos, G., Succi, N.D., *et al.* (2007). Directed differentiation and transplantation of human embryonic stem cell-derived motoneurons. *Stem cells* **25**:1931–1939.
- Leisman, G., Melillo, R. and Carrick, F.R. (2012). Clinical Motor and Cognitive Neurobehavioral Relationships in the Basal Ganglia. *Basal Ganglia - An Integrative View*:1–30.
- Li, C., Zhou, J., Shi, G., Ma, Y., Yang, Y., Gu, J., Yu, H., *et al.* (2009). Pluripotency can be rapidly and efficiently induced in human amniotic fluid-derived cells. *Human Molecular Genetics* **18**:4340–4349.
- Li, H., Wagner, E., McCaffery, P., Smith, D., Andreadis, A. and Dräger, U.C. (2000). A retinoic acid synthesizing enzyme in ventral retina and telencephalon of the embryonic mouse. *Mechanisms of Development* **95**:283–289.
- Li, W., Zhou, H., Abujarour, R., Zhu, S., Joo, J.Y., Lin, T., Hao, E., *et al.* (2009). Generation of Human Induced Pluripotent Stem Cells in the Absence of Exogenous Sox2. *Stem cells* **27**:2992–3000.
- Li, X., Zhang, X., Johnson, M.A., Wang, Z.-B., Lavaute, T. and Zhang, S.-C. (2009). Coordination of sonic hedgehog and Wnt signaling determines ventral and dorsal telencephalic neuron types from human embryonic stem cells. *Development* **136**:4055–4063.
- Liao, J., Wu, Z., Wang, Y., Cheng, L., Cui, C., Gao, Y., Chen, T., *et al.* (2008). Enhanced efficiency of generating induced pluripotent stem (iPS) cells from human somatic cells by a combination of six transcription factors. *Cell research* **18**:600–603.

- Liao, W.-L. and Liu, F.-C. (2005). RARbeta isoform-specific regulation of DARPP-32 gene expression: an ectopic expression study in the developing rat telencephalon. *The European journal of neuroscience* **21**:3262–3268.
- Liao, W.L., Tsai, H.-C., Wang, H.-F., Chang, J., Lu, K.-M., Wu, H.-L., Lee, Y.-C., *et al.* (2008). Modular patterning of structure and function of the striatum by retinoid receptor signaling. *Proceedings of the National Academy of Sciences of the United States of America* **105**:6765–70.
- Liao, W.L., Wang, H.F., Tsai, H.C., Chambon, P., Wagner, M., Kakizuka, A. and Liu, F.C. (2005). Retinoid signaling competence and RAR??-mediated gene regulation in the developing mammalian telencephalon. *Developmental Dynamics* **232**:887–900.
- Lin, C.H., Tallaksen-Greene, S., Chien, W.M., Cearley, J. a, Jackson, W.S., Crouse, A.B., Ren, S., *et al.* (2001). Neurological abnormalities in a knock-in mouse model of Huntington's disease. *Human molecular genetics* **10**:137–44.
- Lin, T., Ambasadhan, R., Yuan, X., Li, W., Hilcove, S., Abujarour, R., Lin, X., *et al.* (2009). A chemical platform for improved induction of human iPSCs. *Nature Methods* **6**:805–808.
- Liu, H., Ye, Z., Kim, Y., Sharkis, S. and Jang, Y.-Y. (2010). Generation of endoderm-derived human induced pluripotent stem cells from primary hepatocytes. *Hepatology (Baltimore, Md.)* **51**:1810–9..
- Liu, J.K., Ghattas, I., Liu, S., Chen, S. and Rubenstein, J.L.R. (1997). Dlx genes encode DNA-binding proteins that are expressed in an overlapping and sequential pattern during basal ganglia differentiation. *Developmental Dynamics* **210**:498–512.
- Liu, P., Wakamiya, M., Shea, M.J., Albrecht, U., Behringer, R.R. and Bradley, a (1999). Requirement for Wnt3 in vertebrate axis formation. *Nature genetics* **22**:361–365.
- Liu, X., Sun, H., Qi, J., Wang, L., He, S., Liu, J., Feng, C., *et al.* (2013). Sequential introduction of reprogramming factors reveals a time-sensitive requirement for individual factors and a sequential EMT-MET mechanism for optimal reprogramming. *Nature Cell Biology* **15**:829–838.
- Liu, Y.F. (1998). CELL BIOLOGY AND METABOLISM : Expression of Polyglutamine-expanded Huntingtin Activates the SEK1-JNK Pathway and Induces Apoptosis in a Hippocampal N. *Cell Biology and Metabolism* **273**:28873-.
- Long, J.E., Swan, C., Liang, W.S., Cobos, I., Potter, G.B. and Rubenstein, J.L. (2009). Dlx1&2 and Mash1 transcription factors control striatal patterning and differentiation through parallel and overlapping pathways. *J Comp Neurol* **512**:556–572.
- Lu, C.C., Brennan, J. and Robertson, E.J. (2001). From fertilization to gastrulation: axis formation in the mouse embryo. *Current Opinion in Genetics & Development* **11**:384–392.
- Lunkes, A. and Mandel, J.L. (1998). A cellular model that recapitulates major pathogenic steps of Huntington's disease. *Human Molecular Genetics* **7**:1355–1361.
- Lupo, G., Novorol, C., Smith, J.R., Vallier, L., Miranda, E., Alexander, M., Biagioni, S., *et al.* (2013). Multiple roles of Activin/Nodal, bone morphogenetic protein, fibroblast growth factor and Wnt/ $\beta$ -catenin signalling in the anterior neural patterning of adherent human embryonic stem cell cultures. *Open biology* **3**:120167.

- Ma, L., Hu, B., Liu, Y., Vermilyea, S., Liu, H., Gao, L., Sun, Y., *et al.* (2012). Human Embryonic Stem Cell-Derived GABA Neurons Correct Locomotion Deficits in Quinolinic Acid-Lesioned Mice. *18*:1199–1216.
- Machold, R., Hayashi, S., Rutlin, M., Muzumdar, M.D., Nery, S., Corbin, J.G., Gritli-Linde, A., *et al.* (2003). Sonic hedgehog is required for progenitor cell maintenance in telencephalic stem cell niches. *Neuron* **39**:937–950.
- Machon, O., Backman, M., Machonova, O., Kozmik, Z., Vacik, T., Andersen, L. and Krauss, S. (2007). A dynamic gradient of Wnt signaling controls initiation of neurogenesis in the mammalian cortex and cellular specification in the hippocampus. *Developmental Biology* **311**:223–237.
- Maden, M. (2002). Retinoid signalling in the development of the central nervous system. *Nature Reviews Neuroscience* [Online] **3**:843–853.
- Maekawa, M., Yamaguchi, K., Nakamura, T., Shibukawa, R., Kodanaka, I., Ichisaka, T., Kawamura, Y., *et al.* (2011). Direct reprogramming of somatic cells is promoted by maternal transcription factor Glis1. *Nature* **474**:225–229.
- Maira, M., Long, J.E., Lee, A.Y., Rubenstein, J.L.R. and Stifani, S. (2010). Role for TGF- $\beta$  superfamily signaling in telencephalic GABAergic neuron development. *Journal of Neurodevelopmental Disorders* **2**:48–60.
- Mali, P., Ye, Z., Hommond, H.H., Yu, X., Lin, J., Chen, G., Zou, J., *et al.* (2008). Improved efficiency and pace of generating induced pluripotent stem cells from human adult and fetal fibroblasts. *Stem cells* **26**:1998–2005.
- Mangiarini, L., Sathasivam, K., Seller, M., Cozens, B., Harper, A., Hetherington, C., Lawton, M., *et al.* (1996). Exon I of the HD gene with an expanded CAG repeat is sufficient to cause a progressive neurological phenotype in transgenic mice. *Cell* **87**:493–506.
- Manuel, M., Martynoga, B., Yu, T., West, J.D., Mason, J.O. and Price, D.J. (2010). The transcription factor Foxg1 regulates the competence of telencephalic cells to adopt subpallial fates in mice. *Development* **137**:487–97.
- Manuel, M.N., Martynoga, B., Molinek, M.D., Quinn, J.C., Kroemmer, C., Mason, J.O. and Price, D.J. (2011). The transcription factor Foxg1 regulates telencephalic progenitor proliferation cell autonomously, in part by controlling Pax6 expression levels. *Neural development* **6**:9.
- Marklund, M., Sjödal, M., Beehler, B.C., Jessell, T.M., Edlund, T. and Gunhaga, L. (2004). Retinoic acid signalling specifies intermediate character in the developing telencephalon. *Development* **131**:4323–4332.
- Maroof, A., Keros, S., Tyson, J. and Ying, S. (2013). Directed differentiation and functional maturation of cortical interneurons from human embryonic stem cells. *Cell Stem Cell* **12**:559–572.
- Martindale, D., Hackam, A., Wiczorek, A., Ellerby, L., Wellington, C., McCutcheon, K., Singaraja, R., *et al.* (1998). Length of huntingtin and its polyglutamine tract influences localization and frequency of intracellular aggregates. *Nature genetics* **18**:150–4.
- Martynoga, B., Morrison, H., Price, D.J. and Mason, J.O. (2005). Foxg1 is required for specification of ventral telencephalon and region-specific regulation of dorsal telencephalic precursor proliferation and apoptosis. *Developmental biology* **283**:113–27.

- Mateizel, I., De Temmerman, N., Ullmann, U., Cauffman, G., Sermon, K., Van de Velde, H., De Rycke, M., *et al.* (2006). Derivation of human embryonic stem cell lines from embryos obtained after IVF and after PGD for monogenic disorders. *Human Reproduction* **21**:503–511.
- Matin, M.M., Walsh, J.R., Gokhale, P.J., Draper, J.S., Bahrami, A.R., Morton, I., Moore, H.D., *et al.* (2004). Specific knockdown of Oct4 and beta2-microglobulin expression by RNA interference in human embryonic stem cells and embryonic carcinoma cells. *Stem cells* **22**:659–668.
- Medicinenet.com (2010). *Stem Cells Symptoms, Treatment, Causes - Why Are Stem Cells Important?*- *MedicineNet*[ *Online*]. Available at: [http://www.medicinenet.com/stem\\_cells/page2.htm](http://www.medicinenet.com/stem_cells/page2.htm)
- Menalled, L., El-Khodori, B.F., Patry, M., Suárez-Fariñas, M., Orenstein, S.J., Zahasky, B., Leahy, C., *et al.* (2009). Systematic behavioral evaluation of Huntington's disease transgenic and knock-in mouse models. *Neurobiology of disease* **35**:319–36.
- Menalled, L.B., Sison, J.D., Dragatsis, I., Zeitlin, S. and Chesselet, M.F. (2003). Time course of early motor and neuropathological anomalies in a knock-in mouse model of Huntington's disease with 140 CAG repeats. *Journal of Comparative Neurology* **465**:11–26.
- Menendez, L., Yatskievych, T.A., Antin, P.B. and Dalton, S. (2012). Wnt signaling and a Smad pathway blockade direct the differentiation of human pluripotent stem cells to multipotent neural crest cells. *Proceedings of the National Academy of Sciences* **109**:9220–9220.
- Milnerwood, A.J., Kaufman, A.M., Sepers, M.D., Gladding, C.M., Zhang, L., Wang, L., Fan, J., *et al.* (2012). Mitigation of augmented extrasynaptic NMDAR signaling and apoptosis in cortico-striatal co-cultures from Huntington's disease mice. *Neurobiology of Disease* **48**:40–51.
- Minami, I., Yamada, K., Otsuji, T.G., Yamamoto, T., Shen, Y., Otsuka, S., Kadota, S., *et al.* (2012). A Small Molecule that Promotes Cardiac Differentiation of Human Pluripotent Stem Cells under Defined, Cytokine- and Xeno-free Conditions. *Cell Reports* **2**:1448–1460.
- Mitsui, K., Tokuzawa, Y., Itoh, H., Segawa, K., Murakami, M., Takahashi, K., Maruyama, M., *et al.* (2003). The homeoprotein nanog is required for maintenance of pluripotency in mouse epiblast and ES cells. *Cell* **113**:631–642.
- Molotkova, N., Molotkov, A. and Duester, G. (2007). Role of retinoic acid during forebrain development begins late when Raldh3 generates retinoic acid in the ventral subventricular zone. *Developmental Biology* **303**:601–610.
- Monuki, E.S., Porter, F.D. and Walsh, C. a. (2001). Patterning of the dorsal telencephalon and cerebral cortex by a roof plate-lhx2 pathway. *Neuron* **32**:591–604.
- Morizane, A., Doi, D., Kikuchi, T., Nishimura, K. and Takahashi, J. (2011). Small-molecule inhibitors of bone morphogenic protein and activin/nodal signals promote highly efficient neural induction from human pluripotent stem cells. *Journal of Neuroscience Research* **89**:117–126.
- Mukhopadhyay, M., Shtrom, S., Rodriguez-Esteban, C., Chen, L., Tsukui, T., Gomer, L., Dorward, D.W., *et al.* (2001). Dickkopf1 Is Required for Embryonic Head Induction and Limb Morphogenesis in the Mouse. *Developmental Cell* **1**:423–434.

- Nakagawa, M., Koyanagi, M., Tanabe, K., Takahashi, K., Ichisaka, T., Aoi, T., Okita, K., *et al.* (2008). Generation of induced pluripotent stem cells without Myc from mouse and human fibroblasts. *Nat.Biotechnol.* **26**:101–106.
- Nasir, J., Floresco, S. and O’Kusky, J. (1995). Targeted disruption of the Huntington’s disease gene results in embryonic lethality and behavioral and morphological changes in heterozygotes. *Cell* **81**:811–823.
- Nat, R., Salti, A., Suci, L., Ström, S. and Dechant, G. (2012). Pharmacological Modulation of the Hedgehog Pathway Differentially Affects Dorsal/Ventral Patterning in Mouse and Human Embryonic Stem Cell Models of Telencephalic Development. *Stem Cells and Development* **21**:1016–1046.
- Neely, M.D., Litt, M.J., Tidball, A.M., Li, G.G., Aboud, A.A., Hopkins, C.R., Chamberlin, R., *et al.* (2012). DMH1, a highly selective small molecule BMP inhibitor promotes neurogenesis of hiPSCs: Comparison of PAX6 and SOX1 expression during neural induction. *ACS Chemical Neuroscience* **3**:482–491.
- Nery, S., Wichterle, H. and Fishell, G. (2001). Sonic hedgehog contributes to oligodendrocyte specification in the mammalian forebrain. *Development* **128**:527–540.
- Nicholas, C.R., Chen, J., Tang, Y., Southwell, D.G., Vogt, D., Arnold, C.M., Chen, Y.J., *et al.* (2014). Functional maturation of hPSC-derived forebrain interneurons requires an extended timeline and mimics human neural development. **12**:573–586.
- Nichols, J., Zevnik, B., Anastassiadis, K., Niwa, H., Klewe-Nebenius, D., Chambers, I., Schöler, H., *et al.* (1998). Formation of pluripotent stem cells in the mammalian embryo depends on the POU transcription factor Oct4. *Cell* **95**:379–391.
- Niclis, J.C., Pinar, A., Haynes, J.M., Alsanie, W., Jenny, R., Dottori, M. and Cram, D.S. (2013). Characterization of forebrain neurons derived from late-onset Huntington’s disease human embryonic stem cell lines. *Frontiers in cellular neuroscience* **7**:37.
- Niclis, J.C., Trounson, A.O., Dottori, M., Ellisdon, A.M., Bottomley, S.P., Verlinsky, Y. and Cram, D.S. (2009). Human embryonic stem cell models of Huntington disease. *Reproductive biomedicine* **19**:106–113.
- Nicoleau, C., Varela, C., Bonnefond, C., Maury, Y., Bugi, A., Aubry, L., Viegas, P., *et al.* (2013). Embryonic stem cells neural differentiation qualifies the role of Wnt/ $\beta$ -Catenin signals in human telencephalic specification and regionalization. *Stem Cells* **31**:1763–1774.
- Niwa, H., Miyazaki, J. and Smith, a G. (2000). Quantitative expression of Oct-3/4 defines differentiation, dedifferentiation or self-renewal of ES cells. *Nature genetics* **24**:372–376.
- Nóbrega-pereira, S., Kessar, N., Du, T., Kimura, S., Anderson, S.A. and Marín, O. (2008). Postmitotic Nkx2-1 controls the migration of telencephalic interneurons by direct repression of guidance receptors. *Neuron* **59**:733–745.
- Ohkubo, Y., Chiang, C. and Rubenstein, J.L.R. (2002). Coordinate regulation and synergistic actions of BMP4, SHH and FGF8 in the rostral prosencephalon regulate morphogenesis of the telencephalic and optic vesicles. *Neuroscience* **111**:1–17
- .Okita, K., Ichisaka, T. and Yamanaka, S. (2007). Generation of germline-competent induced pluripotent stem cells. *Nature* **448**:313–317.
- Okita, K., Yamakawa, T., Matsumura, Y., Sato, Y., Amano, N., Watanabe, A., Goshima, N., *et al.* (2013). An efficient nonviral method to generate integration-free human-induced

- pluripotent stem cells from cord blood and peripheral blood cells. *Stem Cells* **31**:458–466.
- Onorati, M., Castiglioni, V., Biasci, D., Cesana, E., Menon, R., Vuono, R., Talpo, F., *et al.* (2014). Molecular and functional definition of the developing human striatum. *Nature Neuroscience* **17**:1804–1815.
- Ouimet, C.C., Langley-Gullion, K.C. and Greengard, P. (1998). Quantitative immunocytochemistry of DARPP-32-expressing neurons in the rat caudatoputamen. *Brain Research* **808**:8–12.
- Paek, H., Gutin, G. and Hébert, J.M. (2009). FGF signaling is strictly required to maintain early telencephalic precursor cell survival. *Development (Cambridge, England)* **136**:2457–65.
- Panganiban, G. and Rubenstein, J.L.R. (2002). Developmental functions of the Distal-less/Dlx homeobox genes. *Development* **129**:4371–4386.
- Pankratz, M., Li, X., Lavaute, T., Lyons, E., Chen, X. and Zhang, S. (2007). Directed Neural Differentiation of Human Embryonic Stem Cells via an Obligated Primitive Anterior Stage. *Psychiatry: Interpersonal and Biological Processes* **25**:1511–1520.
- Park, I., Arora, N., Huo, H., Maherali, N., Shimamura, A., Lensch, M.W., Cowan, C., *et al.* (2008). Disease-specific induced pluripotent stem (iPS) cells. *October* **134**:877–886.
- Parras, C.M., Galli, R., Britz, O., Soares, S., Galichet, C., Battiste, J., Johnson, J.E., *et al.* (2004). Mash1 specifies neurons and oligodendrocytes in the postnatal brain. *The EMBO journal* **23**:4495–505.
- Pei, Z., Wang, B., Chen, G., Nagao, M., Nakafuku, M. and Campbell, K. (2011). Homeobox genes *Gsx1* and *Gsx2* differentially regulate telencephalic progenitor maturation. *Proceedings of the National Academy of Sciences* **108**:1675–1680.
- Pera, M.F., Andrade, J., Houssami, S., Reubinoff, B., Trounson, A., Stanley, E.G., Ward-van Oostwaard, D., *et al.* (2004). Regulation of human embryonic stem cell differentiation by BMP-2 and its antagonist noggin. *Journal of cell science* **117**:1269–1280.
- Perrier, A.L., Tabar, V., Barberi, T., Rubio, M.E., Bruses, J., Topf, N., Harrison, N.L., *et al.* (2004). Derivation of midbrain dopamine neurons from human embryonic stem cells. *Proceedings of the National Academy of Sciences* **101**:12543–12548.
- Poitras, L., Ghanem, N., Hatch, G. and Ekker, M. (2007). The proneural determinant MASH1 regulates forebrain *Dlx1/2* expression through the I12b intergenic enhancer. *Development* **134**:1755–1765.
- Pouladi, M. a, Morton, a J. and Hayden, M.R. (2013). Choosing an animal model for the study of Huntington’s disease. *Nature reviews. Neuroscience* **14**:708–21.
- Powers, W.J., Videen, T.O., Markham, J., McGee-Minnich, L., Antenor-Dorsey, J. V, Hershey, T. and Perlmutter, J.S. (2007). Selective defect of in vivo glycolysis in early Huntington’s disease striatum. *Proceedings of the National Academy of Sciences of the United States of America* **104**:2945–2949.
- Prensa, L., Gimenez-Amaya Manuel, J. and Parent, A. (1999). Chemical Heterogeneity of the Striosomal Compartment in the Human Striatum. *The Journal of comparative neurology* **413**:603–618.
- Qu, X., Liu, T., Song, K., Li, X. and Ge, D. (2012). Induced pluripotent stem cells generated from human adipose-derived stem cells using a non-viral polycistronic plasmid

in feeder-free conditions. *PLoS one* **7**:e48161.

Van Raamsdonk, J., J. P., DA, R., N, B., AW, V., MR, H. and BR., L. (2005). Loss of wild-type huntingtin influences motor dysfunction and survival in the YAC128 mouse model of Huntington disease. *PLoS one* **14**:1379–1392.

Rajaii, F., Bitzer, Z.T., Xu, Q. and Sockanathan, S. (2008). Expression of the dominant negative retinoid receptor, RAR403, alters telencephalic progenitor proliferation, survival, and cell fate specification. *Developmental Biology* **316**:371–382.

Rallu, M., Machold, R., Gaiano, N., Corbin, J.G., McMahon, A.P. and Fishell, G. (2002). Dorsorostral patterning is established in the telencephalon of mutants lacking both Gli3 and Hedgehog signaling. *Development* **129**:4963–4974.

Ramaswamy, S., McBride, J.L. and Kordower, J.H. (2007). Animal models of Huntington's disease. *ILAR J* **48**:356–373.

Richfield, E.K., Maguire-Zeiss, K. a., Vonkeman, H.E. and Voorn, P. (1995). Preferential loss of preproenkephalin versus preprotachykinin neurons from the striatum of Huntington's disease patients. *Annals of Neurology* **38**:852–861.

Romero, E., Cha, G.H., Verstreken, P., Ly, C. V., Hughes, R.E., Bellen, H.J. and Botas, J. (2008). Suppression of Neurodegeneration and Increased Neurotransmission Caused by Expanded Full-Length Huntingtin Accumulating in the Cytoplasm. *Neuron* **57**:27–40.

Rosas, H.D., Koroshetz, W.J., Chen, Y.I., Skeuse, C., Vangel, M., Cudkovicz, M.E., Caplan, K., *et al.* (2003). Evidence for more widespread cerebral pathology in early HD: An MRI-based morphometric analysis. *Neurology* **60**:1615–1620.

Rubinsztein, D.C., Leggo, J., Coles, R., Almqvist, E., Biancalana, V., Cassiman, J.J., Chotai, K., *et al.* (1996). Phenotypic characterization of individuals with 30-40 CAG repeats in the Huntington disease (HD) gene reveals HD cases with 36 repeats and apparently normal elderly individuals with 36-39 repeats. *American journal of human genetics* **59**:16–22.

Rymar, V. V., Sasseville, R., Luk, K.C. and Sadikot, A.F. (2004). Neurogenesis and Stereological Morphometry of Calretinin-Immunoreactive GABAergic Interneurons of the Neostriatum. *Journal of Comparative Neurology* **469**:325–339.

Samavarchi-Tehrani, P., Golipour, A., David, L., Sung, H.K., Beyer, T.A., Datti, A., Woltjen, K., *et al.* (2010). Functional genomics reveals a BMP-Driven mesenchymal-to-Epithelial transition in the initiation of somatic cell reprogramming. *Cell Stem Cell* **7**:64–77.

Sapp, E., Schwarz, C., Chase, K., Bhide, P.G., Young, A.B., Penney, J., Vonsattel, J.P., *et al.* (1997). Huntingtin localization in brains of normal and Huntington's disease patients. *Annals of neurology* **42**:604–12.

Sasai, Y. and De Robertis, E.M. (1997). Ectodermal patterning in vertebrate embryos. *Developmental biology* **182**:5–20.

Saudou, F., Finkbeiner, S., Devys, D. and Greenberg, M.E. (1998). Huntingtin acts in the nucleus to induce apoptosis but death does not correlate with the formation of intranuclear inclusions. *Cell* **95**:55–56.

Sawa, A., Tomoda, T. and Bae, B. (2003). Mechanisms of neuronal cell death in Huntington's disease. *Cytogenet Genome Res* **100**:287–95.

- Schneider, R. a, Hu, D., Rubenstein, J.L., Maden, M. and Helms, J. a (2001). Local retinoid signaling coordinates forebrain and facial morphogenesis by maintaining FGF8 and SHH. *Development* **128**:2755–2767.
- Schwarcz, R. and Köhler, C. (1983). Differential vulnerability of central neurons of the rat to quinolinic acid. *Neuroscience letters* **38**:85–90.
- Seriola, A., Spits, C., Simard, J.P., Hilven, P., Haentjens, P., Pearson, C.E. and Sermon, K. (2011). Huntington's and myotonic dystrophy hESCs: down-regulated trinucleotide repeat instability and mismatch repair machinery expression upon differentiation. *Human molecular genetics* **20**:176–85.
- Shanmugalingam, S., Houart, C., Picker, a, Reifers, F., Macdonald, R., Barth, a, Griffin, K., *et al.* (2000). *Ace/Fgf8* is required for forebrain commissure formation and patterning of the telencephalon. *Development* **127**:2549–2561.
- Shi, Y., Do, J.T., Desponts, C., Hahm, H.S., Sch??ler, H.R. and Ding, S. (2008). A Combined Chemical and Genetic Approach for the Generation of Induced Pluripotent Stem Cells. *Cell Stem Cell* **2**:525–528.
- Shi, Y., Kirwan, P. and Livesey, F.J. (2012). Directed differentiation of human pluripotent stem cells to cerebral cortex neurons and neural networks. *Nature Protocols* **7**:1836–1846.
- Shi, Y., Kirwan, P., Smith, J., Robinson, H.P. and Livesey, F.J. (2012). Human cerebral cortex development from pluripotent stem cells to functional excitatory synapses. *Nat Neurosci.* **15**:477–86.
- Shimamura, K., Hartigan, D.J., Martinez, S., Puelles, L. and Rubenstein, J.L. (1995). Longitudinal organization of the anterior neural plate and neural tube. *Development* **121**:3923–3933.
- Shimamura, K. and Rubenstein, J.L. (1997). Inductive interactions direct early regionalization of the mouse forebrain. *Development* **124**:2709–2718.
- Shinya, M., Koshida, S., Sawada, A., Kuroiwa, A. and Takeda, H. (2001). Fgf signalling through MAPK cascade is required for development of the subpallial telencephalon in zebrafish embryos. *Development* **128**:4153–4164.
- Singh, A.M., Reynolds, D., Cliff, T., Ohtsuka, S., Mattheyses, A.L., Sun, Y., Menendez, L., *et al.* (2012). Signaling network crosstalk in human pluripotent cells: A Smad2/3-regulated switch that controls the balance between self-renewal and differentiation. *Cell Stem Cell* **10**:312–326.
- Sinha, S. and Chen, J.K. (2006). Purmorphamine activates the Hedgehog pathway by targeting Smoothened. *Nature chemical biology* **2**:29–30.
- Slow, E.J., van Raamsdonk, J., Rogers, D., Coleman, S.H., Graham, R.K., Deng, Y., Oh, R., *et al.* (2003). Selective striatal neuronal loss in a YAC128 mouse model of Huntington disease. *Human Molecular Genetics* **12**:1555–1567.
- Smith, A. (2006). A glossary for stem-cell biology. *Nature* **441**:1060–1060.
- Smith, J.R., Vallier, L., Lupo, G., Alexander, M., Harris, W.A. and Pedersen, R.A. (2008). Inhibition of Activin/Nodal signaling promotes specification of human embryonic stem cells into neuroectoderm. *Developmental biology* **313**:107–17..
- Spemann, H. and Mangold, H. (1924). über Induktion von Embryonalanlagen durch Implantation artfremder Organisatoren. *Archiv für Mikroskopische Anatomie und*

*Entwicklungsmechanik* **100**:599–638..

Squitieri, F., Gellera, C., Cannella, M., Mariotti, C., Cislighi, G., Rubinsztein, D.C., Almqvist, E.W., *et al.* (2003). Homozygosity for CAG mutation in Huntington disease is associated with a more severe clinical course. *Brain* **126**:946–955.

Staal, F.J.T. and Clevers, H.C. (2005). WNT signalling and haematopoiesis: a WNT–WNT situation. *Nature Reviews Immunology* **5**:21–30.

Stack, E.C., Kubilus, J.K., Smith, K., Cormier, K., Del Signore, S.J., Guelin, E., Ryu, H., *et al.* (2005). Chronology of behavioral symptoms and neuropathological sequela in R6/2 Huntington’s disease transgenic mice. *Journal of Comparative Neurology* **490**:354–370.

Stamatakis, D., Ulloa, F., Tsoni, S. V., Mynett, A. and Briscoe, J. (2005). A gradient of Gli activity mediates graded Sonic Hedgehog signaling in the neural tube. *Genes and Development* **19**:626–641.

Stemcellhealthcare.com (2014). *Stem Cell Therapy & Spinal Cord Injury*. *StemcellsHealthCare.com*. [Online]. Available at: <http://www.stemcellshealthcare.com/stem-cell-therapy-spinal-cord-injury.html#respond>.

Storm, E.E., Garel, S., Borello, U., Hebert, J.M., Martinez, S., McConnell, S.K., Martin, G.R., *et al.* (2006). Dose-dependent functions of Fgf8 in regulating telencephalic patterning centers. *Development (Cambridge, England)* **133**:1831–1844.

Stoykova, A., Treichel, D., Hallonet, M. and Gruss, P. (2000). Pax6 Modulates the Dorsoventral Patterning of the Mammalian Telencephalon. *The Journal of Neuroscience* **20**:8042–8050.

Stoykova, a, Götz, M., Gruss, P. and Price, J. (1997). Pax6-dependent regulation of adhesive patterning, R-cadherin expression and boundary formation in developing forebrain. *Development* **124**:3765–3777.

Stoykova, a and Gruss, P. (1994). Roles of Pax-genes in developing and adult brain as suggested by expression patterns. *The Journal of neuroscience : the official journal of the Society for Neuroscience* **14**:1395–1412.

Straccia, M., Barriga, G.G., Sanders, P., Bombau, G., Carrere, J., Mairal, P.B., Vinh, N., *et al.* (2015). Quantitative high-throughput gene expression profiling of human striatal development to screen stem cell – derived medium spiny neurons. *Mol Ther Method Clin* **16**(2):15030.

Sumi, T., Tsuneyoshi, N., Nakatsuji, N. and Suemori, H. (2008). Defining early lineage specification of human embryonic stem cells by the orchestrated balance of canonical Wnt/beta-catenin, Activin/Nodal and BMP signaling. *Development* **135**:2969–2979.

Surmacz, B., Fox, H., Gutteridge, A., Lubitz, S. and Whiting, P. (2012). Directing differentiation of human embryonic stem cells toward anterior neural ectoderm using small molecules. *Stem cells* **30**:1875–84..

Sussel, L., Marin, O., Kimura, S. and Rubenstein, J.L. (1999). Loss of Nkx2.1 homeobox gene function results in a ventral to dorsal molecular respecification within the basal telencephalon: evidence for a transformation of the pallidum into the striatum. *Development* **126**:3359–3370.

Suzuki, A., Raya, A., Kawakami, Y., Morita, M., Matsui, T., Nakashima, K., Gage, F.H., *et al.* (2006). Maintenance of embryonic stem cell pluripotency by Nanog-mediated reversal of mesoderm specification. *Nat Clin Pract Cardiovasc Med*.

- Svenningsson, P., Nishi, A., Fisone, G., Girault, J.-A., Nairn, A.C. and Greengard, P. (2004). DARPP-32: an integrator of neurotransmission. *Annual review of pharmacology and toxicology* **44**:269–96.
- Szkandera, J., Kiesslich, T., Haybaeck, J., Gerger, A. and Pichler, M. (2013). Hedgehog signaling pathway in ovarian cancer. *International Journal of Molecular Sciences* **14**:1179–1196.
- Szucsik, J.C., Witte, D.P., Li, H., Pixley, S.K., Small, K.M. and Potter, S.S. (1997). Altered forebrain and hindbrain development in mice mutant for the Gsh-2 homeobox gene. *Developmental biology* **191**:230–242.
- Tabrizi, S.J., Cleeter, M.W.J., Xuereb, J., Taanman, J.W., Cooper, J.M. and Schapira, a. H. V (1999). Biochemical abnormalities and excitotoxicity in Huntington's disease brain. *Annals of Neurology* **45**:25–32.
- Takahashi, K., Tanabe, K., Ohnuki, M., Narita, M., Ichisaka, T., Tomoda, K. and Yamanaka, S. (2007). Induction of Pluripotent Stem Cells from Adult Human Fibroblasts by Defined Factors. *Cell* **131**:861–872.
- Takahashi, K. and Yamanaka, S. (2006). Induction of Pluripotent Stem Cells from Mouse Embryonic and Adult Fibroblast Cultures by Defined Factors. *Cell* **126**:663–676.
- Tam, P.P. and Steiner, K. a (1999). Anterior patterning by synergistic activity of the early gastrula organizer and the anterior germ layer tissues of the mouse embryo. *Development* **126**:5171–5179.
- Tao, W. and Lai, E. (1992). Telencephalon-restricted expression of BF-1, a new member of the HNF-3/fork head gene family, in the developing rat brain. *Neuron* **8**:957–966.
- Telezhkin, V., Schnell, C., Yarova, P., Yung, S., Cope, E., Hughes, A., Thompson, B.A., *et al.* (2016). Forced cell cycle exit and modulation of GABAA, CREB, and GSK3 $\beta$  signaling promote functional maturation of induced pluripotent stem cell-derived neurons. *American journal of physiology. Cell physiology* **310**:C520-41.
- The HD iPSC Consortium (2012). Induced pluripotent stem cells from patients with huntington's disease show cag-repeat-expansion-associated phenotypes. *Cell Stem Cell* **11**:264–278.
- Theil, T., Alvarez-Bolado, G., Walter, a and R  ther, U. (1999). Gli3 is required for Emx gene expression during dorsal telencephalon development. *Development* **126**:3561–3571.
- Thiery, J.P. and Sleeman, J.P. (2006). Complex networks orchestrate epithelial-mesenchymal transitions. *Nature reviews. Molecular cell biology* **7**:131–42.
- Thomas, P. and Beddington, R. (1996). Anterior primitive endoderm may be responsible for patterning the anterior neural plate in the mouse embryo. *Current Biology* **6**:1487–1496.
- Thomson, J. a, Itskovitz-Eldor, J., Shapiro, S.S., Waknitz, M. a, Swiergiel, J.J., Marshall, V.S. and Jones, J.M. (1998). Embryonic stem cell lines derived from human blastocysts. *Science* **282**:1145–1147.
- Thomson, M., Liu, S.J., Zou, L.N., Smith, Z., Meissner, A. and Ramanathan, S. (2011). Pluripotency factors in embryonic stem cells regulate differentiation into germ layers. *Cell* **145**:875–889..
- Tole, S., Ragsdale, C.W. and Grove, E. a (2000). Dorsoventral patterning of the

- telencephalon is disrupted in the mouse mutant extra-toes(J). *Developmental biology* **217**:254–265.
- Toresson, H. and Campbell, K. (2001). A role for Gsh1 in the developing striatum and olfactory bulb of Gsh2 mutant mice. *Development* **128**:4769–4780.
- Toresson, H., Mata de Urquiza, a, Fagerström, C., Perlmann, T. and Campbell, K. (1999). Retinoids are produced by glia in the lateral ganglionic eminence and regulate striatal neuron differentiation. *Development* **126**:1317–1326.
- Toresson, H., Potter, S.S. and Campbell, K. (2000). Genetic control of dorsal-ventral identity in the telencephalon: opposing roles for Pax6 and Gsh2. *Development* **127**:4361–4371.
- Trettel, F., Rigamonti, D., Hilditch-Maguire, P., Wheeler, V.C., Sharp, a H., Persichetti, F., Cattaneo, E., *et al.* (2000). Dominant phenotypes produced by the HD mutation in STHdh(Q111) striatal cells. *Human molecular genetics* **9**:2799–2809.
- Tropel, P., Tournois, J., Côme, J., Varela, C., Moutou, C., Fagner, P., Cailleret, M., *et al.* (2010). High-efficiency derivation of human embryonic stem cell lines following pre-implantation genetic diagnosis. *In vitro cellular & developmental biology. Animal* **46**:376–85..
- Trottier, Y., D, D., G, I., F, S., I, A., Y, L., C, W., *et al.* (1995). Cellular localization of the Huntington's disease protein and discrimination of the normal and mutated form. *Nature Genetics* **10**:196–201.
- Urist, M.R. (1965). Bone: formation by autoinduction. *Science* **150**:893–9.
- Vallier, L., Mendjan, S., Brown, S., Chng, Z., Teo, A., Smithers, L.E., Trotter, M.W.B., *et al.* (2009). Activin/Nodal signalling maintains pluripotency by controlling Nanog expression. *Development* **136**:1339–49.
- Vazin, T. and Freed, W.J. (2010). Human embryonic stem cells: Derivation, culture, and differentiation: A review. *Restor Neurol Neurosci* **28**:589–603.
- Velier, J., Kim, M., Schwarz, C., Kim, T.W., Sapp, E., Chase, K., Aronin, N., *et al.* (1998). Wild-type and mutant huntingtins function in vesicle trafficking in the secretory and endocytic pathways. *Experimental neurology* **152**:34–40.
- Vogt, J., Traynor, R. and Sapkota, G.P. (2011). The specificities of small molecule inhibitors of the TGFβ and BMP pathways. *Cellular Signalling* **3**:1831–1842.
- Vonsattel, J.-P. and DiFiglia, M. (1998). Huntington Disease. *J Neuropathology Exp Nueurology* **57(5)**:369-84.
- Vonsattel, J.P., Myers, R.H., Stevens, T.J., Ferrante, R.J., Bird, E.D. and Richardson, E.P. (1985). Neuropathological classification of Huntington's disease. *Journal of neuropathology and experimental neurology* **44**:559–77..
- Waclaw, R.R., Wang, B. and Campbell, K. (2004). The homeobox gene Gsh2 is required for retinoid production in the embryonic mouse telencephalon. *Development* **131**:4013–4020.
- Waddington, C.H. (1933). Induction by the primitive streak and its derivatives in the chick. *J. Exp. Biol.* **10**:38–46.
- Walaas, I.S., Aswad, D.W. and Greengard, P. (1983). A dopamine- and cyclic AMP-regulated phosphoprotein enriched in dopamine-innervated brain regions. *Nature* **301**.

- Walker, F.O. (2007). Huntington's disease. *Lancet* **369**:218–28.
- Wallace, D.C., Fan, W. and Procaccio, V. (2010). Mitochondrial energetics and therapeutics. *Annual review of pathology* **5**:297–348.
- Walshe, J. and Mason, I. (2003). Unique and combinatorial functions of Fgf3 and Fgf8 during zebrafish forebrain development. *Development* **130**:4337–4349.
- Wang, B., Long, J.E., Flandin, P., Pla, R., Waclaw, R.R., Campbell, K. and Rubenstein, J.L.R. (2013). Loss of Gsx1 and Gsx2 function rescues distinct phenotypes in Dlx1/2 mutants. *Journal of Comparative Neurology* **521**:1561–1584.
- Wang, H.F. and Liu, F.C. (2001). Developmental restriction of the LIM homeodomain transcription factor Islet-1 expression to cholinergic neurons in the rat striatum. *Neuroscience* **103**:999–1016.
- Wang, W., Yang, J., Liu, H., Lu, D., Chen, X., Zenonos, Z., Campos, L.S., *et al.* (2011). Rapid and efficient reprogramming of somatic cells to induced pluripotent stem cells by retinoic acid receptor gamma and liver receptor homolog 1. *Proceedings of the National Academy of Sciences* **108**:18283–18288.
- Warren, L., Manos, P.D., Ahfeldt, T., Loh, Y.H., Li, H., Lau, F., Ebina, W., *et al.* (2010). Highly efficient reprogramming to pluripotency and directed differentiation of human cells with synthetic modified mRNA. *Cell Stem Cell* **7**:618–630.
- Watanabe, K., Kamiya, D., Nishiyama, A., Katayama, T., Nozaki, S., Kawasaki, H., Watanabe, Y., *et al.* (2005). Directed differentiation of telencephalic precursors from embryonic stem cells. *Nature neuroscience* **8**:288–296.
- Watanabe, K., Ueno, M., Kamiya, D., Nishiyama, A., Matsumura, M., Wataya, T., Takahashi, J.B., *et al.* (2007). A ROCK inhibitor permits survival of dissociated human embryonic stem cells. *Nature Biotechnology* **25**:681–686.
- Wheeler, V.C., Auerbach, W., White, J.K., Srinidhi, J., Auerbach, A., Ryan, A., Duyao, M.P., *et al.* (1999). Length-dependent gametic CAG repeat instability in the Huntington's disease knock-in mouse. *Human Molecular Genetics* **8**:115–122.
- Whitman, M. (1998). Smads and early developmental signaling by the TGFbeta superfamily. *Genes & development* **12**:2445–2462.
- Wichterle, H., Turnbull, D.H., Nery, S., Fishell, G. and Alvarez-Buylla, A. (2001). In utero fate mapping reveals distinct migratory pathways and fates of neurons born in the mammalian basal forebrain. *Development* **128**:3759–3771.
- Victorin, K. (1992). Anatomy and connectivity of intrastriatal striatal transplants. *Progress in Neurobiology* **38**:611–639.
- Wilson, P. a and Hemmati-Brivanlou, a (1995). Induction of epidermis and inhibition of neural fate by Bmp-4. *Nature* **376**:331–333.
- Wilson, S.-W. and Houart, C. (2004). Early steps in the development of the forebrain. *Developmental cell* **6**:167–81.
- Wu, X., Ding, S., Ding, Q., Gray, N.S. and Schultz, P.G. (2002). A small molecule with osteogenesis-inducing activity in multipotent mesenchymal progenitor cells. *J Am Chem Soc* **124**:14520–1.
- Xiao, L., Yuan, X. and Sharkis, S.J. (2006). Activin A maintains self-renewal and regulates fibroblast growth factor, Wnt, and bone morphogenic protein pathways in human

embryonic stem cells. *Stem cells* **24**:1476–1486.

Xu, Q., Guo, L., Moore, H., Waclaw, R.R., Campbell, K., Anderson, A., Cornell, W., *et al.* (2010). Sonic hedgehog signaling confers ventral telencephalic progenitors with distinct cortical interneuron fates. *Neuron* **65**:328–340.

Xu, Q., Wonders, C.P. and Anderson, S. a (2005). Sonic hedgehog maintains the identity of cortical interneuron progenitors in the ventral telencephalon. *Development* **132**:4987–4998.

Xu, R., Barron, T.L., Gu, F., Root, S., Peck, R.M., Yu, J., Antosiewicz-bourget, J., *et al.* (2008). NANOG is a Direct Target of TGF  $\beta$  /Activin Mediated SMAD Signaling in Human ES Cells. *Cell stem cell* **3**:196–206.

Xu, R.-H., Chen, X., Li, D.S., Li, R., Addicks, G.C., Glennon, C., Zwaka, T.P., *et al.* (2002). BMP4 initiates human embryonic stem cell differentiation to trophoblast. *Nature biotechnology* **20**:1261–1264.

Xuan, S., Baptista, C. a, Balas, G., Tao, W., Soares, V.C. and Lai, E. (1995). Winged helix transcription factor BF-1 is essential for the development of the cerebral hemispheres. *Neuron* **14**:1141–1152.

Yang, J., Davies, R.J., Southwood, M., Long, L., Yang, X., Sobolewski, A., Upton, P.D., *et al.* (2008). Mutations in bone morphogenetic protein type II receptor cause dysregulation of *id* gene expression in pulmonary artery smooth muscle cells implications for familial pulmonary arterial hypertension. *Circulation Research* **102**:1212–1221

Yang, S.-H., Cheng, P.-H., Banta, H., Piotrowska-Nitsche, K., Yang, J.-J., Cheng, E.C.H., Snyder, B., *et al.* (2008). Towards a transgenic model of Huntington's disease in a non-human primate. *Nature* **453**:921–924.

Yang, Y.P. and Klingensmith, J. (2006). Roles of organizer factors and BMP antagonism in mammalian forebrain establishment. *Developmental Biology* **296**:458–475.

Ying, Q.L., Nichols, J., Chambers, I. and Smith, A. (2003). BMP induction of *Id* proteins suppresses differentiation and sustains embryonic stem cell self-renewal in collaboration with STAT3. *Cell* **115**:281–292.

Yoshida, Y., Takahashi, K., Okita, K., Ichisaka, T. and Yamanaka, S. (2009). Hypoxia Enhances the Generation of Induced Pluripotent Stem Cells. *Cell Stem Cell* **5**:237–241.

Yu, J., Hu, K., Smuga-otto, K., Tian, S., Stewart, R., Igor, I. and Thomson, J. a (2009). Human Induced Pluripotent Stem Cell Free of Vector Transgene Sequences. *Science* **324**:797–801.

Yu, J., Vodyanik, M. a, Smuga-Otto, K., Antosiewicz-Bourget, J., Frane, J.L., Tian, S., Nie, J., *et al.* (2007). Induced pluripotent stem cell lines derived from human somatic cells. *Science* **318**:1917–20.

Yu, P.B., Deng, D.Y., Lai, C.S., Hong, C.C., Cuny, G.D., Bouxsein, M.L., Hong, D.W., *et al.* (2008). BMP type I receptor inhibition reduces heterotopic ossification. *Nature Medicine* **14**:1363–1369.

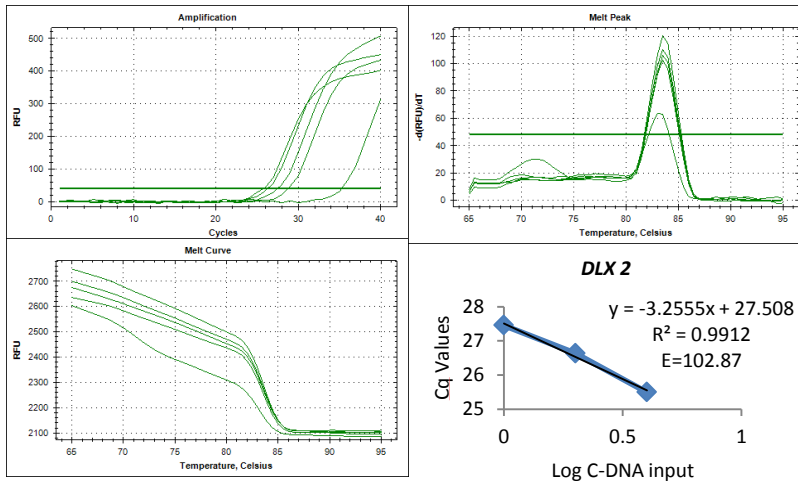
Yu, P.B., Hong, C.C., Sachidanandan, C., Babitt, J.L., Donna, Y., Hoyng, S. a, Lin, H.Y., *et al.* (2008). Dorsomorphin inhibits BMP signals required for embryogenesis and iron metabolism. *Nature chemical biology* **4**:33–41.

Yu, W., Wang, Y., McDonnell, K., Stephen, D. and Bai, C.B. (2009). Patterning of ventral

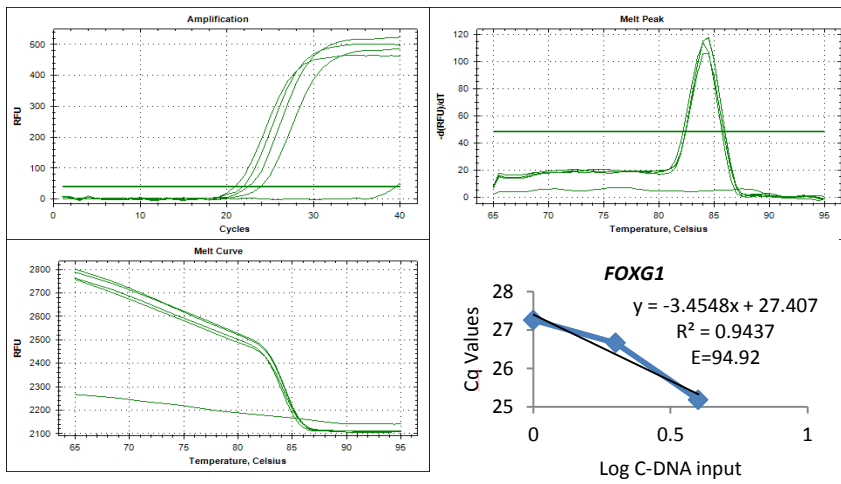
- telencephalon requires positive function of Gli transcription factors. *Developmental Biology* **334**:264–275.
- Yue, W., Li, Y., Zhang, T., Jiang, M., Qian, Y., Zhang, M., Sheng, N., *et al.* (2015). ESC-derived basal forebrain cholinergic neurons ameliorate the cognitive symptoms associated with Alzheimer's disease in mouse models. *Stem Cell Reports* **5**:776–790.
- Yun, K., Fischman, S., Johnson, J., Hrabe de Angelis, M., Weinmaster, G. and Rubenstein, J.L.R. (2002). Modulation of the notch signaling by Mash1 and Dlx1/2 regulates sequential specification and differentiation of progenitor cell types in the subcortical telencephalon. *Development* **129**:5029–5040.
- Yun, K., Potter, S. and Rubenstein, J.L. (2001). Gsh2 and Pax6 play complementary roles in dorsoventral patterning of the mammalian telencephalon. *Development* **128**:193–205.
- Zhang, N., An, M.C., Montoro, D. and Ellerby, L.M. (2010). Characterization of Human Huntington's Disease Cell Model from Induced Pluripotent Stem Cells. *PLoS currents* **2**:RRN1193..
- Zhang, X., Huang, C.T., Chen, J., Pankratz, M.T., Xi, J., Li, J., Yang, Y., *et al.* (2010). Pax6 is a human neuroectoderm cell fate determinant. *Cell Stem Cell* **7**:90–100.
- Zhang, Z., Gao, Y., Gordon, A., Wang, Z.Z., Qian, Z. and Wu, W.S. (2011). Efficient generation of fully reprogrammed human iPS cells via polycistronic retroviral vector and a new cocktail of chemical compounds. *PLoS ONE* **6**:1–9.
- Zhao, Y., Yin, X., Qin, H., Zhu, F., Liu, H., Yang, W., Zhang, Q., *et al.* (2008). Two Supporting Factors Greatly Improve the Efficiency of Human iPSC Generation. *Cell Stem Cell* **3**:475–479.
- Zhong, J., Kim, H.-T., Lyu, J., Yoshikawa, K., Nakafuku, M. and Lu, W. (2011). The Wnt receptor Ryk controls specification of GABAergic neurons versus oligodendrocytes during telencephalon development. *Development* **138**:409–419.
- Zhou, J., Su, P., Li, D., Tsang, S., Duan, E. and Wang, F. (2010). High-efficiency induction of neural conversion in human ESCs and human induced pluripotent stem cells with a single chemical inhibitor of transforming growth factor beta superfamily receptors. *Stem Cells* **28**:1741–1750.
- Zhu, S., Li, W., Zhou, H., Wei, W., Ambasadhan, R., Lin, T., Kim, J., *et al.* (2010). Reprogramming of human primary somatic cells by OCT4 and chemical compounds. *Cell Stem Cell* **7**:651–655.

## Appendix 2.1 Primer Efficiency analysis

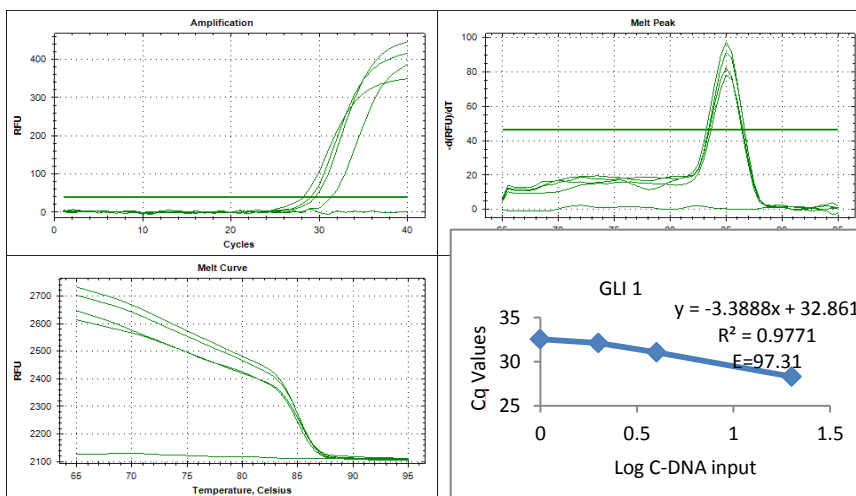
### DLX2



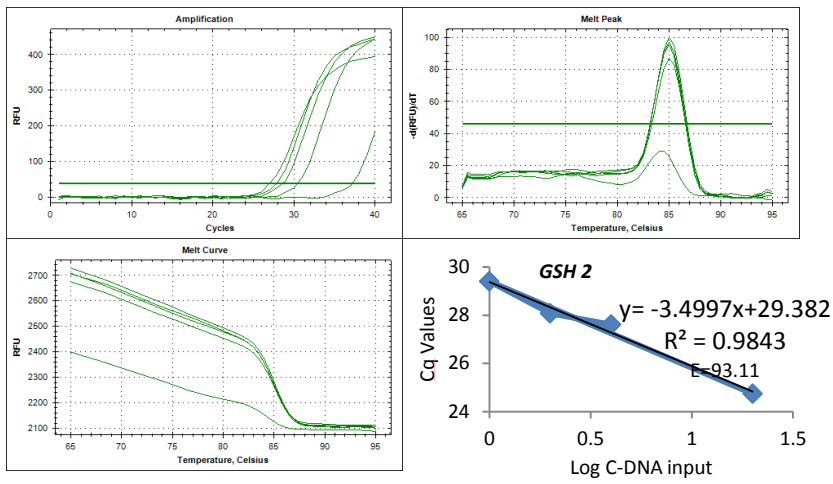
### FOXG1



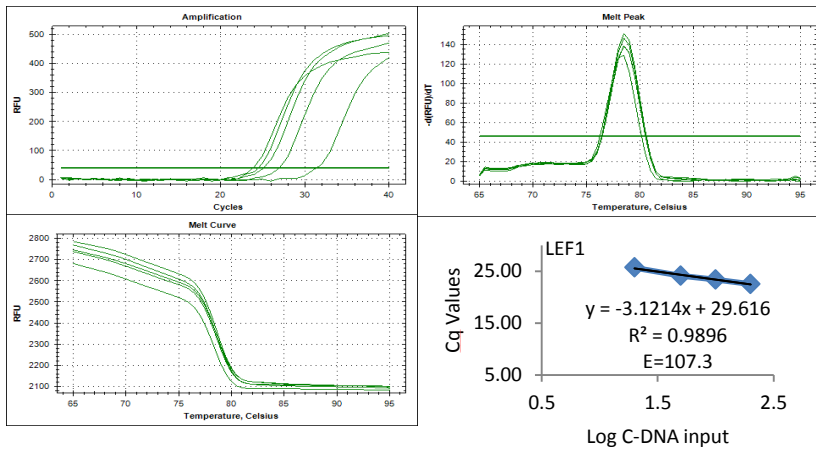
### GLI



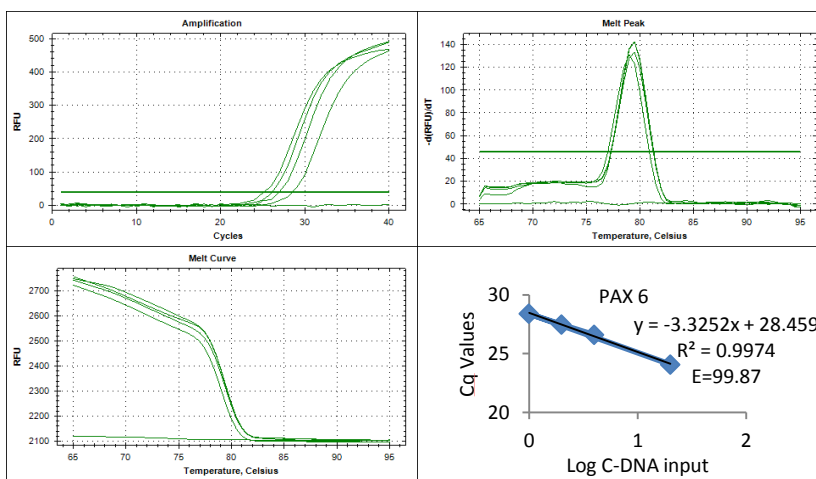
GSX2



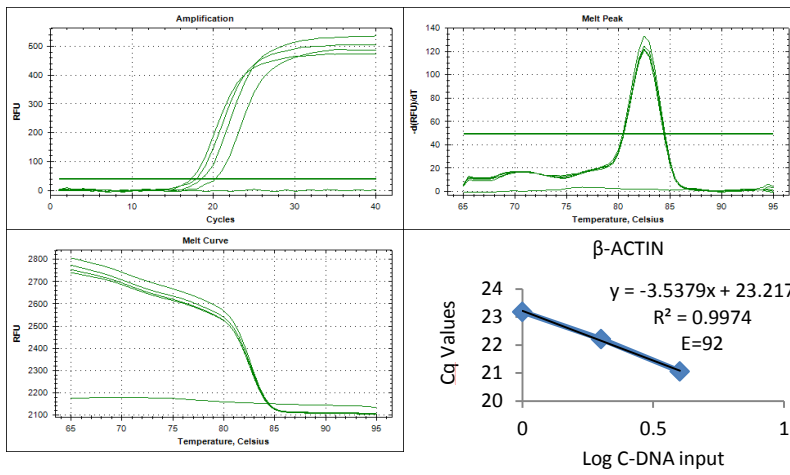
LEF1



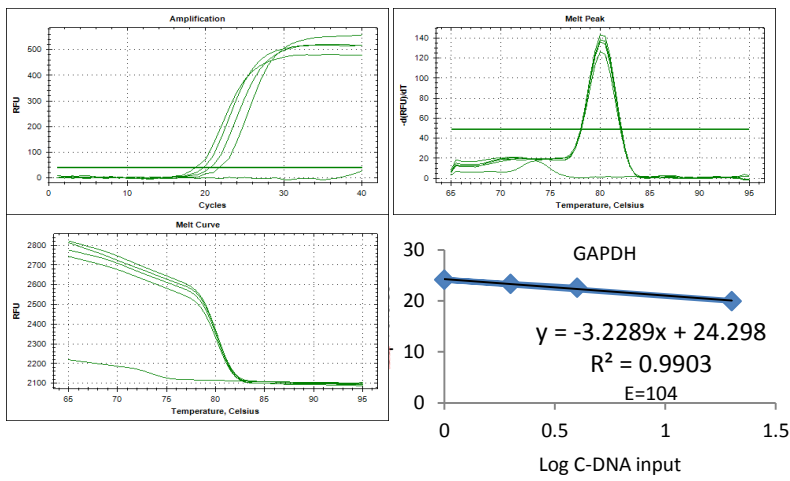
PAX6



B-ACTIN



GAPDH



**Appendix 3.1**Table 3.1  $\Delta Cq$  values of markers analysed in Chapter 3 figure 3.3 to 3.5

Treatment ( $\mu M$ )		$\Delta Cq \pm SEM$ <i>ID1</i>	$\Delta Cq \pm SEM$ <i>ID3</i>	$\Delta Cq \pm SEM$ <i>PAX6</i>	$\Delta Cq \pm SEM$ <i>SLUG</i>	$\Delta Cq \pm SEM$ <i>OCT4</i>
Undifferentiated hESC				13.21 $\pm$ 0.68	12.84 $\pm$ 0.59	3.16 $\pm$ 0.13
Untreated (Vehicle)	0.1% Ethanol	5.73	2.73	8.08 $\pm$ 0.17	5.97 $\pm$ 0.14	9.74 $\pm$ 1.18
SB431542		6.14	2.59	6.32 $\pm$ 0.21	7.76 $\pm$ 0.31	13.85 $\pm$ 0.24
SB431542+ Noggin		6.68	4.17	5.10 $\pm$ 0.12	7.41 $\pm$ 0.37	14.07 $\pm$ 0.34
SB431542+DM	0.25	8.16	5.34	5.20 $\pm$ 0.13	7.75 $\pm$ 0.16	12.28 $\pm$ 1.56
	0.5	8.25	4.53	4.68 $\pm$ 0.08	7.48 $\pm$ 0.14	13.22 $\pm$ 1.29
	1	7.90	4.46	4.67 $\pm$ 0.16	7.90 $\pm$ 0.18	13.08 $\pm$ 0.78
SB431542+LDN193189	0.25	11.00	6.30	4.60 $\pm$ 0.12	8.49 $\pm$ 0.03	11.82 $\pm$ 2.38
	0.5	11.41	6.31	4.58 $\pm$ 0.15	8.47 $\pm$ 0.20	13.53 $\pm$ 1.03
	1	10.88	5.82	4.70 $\pm$ 0.31	8.08 $\pm$ 0.58	12.07 $\pm$ 0.07
SB431542+DMH-1	0.25	9.22	5.24	4.60 $\pm$ 0.29	8.28 $\pm$ 0.22	11.42 $\pm$ 0.00
	0.5	9.56	5.03	4.38 $\pm$ 0.10	7.98 $\pm$ 0.03	11.14 $\pm$ 0.00
	1	10.32	5.01	4.60 $\pm$ 0.29	8.30 $\pm$ 0.40	10.79 $\pm$ 0.00

## Appendix 4.1

Table 4.1  $\Delta Cq$  values of LEF1 in figure 4.1 and 4.2.

Treatment ( $\mu M$ )		$\Delta Cq \pm SEM$ <i>LEF1</i>
WNT3a (on D12)	0	7.32
	25	7.20
	50	7.08
	100	6.87
	200	6.75
WNT3a + IWR $\mu M$ (on D12)	0	6.46 $\pm$ 0.11
	0.001	7.01 $\pm$ 0.25
	0.1	6.64 $\pm$ 0.08
	1	7.18 $\pm$ 0.11
	10	7.25 $\pm$ 0.16
IWR $\mu M$ (on D16)	0 (0.1%DMSO)	5.69 $\pm$ 0.23
	0.001	5.81 $\pm$ 0.09
	0.1	6.81 $\pm$ 0.21
	1	6.68 $\pm$ 0.10

Table 4.2  $\Delta Cq$  values of markers in figure 4.4.

Markers	$\Delta Cq \pm SEM$ D8	$\Delta Cq \pm SEM$ D16
PAX6	4.70 $\pm$ 0.38	4.64 $\pm$ 0.43
SLUG	9.02 $\pm$ 0.37	10.64 $\pm$ 0.71
FOXP1	4.89 $\pm$ 0.38	1.42 $\pm$ 0.33

Table 4.3  $\Delta Cq$  values of FOXP1 in figure 4.5.

	$\Delta Cq \pm SEM$ Untreated	$\Delta Cq \pm SEM$ IWR from D0	$\Delta Cq \pm SEM$ IWR from D8
FOXP1	10.25 $\pm$ 0.73	-6.27 $\pm$ 0.06	-2.87 $\pm$ 0.34

Table 4.4  $\Delta$ Cq values of markers in figure 4.5.

Treatment ( $\mu$ M)	$\Delta$ Cq $\pm$ SEM FOXG1	$\Delta$ Cq $\pm$ SEM PAX6	$\Delta$ Cq $\pm$ SEM GSX2	$\Delta$ Cq $\pm$ SEM DLX2	
IWR	0	12.97 $\pm$ 1.52	2.13 $\pm$ 0.22	14.57 $\pm$ 0.57	14.38 $\pm$ 0.06
	0.1	8.75 $\pm$ 0.96	2.43 $\pm$ 0.46	16.76 $\pm$ 3.64	15.73 $\pm$ 0.06
	1	1.56 $\pm$ 0.06	3.49 $\pm$ 0.38	5.81 $\pm$ 0.40	7.32 $\pm$ 0.60
	10	1.45 $\pm$ 0.45	3.67 $\pm$ 0.48	5.80 $\pm$ 0.02	8.25 $\pm$ 0.37
KY	0.1	8.70 $\pm$ 1.04	2.40 $\pm$ 0.34	13.23 $\pm$ 2.13	13.66 $\pm$ 0.97
	1	2.55 $\pm$ 0.44	3.03 $\pm$ 0.13	7.56 $\pm$ 0.32	11.29 $\pm$ 0.75
	10	0.78 $\pm$ 0.31	3.68 $\pm$ 0.83	7.76 $\pm$ 0.57	7.94 $\pm$ 0.43

Table 4.5  $\Delta$ Cq values of markers analysed by High-through put QRT-PCR.

Gene	$\Delta$ Cq $\pm$ SEM Untreated	$\Delta$ Cq $\pm$ SEM IWR	$\Delta$ Cq $\pm$ SEM KY	In Figure
SOX2	3.65 $\pm$ 0.28	2.70 $\pm$ 0.25	3.54 $\pm$ 0.08	4.11
SOX1	9.92 $\pm$ 0.17	7.95 $\pm$ 0.36	9.13 $\pm$ 0.49	
NES (NESTIN)	2.37 $\pm$ 0.08	2.43 $\pm$ 0.17	2.80 $\pm$ 0.15	
FOXG1	10.25 $\pm$ 0.73	1.22 $\pm$ 0.34	2.86 $\pm$ 0.21	4.12
SIX3	8.82 $\pm$ 1.13	3.98 $\pm$ 0.32	4.07 $\pm$ 0.10	
OTX2	4.17 $\pm$ 0.29	4.17 $\pm$ 0.21	4.35 $\pm$ 1.32	
LMX1B	6.89 $\pm$ 1.16	11.75 $\pm$ 0.35	13.03 $\pm$ 0.50	
PAX6	4.93 $\pm$ 0.20	5.56 $\pm$ 0.16	6.71 $\pm$ 1.56	4.13
EMX2	8.75 $\pm$ 1.03	5.42 $\pm$ 0.31	6.45 $\pm$ 2.22	
TBR1	9.9 $\pm$ 0.56	4.27 $\pm$ 0.46	5.80 $\pm$ 0.44	
GSX2	14.45 $\pm$ 0.21	3.35 $\pm$ 0.29	6.07 $\pm$ 0.82	4.14
GSX1	9.05 $\pm$ 0.00	8.43 $\pm$ 0.36	9.68 $\pm$ 0.31	
DLX1	14.45 $\pm$ 0.21	6.48 $\pm$ 0.80	8.23 $\pm$ 1.30	
DLX2	14.45 $\pm$ 0.21	6.41 $\pm$ 0.69	9.07 $\pm$ 0.82	
DLX5	14.45 $\pm$ 0.21	4.32 $\pm$ 0.22	7.16 $\pm$ 0.38	
ASCL1	8.14 $\pm$ 0.31	6.97 $\pm$ 0.86	8.50 $\pm$ 1.28	4.15
MEIS2	4.75 $\pm$ 0.31	1.73 $\pm$ 0.16	3.72 $\pm$ 0.32	
SP8	5.67 $\pm$ 0.16	4.72 $\pm$ 0.11	4.83 $\pm$ 0.50	
ISL1	9.92 $\pm$ 0.13	6.35 $\pm$ 0.56	9.83 $\pm$ 1.37	
FOXP1	6.79 $\pm$ 0.21	6.91 $\pm$ 0.45	6.96 $\pm$ 0.26	
EBF1	9.86 $\pm$ 0.16	9.12 $\pm$ 0.44	9.53 $\pm$ 0.31	4.16
NCAM1	4.85 $\pm$ 0.13	3.86 $\pm$ 0.25	4.61 $\pm$ 0.52	
CDH2	0.21 $\pm$ 0.06	0.53 $\pm$ 0.16	1.23 $\pm$ 0.15	
DCX	7.15 $\pm$ 0.33	3.51 $\pm$ 0.35	6.11 $\pm$ 1.48	
TUBB3	2.65 $\pm$ 0.23	0.77 $\pm$ 0.27	1.72 $\pm$ 0.10	
MAP2	2.84 $\pm$ 0.16	2.61 $\pm$ 0.41	4.01 $\pm$ 0.37	

## Appendix 5.1

Table 5.1  $\Delta Cq$  values of SHH targets in figure 5.2

Treatment ( $\mu M$ )		$\Delta Cq \pm SEM$ <i>PATCHED1</i>	$\Delta Cq \pm SEM$ <i>GLI1</i>
Control (IWR1)	0	13.61 $\pm$ 1.35	11.81 $\pm$ 0.00
IWR1+ Purmorphamine	0.1	11.86 $\pm$ 0.34	11.99 $\pm$ 0.29
	0.5	9.99 $\pm$ 0.42	6.80 $\pm$ 0.15
	1	8.91 $\pm$ 0.46	5.79 $\pm$ 0.00
IWR-1+ SAG	0.001	13.48 $\pm$ 0.07	14.00 $\pm$ 0.11
	0.01	13.06 $\pm$ 0.43	13.11 $\pm$ 0.05
	0.1	10.57 $\pm$ 0.58	7.65 $\pm$ 0.40

Table 5.2  $\Delta Cq$  values of ventral markers in figure 5.3

Treatment ( $\mu M$ )		$\Delta Cq \pm SEM$ <i>GSX2</i>	$\Delta Cq \pm SEM$ <i>DLX2</i>	$\Delta Cq \pm SEM$ <i>DLX5</i>	$\Delta Cq \pm SEM$ <i>NKX2.1</i>
Control (IWR1)	0	5.16 $\pm$ 0.31	5.24 $\pm$ 0.03	5.51 $\pm$ 1.03	15.79 $\pm$ 0.36
IWR1+ Purmorph- amine	0.1	5.60 $\pm$ 0.14	5.40 $\pm$ 0.29	7.33 $\pm$ 0.42	15.16 $\pm$ 0.06
	0.5	7.25 $\pm$ 0.15	8.01 $\pm$ 0.40	11.93 $\pm$ 0.50	12.61 $\pm$ 0.66
	1	9.86 $\pm$ 0.41	7.54 $\pm$ 0.47	9.49 $\pm$ 0.39	6.15 $\pm$ 0.15
<i>IWR1+ SAG</i>	0.001	5.28 $\pm$ 0.24	5.03 $\pm$ 0.70	6.54 $\pm$ 0.02	14.89 $\pm$ 0.25
	0.01	5.70 $\pm$ 0.41	5.86 $\pm$ 0.31	8.19 $\pm$ 0.63	15.34 $\pm$ 0.00
	0.1	7.13 $\pm$ 0.15	8.07 $\pm$ 0.92	11.85 $\pm$ 0.69	11.42 $\pm$ 0.89

Table 5.3  $\Delta C_q$  values of markers analysed by high-through put QRT-PCR

	H9				34D6		
	Control (IWR1)	IWR1+ Purmorphamine		IWR1+ Activin	Control (IWR1)	IWR1+Purmorphamine	
	0	0.5 $\mu$ M	1 $\mu$ M	20ng/ml	0	0.3 $\mu$ M	1 $\mu$ M
<i>SOX2</i>	2.70 $\pm$ 0.25	2.05 $\pm$ 0.68	1.49 $\pm$ 0.51	2.23 $\pm$ 0.22	1.48 $\pm$ 0.88	1.48 $\pm$ 0.86	0.70 $\pm$ 0.96
<i>SOX1</i>	7.95 $\pm$ 0.36	8.95 $\pm$ 0.24	9.08 $\pm$ 0.19	7.56 $\pm$ 0.00	9.35 $\pm$ 0.05	10.82 $\pm$ 0.47	11.23 $\pm$ 0.75
<i>NES</i>	2.43 $\pm$ 0.17	2.22 $\pm$ 0.44	2.71 $\pm$ 0.26	2.22 $\pm$ 0.25	1.85 $\pm$ 0.56	1.39 $\pm$ 0.27	1.42 $\pm$ 0.51
<i>FOXC1</i>	1.22 $\pm$ 0.34	1.02 $\pm$ 0.05	1.92 $\pm$ 0.63	1.07 $\pm$ 0.19	0.56 $\pm$ 0.87	0.77 $\pm$ 0.66	0.29 $\pm$ 0.96
<i>SIX3</i>	3.98 $\pm$ 0.32	3.79 $\pm$ 0.05	4.56 $\pm$ 0.41	4.11 $\pm$ 0.57	3.62 $\pm$ 0.31	4.34 $\pm$ 0.18	3.80 $\pm$ 0.71
<i>OTX2</i>	4.17 $\pm$ 0.21	4.41 $\pm$ 0.23	3.87 $\pm$ 0.80	6.26 $\pm$ 0.12	3.41 $\pm$ 0.75	3.58 $\pm$ 0.61	3.30 $\pm$ 0.99
<i>LMX1B</i>	11.79 $\pm$ 0.35	11.12 $\pm$ 0.32	11.79 $\pm$ 0.22	11.08 $\pm$ 1.82	10.26 $\pm$ 0.54	12.66 $\pm$ 1.44	11.45 $\pm$ 1.38
<i>FOXA2</i>	12.72 $\pm$ 0.63 (Undetermined)	13.31 $\pm$ 0.89 (Undetermined)	7.68 $\pm$ 0.56	Undetermined	14.10 $\pm$ 0.37	14.37 $\pm$ 0.29	8.20 $\pm$ 0.00
<i>PAX6</i>	5.56 $\pm$ 0.16	4.97 $\pm$ 0.29	7.20 $\pm$ 0.09	8.80 $\pm$ 0.04	5.80 $\pm$ 0.55	7.25 $\pm$ 0.76	12.87 $\pm$ 1.30
<i>GLI3</i>	1.70 $\pm$ 0.13	2.15 $\pm$ 0.52	3.42 $\pm$ 0.35	3.53 $\pm$ 0.75	2.48 $\pm$ 0.42	3.68 $\pm$ 0.43	4.43 $\pm$ 0.81
<i>EMX2</i>	5.42 $\pm$ 0.31	5.70 $\pm$ 1.00	6.54 $\pm$ 0.81	7.55 $\pm$ 0.93	7.34 $\pm$ 0.05	8.93 $\pm$ 0.80	12.93 $\pm$ 1.25
<i>TBR2</i>	5.50 $\pm$ 1.03	4.76 $\pm$ 0.00	6.51 $\pm$ 0.90	11.08 $\pm$ 1.82	8.80 $\pm$ 0.42	11.47 $\pm$ 1.67	11.58 $\pm$ 1.03
<i>TBR1</i>	4.27 $\pm$ 0.46	5.69 $\pm$ 0.47	6.86 $\pm$ 0.78	7.51 $\pm$ 1.09	5.81 $\pm$ 0.51	8.96 $\pm$ 0.81	14.09 $\pm$ 0.53
<i>GSX2</i>	3.35 $\pm$ 0.29	4.60 $\pm$ 0.21	6.99 $\pm$ 0.49	3.79 $\pm$ 0.36	3.47 $\pm$ 0.59	4.30 $\pm$ 0.72	4.81 $\pm$ 0.04
<i>GSX1</i>	8.43 $\pm$ 0.36	10.51 $\pm$ 2.26	8.06 $\pm$ 0.27	7.90 $\pm$ 0.00	6.79 $\pm$ 0.29	6.38 $\pm$ 0.28	5.70 $\pm$ 0.57
<i>DLX2</i>	5.73 $\pm$ 0.20	8.31 $\pm$ 0.11	9.59 $\pm$ 0.33	3.89 $\pm$ 0.18	4.59 $\pm$ 0.70	6.15 $\pm$ 0.72	5.56 $\pm$ 0.93
<i>DLX1</i>	4.27 $\pm$ 0.46	5.69 $\pm$ 0.47	6.86 $\pm$ 0.78	7.51 $\pm$ 1.09	4.58 $\pm$ 0.72	6.32 $\pm$ 0.75	6.40 $\pm$ 1.02
<i>DLX5</i>	4.32 $\pm$ 0.22	7.97 $\pm$ 0.76	8.09 $\pm$ 0.74	4.10 $\pm$ 0.72	3.79 $\pm$ 1.12	5.21 $\pm$ 0.25	5.43 $\pm$ 1.04
<i>ASCL1</i>	6.97 $\pm$ 0.86	7.73 $\pm$ 0.70	6.89 $\pm$ 0.73	5.22 $\pm$ 0.06	5.32 $\pm$ 0.77	5.51 $\pm$ 0.49	5.49 $\pm$ 1.08
<i>MEIS2</i>	1.73 $\pm$ 0.16	3.04 $\pm$ 0.19	3.47 $\pm$ 0.19	0.51 $\pm$ 0.47	1.97 $\pm$ 0.21	3.16 $\pm$ 0.39	3.67 $\pm$ 0.04
<i>SP8</i>	4.72 $\pm$ 0.11	4.68 $\pm$ 0.38	5.39 $\pm$ 0.23	6.42 $\pm$ 0.33	4.56 $\pm$ 0.31	5.49 $\pm$ 0.33	5.59 $\pm$ 0.85

<i>ISL1</i>	6.35 $\pm$ 0.56	10.40 $\pm$ 0.75	10.50 $\pm$ 0.43	4.48 $\pm$ 0.53	6.13 $\pm$ 0.25	7.32 $\pm$ 0.19	7.34 $\pm$ 0.50
<i>FOXP1</i>	6.91 $\pm$ 0.45	6.78 $\pm$ 0.10	7.15 $\pm$ 0.29	5.68 $\pm$ 0.20	7.16 $\pm$ 0.02	7.57 $\pm$ 0.37	8.24 $\pm$ 0.01
<i>EBF1</i>	9.12 $\pm$ 0.44	9.89 $\pm$ 1.35	9.89 $\pm$ 0.91	5.33 $\pm$ 0.72	8.64 $\pm$ 0.83	11.09 $\pm$ 0.47	13.11 $\pm$ 1.09
<i>NOLZ1</i>	8.87 $\pm$ 0.22	8.80 $\pm$ 1.33	6.70 $\pm$ 1.40	4.12 $\pm$ 0.62			
<i>GPR6</i>	9.22 $\pm$ 0.80	Undetermined	Undetermined	2.72 $\pm$ 0.00			
<i>TAC1</i>	6.30 $\pm$ 0.70	7.48 $\pm$ 0.00	10.61 $\pm$ 0.97	1.15 $\pm$ 0.44			
<i>NPY</i>	12.72 $\pm$ 0.63	Undetermined	Undetermined	3.37 $\pm$ 0.47			
<i>SST</i>	10.98 $\pm$ 0.00	8.52 $\pm$ 0.03	8.63 $\pm$ 0.13	5.28 $\pm$ 0.49			
<i>GLI1</i>	11.23 $\pm$ 2.21	10.40 $\pm$ 1.14	4.60 $\pm$ 0.40	8.85 $\pm$ 0.00	4.57 $\pm$ 0.87	3.22 $\pm$ 0.72	1.11 $\pm$ 0.15
<i>NKX2.1</i>	7.03 $\pm$ 0.11	4.8 $\pm$ 0.00	5.38 $\pm$ 0.00	5.34 $\pm$ 0.41	9.22 $\pm$ 0.26	5.76 $\pm$ 0.19	6.24 $\pm$ 0.12
<i>NKX6.2</i>	11.38 $\pm$ 0.74	7.91 $\pm$ 1.32	7.30 $\pm$ 0.60	6.89 $\pm$ 0.00	8.02 $\pm$ 0.43	11.04 $\pm$ 1.89	6.85 $\pm$ 0.14
<i>LHX6</i>	12.72 $\pm$ 0.63	7.48 $\pm$ 0.88	5.71 $\pm$ 0.67	8.15 $\pm$ 0.57	10.16 $\pm$ 0.78	9.04 $\pm$ 0.13	7.82 $\pm$ 0.70
<i>TUBB3</i>	0.77 $\pm$ 0.27	1.22 $\pm$ 0.28	1.63 $\pm$ 0.08	-0.60 $\pm$ 0.20	0.34 $\pm$ 0.29	0.62 $\pm$ 0.21	0.81 $\pm$ 0.04
<i>MAP2</i>	2.61 $\pm$ 0.40	3.55 $\pm$ 0.26	3.44 $\pm$ 0.19	1.91 $\pm$ 0.69	2.65 $\pm$ 0.43	2.94 $\pm$ 0.51	3.38 $\pm$ 0.37
<i>DCX</i>	3.51 $\pm$ 0.35	3.99 $\pm$ 0.49	3.43 $\pm$ 0.79	1.71 $\pm$ 0.11	2.25 $\pm$ 0.88	2.91 $\pm$ 0.72	3.14 $\pm$ 0.98
<i>OLIG2</i>	11.53 $\pm$ 1.68	7.27 $\pm$ 0.73	6.78 $\pm$ 1.28	6.29 $\pm$ 0.50	7.47 $\pm$ 0.50	6.63 $\pm$ 0.48	5.09 $\pm$ 0.25